



WILEY

New Phase Space Formulations and Quantum Dynamics Approaches

Journal:	<i>WIREs Computational Molecular Science</i>
Manuscript ID	CMS-842.R1
Wiley - Manuscript type:	Focus Article
Date Submitted by the Author:	n/a
Complete List of Authors:	He, Xin; Peking University, College of Chemistry and Molecular Engineering Wu, Baihua; Peking University, College of Chemistry and Molecular Engineering Shang, Youhao; Peking University, College of Chemistry and Molecular Engineering Li, Binqi; Peking University, College of Chemistry and Molecular Engineering Cheng, Xiangsong; Peking University, College of Chemistry and Molecular Engineering Liu, Jian; Peking University, College of Chemistry and Molecular Engineering
Keywords:	quantum dynamics, nonadiabatic dynamics, phase space formulation, composite quantum systems, constraint phase space
Choose 1-3 topics to categorize your article:	Molecular Dynamics and Monte-Carlo Methods (CDAC) < Molecular and Statistical Mechanics (CDAA), Reaction Dynamics and Kinetics (CEAB) < Theoretical and Physical Chemistry (CEAA), Statistical Mechanics (CEAE) < Theoretical and Physical Chemistry (CEAA)

SCHOLARONE™
Manuscripts

New Phase Space Formulations and Quantum Dynamics Approaches

Article Type:

- OPINION
- PRIMER
- OVERVIEW
- ADVANCED REVIEW
- FOCUS ARTICLE
- SOFTWARE FOCUS

Authors:

Xin He (co-first author)

Beijing National Laboratory for Molecular Sciences, Institute of Theoretical and Computational Chemistry, College of Chemistry and Molecular Engineering, Peking University, Beijing 100871, China

ORCID ID: 0000-0002-5189-7204

Baihua Wu (co-first author)

Beijing National Laboratory for Molecular Sciences, Institute of Theoretical and Computational Chemistry, College of Chemistry and Molecular Engineering, Peking University, Beijing 100871, China

ORCID ID: 0000-0002-1256-6859

Youhao Shang

Beijing National Laboratory for Molecular Sciences, Institute of Theoretical and Computational Chemistry, College of Chemistry and Molecular Engineering, Peking University, Beijing 100871, China

ORCID ID: 0000-0002-9297-6654

Bingqi Li

Beijing National Laboratory for Molecular Sciences, Institute of Theoretical and Computational Chemistry, College of Chemistry and Molecular Engineering, Peking University, Beijing 100871, China

ORCID ID: 0000-0001-7273-8299

Xiangsong Cheng

1
2
3 Beijing National Laboratory for Molecular Sciences, Institute of Theoretical and Computational
4 Chemistry, College of Chemistry and Molecular Engineering, Peking University, Beijing 100871,
5 China
6
7
8
9 ORCID ID: 0000-0001-8793-5092
10
11

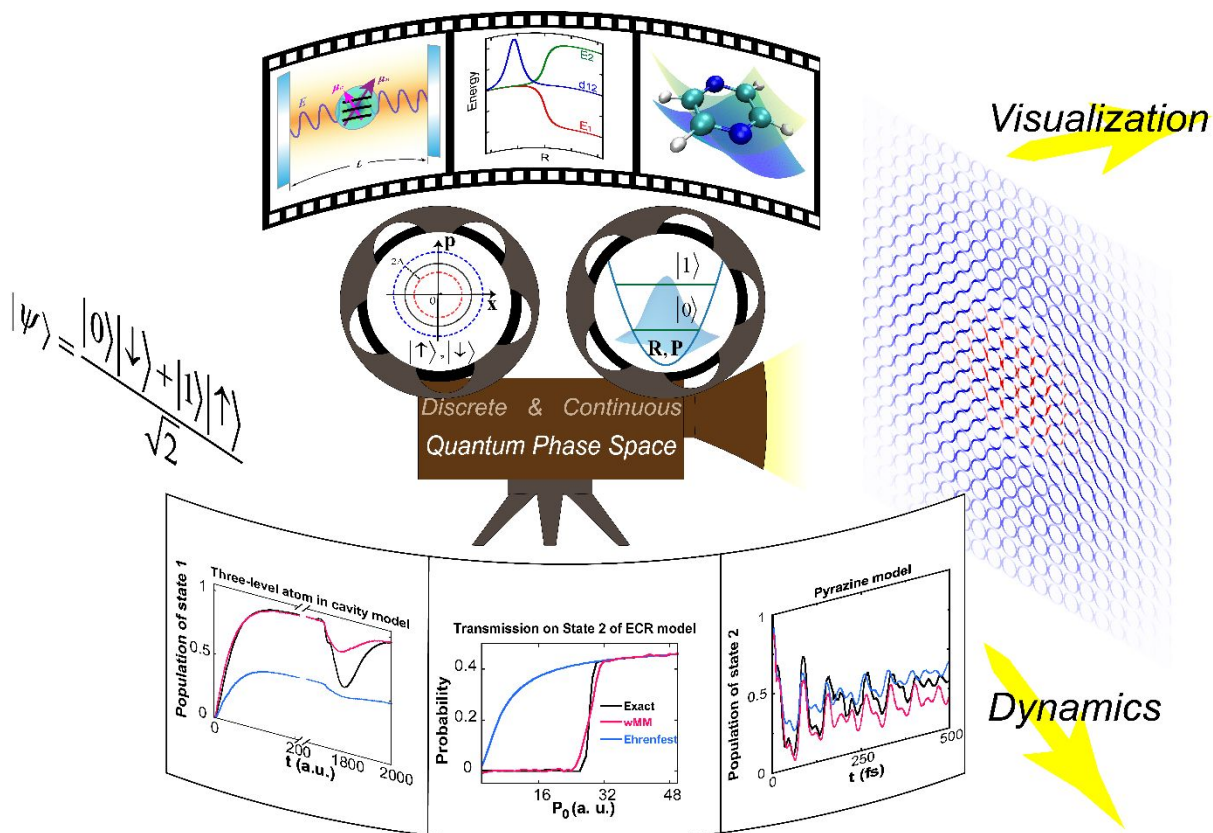
12 **Jian Liu*** (Corresponding author)
13
14

15 Beijing National Laboratory for Molecular Sciences, Institute of Theoretical and Computational
16 Chemistry, College of Chemistry and Molecular Engineering, Peking University, Beijing 100871,
17 China
18
19 ORCID ID: 0000-0002-2906-5858
20
21 Email: jianliupku@pku.edu.cn
22

23 **Abstract**

24 We report recent progress on the phase space formulation of quantum mechanics with coordinate-momentum
25 variables, focusing more on new theory of (weighted) constraint coordinate-momentum phase space for discrete-
26 variable quantum systems. This leads to a general coordinate-momentum phase space formulation of composite
27 quantum systems, where conventional representations on infinite phase space are employed for continuous
28 variables. It is convenient to utilize (weighted) constraint coordinate-momentum phase space for representing
29 the quantum state and describing nonclassical features. Various numerical tests demonstrate that new trajectory-
30 based quantum dynamics approaches derived from the (weighted) constraint phase space representation are useful
31 and practical for describing dynamical processes of composite quantum systems in gas phase as well as in
32 condensed phase.
33
34
35
36
37
38
39
40
41
42
43
44
45
46
47
48
49
50
51
52
53
54
55
56
57
58
59
60

Graphical/Visual Abstract and Caption



Schematic representation of dynamics of composite quantum systems *via* phase space formulations.

1. INTRODUCTION

Phase space with coordinate-momentum variables is a fundamental concept and offers a convenient tool to describe statistics as well as dynamics in classical mechanics. In comparison to other equivalent interpretations of quantum mechanics, phase space formulations offer more insight and understanding between quantum and classical counterpart concepts, which are widely used in chemical and biological dynamics and spectroscopy¹⁻⁶⁰, quantum optics^{51, 61-70}, cryogenic physics/chemistry⁷¹⁻⁷⁵, quantum information and computation⁷⁶⁻⁸⁷, etc.

Phase space formulations of quantum mechanics have been developed since two important pioneering works, the Weyl transform in 1927, of which the original formulation converted a Hamiltonian on classical phase space into a quantum mechanical operator⁸⁸, and the Wigner function in 1932 that in principle depicts the inverse transform although a pure state was used for demonstration⁸⁹. The most essential element is the one-to-one correspondence mapping between quantum operators and classical functions often defined on a smooth manifold, namely, phase space. Because of the commutation relation of conjugate operators, the mapping is not unique in quantum mechanics^{90, 91}.

When infinite phase space is employed for a continuous-variable quantum system, most phase space formulations can be described by Cohen's generalized form⁹² in 1966. Quantum dynamics with phase space variables is expressed by the Moyal or Moyal-like bracket as first proposed by Groenewold⁹³ in 1946 and Moyal⁹⁴ in 1949. The Wigner and Husimi representations are most often used for the continuous-variable system. When the Moyal bracket is approximated by the Poisson bracket in the Wigner phase space expression of the quantum Liouville theorem, which was also derived as the linearized semiclassical initial value representation (LSC-IVR) or classical Wigner model^{4-8, 11, 20, 23} for the quantum correlation function, it reproduces exact quantum correlation functions even of nonlinear operators (i.e., nonlinear functions of the coordinate or momentum operator) in the harmonic or classical limit. The truncated Wigner approximation⁷⁴ with the time-dependent generalization of the Bopp representation^{90, 95} is similar to the LSC-IVR, but the former requests more demanding evaluation of the stability matrix elements along the trajectory when nonlinear operators are involved in the correlation function. Ref. ¹⁵ suggests a practical way to implement the imaginary time path integral treatment of the Boltzmann density operator in the LSC-IVR for general molecular systems that often contain imaginary frequencies. Its recent application illustrates that quantum dynamical effects play a critical role in reproducing the peaks in the intermediate region between the librational and bending bands, those between the bending and stretching bands, and the double-peak in the stretching band in the experimental isotropic Raman spectrum of liquid water¹⁹ (as shown in Figure 1). In addition that more advanced versions of SC-IVR⁹⁶⁻⁹⁹ are capable of

improving over the LSC-IVR, in ref¹¹ we first employed the quantum Liouville theorem in the phase space formulation to develop trajectory-based approaches to satisfy the two fundamental criteria: conservation of the quantum Boltzmann distribution for the thermal equilibrium system and being exact for any quantum thermal correlation functions in the classical and harmonic limits. Such trajectory-based approaches can in principle be further improved by higher order corrections of the exact series expansion of the phase space propagator as demonstrated in ref⁴⁴. More progress along this line can be found in refs³⁷⁻⁴⁷. (Figure 2 shows molecular vibrational spectra produced by the new phase space quantum dynamics methods.)

Phase space representations of a finite discrete F -state quantum system were first independently described by Stratonovich¹⁰⁰ in 1956, Feynman¹⁰¹ in 1987, and Wootters¹⁰² in 1987. Further developments of Stratonovich's formulation have focused on an SU(2) or SU(F) structure of phase space¹⁰³⁻¹¹⁷, while those on the construction of a discrete phase space are described in Refs^{78, 118-126}. Other than the 2-state (or spin 1/2) system, the exact equations of motion (EOMs) of phase variables (expressed by the Moyal-like bracket) involved in these approaches for the finite discrete multi-state system are often tedious (and nonlinear)^{109, 127-130}. Recent theoretical progress on exactly mapping the finite discrete F -state quantum system onto *constraint* coordinate-momentum phase space suggests that there exists a novel unified framework to derive comprehensive exact mapping Hamiltonians^{44, 57, 131, 132}, of which the quantum EOMs of mapping coordinate-momentum variables are simply linear^{44, 57, 131-134}.

The unified mapping formulation on coordinate-momentum phase space^{44, 57, 131-134} then offers a useful tool to treat dynamics of a composite quantum system, in which both continuous and finite discrete degrees of freedom (DOFs) are involved and coupled with one another. Because a typical molecular system has vibrational, rotational, and translational motion, it is often much more convenient to employ continuous coordinate space rather than Hilbert space with dense states to describe the nuclear DOFs. On the other hand, the energy gap between different electronic states of interest is often significantly larger such that the (adiabatic or diabatic) state representation is more useful to depict the electronic DOFs. It is evident that a general description of the molecular system leads to a composite quantum system, especially in the nonadiabatic region¹³⁵⁻¹⁵². A comprehensive version of the Meyer-Miller mapping Hamiltonian model^{153, 154} can rigorously be formulated in the general coordinate-momentum phase space formulation^{44, 57, 131-134}.

In the Focus Article we focus on novel developments on the phase space formulation of quantum mechanics with coordinate-momentum variables for discrete-variable systems as well as for composite systems^{44, 57, 131-134}. In Section 2 we first review the general coordinate-momentum phase space formulation, where infinite space is

used for describing continuous variables and constraint space is employed for mapping discrete variables. We then propose a weighted constraint phase space representation that is also an exact formulation for mapping discrete-variable quantum systems. Section 3 demonstrates several examples and discusses implications of the (weighted) constraint coordinate-momentum phase space for studying and illustrating discrete-variable or composite quantum systems. When we use the weighted constraint phase space representation for mapping composite quantum systems, the mapping Hamiltonian (we use the Meyer-Miller mapping Hamiltonian for demonstration throughout the article, albeit that other mapping Hamiltonians are also available^{57, 58, 131, 132}) yields a novel trajectory-based approximate approach for composite systems. Such a new method satisfies the frozen nuclei limit [i.e., the dynamics reproduces the exact evolution when only finite discrete (electronic) DOFs are involved]. In Section 4 the performance of new trajectory-based quantum dynamics approaches on (weighted) constraint phase space is extensively tested for a few typical benchmark composite systems in gas phase as well as in condensed phase. Finally, conclusion remarks are presented in Section 5.

2. GENERAL COORDINATE-MOMENTUM PHASE SPACE FORMULATION OF QUANTUM MECHANICS

Consider a (molecular) system with N continuous (nuclear) DOFs and F discrete (electronic) states, of which the Hamiltonian reads

$$\hat{H} = \sum_{n,m=1}^F H_{nm}(\hat{\mathbf{R}}, \hat{\mathbf{P}}) |n\rangle\langle m| = \sum_{n,m=1}^F \left[\frac{1}{2} \hat{\mathbf{P}}^T \mathbf{M}^{-1} \hat{\mathbf{P}} \delta_{nm} + V_{nm}(\hat{\mathbf{R}}) \right] |n\rangle\langle m| , \quad 2$$

where \mathbf{R} and \mathbf{P} are the nuclear coordinate and momentum variables, respectively, \mathbf{M} is the diagonal mass matrix, and the F states form an orthonormal complete basis sets, i.e.,

$$\langle m | n \rangle = \delta_{mn}, \quad \hat{I}_{\text{ele}} = \sum_{n=1}^F |n\rangle\langle n| . \quad 3$$

\hat{I}_{ele} and \hat{I}_{nuc} stand for the identity operator of the discrete (electronic) DOFs and that of the continuous (nuclear) DOFs. For simplicity, eq 2 employs the (electronically) diabatic representation, where the Hermitian potential matrix $\mathbf{V}(\mathbf{R})$ is a function of only the coordinate vector. (In applications $\mathbf{V}(\mathbf{R})$ is often a real symmetric matrix.) More discussion on the adiabatic representation of discrete (electronic) DOFs is available in Section-4.1.

The unified formulation of mapping phase space with coordinate-momentum variables offers a useful exact approach to describe the composite system. The trace of a product of two quantum operators is expressed as an integral of two functions on mapping phase space, *i.e.*,

$$\text{Tr}_{n,e} [\hat{A}\hat{B}] = \int d\mu_{\text{nuc}}(\mathbf{R}, \mathbf{P}) \int_{S(x,p)} d\mu_{\text{ele}}(\mathbf{x}, \mathbf{p}) A_C(\mathbf{R}, \mathbf{P}; \mathbf{x}, \mathbf{p}) \mathcal{B}_C^o(\mathbf{R}, \mathbf{P}; \mathbf{x}, \mathbf{p}) \quad 4$$

with

$$A_C(\mathbf{R}, \mathbf{P}; \mathbf{x}, \mathbf{p}) = \text{Tr}_{n,e} [\hat{A} \hat{K}_{\text{nuc}}(\mathbf{R}, \mathbf{P}) \otimes \hat{K}_{\text{ele}}(\mathbf{x}, \mathbf{p})] \quad 5$$

$$\mathcal{B}_C^o(\mathbf{R}, \mathbf{P}; \mathbf{x}, \mathbf{p}) = \text{Tr}_{n,e} [\hat{K}_{\text{nuc}}^{-1}(\mathbf{R}, \mathbf{P}) \otimes \hat{K}_{\text{ele}}^{-1}(\mathbf{x}, \mathbf{p}) \hat{B}] \quad 6$$

$d\mu_{\text{nuc}}(\mathbf{R}, \mathbf{P}) = (2\pi\hbar)^{-N} d\mathbf{R} d\mathbf{P}$ and $d\mu_{\text{ele}}(\mathbf{x}, \mathbf{p}) = F d\mathbf{x} d\mathbf{p}$ as the integration measure on nuclear phase space and that on electronic phase space, respectively, and $\text{Tr}_{n,e}$ represents the trace over the corresponding nuclear and electronic Hilbert space. The integral over the mapping phase space variables for the finite discrete (electronic) DOFs in eq 4 is performed as

$$\int_{S(x,p)} F d\mathbf{x} d\mathbf{p} g(\mathbf{x}, \mathbf{p}) = \int F d\mathbf{x} d\mathbf{p} \frac{1}{\Omega} S(\mathbf{x}, \mathbf{p}) g(\mathbf{x}, \mathbf{p}) = \int F d\mathbf{x} d\mathbf{p} \bar{S}(\mathbf{x}, \mathbf{p}) g(\mathbf{x}, \mathbf{p}) \quad 7$$

where the area of constraint space $S(\mathbf{x}, \mathbf{p})$

$$\Omega = \int d\mathbf{x} d\mathbf{p} S(\mathbf{x}, \mathbf{p}) \quad 8$$

is the normalization constant, and $\bar{S}(\mathbf{x}, \mathbf{p})$ is the normalized constraint space.

The normalization of the (inverse) mapping kernel reads

$$\text{Tr}_n [\hat{K}_{\text{nuc}}(\mathbf{R}, \mathbf{P})] = \text{Tr}_n [\hat{K}_{\text{nuc}}^{-1}(\mathbf{R}, \mathbf{P})] = 1 \quad 9$$

$$\text{Tr}_e [\hat{K}_{\text{ele}}(\mathbf{x}, \mathbf{p})] = \text{Tr}_e [\hat{K}_{\text{ele}}^{-1}(\mathbf{x}, \mathbf{p})] = 1 \quad 10$$

and

$$\int d\mu_{\text{nuc}}(\mathbf{R}, \mathbf{P}) \hat{K}_{\text{nuc}}(\mathbf{R}, \mathbf{P}) = \int d\mu_{\text{nuc}}(\mathbf{R}, \mathbf{P}) \hat{K}_{\text{nuc}}^{-1}(\mathbf{R}, \mathbf{P}) = \hat{I}_{\text{nuc}} \quad 11$$

$$\int_{S(x,p)} d\mu_{\text{ele}}(\mathbf{x}, \mathbf{p}) \hat{K}_{\text{ele}}(\mathbf{x}, \mathbf{p}) = \int_{S(x,p)} d\mu_{\text{ele}}(\mathbf{x}, \mathbf{p}) \hat{K}_{\text{ele}}^{-1}(\mathbf{x}, \mathbf{p}) = \hat{I}_{\text{ele}} \quad 12$$

The one-to-one correspondence mapping from phase space function $A_C(\mathbf{R}, \mathbf{P}; \mathbf{x}, \mathbf{p})$ or $\beta_C^0(\mathbf{R}, \mathbf{P}; \mathbf{x}, \mathbf{p})$ of Eq 5 back to operator \hat{A} or \hat{B} is

$$\begin{aligned}\hat{A} &= \int d\mu_{\text{nuc}}(\mathbf{R}, \mathbf{P}) \int_{S(x, p)} d\mu_{\text{ele}}(\mathbf{x}, \mathbf{p}) A_C(\mathbf{R}, \mathbf{P}; \mathbf{x}, \mathbf{p}) \hat{K}_{\text{nuc}}^{-1}(\mathbf{R}, \mathbf{P}) \otimes \hat{K}_{\text{ele}}^{-1}(\mathbf{x}, \mathbf{p}) \\ \hat{B} &= \int d\mu_{\text{nuc}}(\mathbf{R}, \mathbf{P}) \int_{S(x, p)} d\mu_{\text{ele}}(\mathbf{x}, \mathbf{p}) \beta_C^0(\mathbf{R}, \mathbf{P}; \mathbf{x}, \mathbf{p}) \hat{K}_{\text{nuc}}(\mathbf{R}, \mathbf{P}) \otimes \hat{K}_{\text{ele}}(\mathbf{x}, \mathbf{p})\end{aligned}. \quad 13$$

The nuclear or electronic kernel should satisfy five criteria, namely, linearity, reality, standardization (normalization), traciality, and covariance^{93, 94, 100, 115}.

2.1 Mapping kernel for continuous (nuclear) degrees of freedom

The integrals for (\mathbf{R}, \mathbf{P}) in eqs 4, 11, and 13 are over infinite (nuclear) phase space. The mapping kernel and its inverse for the nuclear DOFs are

$$\begin{aligned}\hat{K}_{\text{nuc}}(\mathbf{R}, \mathbf{P}) &= \left(\frac{\hbar}{2\pi} \right)^N \int d\zeta \int d\eta e^{i\zeta \cdot (\hat{\mathbf{R}} - \mathbf{R}) + i\eta \cdot (\hat{\mathbf{P}} - \mathbf{P})} f(\zeta, \eta) \\ \hat{K}_{\text{nuc}}^{-1}(\mathbf{R}, \mathbf{P}) &= \left(\frac{\hbar}{2\pi} \right)^N \int d\zeta \int d\eta e^{i\zeta \cdot (\hat{\mathbf{R}} - \mathbf{R}) + i\eta \cdot (\hat{\mathbf{P}} - \mathbf{P})} [f(-\zeta, -\eta)]^{-1}\end{aligned}, \quad 14$$

where $f(\zeta, \eta)$ is a scalar function. E.g., we have the Wigner function^{89, 155}

$$f(\zeta, \eta) = 1, \quad 15$$

the Husimi function¹⁵⁶

$$f(\zeta, \eta) = \exp \left(-\frac{\zeta^T \Gamma^{-1} \zeta}{4} - \frac{\hbar^2}{4} \eta^T \Gamma \eta \right), \quad 16$$

the anti-Husimi function

$$f(\zeta, \eta) = \exp \left(\frac{\zeta^T \Gamma^{-1} \zeta}{4} + \frac{\hbar^2}{4} \eta^T \Gamma \eta \right), \quad 17$$

the Glauber-Sudarshan P function^{61, 62, 66} (with the characteristic frequency matrix ω of the system)

$$f(\zeta, \eta) = \exp \left[\frac{\hbar}{4} \zeta^T \mathbf{M}^{-1/2} \omega^{-1} \mathbf{M}^{-1/2} \zeta + \frac{\hbar}{4} \eta^T \mathbf{M}^{1/2} \omega \mathbf{M}^{1/2} \eta \right] \quad 18$$

and its generalized versions⁶⁶, the Glauber Q function¹⁵⁷

$$f(\zeta, \eta) = \exp \left[-\frac{\hbar}{4} \zeta^T \mathbf{M}^{-1/2} \boldsymbol{\omega}^{-1} \mathbf{M}^{-1/2} \zeta - \frac{\hbar}{4} \eta^T \mathbf{M}^{1/2} \boldsymbol{\omega} \mathbf{M}^{1/2} \eta \right] , \quad 19$$

the normal-antinormal ordered function⁹¹

$$f(\zeta, \eta) = \cosh \left[\frac{\hbar}{4} \zeta^T \mathbf{M}^{-1/2} \boldsymbol{\omega}^{-1} \mathbf{M}^{-1/2} \zeta + \frac{\hbar}{4} \eta^T \mathbf{M}^{1/2} \boldsymbol{\omega} \mathbf{M}^{1/2} \eta \right] , \quad 20$$

the Kirkwood antistandard-ordered function^{158, 159}

$$f(\zeta, \eta) = e^{i \hbar \zeta^T \eta / 2} , \quad 21$$

the Mehta standard-ordered function¹⁶⁰

$$f(\zeta, \eta) = e^{-i \hbar \zeta^T \eta / 2} , \quad 22$$

the Rivier function^{161, 162}

$$f(\zeta, \eta) = \cos \left[\frac{1}{2} \hbar \zeta^T \eta \right] , \quad 23$$

and the distribution function of Born and Jordan¹⁶³

$$f(\zeta, \eta) = \frac{\sin \left[\frac{1}{2} \hbar \zeta^T \eta \right]}{\frac{1}{2} \hbar \zeta^T \eta} , \quad 24$$

etc.

When operator \hat{A} is a function of only the nuclear DOFs, its phase space function from Eq 5 and the dual function from eq 6 become

$$A_{\text{nuc}}(\mathbf{R}, \mathbf{P}) = \text{Tr}_n \left[\hat{A} \hat{K}_{\text{nuc}}(\mathbf{R}, \mathbf{P}) \right] \quad 25$$

and

$$\%_{\text{nuc}}(\mathbf{R}, \mathbf{P}) = \text{Tr}_n \left[\hat{K}_{\text{nuc}}^{-1}(\mathbf{R}, \mathbf{P}) \hat{A} \right] . \quad 26$$

When the Wigner function eq 15 is used, the mapping kernel and its inverse are the same, i.e., $\hat{K}_{\text{nuc}}(\mathbf{x}, \mathbf{p}) = \hat{K}_{\text{nuc}}^{-1}(\mathbf{x}, \mathbf{p})$. The Wigner phase space function of operator \hat{A} (from eq 25) is identical to its dual (from eq 26),

$$A_{\text{nuc}}^W(\mathbf{R}, \mathbf{P}) = A_{\text{nuc}}^{\mathcal{H}}(\mathbf{R}, \mathbf{P}) . \quad 27$$

When the Husimi phase space (eq 16) is employed, it is straightforward to show the relation between the Wigner and Husimi phase space functions (obtained from eq 25)

$$A_{\text{nuc}}^H(\mathbf{R}, \mathbf{P}) = \exp \left[\frac{1}{4} \left(\frac{d}{d\mathbf{R}} \right)^T \Gamma^{-1} \left(\frac{d}{d\mathbf{R}} \right) + \frac{\hbar^2}{4} \left(\frac{d}{d\mathbf{P}} \right)^T \Gamma \left(\frac{d}{d\mathbf{P}} \right) \right] A_{\text{nuc}}^W(\mathbf{R}, \mathbf{P}) , \quad 28$$

and the relation between the dual function of Husimi phase space $A_{\text{nuc}}^{\mathcal{H}}(\mathbf{R}, \mathbf{P})$ and the Wigner phase space function $A_{\text{nuc}}^W(\mathbf{R}, \mathbf{P})$

$$A_{\text{nuc}}^{\mathcal{H}}(\mathbf{R}, \mathbf{P}) = \exp \left[-\frac{1}{4} \left(\frac{d}{d\mathbf{R}} \right)^T \Gamma^{-1} \left(\frac{d}{d\mathbf{R}} \right) - \frac{\hbar^2}{4} \left(\frac{d}{d\mathbf{P}} \right)^T \Gamma \left(\frac{d}{d\mathbf{P}} \right) \right] A_{\text{nuc}}^W(\mathbf{R}, \mathbf{P}) . \quad 29$$

Because any choice of $f(\zeta, \eta)$ in eq 14 leads to an informationally complete representation of the continuous-variable quantum system, it is not difficult to establish the relation between different (dual) phase space functions in addition to eq 28 and eq 29.

2.2 Mapping kernel on constraint space for discrete (electronic) degrees of freedom

As derived first in Appendix A of ref¹³² in the spirit of Ref¹³¹ and then in the Supporting Information of ref¹³⁴, the kernel that maps a set of F states onto constraint phase space $\mathbf{S}(\mathbf{x}, \mathbf{p})$ reads

$$\hat{K}_{\text{ele}}(\mathbf{x}, \mathbf{p}) = \sum_{n,m=1}^F \left[\frac{1}{2} (x^{(n)} + ip^{(n)}) (x^{(m)} - ip^{(m)}) - \gamma \delta_{nm} \right] |n\rangle\langle m| \quad 30$$

and the corresponding inverse kernel is

$$\hat{K}_{\text{ele}}^{-1}(\mathbf{x}, \mathbf{p}) = \sum_{n,m=1}^F \left[\frac{1+F}{2(1+F\gamma)^2} (x^{(n)} + ip^{(n)}) (x^{(m)} - ip^{(m)}) - \frac{1-\gamma}{1+F\gamma} \delta_{nm} \right] |n\rangle\langle m| . \quad 31$$

As naturally required by eq 10, constraint phase space $\mathbf{S}(\mathbf{x}, \mathbf{p})$ is defined by

$$\delta \left(\sum_{n=1}^F \frac{(x^{(n)})^2 + (p^{(n)})^2}{2} - (1+F\gamma) \right) , \quad 32$$

of which the area is

$$\Omega(\gamma) = \int d\mathbf{x}d\mathbf{p} \delta \left(\sum_{n=1}^F \frac{(x^{(n)})^2 + (p^{(n)})^2}{2} - (1+F\gamma) \right) . \quad 33$$

The normalized constraint phase space is $\bar{\mathbb{S}}(\mathbf{x}, \mathbf{p}) = \mathbb{S}(\mathbf{x}, \mathbf{p})/\Omega(\gamma)$.

Equations 30-33 define the mapping kernel and inverse kernel as well as constraint phase space, which are the key elements of the coordinate-momentum phase space formulation of the discrete-variable quantum system that we first established in refs^{131, 132} and further developed in refs^{57, 58, 134}. As yielded from eq 5, when the Wigner function eq 15 is used for the nuclear DOFs, the mapping Hamiltonian for the quantum Hamiltonian operator eq 2 reads

$$H_C(\mathbf{R}, \mathbf{P}; \mathbf{x}, \mathbf{p}; \gamma) = \frac{1}{2} \mathbf{P}^T \mathbf{M}^{-1} \mathbf{P} + \sum_{n,m=1}^F V_{mn}(\mathbf{R}) \left[\frac{1}{2} (x^{(n)} + ip^{(n)}) (x^{(m)} - ip^{(m)}) - \gamma \delta_{nm} \right] . \quad 34$$

Because $\mathbf{V}(\mathbf{R})$ is Hermitian, the mapping Hamiltonian is real. As $\mathbf{V}(\mathbf{R})$ is often a real symmetric matrix, eq 34 becomes

$$H_C(\mathbf{R}, \mathbf{P}; \mathbf{x}, \mathbf{p}; \gamma) = \frac{1}{2} \mathbf{P}^T \mathbf{M}^{-1} \mathbf{P} + \sum_{n,m=1}^F \left[\frac{1}{2} (x^{(n)} x^{(m)} + p^{(n)} p^{(m)}) - \gamma \delta_{nm} \right] V_{mn}(\mathbf{R}) , \quad 35$$

which is the seminal Meyer-Miller Hamiltonian¹⁵³ that has extensively been implemented for nonadiabatic dynamics in the literature^{4, 56, 60, 138, 154, 164-218}. In refs^{58, 131, 132} it is shown that there also exist other comprehensive mapping Hamiltonian models in the general coordinate-momentum phase space formulation of quantum mechanics. When the mapping Hamiltonian is employed to generate trajectory-based dynamics in the phase space formulation for a composite quantum system, we denote it the classical mapping model (CMM) approach. It satisfies the frozen nuclei limit. We use the Meyer-Miller Hamiltonian for demonstration throughout the Focus Article.

When Meyer and Miller proposed the conventional Meyer-Miller mapping Hamiltonian model for the nonadiabatic system in 1979, they did not invoke the phase space formulation. In 1997 Stock and Thoss¹⁵⁴ utilized the Schwinger oscillator theory of angular momentum^{219, 220} to derive the Meyer-Miller mapping Hamiltonian¹⁵³. Its LSC-IVR approximation⁴ in principle includes *infinite* Wigner phase space for the finite set of (electronic) states. The applications, however, suggest that the LSC-IVR approximation in the framework of

refs^{4, 154, 170} is not good^{172, 177, 181, 187, 195, 200, 202}. More advanced semiclassical approaches^{96, 97} improve the performance but request more computational effort^{172, 173}. The symmetric-window-function and other techniques have been introduced to practically overcome the drawbacks^{177, 181, 187, 195, 200, 202}. Recent progress along this line is briefly summarized in ref¹³⁸.

Equation 32 indicates that parameter γ lies in region $(-1/F, \infty)$. It is shown that parameter γ can be either positive or negative^{131, 134} and should be interpreted as a special case of the commutator matrix^{57, 58, 131, 134} rather than the conventional zero-point-energy parameter^{153, 154}. There exist three key elements for a trajectory-based quantum dynamics method to evaluate the evolution of the expectation/ensemble average of a physical property, namely,

- 1) the EOMs of the trajectory,
- 2) the initial condition of the trajectory, and
- 3) the integral expression for the expectation/ensemble average of the physical property of interest.

In the frozen-nuclei limit, Hamilton's EOMs governed by the Meyer-Miller mapping Hamiltonian is isomorphic to exact dynamics. While it is reasonable to employ the mapping Hamiltonian to define the EOMs of the trajectory, the left two elements are also important to consider such that the trajectory-based dynamics method is consistent. The constraint coordinate-momentum phase space formulation then offers a more advanced platform to consider all the three key elements.

It is evident that eq 32 is a special choice of constraint phase space $S(x, p)$. The interpretation of parameter γ in refs^{57, 58, 131, 134} hints that a more comprehensive choice of normalized constraint phase space $\bar{S}(x, p)$ is

$$\int_{-1/F}^{\infty} d\gamma w(\gamma) \frac{1}{\Omega(\gamma)} \delta\left(\sum_{n=1}^F \frac{(x^{(n)})^2 + (p^{(n)})^2}{2} - (1+F\gamma)\right) , \quad 36$$

with the *quasi*-probability distribution function

$$\int_{-1/F}^{\infty} d\gamma w(\gamma) = 1 . \quad 37$$

Equation 7, the integral over the mapping phase space variables for the finite discrete (electronic) DOFs then becomes

$$\int_{S(x,p)} F dx dp g(x,p) = \int_{-1/F}^{\infty} d\gamma w(\gamma) \int F dx dp \frac{1}{\Omega(\gamma)} \delta \left(\sum_{n=1}^F \frac{(x^{(n)})^2 + (p^{(n)})^2}{2} - (1+F\gamma) \right) g(x,p) . \quad 38$$

If we require that the kernel is the same as its inverse, i.e.,

$$\hat{K}_{\text{ele}}(x,p) = \hat{K}_{\text{ele}}^{-1}(x,p) = \sum_{n,m=1}^F \left[\frac{1}{2} (x^{(n)} + ip^{(n)}) (x^{(m)} - ip^{(m)}) - \gamma \delta_{nm} \right] |n\rangle\langle m| , \quad 39$$

it is then not difficult to obtain

$$\int_{-1/F}^{\infty} d\gamma w(\gamma) \chi(\gamma) = 1 \quad 40$$

with

$$\chi(\gamma) = F\gamma^2 + 2\gamma . \quad 41$$

(See Appendix 1 of Supporting Information for more discussion.) Equations 36-41 define normalized constraint phase space $\bar{S}(x,p)$, the mapping kernel and inverse kernel, and the *quasi*-probability distribution function $w(\gamma)$ of parameter γ . The weighted constraint phase space formulation for the discrete-variable quantum system is the key new theoretical result of the Focus Article. When the Wigner function eq 15 is used for the nuclear DOFs, where $\hat{K}_{\text{nuc}}(x,p) = \hat{K}_{\text{nuc}}^{-1}(x,p)$, eq 5 is then identical to eq 6 when $\hat{A} = \hat{B}$. The mapping Hamiltonian for the quantum Hamiltonian operator eq 2 produced by either of eq 5 and eq 6 leads to the same expression as eq 35. When the mapping Hamiltonian is utilized to produce the trajectory-based dynamics for a composite system, it is denoted the weighted mapping model (wMM) approach. The frozen nuclei limit is satisfied in wMM.

Many choices are possible for the discrete or continuous version of the normalized quasi-probability distribution function $w(\gamma)$ in the weighted constraint phase space mapping theory. In the Focus Article we consider only the simplest cases of the discrete version. When but a single value of parameter γ is chosen in eq 40, i.e., $w(\gamma) = \delta(\gamma - \gamma_1)$, we obtain

$$F\gamma^2 + 2\gamma = 1 , \quad 42$$

of which the non-trivial solution is

$$\gamma = \frac{\sqrt{1+F} - 1}{F} \quad . \quad 43$$

In this case, the weighted constraint phase space formulation is identical to the constraint phase space formulation, and wMM becomes CMM when trajectory-based dynamics is considered. When only two values of parameter γ are selected, i.e.,

$$w(\gamma) = \sum_{j=1}^2 w(\gamma_j) \delta(\gamma - \gamma_j) \quad , \quad 44$$

eq 37 and eq 40 lead to

$$\begin{aligned} w(\gamma_1) &= \frac{1 - \chi(\gamma_2)}{\chi(\gamma_1) - \chi(\gamma_2)} \\ w(\gamma_2) &= \frac{\chi(\gamma_1) - 1}{\chi(\gamma_1) - \chi(\gamma_2)} \end{aligned} \quad . \quad 45$$

When the values of parameter γ are close to zero or smaller than zero in region $(-1/F, \infty)$, trajectories produced by the Meyer-Miller mapping Hamiltonian eq 35 for nonadiabatic molecular dynamics are stable. For demonstration in the paper we choose

$$\gamma_1 = -\gamma_2 = \Delta \quad 46$$

with Δ a reasonably small positive real number in region $(0, 1/F)$. Figure 3 presents the constraint coordinate-momentum phase space formulation when a single value of parameter γ is used (Figure 3a) as well as the weighted formulation when two values of parameter γ suggested by eq 46 are used (Figure 3b).

3. PHASE SPACE REPRESENTATION OF THE NONCLASSICAL FEATURE OF QUANTUM SYSTEMS

Recent advance on quantum technologies makes it possible to control and manipulate quantum states in experiment. Because the phase space formulation offers an informationally complete description of the density matrix, direct measurements of phase space of the quantum system with continuous DOFs, those of the quantum system with discrete DOFs, and those of the composite quantum system have been realized in experiment^{70, 85, 221-234}. While the celebrated Wigner phase space has long been used for illustration of the negative *quasi*-probability for continuous-variable systems^{225, 235}, Stratonovich phase space has recently been proposed for visualization and tomography of discrete-variable systems^{85, 113, 227-229, 231, 236, 237}. A combination of these two spaces has been used for illustration of nonclassical correlations or entanglement between the discrete DOF and the continuous DOF of

the composite system^{238, 239}. (In Appendix 3 of Supporting Information, we briefly review Stratonovich phase space with an either SU(2) or SU(F) structure, as well as the relationship between Stratonovich phase space and constraint coordinate-momentum phase space as already pointed out in refs^{57, 58}.)

As coordinate-momentum phase space is well-established in classical mechanics, the formulation of (weighted) constraint coordinate-momentum phase space described in Section 2 offers a potentially useful approach for describing correlations and dynamics in the discrete-variable system as well as the composite system in quantum mechanics. When (weighted) constraint coordinate-momentum phase space is used for mapping an F -state system, the phase space distribution is

$$\rho_C(\mathbf{x}, \mathbf{p}) = \sum_{m,n=1}^F \rho_{mn} K_{nm}(\mathbf{x}, \mathbf{p}), \quad 47$$

where $\rho_{mn} = \langle m | \hat{\rho} | n \rangle$ and $K_{nm}(\mathbf{x}, \mathbf{p}) = \langle n | \hat{K}_{\text{ele}}(\mathbf{x}, \mathbf{p}) | m \rangle$ with $\hat{K}_{\text{ele}}(\mathbf{x}, \mathbf{p})$ defined in eq 39. For the sake of visualization, it is convenient to further reduce constraint phase space variables (\mathbf{x}, \mathbf{p}) to two relevant variables, $(x^{(n)}, x^{(m)})$ or $(x^{(n)}, p^{(m)})$ for describing the correlation on arbitrary two states $|n\rangle$ and $|m\rangle$.

We define the marginal function, $K_{(n,m)}(x^{(n)}, x^{(m)})$, on constraint coordinate-momentum phase space (Figure 4),

$$K_{(n,m)}(x^{(n)}, x^{(m)}) = \int F d\mathbf{x}_\perp d\mathbf{p} \frac{1}{\Omega(\gamma)} \delta \left(\sum_{j=1}^F \frac{(x^{(j)})^2 + (p^{(j)})^2}{2} - (1+F\gamma) \right) K_{nm}(\mathbf{x}, \mathbf{p}; \gamma), \quad 48$$

where \mathbf{x}_\perp represents all $x^{(i)}$ other than $\{x^{(n)}, x^{(m)}\}$, and that on weighted constraint phase space,

$$K_{(n,m)}(x^{(n)}, x^{(m)}) = \int_{-1/F}^{\infty} d\gamma w(\gamma) \frac{1}{\Omega(\gamma)} \int F d\mathbf{x}_\perp d\mathbf{p} \delta \left(\sum_{j=1}^F \frac{(x^{(j)})^2 + (p^{(j)})^2}{2} - (1+F\gamma) \right) K_{nm}(\mathbf{x}, \mathbf{p}; \gamma). \quad 49$$

Figure 5 demonstrates the case of eq 49 when the quasi-probability distribution function $w(\gamma)$ is defined by eqs 44-46 where two symmetrical values of parameter γ are used. Similar definitions also apply for $K_{(n,m)}(x^{(n)}, p^{(m)})$. The explicit formula of these marginal functions can be derived by using the integral techniques in Appendix 1 of Supporting Information.

Figures 4-5 demonstrate a composite system that consists of a discrete DOF for spin-1/2 and a continuous DOF for a harmonic oscillator. The marginal joint distribution function of the composite system reads

$$\rho_C^{(n,m)}(\mathbf{R}, \mathbf{P}; x^{(n)}, x^{(m)}) = \text{Tr}_{n,e} \left[\hat{\rho} \hat{K}_{\text{nuc}}(\mathbf{R}, \mathbf{P}) \otimes |n\rangle \langle m| K_{(n,m)}(x^{(n)}, x^{(m)}) \right]. \quad 50$$

The marginal quasi-probability distribution functions of the continuous variable for both the pure state and the mixed state are presented in Figure 4a, where infinite Wigner phase space is employed. The marginal functions of the discrete variables (based on eq 48) of the spin-1/2 system read

$$\begin{aligned} & \begin{pmatrix} K_{\uparrow\uparrow}(x^{(1)}, x^{(2)}) & K_{\uparrow\downarrow}(x^{(1)}, x^{(2)}) \\ K_{\downarrow\uparrow}(x^{(1)}, x^{(2)}) & K_{\downarrow\downarrow}(x^{(1)}, x^{(2)}) \end{pmatrix} \\ &= \frac{1}{2\pi(1+2\gamma)} \begin{pmatrix} 1 + \frac{1}{2}(x^{(1)})^2 - \frac{1}{2}(x^{(2)})^2 & x^{(1)}x^{(2)} \\ x^{(1)}x^{(2)} & 1 - \frac{1}{2}(x^{(1)})^2 + \frac{1}{2}(x^{(2)})^2 \end{pmatrix}, \end{aligned} \quad 51$$

where notations \uparrow, \downarrow are used to represent the two discrete states.

The marginal functions for the discrete variable are demonstrated on constraint coordinate-momentum phase space in Figure 4b and on weighted constraint space in Figure 5b. More interestingly, the identical angular behaviour and the radial cancellation behaviour of two weighted components lead to a hollow ring structure on weighted constraint phase space (Figure 5a, also see Appendix 4 of Supporting Information). The difference between the Schrodinger cat state and the mixed state is distinct in either Figure 4b on constraint space or Figure 5b on weighted constraint space.

The marginal joint function of a pure Bell entangled state, $(|0\rangle|\downarrow\rangle + |1\rangle|\uparrow\rangle)/2$, of the composite system is demonstrated in Figure 4c (by adopting the similar strategy of refs ^{238, 239}), where constraint coordinate-momentum phase space is used for the discrete DOF at each grid, as well as in Figure 5c where weighted constraint space is employed for the discrete DOF at each grid. The two-dimensional grids represent variables (R, P) of infinite Wigner phase space for the continuous DOF in either of Figure 4c and Figure 5c. When the pure Bell entangled state is studied, both Figure 4c and Figure 5c clearly demonstrate a Gaussian decay of the joint marginal function against Wigner phase space variables (R, P) of the continuous DOF. Either Figure 4c or Figure 5c also shows the pattern of the correlation between the continuous DOF and the discrete DOF. It is convenient to distinguish the pure Bell entangled state, $(|0\rangle|\downarrow\rangle + |1\rangle|\uparrow\rangle)/2$, from the direct product of the Schrodinger cat states, $(|0\rangle + |1\rangle) \otimes (|\uparrow\rangle + |\downarrow\rangle)/2$, when the hybrid representation of the general coordinate-momentum phase space is used.

4. DYNAMICS OF COMPOSITE QUANTUM SYSTEMS

The quantum Liouville theorem can be expressed as a generalized Moyal bracket on hybrid coordinate-momentum phase space. When the Poisson bracket for classical Hamilton's EOMs governed by the mapping Hamiltonian, eq 35, is used to approximate the generalized Moyal bracket on phase space, we have CMM when constraint space is used, and wMM when weighted constraint space is employed. We compare the new wMM and CMM approaches to Ehrenfest dynamics^{240, 241} as well as the fewest-switches surface hopping (FSSH) method²⁴²⁻²⁴⁴, two prevailing trajectory-based dynamics methods for a few typical composite quantum systems. (In this section we set $\hbar = 1$ for simplicity if it is not specifically stated).

4.1 Equations of motion governed by the mapping Hamiltonian

In eq 2, the 'complete' set of diabatic states $\{|n\rangle\}$ is independent of nuclear coordinate/configuration \mathbf{R} . The mapping variables for discrete (electronic) DOFs, (\mathbf{x}, \mathbf{p}) , are independent of \mathbf{R} . Define $\mathbf{g} = \mathbf{x} + i\mathbf{p}$. The EOMs governed by eq 34, the mapping Hamiltonian of eq 2, then read,

$$\dot{\mathbf{g}} = -i\mathbf{V}(\mathbf{R})\mathbf{g} \quad . \quad 52$$

$$\dot{\mathbf{R}} = \mathbf{M}^{-1}\mathbf{P} \quad 53$$

$$\dot{\mathbf{P}} = -\sum_{n,m=1}^F (\nabla_{\mathbf{R}} V_{mn}(\mathbf{R})) \left(\frac{1}{2} (x^{(n)} + ip^{(n)}) (x^{(m)} - ip^{(m)}) - \gamma \delta_{nm} \right) \quad . \quad 54$$

Diabatic potential matrix $\mathbf{V}(\mathbf{R})$ is Hermitian, so is the force matrix, $\{\nabla_{\mathbf{R}} V_{mn}(\mathbf{R})\}$. It is trivial to verify that the mean force of the right-hand side (RHS) of eq 54 is always real. When $\mathbf{V}(\mathbf{R})$ is a real symmetric matrix, the EOMs become

$$\begin{aligned} \dot{\mathbf{x}} &= \mathbf{V}(\mathbf{R})\mathbf{p} \\ \dot{\mathbf{p}} &= -\mathbf{V}(\mathbf{R})\mathbf{x} \\ \dot{\mathbf{R}} &= \mathbf{M}^{-1}\mathbf{P} \end{aligned} \quad . \quad 55$$

$$\dot{\mathbf{P}} = -\sum_{n,m=1}^F (\nabla_{\mathbf{R}} V_{mn}(\mathbf{R})) \left[\frac{1}{2} (x^{(n)}x^{(m)} + p^{(n)}p^{(m)}) - \gamma \delta_{nm} \right]$$

Consider the full Hamiltonian of nuclei and electrons of the molecular system,

$$\hat{H} = \frac{1}{2} \hat{\mathbf{P}}^T \mathbf{M}^{-1} \hat{\mathbf{P}} + \hat{H}_{el}(\hat{\mathbf{R}}) \quad , \quad 56$$

where $\hat{H}_{el}(\hat{\mathbf{R}})$ is the electronic Hamiltonian. Its representation in the diabatic basis reads

$$\hat{H}_{el}(\mathbf{R}) = \sum_{n,m} V_{nm}(\mathbf{R}) |n\rangle \langle m| \quad 57$$

and that in the adiabatic basis is

$$\hat{H}_{el}(\mathbf{R}) = \sum_k E_k(\mathbf{R}) |\phi_k(\mathbf{R})\rangle\langle\phi_k(\mathbf{R})| , \quad 58$$

where $E_k(\mathbf{R})$ denotes the adiabatic potential energy surface of the k -th adiabatic electronic state. Assume that the unitary transformation between a set of diabatic basis states, $\{|m\rangle\}$, and a set of adiabatic basis states, $\{|\phi_k(\mathbf{R})\rangle\}$, is

$$|\phi_k(\mathbf{R})\rangle = \sum_m U_{mk}(\mathbf{R}) |m\rangle , \quad 59$$

$$|n\rangle = \sum_k U_{nk}^*(\mathbf{R}) |\phi_k(\mathbf{R})\rangle$$

where $U_{mk}(\mathbf{R}) = \langle m | \phi_k(\mathbf{R}) \rangle$. This states the diagonalization of the diabatic potential matrix,

$$\sum_{n,m} U_{nj}^*(\mathbf{R}) V_{nm}(\mathbf{R}) U_{mk}(\mathbf{R}) = E_k(\mathbf{R}) \delta_{kj} , \quad 60$$

or equivalently,

$$V_{mn}(\mathbf{R}) = \sum_k U_{mk}(\mathbf{R}) E_k(\mathbf{R}) U_{nk}^*(\mathbf{R}) . \quad 61$$

Define the nonadiabatic coupling vector,

$$\mathbf{d}_{mn}(\mathbf{R}) = \left\langle \phi_m(\mathbf{R}) \left| \frac{\partial \phi_n(\mathbf{R})}{\partial \mathbf{R}} \right. \right\rangle . \quad 62$$

It is trivial to show

$$\mathbf{d}_{mn}(\mathbf{R}) = -\mathbf{d}_{nm}^*(\mathbf{R}) \quad 63$$

because of the orthonormality of the basis set, i.e., $\langle \phi_m(\mathbf{R}) | \phi_n(\mathbf{R}) \rangle = \delta_{mn}$. We then obtain

$$\nabla_{\mathbf{R}} U_{mk}^*(\mathbf{R}) = \langle \nabla_{\mathbf{R}} \phi_k(\mathbf{R}) | m \rangle = \sum_n \langle \nabla_{\mathbf{R}} \phi_k(\mathbf{R}) | \phi_n \rangle \langle \phi_n | m \rangle$$

$$= \sum_n \mathbf{d}_{nk}^*(\mathbf{R}) U_{mn}^*(\mathbf{R}) = -\sum_n \mathbf{d}_{kn}(\mathbf{R}) U_{mn}^*(\mathbf{R}) \quad 64$$

and

$$\nabla_{\mathbf{R}} U_{mk}(\mathbf{R}) = -\sum_n \mathbf{d}_{kn}^*(\mathbf{R}) U_{mn}(\mathbf{R}) = \sum_n U_{mn}(\mathbf{R}) \mathbf{d}_{nk}(\mathbf{R}) . \quad 65$$

Below we show the explicit form of the EOMs, eqs 52-54, under the diabatic-to-adiabatic transformation, eq 59.

The covariant transformation for mapping variables corresponding to the diabatic-to-adiabatic transformation, eq 59, reads

$$\mathcal{X}_0^{(m)}(\mathbf{R}) + i\mathcal{P}_0^{(m)}(\mathbf{R}) = \sum_m U_{mn}^*(\mathbf{R}) (x^{(m)} + ip^{(m)}) \quad 66$$

or

$$x^{(n)} + ip^{(n)} = \sum_m U_{nm}(\mathbf{R}) (\mathcal{X}_0^{(m)}(\mathbf{R}) + i\mathcal{P}_0^{(m)}(\mathbf{R})) \quad 67$$

Denote $\mathbf{g}(\mathbf{R}) = \mathcal{X}_0(\mathbf{R}) + i\mathcal{P}_0(\mathbf{R})$. Equations 66-67 become

$$\begin{aligned} \mathcal{X}_0(\mathbf{R}) &= \mathbf{U}^\dagger(\mathbf{R}) \mathbf{g} \\ \mathbf{g} &= \mathbf{U}(\mathbf{R}) \mathcal{X}_0(\mathbf{R}) \end{aligned} \quad 68$$

The electronic mapping kernel, eq 30, is

$$\hat{K}_{\text{ele}} = \sum_{n,m} \left[\frac{1}{2} (\mathcal{X}_0^{(m)} + i\mathcal{P}_0^{(m)}) (\mathcal{X}_0^{(m)} - i\mathcal{P}_0^{(m)}) - \gamma \delta_{nm} \right] |\phi_n\rangle \langle \phi_m| \quad 69$$

under the transformation for a specific nuclear configuration, \mathbf{R} . Substitution of eq 64 into eq 66 yields

$$\nabla_{\mathbf{R}} (\mathcal{X}_0^{(n)}(\mathbf{R}) + i\mathcal{P}_0^{(n)}(\mathbf{R})) = - \sum_k \mathbf{d}_{nk}(\mathbf{R}) (\mathcal{X}_0^{(k)}(\mathbf{R}) + i\mathcal{P}_0^{(k)}(\mathbf{R})) \quad 70$$

The total time derivative of $\mathcal{X}_0^{(n)} + i\mathcal{P}_0^{(n)}$ reads

$$\begin{aligned} \frac{d}{dt} (\mathcal{X}_0^{(n)} + i\mathcal{P}_0^{(n)}) &= \sum_m U_{mn}^*(\mathbf{R}) \left(\frac{d}{dt} (x^{(m)} + ip^{(m)}) \right) + \sum_m \left(\frac{d}{dt} U_{mn}^*(\mathbf{R}) \right) (x^{(m)} + ip^{(m)}) \\ &= -i \sum_k \delta_{nk} E_k(\mathbf{R}) (\mathcal{X}_0^{(k)} + i\mathcal{P}_0^{(k)}) - \sum_k \mathbf{R} \cdot \mathbf{d}_{nk}(\mathbf{R}) (\mathcal{X}_0^{(k)} + i\mathcal{P}_0^{(k)}) \\ &= -i \sum_k [E_k(\mathbf{R}) \delta_{nk} - i \mathbf{R} \cdot \mathbf{d}_{nk}(\mathbf{R})] (\mathcal{X}_0^{(k)} + i\mathcal{P}_0^{(k)}) \end{aligned} \quad 71$$

Equation 71 is the EOMs for mapping variables of electronic DOFs in the adiabatic representation.

We then consider the EOMs of nuclear mapping variables under the transformation eq 59. Equation 53 remains invariant under the transformation. Substitution of eqs 61, 64, 65, and 69 into eq 54 produces

$$\begin{aligned}
 \mathbf{\dot{P}} &= -\sum_{n,m=1}^F (\nabla_{\mathbf{R}} V_{mn}(\mathbf{R})) \left[\frac{1}{2} (x^{(n)} + ip^{(n)}) (x^{(m)} - ip^{(m)}) - \gamma \delta_{nm} \right] \\
 &= -\sum_{n,m} \nabla_{\mathbf{R}} \left(\sum_k U_{mk}(\mathbf{R}) E_k(\mathbf{R}) U_{nk}^*(\mathbf{R}) \right) \left[\frac{1}{2} (x^{(n)} + ip^{(n)}) (x^{(m)} - ip^{(m)}) - \gamma \delta_{nm} \right] \\
 &= \sum_{k,l} \mathbf{d}_{lk}(\mathbf{R}) (E_l(\mathbf{R}) - E_k(\mathbf{R})) \left[\frac{1}{2} (\mathbf{x}_0^{(k)} + i\mathbf{p}_0^{(k)}) (\mathbf{x}_0^{(l)} - i\mathbf{p}_0^{(l)}) - \gamma \delta_{kl} \right] \\
 &\quad - \sum_{k,l} \nabla_{\mathbf{R}} E_k(\mathbf{R}) \delta_{kl} \left[\frac{1}{2} (\mathbf{x}_0^{(k)} + i\mathbf{p}_0^{(k)}) (\mathbf{x}_0^{(l)} - i\mathbf{p}_0^{(l)}) - \gamma \delta_{kl} \right]
 \end{aligned} \tag{72}$$

Since force matrix $\{\mathbf{F}_{kl} = \nabla_{\mathbf{R}} E_k(\mathbf{R}) \delta_{kl} + (E_k(\mathbf{R}) - E_l(\mathbf{R})) \mathbf{d}_{lk}(\mathbf{R})\}$ is Hermitian, the mean force of the RHS of eq 72 stays real. Under the diabatic-to-adiabatic transformation, eq 59, the EOMs of nuclear phase variables (eqs 53-54) are then recast into

$$\begin{aligned}
 \mathbf{\dot{R}} &= \mathbf{M}^{-1} \mathbf{P} \\
 \mathbf{\dot{P}} &= -\sum_{k,l} \left[\nabla_{\mathbf{R}} E_k(\mathbf{R}) \delta_{kl} + (E_k(\mathbf{R}) - E_l(\mathbf{R})) \mathbf{d}_{lk}(\mathbf{R}) \right] \left[\frac{1}{2} (\mathbf{x}_0^{(k)} + i\mathbf{p}_0^{(k)}) (\mathbf{x}_0^{(l)} - i\mathbf{p}_0^{(l)}) - \gamma \delta_{kl} \right].
 \end{aligned} \tag{73}$$

Define the effective potential matrix, $\mathbf{V}^{(\text{eff})}$, whose element is a function of the nuclear phase variables,

$$V_{nk}^{(\text{eff})}(\mathbf{R}, \mathbf{P}) = E_n(\mathbf{R}) \delta_{nk} - i \mathbf{\dot{R}} \cdot \mathbf{d}_{nk}(\mathbf{R}) = E_n(\mathbf{R}) \delta_{nk} - i \mathbf{M}^{-1} \mathbf{P} \cdot \mathbf{d}_{nk}(\mathbf{R}). \tag{74}$$

A more compact form of eq 71 for the electronic phase variables becomes

$$\mathbf{\dot{g}}_0 = -i \mathbf{V}^{(\text{eff})}(\mathbf{R}, \mathbf{P}) \mathbf{g}_0. \tag{75}$$

Equations 73 and 75 are the final EOMs under the covariant transformation eq 66.

When the electronic wavefunction of the basis set is always real, i.e., $\langle r | \phi_n(\mathbf{R}) \rangle$ is real for any n , which is often the case for molecular systems, eq 63 leads to

$$\mathbf{d}_{mn}(\mathbf{R}) = -\mathbf{d}_{nm}(\mathbf{R}). \tag{76}$$

Equation 73 is simplified to

$$\begin{aligned}
 \mathbf{\dot{R}} &= \mathbf{M}^{-1} \mathbf{P} \\
 \mathbf{\dot{P}} &= -\sum_{k,l} \left[\nabla_{\mathbf{R}} E_k(\mathbf{R}) \delta_{kl} + (E_k(\mathbf{R}) - E_l(\mathbf{R})) \mathbf{d}_{lk}(\mathbf{R}) \right] \left[\frac{1}{2} (\mathbf{x}_0^{(k)} \mathbf{x}_0^{(l)} + \mathbf{p}_0^{(k)} \mathbf{p}_0^{(l)}) - \gamma \delta_{kl} \right].
 \end{aligned} \tag{77}$$

Note that the mapping Hamiltonian of eq 34 (obtained in the diabatic representation) becomes

$$H_C(\mathbf{R}, \mathbf{P}, \mathbf{x}(\mathbf{x}_0, \mathbf{p}), \mathbf{p}(\mathbf{x}_0, \mathbf{p})) = \frac{1}{2} \mathbf{P}^T \mathbf{M}^{-1} \mathbf{P} + \sum_{n=1}^F E_n(\mathbf{R}) \left(\frac{1}{2} \left((\mathbf{x}_0^{(n)})^2 + (\mathbf{p}_0^{(n)})^2 \right) - \gamma \right) \tag{78}$$

under the transformation defined by eq 61 and eq 66. The new EOMs, eq 73 and eq 75, conserve the mapping Hamiltonian of eq 78. The diabatic-to-adiabatic transformation depends on nuclear coordinate \mathbf{R} , which is also a time-dependent variable of the evolution. The time-dependent canonical transformation for the Hamiltonian system yields a new set of EOMs by the chain rule²⁴⁵.

In eqs 72-75 and eqs 77-78 \mathbf{P} corresponds to the mapping momentum in the diabatic representation, but *not* the canonical momentum in the adiabatic representation because eq 72 is *not* generated from Hamilton's equations of motion. Equations 75 and 77 share a similar form to the EOMs proposed by Cotton *et al* in ref¹⁸⁴ and discussed in the Supporting Information of ref⁵⁷. Define the covariant transformation for nuclear phase variables,

$$\mathbf{R} = \mathbf{R}^0 + i \sum_{m,n} \left[\frac{1}{2} (\mathbf{P}_0^{(n)} + i\mathbf{P}_0^{(n)}) (\mathbf{R}_0^{(m)} - i\mathbf{R}_0^{(m)}) - \gamma \delta_{nm} \right] \mathbf{d}_{mn}(\mathbf{R}) \quad 79$$

The Hamiltonian of eq 78 becomes

$$H_C(\mathbf{R}, \mathbf{P}, \mathbf{X}, \mathbf{P}) = \frac{1}{2} \mathbf{P}(\mathbf{P}_0^0, \mathbf{P}_0^0, \mathbf{R}_0^0)^T \mathbf{M}^{-1} \mathbf{P}(\mathbf{P}_0^0, \mathbf{P}_0^0, \mathbf{R}_0^0) + \sum_{n=1}^F E_n(\mathbf{R}_0^0) \left(\frac{1}{2} \left((\mathbf{P}_0^{(n)}(\mathbf{R}_0^0))^2 + (\mathbf{P}_0^{(n)}(\mathbf{R}_0^0))^2 \right) - \gamma \right), \quad 80$$

of which the canonical variables are $\{\mathbf{R}_0^0, \mathbf{P}_0^0, \mathbf{X}_0^0, \mathbf{P}_0^0\}$ instead of $\{\mathbf{R}, \mathbf{P}, \mathbf{X}, \mathbf{P}\}$. (See more discussions in Appendix 2 of Supporting Information). The mapping diabatic momentum, \mathbf{P} , is related to the kinematic momentum of the adiabatic representation. Although we can directly use Hamilton's EOMs for $\{\mathbf{R}_0^0, \mathbf{P}_0^0, \mathbf{X}_0^0, \mathbf{P}_0^0\}$, it is more convenient to employ the EOMs for $\{\mathbf{R}, \mathbf{P}, \mathbf{X}, \mathbf{P}\}$ instead to avoid the derivative of nonadiabatic coupling terms. This is indeed the strategy suggested by Cotton *et al* in ref¹⁸⁴. When the initial condition does not involve nonadiabatic coupling terms, the sampling of \mathbf{P} in the diabatic representation is the same for that of \mathbf{P}^0 in the adiabatic representation. This is the case in the following applications, where FSSH has to be used in the adiabatic representation. By applying the covariance relation under the diabatic-to-adiabatic transformation, the EOMs on mapping phase space are independent of the representation of the (electronic) basis set, which is also the merit of Ehrenfest dynamics.

We note that either eq 52 or eq 75 can analytically be solved by a symplectic approach that employs an exact propagator on electronic phase space at each nuclear phase point. For example, for eq 75 we use

$$\mathbf{U}(\mathbf{R}, \mathbf{P}; \Delta t) = \exp[-i\Delta t \mathbf{V}^{(\text{eff})}]$$

81

such that the evolution of electronic phase variables follows $\mathbf{g}(t + \Delta t) = \mathbf{U}(\mathbf{R}, \mathbf{P}; \Delta t)\mathbf{g}(t)$.

We then test a range of benchmark systems, including two-site dissipative models, Tully's scattering models, atomic systems in cavity interacted with a number of field modes, and linear vibronic coupling model systems that involve the conical intersection^{135, 246-248}. They are typical composite quantum systems in chemistry, physics, condensed matter science, quantum optics, and quantum information.

4.2 Spin-boson models at low-temperature in condensed phase

The first model illustrated is the spin-boson model, which describes a two-site system interacted with an environmental bath in condense phase. It is also a simplified model for electron transfer and energy transfer in chemical and biological reactions. Several numerically exact benchmark methods for solving the spin-boson model include quasi-adiabatic propagator path integral (QuAPI)²⁴⁹⁻²⁵², hierarchy equations of motion (HEOM)²⁵³⁻²⁶¹, (multi-layer) multi-configuration time-dependent Hartree [(ML-)MCTDH]²⁶²⁻²⁶⁸, but their numerical costs typically increase exponentially as the number of DOFs increases. Quantum dynamics of the spin-boson model exhibits interesting dissipative characters, of which the asymptotic behaviours are often missed by either of Ehrenfest dynamics and FSSH in the low temperature regime⁵⁸. Spin-boson models with strong coupling in the low temperature regime presents challenging tests for trajectory-based dynamics methods.

The Hamiltonian of the spin-boson model is divided to three parts, $\hat{H} = \hat{H}_s + \hat{H}_b + \hat{H}_{sb}$. Here $\hat{H}_s = \varepsilon \hat{\sigma}_z + \Delta_c \hat{\sigma}_x$ describes a two-site system with the bias ε and tunneling Δ_c , while the bath part of the Hamiltonian is discretized into a combination of a number of quantum harmonic oscillators $\hat{H}_b = \sum_{j=1}^{N_b} (\hat{P}_j^2 + \omega_j^2 \hat{R}_j^2)/2$. The system-bath coupling adopts a bilinear interaction, $\hat{H}_{sb} = -\sum_{j=1}^{N_b} c_j \hat{R}_j \hat{\sigma}_z$. Here we use an Ohmic bath spectral density $J(\omega) = (\pi/2)\alpha\omega e^{-\omega/\omega_c}$, where α is the Kondo parameter and ω_c is the cut-off frequency. Its discrete frequencies and coupling strengths $\{\omega_j, c_j\}$ are sampled^{269, 270} from

$$\begin{cases} \omega_j = -\omega_c \ln[1 - j/(1+N_b)] \\ c_j = \omega_j \sqrt{\alpha \omega_c / (1+N_b)} \end{cases}, \quad j = 1, \dots, N_b$$

82

The initial density is set as $|1\rangle_s\langle 1|_s \otimes \hat{\rho}_b$, where the system is in excited state $|1\rangle_s$ while all bath modes are at thermal equilibrium with $\hat{\rho}_b = e^{-\beta\hat{H}_b} / Z_b$. Initial nuclear DOFs are sampled from the Wigner distribution of $\hat{\rho}_b$, while initial electronic DOFs are sampled from (weighted) constraint coordinate-momentum phase space $S(\mathbf{x}, \mathbf{p})$. The continuous spectral density is discretized into $N_b = 300$ effective bath modes to guarantee numerical convergence in simulations.

In Figure 6, we demonstrate results produced by wMM with parameter $\Delta = 0.05$, by wMM with $\Delta = 0.1$, and by CMM with $\gamma = (\sqrt{F+1} - 1) / F = 0.366$ that is a special case of CMM of ref.¹³⁴. Numerically exact results, as well as results yielded by Ehrenfest dynamics and FSSH, are also shown for comparison. Figure 6 indicates that wMM, as well as CMM, outperforms both Ehrenfest dynamics and FSSH dynamics, either for short-time coherences or for long-time dissipations.

4.3 Tully's gas phase scattering models

Tully's scattering models²⁴² mimic different intersection types of molecular systems, which have widely been tested for various nonadiabatic dynamics methods. They describe a two-state Hamiltonian with a central coupling area and asymptotic plateau regions where diabatic potential function $V_{nn}(R \rightarrow \pm\infty)$ is flat. All the three models, including the single avoided crossing (SAC), dual avoided crossing (DAC), and extended coupling region (ECR) problems, are used in our numerical tests.

Atomic units are used in the simulations of the Tully models. The SAC model (Panel (a1) of Figure 7) describes the simplest but essential surface crossing in molecular systems. In the diabatic representation, its diagonal potential energy surfaces (PESes) are $V_{11} = -V_{22} = A(1 - e^{-B|R|})\text{sgn}(R)$ and off-diagonal coupling terms are $V_{12} = V_{21} = Ce^{-DR^2}$. Here, the parameters are $A = 0.01$, $B = 1.6$, $C = 0.005$, and $D = 1.0$. The DAC model (Panel (b1) of Figure 7) includes two crossing points, thus different (electronic) paths are interfered with the dependence on the initial momentum. Its diagonal PESes are $V_{11} = 0$ and $V_{22} = -Ae^{-BR^2} + E_0$, and off-diagonal coupling terms are $V_{12} = V_{21} = Ce^{-DR^2}$ in the diabatic representation with parameters $A = 0.10$, $B = 0.28$, $E_0 = 0.05$, $C = 0.015$ and $D = 0.06$. The ECR model in the diabatic representation (Panel (c1) of Figure 7) has diagonal PESes $V_{11} = -V_{22} = E_0$ and coupling terms $V_{12} = V_{21} = C[e^{BR}\Theta(-R) + (2 - e^{-BR})\Theta(R)]$, with $E_0 = -0.0006$, $B = 0.9$, $C = 0.1$. Here

1
2
3 $\Theta(R)$ is the Heaviside function of coordinate R . The adiabatic PESes and nonadiabatic coupling vector of
4
5 the ECR model are also illustrated in Panel (c2) of Figure 7.
6

7 We investigate the transmission and reflection coefficients of each state. In the simulations, the initial
8 condition is a nuclear wavepacket, $\Psi(R; t = 0) \propto \exp[-\alpha(R - R_0)^2/2 + i(R - R_0)P_0]$ (here we adopt
9
10 $\hbar = 1$), occupied in state 1, where $\alpha = 1$ is the Gaussian width parameter, and R_0 and P_0 are the initial
11 average coordinate and momentum. The initial average coordinate is set at $R_0 = -3.8$, -10 , and -13
12
13 for the SAC, DAC and ECR models, respectively. The initial Wigner distribution for the nuclear DOF is then
14
15 $\rho_W^{\text{nuc}}(R, P) \propto \exp[-\alpha(R - R_0)^2 - (P - P_0)^2 / \alpha]$.
16
17

18 Figure 7a shows that all methods are capable of quantitatively describing transmission coefficients in
19 (diabatic) state 1 and state 2 of the SAC model. Figure 7b demonstrates that either wMM or CMM outperforms
20
21 Ehrenfest dynamics and FSSH in predicting the peak shape when the initial momentum is relatively high, e.g.,
22
23 $P_0 \geq 15$ au. This indicates that the trajectory-based approximate dynamics approaches in the mapping phase
24
25 space formulation are good for fast processes in the gas phase composite/nonadiabatic system. However, the
26
27 performance of either wMM or CMM in the low initial momentum region should be improved. It is important
28
29 to note that the EOMs of wMM/CMM are invariant with the representation of the electronic state, as described in
30
31 the Supporting Information of ref⁵⁷. (More discussion is also available in Appendix 2 of Supporting
32
33 Information.) That is, both the diabatic and adiabatic representations produce the same results for wMM or
34
35 CMM, which is often not satisfied in FSSH and other nonadiabatic dynamics approaches.
36
37
38
39

40 For the ECR model of Figure 7c, the numerically exact DVR solution indicates an energy threshold for a
41
42 bifurcation. Ehrenfest dynamics totally misses the step-like behaviours for the transmission coefficient in state
43
44 1, and for the reflection coefficient in either state 1 or state 2. CMM greatly improves over Ehrenfest dynamics.
45
46 It is more encouraging that wMM is capable of faithfully describing such step-like behaviours. Tully's original
47
48 FSSH algorithm is not able to well describe the ECR model²⁴², but a modified version for treating frustrated
49
50 hopping of FSSH (e.g., see ref.²⁴⁴) is capable of qualitatively capturing the step-like behaviours. As shown in
51
52 Figure 7c, in comparison to the traditional FSSH approach^{242, 244}, the overall performance of wMM for the ECR
53
54 model is better.
55

56 4.4 Atom/molecule-in-cavity models of quantum electrodynamic light-matter systems 57

58 The cavity quantum electrodynamics (cQED) focuses on studying the interaction between light and a multi-
59
60 level system (e.g., an atom or a molecule) in an optical cavity, which has many applications in the field of quantum

information and quantum computation. There exist many interesting and important phenomena in cQED, e.g., the Purcell effect when coupling is weak and the vacuum Rabi splitting when coupling becomes strong²⁷¹⁻²⁸⁵. When the general atomic/molecular system is coupled to multi-cavity modes, it is often intractable to solve the exact evolution in real time due to the curse of dimensionality. We test wMM for two typical models that describe an imprisoned multi-level atom coupled with a series of optical modes in a one-dimensional lossless cavity^{57, 204, 286-289}.

The total Hamiltonian consists of three parts. The optical field is depicted by N effective modes

$$\hat{H}_p = \sum_{j=1}^N \frac{1}{2} (\hat{P}_j^2 + \omega_j^2 \hat{R}_j^2) , \quad 83$$

where $\{\hat{R}_j, \hat{P}_j\}$ denote the canonical coordinate-momentum variables of j -th optical field mode with the corresponding photonic frequency ω_j . The atomic system is described by $\hat{H}_a = \sum_{n=1}^F \varepsilon_n |n\rangle\langle n|$ with ε_n representing the n -th atomic energy level. Employing the dipole approximation, one can formulate the interaction between atom and optical field as

$$\hat{H}_c = \sum_{n \neq m} \left(\sum_{j=1}^N \omega_j \lambda_j(r_0) \hat{R}_j \right) \mu_{nm} |n\rangle\langle m| . \quad 84$$

Here μ_{nm} denotes the transitional dipole moment between the n -th and m -th atomic levels, and the coupling between the j -th mode and the atom is

$$\lambda_j(r_0) = \sqrt{\frac{2}{\varepsilon_0 L}} \sin\left(\frac{j\pi r_0}{L}\right) , \quad 85$$

where L is the volume length of cavity, ε_0 denotes the vacuum permittivity, and r_0 represents the location of the atom. In the simulation, the volume length of the cavity is set to 236200 au and the atom is frozen at the central location, i.e., $r_0 = L / 2$. The optical field is depicted by 400 standing-wave modes in cavity, of which the j -th frequency is $\omega_j = j\pi c / L$ with c the light speed in vacuum. We use two benchmark models for studying cQED processes, a three-level model with $\varepsilon_1 = -0.6738$, $\varepsilon_2 = -0.2798$, $\varepsilon_3 = -0.1547$, $\mu_{12} = -1.034$, $\mu_{23} = -2.536$ (all in atomic units), and a reduced two-level model where only the two lowest atomic levels are employed.

The highest atomic level of each model is initially occupied with no photon in cavity, i.e., all cavity modes are in the corresponding vacuum state. The spontaneous emission occurs at the beginning, the released photon evolves in the cavity, and the re-absorption and re-emission happen later when the photon is reflected to meet the atom. Figure 8 shows the population transfer of each atomic level of the two models. The wMM results are compared with CMM, Ehrenfest dynamics, FSSH, and exact results^{287, 288}. Results of Ehrenfest dynamics and of FSSH significantly deviate from exact results even since very short time, while CMM and wMM yield much more reasonable descriptions for all energy levels, including the transfer behaviour at short time and the revival at around $t = 1800$ au. The wMM approach shows overall better performance than CMM in most of the cases. Figure 8 implies that the trajectory-based methods in the general coordinate-momentum phase space formulation will be useful for studying cQED phenomena in the field of quantum optics and quantum information.

4.5 Linear vibronic coupling model for the molecular system involving the conical intersection

The conical intersection widely exists in molecular systems and plays a central role in many photophysical and photochemical phenomena^{135, 139, 214, 246, 247, 290-293}. The linear vibronic coupling model (LVCM) is the simplest but effective model widely used to describe dynamic properties around the conical intersection region, of which Hamiltonian in the diabatic representation is

$$\hat{H} = \hat{H}_0 + \hat{H}_l + \hat{H}_c \quad . \quad 86$$

Here, $\hat{H}_0 = \sum_{k=1}^N \omega_k (\hat{P}_k^2 + \hat{R}_k^2)/2$ is the zeroth-order harmonic oscillator Hamiltonian in normal-mode space of the electronic ground state, where $\hat{P}_k, \hat{R}_k (k=1, \dots, N)$ denote the k -th effective weighted normal-mode variables with frequency ω_k (i.e., $P_k = p_k / \sqrt{\omega_k}$, $R_k = \sqrt{\omega_k} r_k$, where p_k, r_k are the canonical momentum, and canonical coordinate of k -th normal-mode). In eq 86, $\hat{H}_l = \sum_{n=1}^F \left(E_n + \sum_{k=1}^N \kappa_k^{(n)} \hat{R}_k \right) |n\rangle\langle n|$ contains the vertical excitation energy, $E_n (n=1, \dots, F)$ of F electronic states, and the linear coupling term $\kappa_k^{(n)}$ of each nuclear DOF for diagonal Hamiltonian elements, while $\hat{H}_c = \sum_{n \neq m}^F \left(\sum_{k=1}^N \lambda_k^{(nm)} \hat{R}_k \right) |n\rangle\langle m|$ includes linear coupling $\lambda_k^{(nm)}$ for each normal-mode between two different electronic states, $|n\rangle$ and $|m\rangle$.

A typical two-level 3-mode LVCM describes the S1/S2 conical intersection of the pyrazine molecule. The parameters of this model are fitted from semi-empirical electronic structure calculations by Schneiders and

Domcke in ref²⁹⁴. The excitation energies for the two electronic states are $E_1 = 3.94$ eV and $E_2 = 4.84$ eV. The diagonal linear coupling terms of first two modes $\{\hat{R}_1, \hat{R}_2\}$ are $\kappa_1^{(1)} = 0.037$ eV, $\kappa_2^{(1)} = -0.105$ eV for the first electronic state, and $\kappa_1^{(2)} = -0.254$ eV, $\kappa_2^{(2)} = 0.149$ eV for the second electronic state, respectively. The off-diagonal linear coupling of third mode \hat{R}_3 is $\lambda_3^{(12)} = \lambda_3^{(21)} = 0.262$ eV. The normal-mode vibronic frequency of each mode is $\omega_1 = 0.126$ eV, $\omega_2 = 0.074$ eV, and $\omega_3 = 0.118$ eV, respectively. Initial conditions of nuclear DOFs are sampled from the corresponding Wigner function of the vibronic ground state while the second electronic state is occupied. All simulations employ 10^5 trajectories and time stepsize $\Delta t = 0.01$ fs for fully converged results. Numerically exact result of this model calculated by ML-MCTDH are available in ref²¹².

Figure 9 shows population dynamics of state 2 yielded by wMM, CMM, Ehrenfest dynamics, FSSH and ML-MCTDH. It is evident that Ehrenfest dynamics performs poorly even for the short-time behaviour (before 100 fs). In comparison, wMM, CMM, and FSSH more reasonably describe the radiationless energy transfer process at short time. Interestingly, wMM describes the oscillating behaviours in the long-time region (after 300 fs) better than other approximate methods. Such oscillating behaviour in population dynamics indicates the molecular system passes through the “slopped” conical intersection region²⁹⁴.

Figures 6-9 demonstrate that the overall performance of wMM is better than CMM, especially in the gas phase scattering case of Figure 7c and the quantum electrodynamic light-matter systems of Figure 8. Both wMM and CMM approaches are able to outperform Ehrenfest dynamics as well as FSSH for condensed phase systems (e.g., in Figure 6 and Figure 8).

5. CONCLUSION REMARKS

The phase space formulation of quantum mechanics not only presents a type of convenient interpretation to describe quantum-classical correspondences as well as nonclassical correlations/entanglement, but also sets the insightful scene for developing practical and useful trajectory-based quantum dynamics approaches.

In the Focus Article we show that the constraint coordinate-momentum phase space formulation for the discrete-variable system which we have recently developed, and the weighted representation that we propose in the Focus Article are useful approaches for illustration of nonclassical features of quantum systems. The novel formulation is expected to have potential use for illustration of nonclassical features of quantum states, as well as for future phase point measurement experiment^{70, 85, 221-234}.

1
2
3 It is straightforward to show the relation between the $SU(F)/U(F-1)$ Stratonovich phase space¹¹⁴ and
4 constraint coordinate-momentum phase space, which is diffeomorphic to $U(F)/U(F-1)$. When $F > 2$, it is
5 inevitable to meet singularities in dynamics for discrete-variable systems when Stratonovich phase space is used.
6 In comparison, (weighted) constraint coordinate-momentum phase space does not cause any singularities in
7 trajectory-based exact dynamics, which is much more numerically favourable. (See more discussion in
8 Appendix 3 of Supporting Information).

9
10
11 When the general Moyal bracket of the quantum Liouville theorem is approximated by the corresponding
12 Poisson bracket on (weighted) constraint phase space, it reproduces the correct frozen-nuclei limit of
13 composite/nonadiabatic systems. Such trajectory-based EOMs on (weighted) constraint coordinate-momentum
14 phase space do not rely on the choice of representation of electronic states and are straightforward to obtain the
15 form under covariant transformations. Because second-order nonadiabatic coupling terms are avoided in the
16 EOMs of the adiabatic representation, it is especially useful for applications to realistic molecular systems.
17 Various benchmark model tests of from gas phase to condensed phase quantum systems (as shown in Figures 6-
18 9) indicate that wMM, the new trajectory-based approximate approach with the weighted constraint coordinate-
19 momentum phase space representation, demonstrates overall better performance than FSSH as well as Ehrenfest
20 dynamics. It is expected that more investigations on the (weighted) constraint phase space formulation will shed
21 light on more numerically favourable dynamics approaches with the Meyer-Miller mapping Hamiltonian or other
22 mapping Hamiltonians (e.g., those of ref¹³¹ and discussed in ref⁵⁸).

23
24 We note that the (weighted) constraint coordinate-momentum phase space formulation is established for any
25 systems with a finite set of states, not only limited to discrete electronic states, but also for finite discrete nuclear
26 states. The weighted phase space strategy that we propose can also be applied to other types of phase space
27 formulations of the discrete-variable system, such as Stratonovich phase space, and Wootters phase space, albeit
28 that the general coordinate-momentum phase space formulation presented in the Focus Article will be more
29 convenient, for experimental measurements, tomography, or characterizations of fidelity, coherence, inequalities,
30 displaced parity, atomic/molecular/optical Schrodinger cat states, and entanglement in quantum information and
31 computation^{70, 85, 221-234, 295, 296} as well as for studying dynamic processes of composite systems in physics,
32 chemistry, materials, biology, and environmental science.

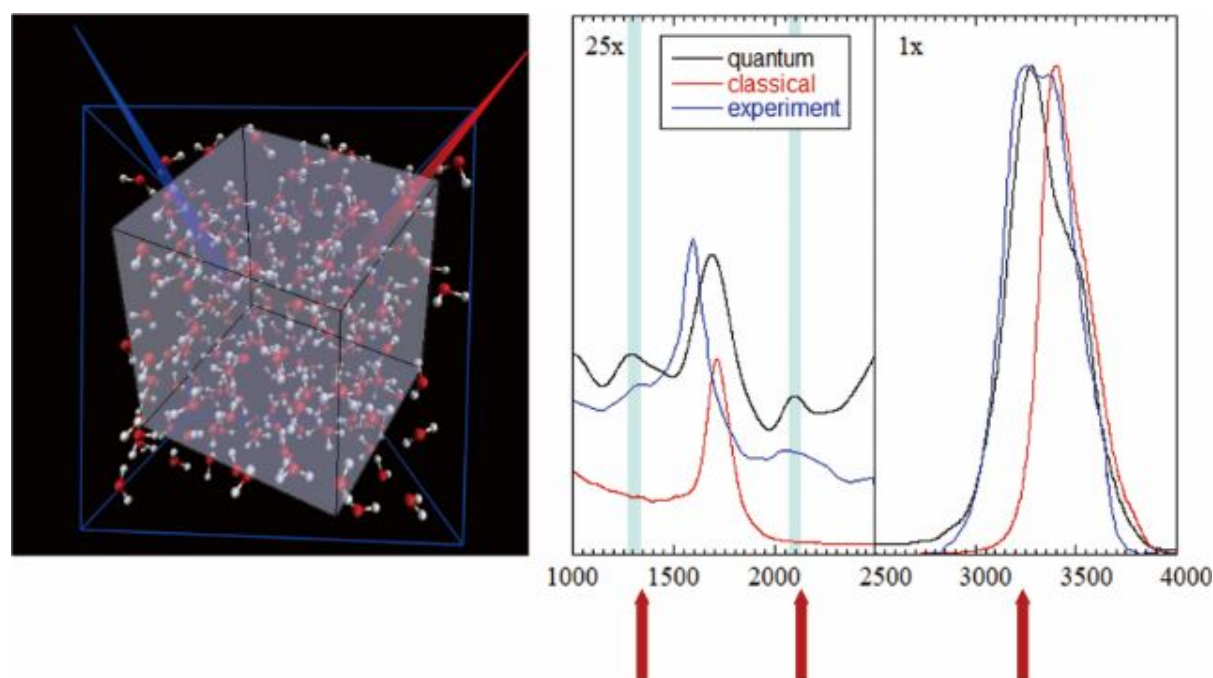
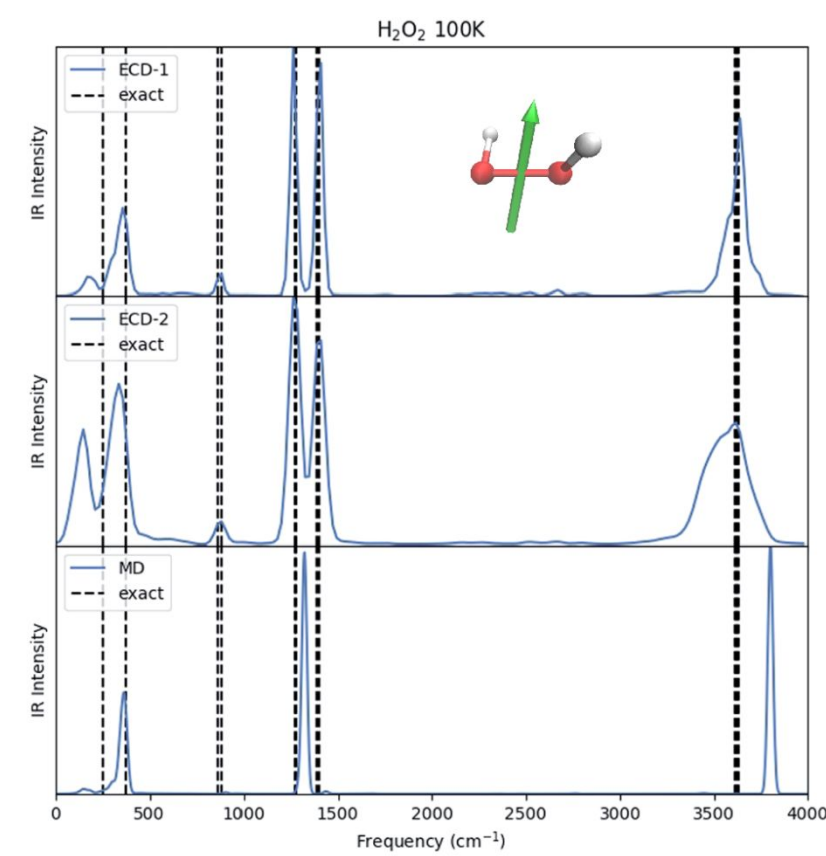
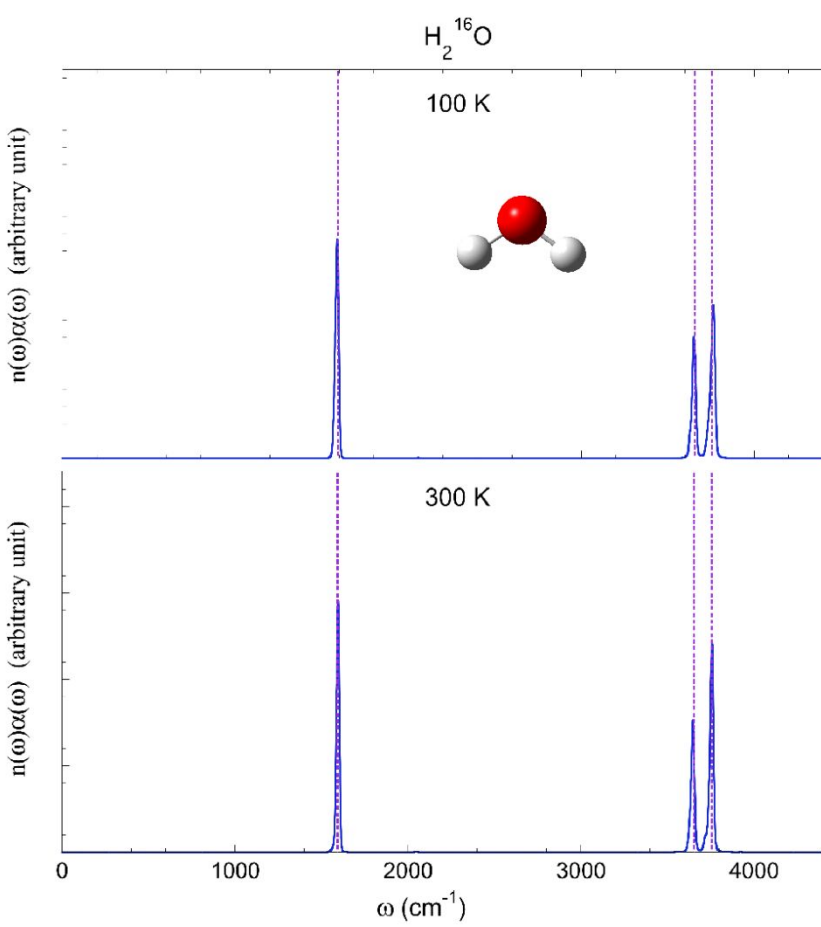
Figures and Tables

Figure 1. Quantum dynamical effects are decisive in reproducing the experimental isotropic Raman spectrum of liquid water at room temperature, as illustrated by the LSC-IVR simulation where infinite (Wigner) phase space for nuclear DOFs is used. Converged results were obtained with 216 water molecules in a box with periodic boundary conditions. (Reprinted with permission from ref¹⁹. Copyright 2018 Taylor & Francis.)



1
2
3 **Figure 2.** Molecular vibrational spectra produced by more advanced trajectory-based dynamics methods with
4 infinite (Wigner) phase space used for nuclear DOFs, which satisfy the two fundamental criteria: conservation of
5 the quantum Boltzmann distribution for the thermal equilibrium system and being exact for any quantum thermal
6 correlation functions in the classical and harmonic limits. (a) Vibrational spectrum of the H_2O molecule at
7 100K and that at 300K. Adapted with permission from ref⁴¹. Copyright 2016 American Institute of Physics
8
9 Publishing. (b) Vibrational spectrum of the H_2O_2 molecule at 100K. Adapted with permission from ref⁴⁴.
10
11 Copyright 2021 American Institute of Physics Publishing.
12
13
14
15
16
17
18
19
20
21
22
23
24
25
26
27
28
29
30
31
32
33
34
35
36
37
38
39
40
41
42
43
44
45
46
47
48
49
50
51
52
53
54
55
56
57
58
59
60

For Peer Review

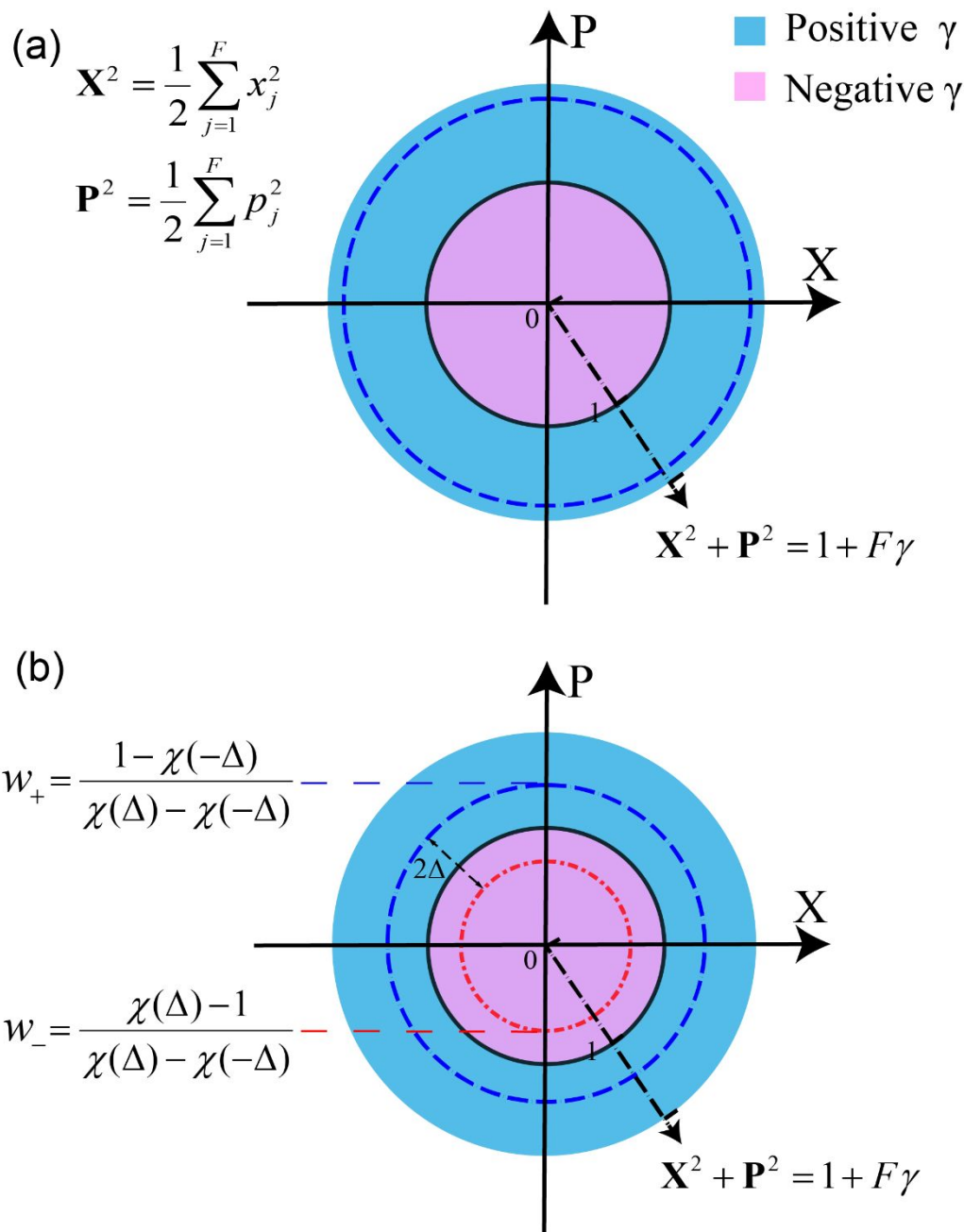
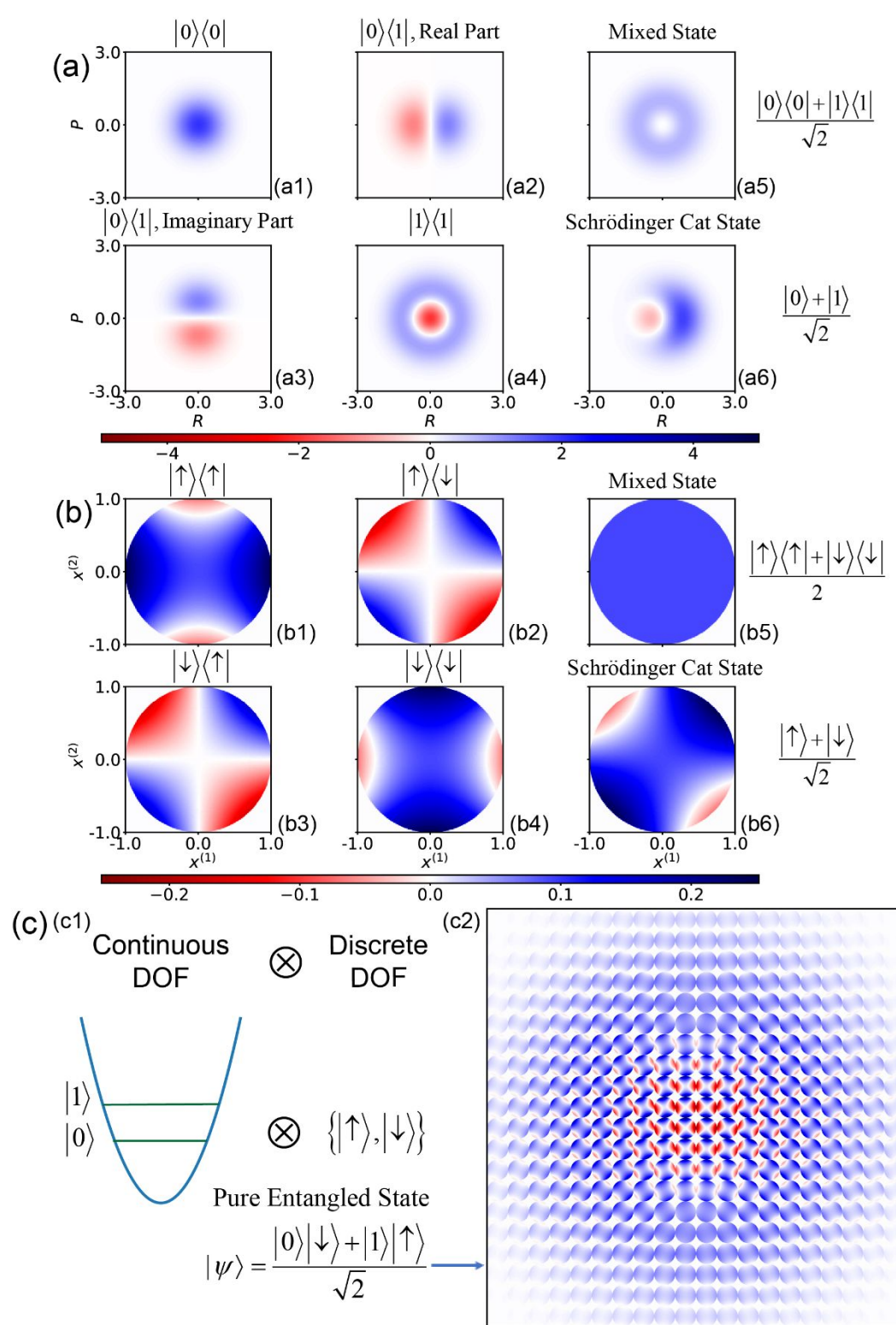


Figure 3: Illustration of the exact mapping formulation with constraint coordinate-momentum phase space. Panel (a) presents constraint phase space with only a single value of parameter γ . Panel (b) demonstrates weighted constraint phase space with two values of parameter γ , where the quasi-probability distribution function is $w(\gamma) = w_+ \delta(\gamma - \Delta) + w_- \delta(\gamma + \Delta)$. Constraint phase space with the positive weight is blue-dashed, while that with the negative weight is red dot-dashed. (Panel (a) is adapted with permission from ref¹³⁴. Copyright 2021 American Chemical Society.)

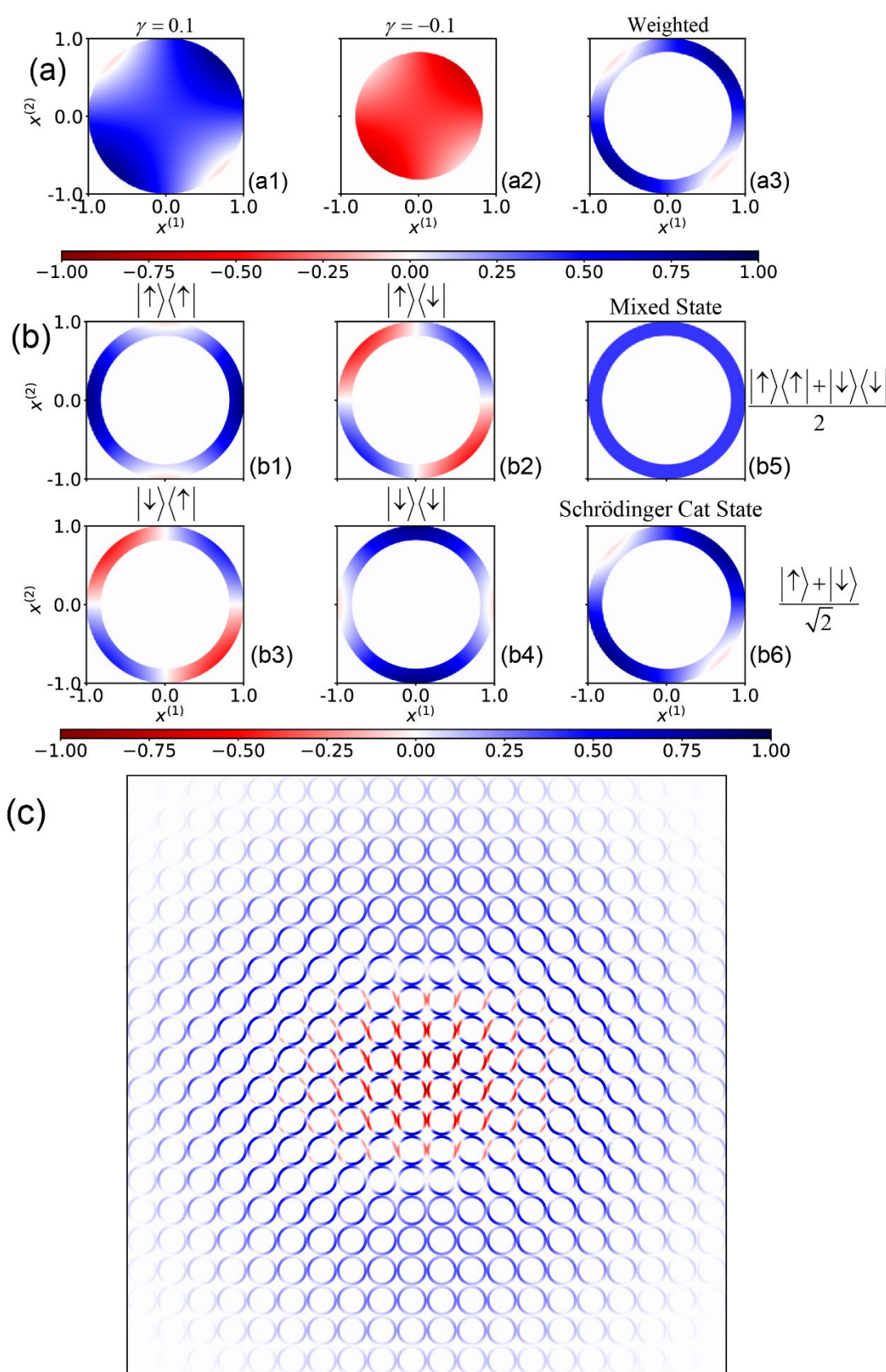


1
2
3 **Figure 4:** Illustrations of (a) Wigner representation of a continuous-variable system, (b) constraint phase space
4 representation of a discrete-variable system, and (c) hybrid coordinate-momentum phase space representation of
5 a composite system with both discrete and continuous DOFs.
6
7

8 (a) Wigner distribution for $|0\rangle\langle 0|$ (Panel a1), that for $|1\rangle\langle 1|$ (Panel a4), real part (Panel a2) and imaginary
9 part (Panel a3) of the Wigner distribution for $|0\rangle\langle 1|$, Wigner distribution for mixed state
10 $(|0\rangle\langle 0|+|1\rangle\langle 1|)/2$ (Panel a5), and that for Schrödinger cat state $(|0\rangle+|1\rangle)/\sqrt{2}$ (Panel a6). Here,
11
12 $|0\rangle$ and $|1\rangle$ are two energy levels of a continuous-variable system.
13
14

15 (b) Marginal distribution of constraint phase space coordinates $(x^{(1)}, x^{(2)})$ for $|\uparrow\rangle\langle \uparrow|$ (Panel b1), $|\downarrow\rangle\langle \downarrow|$
16 (Panel b4), that for $|\uparrow\rangle\langle \downarrow|$ (Panel b2), that for $|\downarrow\rangle\langle \uparrow|$ (Panel b3), that for mixed state
17 $(|\uparrow\rangle\langle \uparrow|+|\downarrow\rangle\langle \downarrow|)/2$ (Panel b5), and that for Schrödinger cat state $(|\uparrow\rangle+|\downarrow\rangle)/\sqrt{2}$ (Panel b6). Here,
18
19 $|\uparrow\rangle$ and $|\downarrow\rangle$ represent two discrete states of a discrete-variable system.
20
21

22 (c) Panel c1: Schematic representaton of the composite system and the pure entangled state
23 $(|0\rangle|\downarrow\rangle+|1\rangle|\uparrow\rangle)/2$; Panel c2: hybrid coordinate-momentum phase space representation of the entangled
24 state. The grid is on the Wigner phase space (R, P) for the continuos DOF, and each circle of a grid stands
25 for the local marginal distribution function of constraint phase space variables $(x^{(1)}, x^{(2)})$. The notations
26 are identical to those in Panels (a)-(b).
27
28
29
30
31
32
33
34
35
36
37
38
39
40
41
42
43
44
45
46
47
48
49
50
51
52
53
54
55
56
57
58
59
60



1
2
3 **Figure 5:** Illustrations of (a) components and (b) marginal distribution functions of the weighted constraint phase
4 space representation of a discrete-variable system, and (c) weighted hybrid representation of the same composite
5 system as that of Figure 4(c).
6
7

- 8 (a) Marginal distribution of constraint phase space coordinates $(x^{(1)}, x^{(2)})$ for Schrödinger cat state
9 $(|\uparrow\rangle + |\downarrow\rangle)/\sqrt{2}$ with $\gamma = \Delta$ weighted by w_+ (Panel a1), with $\gamma = -\Delta$ weighted by w_- (Panel
10 a2). The sum of the two components yields the marginal distribution of constraint phase space coordinates
11 (x_1, x_2) of the weighted representation with two values of parameter γ for the Schrödinger cat state
12 (Panel a3). Coordinates are scaled by the larger radius $\sqrt{2(1+F\Delta)}$.
13
14 (b) Weighted marginal distribution of constraint phase space coordinates $(x^{(1)}, x^{(2)})$ for the same properties
15 as those in Figure 4(b).
16
17 (c) Same as Figure 4(c), but using weighted marginal distribution for the discrete DOF.
18
19
20
21
22
23
24
25
26
27
28
29
30
31
32
33
34
35
36
37
38
39
40
41
42
43
44
45
46
47
48
49
50
51
52
53
54
55
56
57
58
59
60

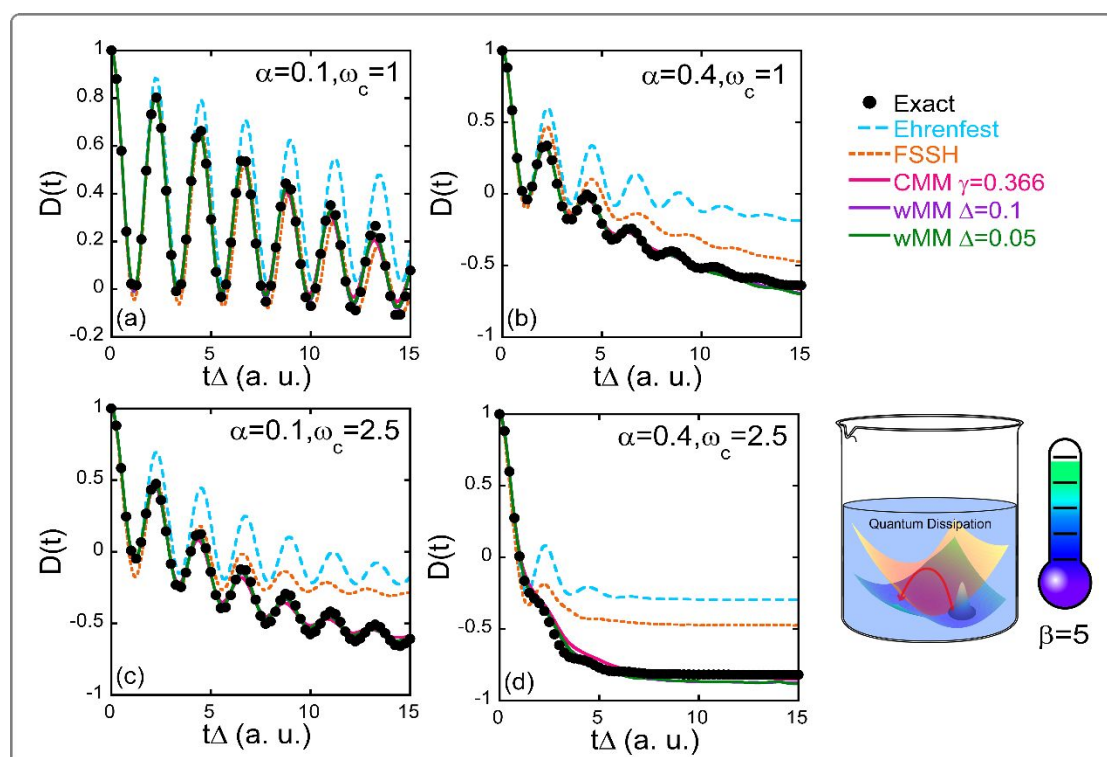
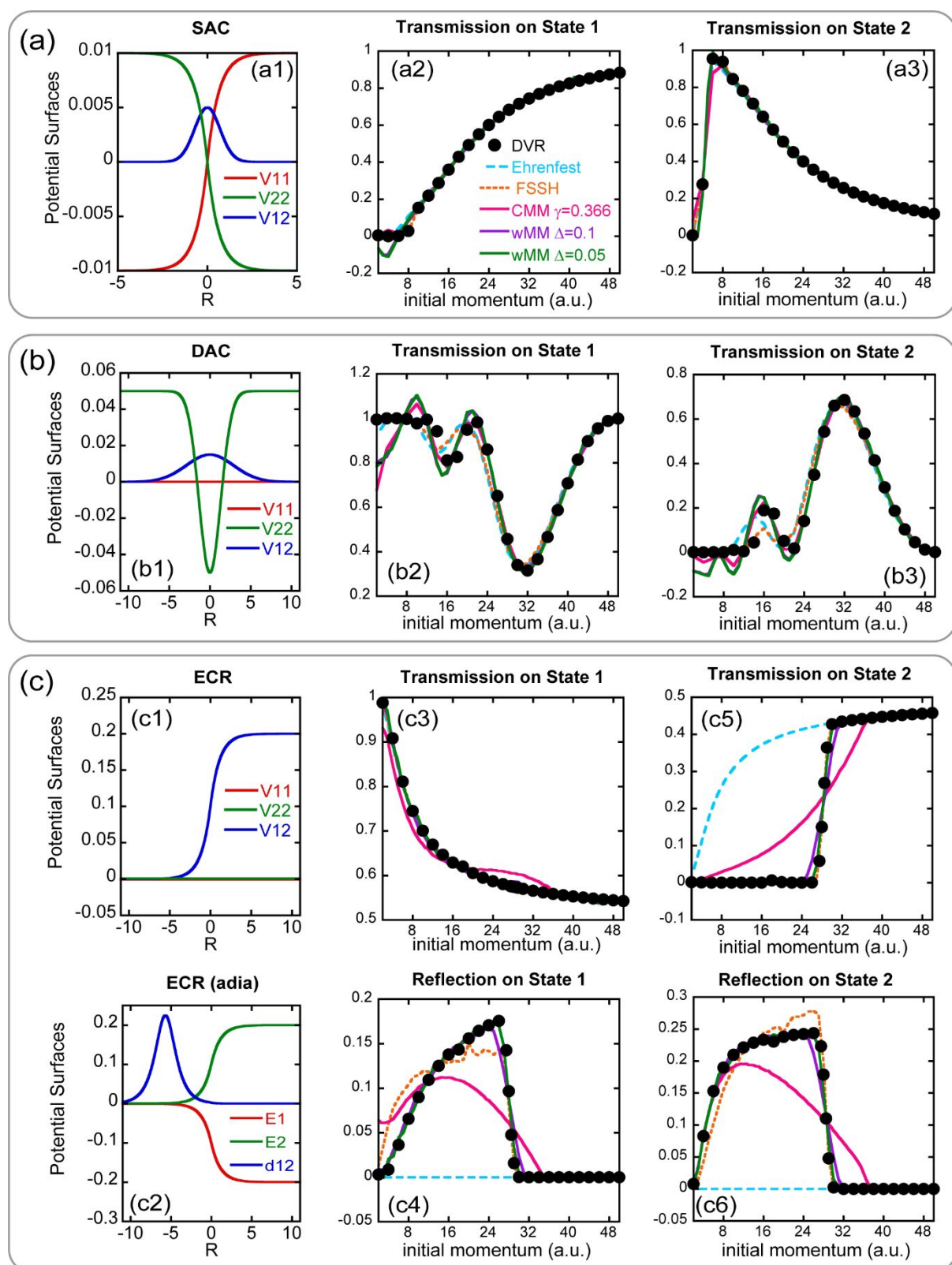


Figure 6: Results of population difference $D(t) = P_1(t) - P_0(t)$ between two states for the spin-boson model at low-temperature ($\beta = 1 / (k_B T) = 5$) with the Ohmic bath. Panel (a) reports the population dynamics of the spin-boson model with parameters $\varepsilon = \Delta_c = 1$, $\beta = 5$, $\omega_c = 1$, $\alpha = 0.1$ in Panel (a). Solid circles: Exact results produced by eHEOM reported in ref¹³⁴. Cyan dashed lines: Ehrenfest dynamics. Orange dashed lines: FSSH. Magenta solid lines: CMM with $\gamma = 0.366$. Purple and green solid lines: wMM with $\Delta = 0.1$ and 0.05, respectively. Panel (b) is similar to Panel (a) but for $\alpha = 0.4$; Panel (c) is similar to Panel (a) but for $\omega_c = 2.5$; Panel (d) is similar to Panel (a) but for $\omega_c = 2.5$, $\alpha = 0.4$. In each model 300 continuous DOFs (i.e., effective bath modes) are used.



1
2
3 **Figure 7:** Illustration of three Tully models and simulation results. Panel (a1) denotes diabatic PESes $V_{11}(R)$
4 and $V_{22}(R)$, as well as coupling term $V_{12}(R)$ for the SAC model; Panel (b1) does so for the DAC model;
5
6 Panel (c1) does so for the ECR model. Panel (c2) demonstrates adiabatic PESes $E_1(R)$ and $E_2(R)$, as well
7
8 as nonadiabatic coupling vector $d_{12}(R)$.
9

10 Panels (a2)-(a3): transmission coefficients on diabatic state 1, and those on diabatic state 2 of the SAC model,
11 respectively. Panels (b2)-(b3): similar to Panels (a2)-(a3), but for the DAC model. Panels (c3) and (c4):
12 transmission/reflection coefficients on adiabatic state 1 of the ECR model; Panels (c5) and (c6): those on adiabatic
13 state 2.
14

15 In Panels (a2)-(a3), (b2)-(b3), and (c3)-(c6), magenta, purple and green lines stand for transmission coefficients
16 results for CMM with $\gamma = 0.366$, wMM with $\Delta = 0.1$, and wMM with $\Delta = 0.05$, respectively. Long-
17 dashed blue lines: Ehrenfest dynamics; Short-dashed orange lines: FSSH; Black points: exact DVR benchmarks.
18
19
20
21
22
23
24
25
26
27
28
29
30
31
32
33
34
35
36
37
38
39
40
41
42
43
44
45
46
47
48
49
50
51
52
53
54
55
56
57
58
59
60

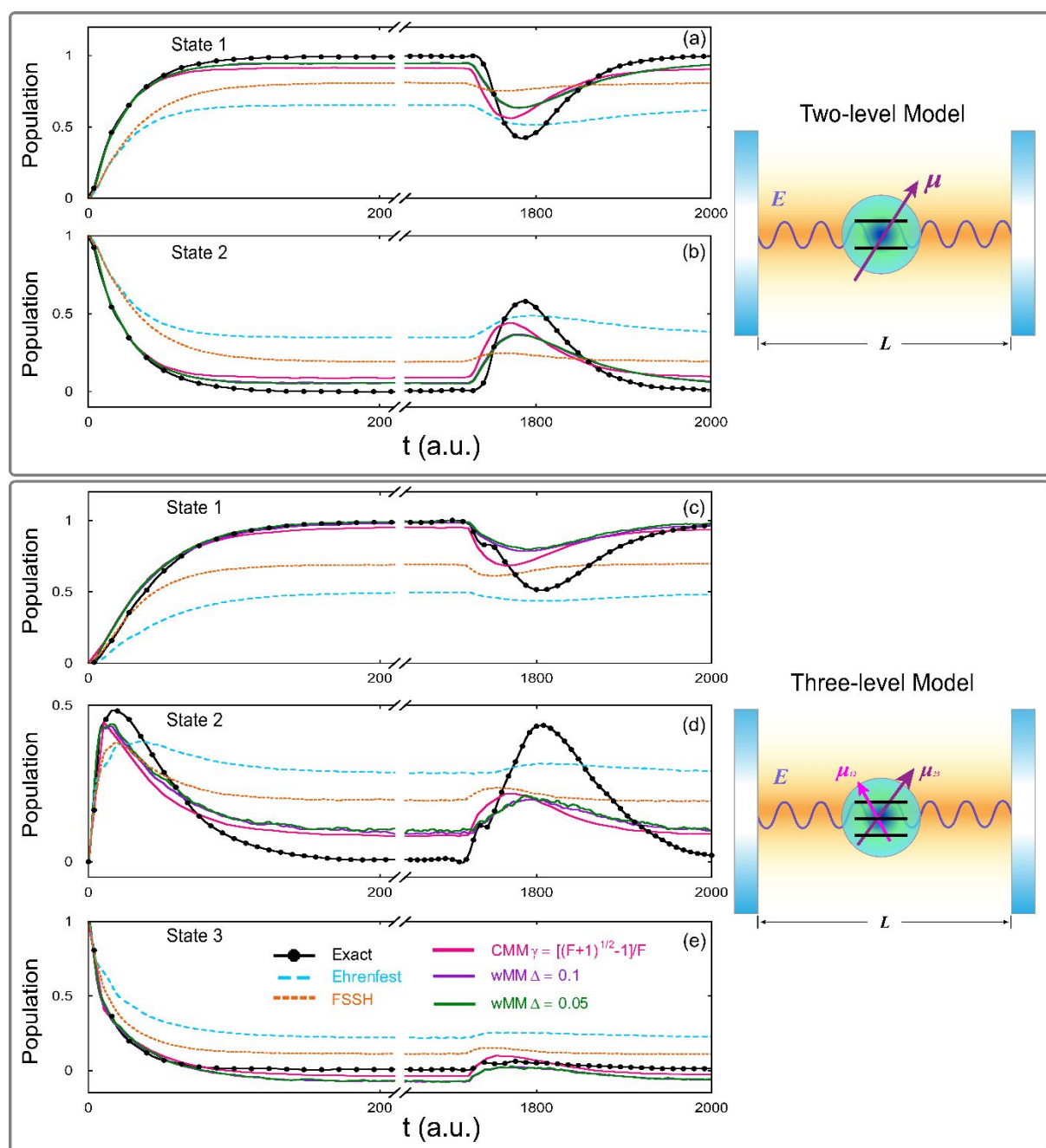


Figure 8: Results of population dynamics for the atom-in-cavity models. Panels (a)-(b) represent data of the first and second states of the two-level model, respectively. Panels (c)-(e) denote data of the first, second and third states of the three-level model, respectively. Magenta solid lines: CMM with $\gamma = (\sqrt{F+1} - 1)/F$; Purple solid lines: wMM with $\Delta = 0.1$; Green solid lines: wMM with $\Delta = 0.05$; Cyan long-dashed lines: Ehrenfest dynamics; Orange short-dashed lines: FSSH; Black solid-dotted lines: exact results from refs^{287, 288}. In each model 400 continuous DOFs (i.e., standing-wave modes) are involved.

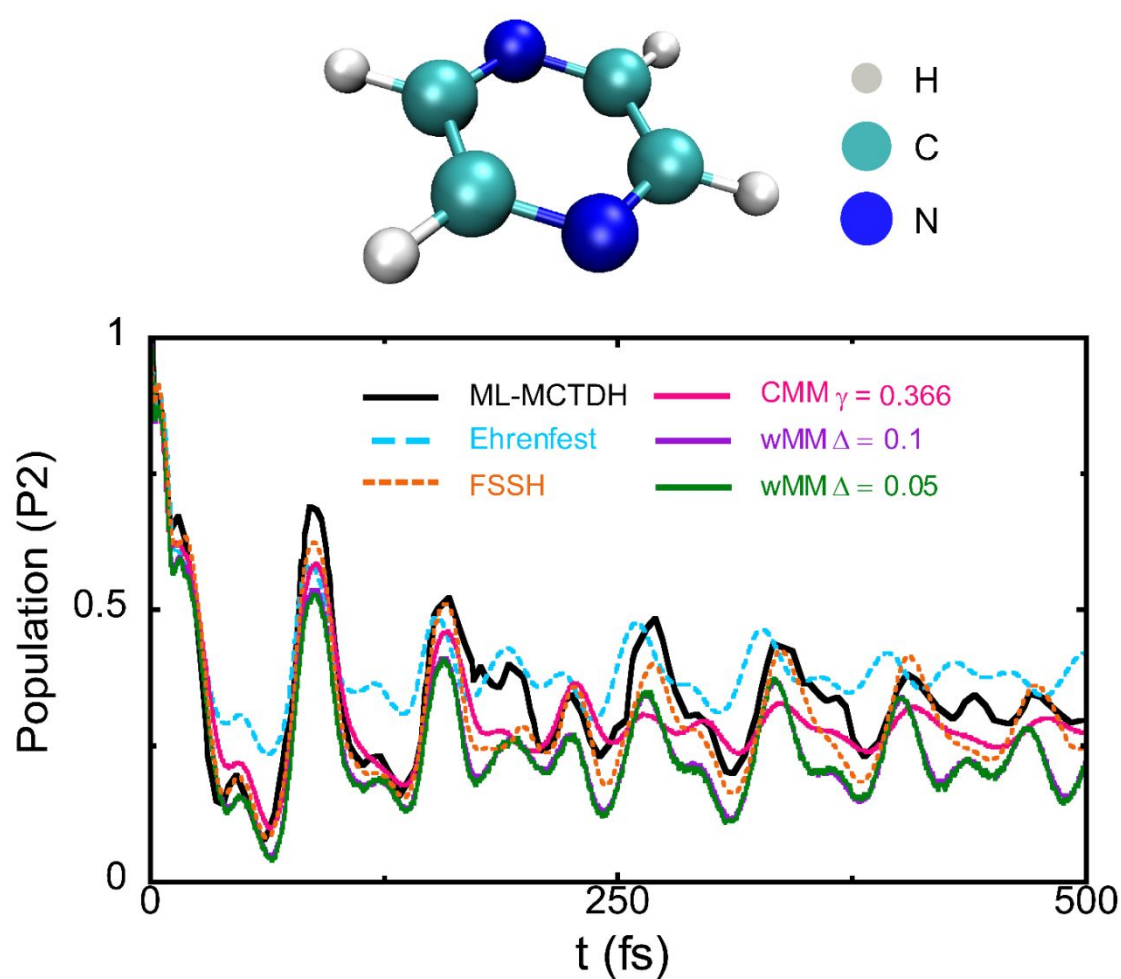


Figure 9: Results of population dynamics of the second electronic state of the 2-level 3-mode pyrazine model.

Magenta solid lines: CMM with $\gamma = (\sqrt{F+1} - 1) / F \approx 0.366$; Purple solid lines: wMM with $\Delta = 0.1$; Green solid lines: wMM with $\Delta = 0.05$. Cyan dashed lines: Ehrenfest dynamics; Orange short-dashed lines: FSSH; Black solid lines: ML-MCTDH results of ref²¹².

Funding Information

National Natural Science Foundation of China (NSFC) Grant No. 21961142017; Ministry of Science and Technology of China (MOST) Grant No. 2017YFA0204901

Research Resources

High-performance Computing Platform of Peking University, Beijing PARATERA Tech CO., Ltd., and Guangzhou supercomputer center

Acknowledgments

This work was supported by the National Natural Science Foundation of China (NSFC) Grant No. 21961142017, and by the Ministry of Science and Technology of China (MOST) Grant No. 2017YFA0204901. We acknowledge the High-performance Computing Platform of Peking University, Beijing PARATERA Tech CO., Ltd., and Guangzhou supercomputer center for providing computational resources.

Notes

The authors declare no competing financial interest.

Further Reading**Appendices****1. Derivation of the formulation of (weighted) constraint coordinate-momentum phase space.**

In this appendix, we introduce the techniques for performing integrals on constraint coordinate-momentum phase space, and show the brief derivation of the formulation of (weighted) constraint coordinate-momentum phase space. Such techniques have been expressed in Appendix A of ref¹³² as well as in Section S1 of the Supporting Information of ref¹³⁴.

Consider the expectation of any function $f(X_1, X_2, \dots, X_L)$ under the L -dimensional independent standard normal distribution (i.e., $\{X_i\} : N^{(L)}(0, 1)$). It is closely related to that under the uniform distribution on the $(L-1)$ -dimensional constraint space, i.e.,

$$\begin{aligned}
 \langle f \rangle_{N^{(L)}(0,1)} &= \frac{1}{(2\pi)^{L/2}} \int dX_1 dX_2 \dots dX_L e^{-\frac{1}{2} \sum_{k=1}^L X_k^2} f(X_1, X_2, \dots, X_L) \\
 &= \frac{1}{(2\pi)^{L/2}} \int_0^\infty d\xi \int dX_1 dX_2 \dots dX_L e^{-\xi} \delta\left(\frac{1}{2} \sum_{k=1}^L X_k^2 - \xi\right) f(X_1, X_2, \dots, X_L) . \quad 87 \\
 &= \frac{1}{(2\pi)^{L/2}} \int_0^\infty d\xi e^{-\xi} S_{L-1}(\sqrt{\xi}) \langle f \rangle_{S_{L-1}(\sqrt{\xi})}
 \end{aligned}$$

Here,

$$S_{L-1}(R) = \int dX_1 dX_2 \dots dX_L \delta\left(\frac{1}{2} \sum_{k=1}^L X_k^2 - R^2\right) \quad 88$$

denotes the area of the constraint space with radius R , and the expectation under the uniform distribution on the $(L-1)$ -dimensional constraint space, $\langle L \rangle_{S_{L-1}(R)}$, is given by

$$\langle f \rangle_{S_{L-1}(R)} = \frac{1}{S_{L-1}(R)} \int dX_1 dX_2 \dots dX_L \delta\left(\frac{1}{2} \sum_{k=1}^L X_k^2 - R^2\right) f(X_1, X_2, \dots, X_L) . \quad 89$$

(Note that the constraint space with radius R defined in eq 88 is slightly different from the $(L-1)$ -sphere in mathematics.) It is trivial to verify that $S_{L-1}(R) = R^{L-2} S_{L-1}(1)$ is the scaling relation of $S_{L-1}(R)$. We can calculate $S_{L-1}(1)$ by setting $f(X_1, X_2, \dots, X_L) \equiv 1$ in eq 87, i.e.,

$$1 = \frac{1}{(2\pi)^{L/2}} \int_0^\infty d\xi e^{-\xi} S_{L-1}(\sqrt{\xi}) = \frac{1}{(2\pi)^{L/2}} S_{L-1}(1) \int_0^\infty d\xi e^{-\xi} \xi^{\frac{L-2}{2}} . \quad 90$$

Equation 90 yields

$$S_{L-1}(1) = \frac{(2\pi)^{L/2}}{\Gamma(L/2)} \quad 91$$

after we use the equality $\int_0^\infty de^{-x} x^\alpha = \Gamma(\alpha+1)$ for $\alpha > -1$, where the Gamma function is defined by

$$\Gamma(s) = \int_0^\infty dt e^{-t} t^{s-1} \quad (s > 0).$$

The k -th order moment of the uniform distribution on the $(L-1)$ -dimensional constraint space has the scaling relation,

$$\begin{aligned} \langle X_{n_1} X_{n_2} \text{L}_+ X_{n_k} \rangle_{S_{L-1}(\sqrt{\xi})} &= \frac{1}{S_{L-1}(\sqrt{\xi})} \int dX_1 dX_2 \text{L}_+ dX_L \delta\left(\frac{1}{2} \sum_{l=1}^L X_l^2 - \xi\right) X_{n_1} X_{n_2} \text{L}_+ X_{n_k} \\ &= \xi^{k/2} \langle X_{n_1} X_{n_2} \text{L}_+ X_{n_k} \rangle_{S_{L-1}(1)} \end{aligned} \quad 92$$

Substitution of eq 92 into eq 87 produces

$$\begin{aligned} \langle X_{n_1} X_{n_2} \text{L}_+ X_{n_k} \rangle_{N^{(L)}(0,1)} &= \frac{\Gamma\left(\frac{L+k}{2}\right)}{\Gamma(L/2)} \langle X_{n_1} X_{n_2} \text{L}_+ X_{n_k} \rangle_{S_{L-1}(1)} \\ &= \frac{\Gamma\left(\frac{L+k}{2}\right)}{\xi^{k/2} \Gamma(L/2)} \langle X_{n_1} X_{n_2} \text{L}_+ X_{n_k} \rangle_{S_{L-1}(\sqrt{\xi})} \end{aligned} \quad 93$$

The well-known Wick theorem (also called Isserlis's theorem)^{297, 298} for the independent and identical standard normal distribution reads

$$\langle X_{n_1} X_{n_2} \text{L}_+ X_{n_k} \rangle_{N^{(L)}(0,1)} = \begin{cases} 0, & k \text{ is odd} \\ \sum \left(\prod \langle X_{n_i} X_{n_j} \rangle_{N^{(L)}(0,1)} \right), & k \text{ is even} \end{cases} \quad 94$$

Here, the notation $\sum \left(\prod \text{L}_+ \right)$ stands for the summation of the products over all possible pair partitions of $\{X_{n_1}, X_{n_2}, \text{L}_+, X_{n_k}\}$. It is straightforward to obtain the second order moment and fourth order moment of $N^{(L)}(0,1)$,

$$\begin{aligned} \langle X_i X_j \rangle_{N(0,1)} &= \delta_{ij} \\ \langle X_i X_j X_k X_l \rangle_{N(0,1)} &= \delta_{ij} \delta_{kl} + \delta_{ik} \delta_{jl} + \delta_{il} \delta_{jk} \end{aligned} \quad 95$$

Substitution of eq 95 into eq 93 leads to

$$\begin{aligned} \langle X_i X_j \rangle_{S_{L-1}(\sqrt{\xi})} &= \frac{\xi}{L/2} \delta_{ij} \\ \langle X_i X_j X_k X_l \rangle_{S_{L-1}(\sqrt{\xi})} &= \frac{\xi^2}{\frac{L}{2} \left(\frac{L}{2} + 1 \right)} (\delta_{ij} \delta_{kl} + \delta_{ik} \delta_{jl} + \delta_{il} \delta_{jk}) \end{aligned} \quad 96$$

We then set $L = 2F$ as well as $\xi = 1 + F\gamma$ and relabel the constraint space (defined by eq 32) as $S_\gamma(\mathbf{x}, \mathbf{p})$ parameterized by γ . The comparison between eq 33 and eq 88 states that the area of constraint phase space is

$$\Omega(\gamma) = S_{2F-1} \left(R = \sqrt{1+F\gamma} \right) = \frac{(2\pi)^F}{\Gamma(F)} (1+F\gamma)^{F-1}$$

We then obtain

$$\begin{aligned} \langle g(\mathbf{x}, \mathbf{p}) \rangle_{S_{L-1}(\sqrt{\xi})} &= \int_{S_\gamma(\mathbf{x}, \mathbf{p})} d\mathbf{X} g(\mathbf{x}, \mathbf{p}) \\ &= \int F d\mathbf{x} d\mathbf{p} \frac{1}{\Omega(\gamma)} \delta \left(\sum_{n=1}^F \frac{(x^{(n)})^2 + (p^{(n)})^2}{2} - (1+F\gamma) \right) g(\mathbf{x}, \mathbf{p}) \end{aligned} \quad 98$$

where $\mathbf{X} = (\mathbf{x}, \mathbf{p})$. The second order moment and fourth order moment on the constraint space of eq 32 read

$$\begin{aligned} \int_{S_\gamma(\mathbf{x}, \mathbf{p})} d\mathbf{X} (X_i X_j) &= \frac{1+F\gamma}{F} \delta_{ij} \\ \int_{S_\gamma(\mathbf{x}, \mathbf{p})} d\mathbf{X} (X_i X_j X_k X_l) &= \frac{(1+F\gamma)^2}{F(F+1)} (\delta_{ij}\delta_{kl} + \delta_{ik}\delta_{jl} + \delta_{il}\delta_{jk}) \end{aligned} \quad 99$$

Consider $\hat{A} = |m\rangle\langle n|$ and $\hat{B} = |k\rangle\langle l|$. We have

$$\text{Tr}[\hat{A}\hat{B}] = \delta_{nk}\delta_{ml} \quad 100$$

The constraint phase space expression (i.e., eqs 4-6 when only discrete electronic DOFs exist) of the left-hand side (LHS) of eq 100 is equivalent to

$$\begin{aligned} \text{Tr}[\hat{A}\hat{B}] &= F \int_{S_\gamma(\mathbf{x}, \mathbf{p})} d\mathbf{X} \langle n | \hat{K}_{\text{ele}}(\mathbf{x}, \mathbf{p}) | m \rangle \langle l | K_{\text{ele}}^{-1}(\mathbf{x}, \mathbf{p}) | k \rangle \\ &= F \int_{S_\gamma(\mathbf{x}, \mathbf{p})} d\mathbf{X} K_{nm}^{(\text{ele})}(\mathbf{x}, \mathbf{p}) K_{(ele), lk}^{-1}(\mathbf{x}, \mathbf{p}) \end{aligned} \quad 101$$

In eq 101, $K_{nm}^{(\text{ele})}(\mathbf{x}, \mathbf{p})$ is the element of operator $\hat{K}_{\text{ele}}(\mathbf{x}, \mathbf{p})$, and $K_{(ele), lk}^{-1}(\mathbf{x}, \mathbf{p})$ is the element of operator $K_{\text{ele}}^{-1}(\mathbf{x}, \mathbf{p})$. When the mapping kernel is given by eq 30, it is straightforward to derive that its corresponding inverse kernel is eq 31 by employing eqs 99-101. Specifically, when the mapping kernel is identical to its inverse (i.e., eq 39), the element of the (inverse) kernel operator is

$$K_{nm}(\mathbf{x}, \mathbf{p}) = K_{nm}^{-1}(\mathbf{x}, \mathbf{p}) = \frac{1}{2} (x^{(n)} + ip^{(n)}) (x^{(m)} - ip^{(m)}) - \gamma \delta_{nm} \quad 102$$

It is trivial to use eq 99 and eq 102 to achieve the equality

$$F \int_{S_\gamma(\mathbf{x}, \mathbf{p})} d\mathbf{X} K_{nm}(\mathbf{x}, \mathbf{p}) K_{lk}^{-1}(\mathbf{x}, \mathbf{p}) = \frac{(1+F\gamma)^2}{(F+1)} \delta_{nk}\delta_{ml} + \left[\frac{(1+F\gamma)^2}{(F+1)} - 2\gamma - F\gamma^2 \right] \delta_{lk}\delta_{nm} \quad 103$$

After employing eqs 100-101, we obtain $\gamma = (\sqrt{F+1} - 1) / F$ from eq 103 where the mapping kernel is identical to its inverse (i.e., eq 39).

Similarly, the weighting constraint phase space formulation (eqs 4-6 when only discrete electronic DOFs exist, and eq 38) leads to

$$\begin{aligned}\text{Tr}_e [\hat{A}\hat{B}] &= \int_{S(x,p)} F dxdp A_C(x,p) \hat{B}_C^0(x,p) \\ &= \int_{-1/F}^{\infty} d\gamma w(\gamma) \int F dxdp \frac{1}{\Omega(\gamma)} \delta\left(\sum_{n=1}^F \frac{(x^{(n)})^2 + (p^{(n)})^2}{2} - (1+F\gamma)\right) A_C(x,p) \hat{B}_C^0(x,p) \\ &= \int_{-1/F}^{\infty} d\gamma w(\gamma) \langle A_C(x,p) \hat{B}_C^0(x,p) \rangle_{S_{L-1}(\sqrt{\xi})}\end{aligned}\quad 104$$

Employing eq 100, we obtain an equation similar to eq 101

$$F \int d\gamma w(\gamma) \int_{S_\gamma(x,p)} dX K_{nm}(x,p) K_{lk}^{-1}(x,p) = \delta_{nk} \delta_{ml} \quad . \quad 105$$

Because we request eq 39 that the mapping kernel is identical to its inverse in the weighted constraint phase space formulation, eqs 102-103 also hold. Substitution of eq 103 into eq 105 generates

$$\int d\gamma w(\gamma) (F\gamma^2 + 2\gamma) = \int d\gamma w(\gamma) \chi(\gamma) = 1 \quad , \quad 106$$

which is eq 40 of the main text. When $w(\gamma)$, the quasi-probability distribution function of parameter γ , is a single Dirac delta function, the constraint coordinate-momentum phase space formulation with $\gamma = (\sqrt{F+1} - 1) / F$ is a special case of eq 106, or of eq 40 of the main text. When in eq 106 or eq 40 $w(\gamma)$ is represented by a linear combination of two symmetrical delta functions (i.e., eqs 44-46), we achieve the symmetrically weighted constraint phase space formulation employed in wMM of the Focus Article. Apparently, various other choices for quasi-probability distribution function $w(\gamma)$ are also available and can be investigated in the future.

2. More discussion on the equations of motion in the adiabatic representation

Below we will show that eq 75 and eq 77, the equations of motion (EOMs) under the diabatic-to-adiabatic transformation are intrinsically equivalent to Hamilton's EOMs generated by the Hamiltonian, eq 80, when (nuclear) canonical phase variables $(\mathbf{R}; \mathbf{P})$ are defined by eq 79. For simplicity, assume that all nonadiabatic coupling terms $\{\mathbf{d}_{mn}^{(I)}(\mathbf{R})\}$ are real. It leads to a simplified relation

$$\mathbf{P}_0 = \mathbf{P} + h \sum_{n,m=1}^F \mathbf{x}_0^{(m)} \beta_0^{(m)} \mathbf{d}_{mn}(\mathbf{R})$$

in eq 79. In the adiabatic representation, $\mathbf{P} = \mathbf{P}_0 - h \sum_{n,m=1}^F \mathbf{x}_0^{(m)} \beta_0^{(m)} \mathbf{d}_{mn}(\mathbf{R})$ is denoted the kinematic momentum (e.g., in ref¹⁸⁴), which is different from canonical momentum \mathbf{P} . The Hamiltonian, eq 80, is recast into

$$H_C(\mathbf{R}, \mathbf{P}, \mathbf{x}_0, \mathbf{p}_0) = \sum_{I=1}^N \frac{\left(\dot{\mathbf{P}}_I - h \sum_{n,m=1}^F \mathbf{x}_0^{(m)} \beta_0^{(m)} d_{mn}^{(I)}(\mathbf{R}) \right)^2}{2M_I} + \sum_{k=1}^F E_k(\mathbf{R}) \left(\frac{1}{2} \left((\mathbf{x}_0^{(k)})^2 + (\mathbf{p}_0^{(k)})^2 \right) - \gamma \right) . \quad 108$$

Here, $d_{mn}^{(I)}(\mathbf{R})$ and $\dot{\mathbf{P}}_I$ are the the I -th DOF component of $\mathbf{d}_{mn}(\mathbf{R})$ and that of \mathbf{P} , respectively. Note that canonical variables $(\mathbf{R}, \mathbf{P}, \mathbf{x}_0, \mathbf{p}_0)$ are independent of one another. Hamilton's EOMs produced by eq 108 are

$$\begin{aligned} \dot{\mathbf{x}}_0^{(m)} &= \frac{1}{h} \frac{\partial}{\partial \mathbf{p}_0^{(m)}} H_C(\mathbf{R}, \mathbf{P}, \mathbf{x}_0, \mathbf{p}_0) \\ &= - \sum_{J=1}^N \sum_{n=1}^F \frac{\dot{\mathbf{P}}_J - h \sum_{k,l=1}^F \mathbf{x}_0^{(k)} \beta_0^{(l)} d_{lk}^{(J)}(\mathbf{R})}{M_J} \mathbf{x}_0^{(m)} d_{mn}^{(J)}(\mathbf{R}) + \frac{1}{h} E_m(\mathbf{R}) \beta_0^{(m)} , \end{aligned} \quad 109$$

$$\begin{aligned} \dot{\mathbf{p}}_0^{(m)} &= - \frac{1}{h} \frac{\partial}{\partial \mathbf{x}_0^{(m)}} H_C(\mathbf{R}, \mathbf{P}, \mathbf{x}_0, \mathbf{p}_0) \\ &= \sum_{J=1}^N \sum_{n=1}^F \frac{\dot{\mathbf{P}}_J - h \sum_{k,l=1}^F \mathbf{x}_0^{(k)} \beta_0^{(l)} d_{lk}^{(J)}(\mathbf{R})}{M_J} \beta_0^{(m)} d_{nm}^{(J)}(\mathbf{R}) - \frac{1}{h} E_m(\mathbf{R}) \mathbf{x}_0^{(m)} , \end{aligned} \quad 110$$

$$\dot{\mathbf{R}}_I = \frac{\partial}{\partial \dot{\mathbf{P}}_I} H_C(\mathbf{R}, \mathbf{P}, \mathbf{x}_0, \mathbf{p}_0) = \frac{\dot{\mathbf{P}}_I - h \sum_{n,m=1}^F \mathbf{x}_0^{(m)} \beta_0^{(m)} d_{mn}^{(I)}(\mathbf{R})}{M_I} , \quad 111$$

$$\begin{aligned} \dot{\mathbf{P}}_I &= - \frac{\partial}{\partial \mathbf{R}_I} H_C(\mathbf{R}, \mathbf{P}, \mathbf{x}_0, \mathbf{p}_0) \\ &= h \sum_{J=1}^N \sum_{n,m=1}^F \frac{\dot{\mathbf{P}}_J - h \sum_{k,l=1}^F \mathbf{x}_0^{(k)} \beta_0^{(l)} d_{lk}^{(J)}(\mathbf{R})}{M_J} \mathbf{x}_0^{(m)} \beta_0^{(m)} \frac{\partial d_{mn}^{(J)}(\mathbf{R})}{\partial \mathbf{R}_I} \\ &\quad - \sum_{k=1}^F \frac{\partial E_k(\mathbf{R})}{\partial \mathbf{R}_I} \left(\frac{1}{2} \left((\mathbf{x}_0^{(k)})^2 + (\mathbf{p}_0^{(k)})^2 \right) - \gamma \right) . \end{aligned} \quad 112$$

It is evident that eqs 109-110 are identical to eq 71 and that eq 111 is the same as the first equation of eq 77.

We will then prove that eq 112 is equivalent to the second equation of eq 77.

Consider the full time-derivative of canonical momentum \dot{P}_I^{α} ,

$$\begin{aligned} \dot{P}_I^{\alpha} &= \dot{P}_I^{\alpha}(\mathbf{R}^0, \mathbf{P}^0, \mathbf{x}^0, \mathbf{p}^0) + \hbar \frac{d}{dt} \sum_{n,m=1}^F \mathcal{X}_0^{(m)} \mathcal{P}_0^{(n)} d_{nm}^{(I)}(\mathbf{R}^0) \\ &= \dot{P}_I^{\alpha} + \hbar \sum_{n,m=1}^F \mathcal{X}_0^{(m)} \mathcal{P}_0^{(n)} d_{nm}^{(I)}(\mathbf{R}^0) + \hbar \sum_{n,m=1}^F \mathcal{X}_0^{(m)} \mathcal{P}_0^{(n)} d_{nm}^{(I)}(\mathbf{R}^0) + \hbar \sum_{n,m=1}^F \mathcal{X}_0^{(m)} \mathcal{P}_0^{(n)} \sum_{J=1}^N \frac{\partial d_{nm}^{(I)}(\mathbf{R}^0)}{\partial R_J^0} \dot{R}_J^{\alpha} . \end{aligned} \quad 113$$

Substitution of eqs 109-112 into eq 113 yields,

$$\begin{aligned} \dot{P}_I^{\alpha}(\mathbf{R}^0, \mathbf{P}^0, \mathbf{x}^0, \mathbf{p}^0) &= \hbar \sum_{J=1}^N \sum_{n,m=1}^F \frac{P_J(\mathbf{R}^0, \mathbf{P}^0, \mathbf{x}^0, \mathbf{p}^0) \mathcal{X}_0^{(m)} \mathcal{P}_0^{(n)}}{M_J} \left(\frac{\partial d_{mn}^{(J)}(\mathbf{R}^0)}{\partial R_I^0} - \frac{\partial d_{mn}^{(I)}(\mathbf{R}^0)}{\partial R_J^0} \right) \\ &\quad - \sum_{k=1}^F \frac{\partial E_k(\mathbf{R}^0)}{\partial R_I^0} \left(\frac{1}{2} \left((\mathcal{X}_0^{(k)})^2 + (\mathcal{P}_0^{(k)})^2 \right) - \gamma \right) \\ &\quad + \hbar \sum_{n,m=1}^F \sum_{J=1}^N \sum_{k=1}^F \frac{P_J(\mathbf{R}^0, \mathbf{P}^0, \mathbf{x}^0, \mathbf{p}^0) d_{nk}^{(I)}(\mathbf{R}^0) d_{km}^{(J)}(\mathbf{R}^0) (\mathcal{X}_0^{(m)} \mathcal{P}_0^{(n)} - \mathcal{X}_0^{(n)} \mathcal{P}_0^{(m)})}{M_J} \\ &\quad + \sum_{n,m=1}^F \left(E_n(\mathbf{R}^0) \mathcal{X}_0^{(m)} \mathcal{X}_0^{(n)} - E_m(\mathbf{R}^0) \mathcal{P}_0^{(m)} \mathcal{P}_0^{(n)} \right) d_{nm}^{(I)}(\mathbf{R}^0) . \end{aligned} \quad 114$$

Since the derivative of the first-order nonadiabatic coupling is

$$\begin{aligned} \frac{\partial d_{mn}^{(J)}}{\partial R_I^0} &= \frac{\partial}{\partial R_I^0} \left\langle \phi_m \left| \frac{\partial}{\partial R_J^0} \phi_n \right. \right\rangle = \left\langle \frac{\partial}{\partial R_I^0} \phi_m \left| \frac{\partial}{\partial R_J^0} \phi_n \right. \right\rangle + \left\langle \phi_m \left| \frac{\partial^2}{\partial R_I^0 \partial R_J^0} \phi_n \right. \right\rangle , \\ &= \sum_{k=1}^F d_{km}^{(I)} d_{kn}^{(J)} + D_{mn}^{(IJ)} \end{aligned} \quad 115$$

where $D_{mn}^{(IJ)} = \left\langle \phi_m \left| \frac{\partial^2}{\partial R_I^0 \partial R_J^0} \phi_n \right. \right\rangle$ is a symmetric tensor of nuclear index, i.e., $D_{mn}^{(IJ)} = D_{mn}^{(JI)}$, the first term of

the RHS of eq 114 becomes

$$\begin{aligned} &\hbar \sum_{J=1}^N \sum_{n,m=1}^F \frac{P_J(\mathbf{R}^0, \mathbf{P}^0, \mathbf{x}^0, \mathbf{p}^0) \mathcal{X}_0^{(m)} \mathcal{P}_0^{(n)}}{M_J} \left(\frac{\partial d_{mn}^{(J)}(\mathbf{R}^0)}{\partial R_I^0} - \frac{\partial d_{mn}^{(I)}(\mathbf{R}^0)}{\partial R_J^0} \right) \\ &= -\hbar \sum_{J=1}^N \sum_{n,m=1}^F \sum_{k=1}^F \frac{P_J(\mathbf{R}^0, \mathbf{P}^0, \mathbf{x}^0, \mathbf{p}^0) (\mathcal{X}_0^{(m)} \mathcal{P}_0^{(n)} - \mathcal{X}_0^{(n)} \mathcal{P}_0^{(m)})}{M_J} d_{nk}^{(I)}(\mathbf{R}^0) d_{km}^{(J)}(\mathbf{R}^0) . \end{aligned} \quad 116$$

1
2
3
4 It is important to note that, in general $\frac{\partial d_{mn}^{(J)}(\mathbf{R})}{\partial R_I^0} - \frac{\partial d_{mn}^{(I)}(\mathbf{R})}{\partial R_J^0} = 0$ does not always hold for $I \neq J$, except
5
6

7 for two-electronic-state systems. So eq 116 is not always equal to zero. The term of eq 116 cancels out the
8 third term of eq 114. The last term of the RHS of eq 114 can be recast into
9
10

$$\begin{aligned} & \sum_{n,m=1}^F \left(E_n(\mathbf{R}) \mathcal{X}_0^{(m)} \mathcal{X}_0^{(m)} - E_m(\mathbf{R}) \mathcal{P}_0^{(m)} \mathcal{P}_0^{(m)} \right) d_{nm}^{(I)}(\mathbf{R}) \\ &= \frac{1}{2} \sum_{n,m=1}^F \left(E_n(\mathbf{R}) - E_m(\mathbf{R}) \right) \left(\mathcal{X}_0^{(m)} \mathcal{X}_0^{(m)} + \mathcal{P}_0^{(m)} \mathcal{P}_0^{(m)} \right) d_{nm}^{(I)}(\mathbf{R}) \end{aligned} \quad . \quad 117$$

18 Equation 114 then becomes
19

$$\begin{aligned} & \dot{\mathbf{P}}_I(\mathbf{R}, \mathbf{P}, \mathbf{x}, \mathbf{p}) \\ &= - \sum_{k=1}^F \frac{\partial E_k(\mathbf{R})}{\partial R_I} \left(\frac{1}{2} \left((\mathcal{X}_0^{(k)})^2 + (\mathcal{P}_0^{(k)})^2 \right) - \gamma \right) - \sum_{n,m=1}^F \left(E_n(\mathbf{R}) - E_m(\mathbf{R}) \right) d_{mn}^{(I)}(\mathbf{R}) \frac{1}{2} \left(\mathcal{X}_0^{(n)} \mathcal{X}_0^{(m)} + \mathcal{P}_0^{(n)} \mathcal{P}_0^{(m)} \right) \end{aligned}$$

20
21
22
23
24
25
26
27
28
29
30
31
32
33
34
35
36
37
38
39
40
41
42
43
44
45
46
47
48
49
50
51
52
53
54
55
56
57
58
59
60

which is equivalent to the second equation of eq 77 of the main text. It indicates that the canonical momentum in the diabatic representation is covariant with *kinematic* momentum \mathbf{P} rather than canonical momentum $\dot{\mathbf{P}}$ in adiabatic representation unless all nonadiabatic coupling terms vanish. This is consistent with the spirit of the work of Cotton *et. al.* in ref¹⁸⁴. Because the EOMs (eq 71 and eq 77) of the main text are identical to Hamilton's EOMs generated by eq 108, the mapping Hamiltonian (eq 80 or eq 108) is conserved during the evolution in the adiabatic representation.

3. The relationship between the constraint coordinate-momentum phase space and Stratonovich phase space

Stratonovich's original work¹⁰⁰ in 1956 maps a 2-state (spin-1/2) system onto a two-dimensional sphere. We review two kinds of further developments of the Stratonovich-Weyl mapping phase space representations for F -state quantum system: the first one based on the SU(2) structure^{103, 113} and the second one based on the SU(F) structure¹¹⁴. We show the relationship between constrained coordinate-momentum phase space representation that we use in the Focus Article and the two kinds of Stratonovich phase space representations.

In the SU(2) Stratonovich phase space representation, an F -state system is treated as a spin- j system (where $F = 2j + 1$). The basis set consists of $| j, m \rangle$, the eigenstate of the square of total angular momentum

\hat{J}^2 and the z -component of angular momentum \hat{J}_z with quantum numbers j and m , respectively. The mapping kernel is

$$\hat{K}_{\text{ele}}^{\text{SU}(2)}(\theta, \varphi; s) = \sqrt{\frac{\pi}{2j+1}} \sum_{l=0}^{2j} (C_{jj,l0}^{jj})^{-s} \sum_{m=-l}^l Y_{lm}^*(\theta, \varphi) \hat{T}_{lm}^j, \quad s \in \mathbb{I} \quad 119$$

where \hat{T}_{lm}^j is the irreducible tensor operator defined as²⁹⁹

$$\hat{T}_{lm}^j = \sqrt{\frac{2l+1}{2j+1}} \sum_{m',n=-j}^j C_{jm',lm}^{jn} |j,n\rangle\langle j,m'|. \quad 120$$

Here $C_{j_1 m_1, j_2 m_2}^{jm} = \langle jm | j_1 m_1, j_2 m_2 \rangle$ is the well-known Clebsch-Gordan coefficient for the angular momentum coupling, and $Y_{lm}(\theta, \varphi)$ is the spherical harmonic function. The inverse kernel of $\hat{K}_{\text{ele}}^{\text{SU}(2)}(\theta, \varphi; s)$ is simply $\hat{K}_{\text{ele}}^{\text{SU}(2)}(\theta, \varphi; -s)$. We note that, although $s = 1, 0$, and -1 are traditionally associated with the Q , Wigner, and P -functions respectively and used in the literature^{111, 128}, parameter s of eq 119 can in principle take *any* real value.

When $F > 2$, the SU(2) Stratonovich phase space (θ, φ) does *not* have a phase point-to-phase point mapping to constraint coordinate-momentum phase space, although the relation can only be constructed by virtue of the density matrix. Only when $F = 2$ as in the original work of Stratonovich, there exists a phase point-to-phase point mapping to constraint coordinate-momentum phase space. The mapping kernel can be expressed in terms of the spin-coherent state,

$$\hat{K}_{\text{ele}}^{\text{SU}(2)}(\theta, \varphi; s) = 3^{(1+s)/2} |\theta, \varphi\rangle\langle\theta, \varphi| + \frac{\hat{\mathbf{I}}}{2} [1 - 3^{(1+s)/2}]. \quad 121$$

In eq 121 spin coherent state $|\theta, \varphi\rangle$ is

$$|\theta, \varphi\rangle = \begin{pmatrix} e^{-i\varphi} \sin(\theta/2) \\ \cos(\theta/2) \end{pmatrix}, \quad 122$$

where (θ, φ) are the spherical coordinate variables on the two-dimensional spherical phase space. The range of θ is $[0, \pi]$ and that for φ is $[0, 2\pi]$. When $F = 2$, the explicit transformation of (θ, φ) to the constrained coordinate-momentum phase space $(x^{(1)}, x^{(2)}, p^{(1)}, p^{(2)})$ is

$$\begin{aligned} \begin{pmatrix} x^{(1)} \\ p^{(1)} \end{pmatrix} &= \sqrt{2(1+2\gamma)} \begin{pmatrix} \cos\psi & -\sin\psi \\ \sin\psi & \cos\psi \end{pmatrix} \begin{pmatrix} \cos\varphi \sin(\theta/2) \\ -\sin\varphi \sin(\theta/2) \end{pmatrix}, \\ \begin{pmatrix} x^{(2)} \\ p^{(2)} \end{pmatrix} &= \sqrt{2(1+2\gamma)} \begin{pmatrix} \cos\psi & -\sin\psi \\ \sin\psi & \cos\psi \end{pmatrix} \begin{pmatrix} \cos(\theta/2) \\ 0 \end{pmatrix} \end{aligned} \quad , \quad 123$$

where ψ is an additional global phase.

The second kind of representation is the $SU(F)$ Stratonovich phase space¹¹⁴, which is diffeomorphic to the quotient set $SU(F)/U(F-1)$, parameterized by $(2F-2)$ angle variables $(\boldsymbol{\theta}, \boldsymbol{\varphi}) = (\theta_1, \theta_2, \dots, \theta_{F-1}, \varphi_1, \varphi_2, \dots, \varphi_{F-1})$. The range of each angle θ_i is $[0, \pi/2]$ and that for each angle φ_i is $[0, 2\pi)$. The $SU(F)$ Stratonovich phase space of Tilma *et.al.*¹¹⁴ has been used to prepare the initial condition for the Meyer-Miller mapping model of non-adiabatic dynamics in ref¹⁹⁷.

The mapping kernel of the $SU(F)$ Stratonovich phase space is

$$\hat{K}_{\text{ele}}^{\text{SU}(F)}(\boldsymbol{\theta}, \boldsymbol{\varphi}; s) = (1+F)^{(1+s)/2} |\boldsymbol{\theta}, \boldsymbol{\varphi}\rangle \langle \boldsymbol{\theta}, \boldsymbol{\varphi}| + \frac{\hat{\mathbf{I}}}{F} (1 - (1+F)^{(1+s)/2}), \quad s \in \mathbb{i} \quad 124$$

and the inverse kernel is $\hat{K}_{\text{ele}}^{\text{SU}(F)}(\boldsymbol{\theta}, \boldsymbol{\varphi}; -s)$. The explicit form of the generalized coherent state $|\boldsymbol{\theta}, \boldsymbol{\varphi}\rangle$ is^{300, 301}

$$|\boldsymbol{\theta}, \boldsymbol{\varphi}\rangle = \sum_{n=1}^F c_n |n\rangle, \quad 125$$

where the coefficients are

$$\begin{pmatrix} c_1 \\ c_2 \\ c_3 \\ \vdots \\ c_{F-3} \\ c_{F-2} \\ c_{F-1} \\ c_F \end{pmatrix} = \begin{pmatrix} e^{i(\varphi_1+\varphi_2+\dots+\varphi_{F-1})} \cos(\theta_1) \cos(\theta_2) \dots \cos(\theta_{F-2}) \sin(\theta_{F-1}) \\ -e^{i(-\varphi_1+\varphi_2+\dots+\varphi_{F-1})} \sin(\theta_1) \cos(\theta_2) \dots \cos(\theta_{F-2}) \sin(\theta_{F-1}) \\ -e^{i(\varphi_3+\varphi_4+\dots+\varphi_{F-1})} \sin(\theta_2) \cos(\theta_3) \dots \cos(\theta_{F-2}) \sin(\theta_{F-1}) \\ \vdots \\ -e^{i(\varphi_{F-3}+\varphi_{F-2}+\varphi_{F-1})} \sin(\theta_{F-4}) \cos(\theta_{F-3}) \cos(\theta_{F-2}) \sin(\theta_{F-1}) \\ -e^{i(\varphi_{F-2}+\varphi_{F-1})} \sin(\theta_{F-3}) \cos(\theta_{F-2}) \sin(\theta_{F-1}) \\ -e^{i(\varphi_{F-1})} \sin(\theta_{F-2}) \sin(\theta_{F-1}) \\ \cos(\theta_{F-1}) \end{pmatrix}. \quad 126$$

As derived first in Appendix A of ref¹³² in the spirit of ref¹³¹ and then in the Supporting Information of ref¹³⁴, the mapping kernel of constraint coordinate-momentum phase space for a set of F states (eq 30 of the main text) is denoted as,

$$\hat{K}_{\text{ele}}(\mathbf{x}, \mathbf{p}; \gamma) = \sum_{m,n=1}^F \left[\frac{(x^{(m)} - i p^{(m)})(x^{(n)} + i p^{(n)})}{2} - \gamma \delta_{mn} \right] |n\rangle \langle m| = |\mathbf{x}, \mathbf{p}\rangle \langle \mathbf{x}, \mathbf{p}| - \gamma \hat{\mathbf{I}}, \quad 127$$

1
2 where the non-normalized state $|\mathbf{x}, \mathbf{p}\rangle$ is
3
4

$$5 \quad 6 \quad 7 \quad 8 \quad 9 \quad 10 \quad 11 \quad 12 \quad 13 \quad 14 \quad 15 \quad 16 \quad 17 \quad 18 \quad 19 \quad 20 \quad 21 \quad 22 \quad 23 \quad 24 \quad 25 \quad 26 \quad 27 \quad 28 \quad 29 \quad 30 \quad 31 \quad 32 \quad 33 \quad 34 \quad 35 \quad 36 \quad 37 \quad 38 \quad 39 \quad 40 \quad 41 \quad 42 \quad 43 \quad 44 \quad 45 \quad 46 \quad 47 \quad 48 \quad 49 \quad 50 \quad 51 \quad 52 \quad 53 \quad 54 \quad 55 \quad 56 \quad 57 \quad 58 \quad 59 \quad 60$$

$$\sum_{n=1}^F \frac{x^{(n)} + i p^{(n)}}{\sqrt{2}} |n\rangle. \quad 128$$

The $U(F)$ constraint coordinate-momentum phase space of the $(2F-1)$ -dimensional sphere is diffeomorphic to $U(F)/U(F-1)$. (The difference between $U(F)$ and $SU(F) \times U(1)$ is excluded by the division over $U(F-1)$.) Comparison of $\hat{K}_{\text{ele}}^{\text{SU}(F)}(\boldsymbol{\theta}, \boldsymbol{\varphi}; s)$ to $\hat{K}_{\text{ele}}(\mathbf{x}, \mathbf{p}; \gamma)$ implies that the two kernels are closely related. The correspondence between parameters s and γ reads

$$1 + F\gamma = (1 + F)^{(1+s)/2}. \quad 129$$

It is evident (from eq 129, the relation between constraint coordinate-momentum phase space and the $SU(F)$ Stratonovich phase space) that parameter s can be any real number in eq 124, *not* limited to $s = 1, 0$, or -1 , where the corresponding value of parameter γ of constraint coordinate-momentum phase space is $\gamma = 1, (\sqrt{1+F} - 1)/F$, or 0 . This has been clearly mentioned in refs^{57, 58, 134}.

Any normalized pure state of the F -dimensional Hilbert space uniquely corresponds to a state on constraint coordinate-momentum phase space, $|\mathbf{x}, \mathbf{p}\rangle$, which is equivalent to $\exp[i\psi]|\boldsymbol{\theta}, \boldsymbol{\varphi}\rangle$ with ψ as the global phase. That is, the correspondence between $(\boldsymbol{\theta}, \boldsymbol{\varphi})$ and (\mathbf{x}, \mathbf{p}) is

$$\begin{pmatrix} x^{(n)} \\ p^{(n)} \end{pmatrix} = \sqrt{2(1+F\gamma)} \begin{pmatrix} \cos\psi & -\sin\psi \\ \sin\psi & \cos\psi \end{pmatrix} \begin{pmatrix} \text{Re}\langle n | \boldsymbol{\theta}, \boldsymbol{\varphi} \rangle \\ \text{Im}\langle n | \boldsymbol{\theta}, \boldsymbol{\varphi} \rangle \end{pmatrix}. \quad 130$$

Under the transformation, eq 130, mapping functions $A_C(\boldsymbol{\theta}, \boldsymbol{\varphi}; s) = \text{Tr}[\hat{A} \hat{K}_{\text{ele}}^{\text{SU}(F)}(\boldsymbol{\theta}, \boldsymbol{\varphi}; s)]$ and $A_C(\mathbf{x}, \mathbf{p}; \gamma) = \text{Tr}[\hat{A} \hat{K}_{\text{ele}}(\mathbf{x}, \mathbf{p}; \gamma)]$ of an operator \hat{A} share the same value. The global phase, ψ , which is missing in the $SU(F)$ Stratonovich phase space, however, is important for the expression of quantum dynamics.

When we consider quantum dynamics in a finite F -dimensional Hilbert space, if the Hamiltonian operator includes linear components beyond the identity operator and generator operators of phase space group, it is impossible to derive trajectory-based exact dynamics. The $SU(2)$ group involves the identity operator and angular momentum operators as generators on \mathbf{S}^2 sphere. It produces trajectory-based exact dynamics only for two-state systems, but fails to do so for all $F > 2$ cases. It is claimed that trajectory-based dynamics is a

good approximation for the large spin limit ($F \rightarrow \infty$) though^{109, 111, 302}. Except for the $F = 2$ case, the expression of quantum dynamics on the $SU(2)$ Stratonovich phase space has no direct relation to the trajectory-based exact dynamics on constrained coordinate-momentum phase space.

The $SU(F)$ Stratonovich phase space, however, produces trajectory-based exact dynamics for the finite F -dimensional Hilbert space. This is because that the evolution generated by any Hamiltonian of the F -dimensional Hilbert space is the action of some group element of $SU(F)$.³⁰³ The inherent symplectic structure of Stratonovich phase space indicates that the trajectory-based exact dynamics can be produced by the corresponding mapping Hamiltonian function $H_C = \text{Tr}[\hat{H}\hat{K}_{\text{ele}}^{\text{SU}(F)}(\boldsymbol{\theta}, \boldsymbol{\varphi}; s)]$, i.e.,

$$\begin{cases} \dot{\boldsymbol{\theta}}_i = -\sum_{j=1}^{F-1} \frac{A_{ji}}{(1+F)^{(1+s)/2}} \frac{\partial H_C}{\partial \varphi_j} \\ \dot{\boldsymbol{\varphi}}_i = +\sum_{j=1}^{F-1} \frac{A_{ij}}{(1+F)^{(1+s)/2}} \frac{\partial H_C}{\partial \theta_j} \end{cases} \quad 131$$

The elements, $\{A_{ij}\}$, of the $(F-1) \times (F-1)$ matrix, \mathbf{A} , are

$$A_{ij} = \begin{cases} \frac{1}{2} \csc(2\theta_1) \csc^2 \theta_{F-1} \prod_{k=2}^{F-2} \sec^2 \theta_k, & i = j = 1; \\ -\frac{1}{2} \cot(2\theta_1) \csc^2 \theta_{F-1} \prod_{k=2}^{F-2} \sec^2 \theta_k, & (i-1) = j = 1; \\ \csc(2\theta_i) \csc^2 \theta_{F-1} \prod_{k=i+1}^{F-2} \sec^2 \theta_k, & 2 \leq i = j \leq F-2; \\ -\frac{1}{2} \cot(\theta_i) \csc^2 \theta_{F-1} \prod_{k=i+1}^{F-2} \sec^2 \theta_k, & 2 \leq (i-1) = j \leq F-2; \\ -\csc(2\theta_{F-1}), & i = j = (F-1). \end{cases} \quad 132$$

The explicit expression of the EOMs of eq 131 is, however, much complicated. In addition, because trigonometric functions are involved in eq 132, singularities are inevitable in the EOMs on the $SU(F)$ Stratonovich phase space for $F > 2$. This makes the expression of quantum dynamics on the $SU(F)$ Stratonovich phase space numerically unfavorable. In comparison, on (weighted) constrained coordinate-momentum phase space, Hamilton's EOMs are simply linear in derivatives with coefficients independent of phase variables, as well as exact.

The relation of eq 130 implies that there exists a one-to-one correspondence between exact trajectory-base dynamics on the $SU(F)$ Stratonovich phase space and that on constraint coordinate-momentum phase space.

The addition of the global phase, ψ , is critical to obtain the one-to-one correspondence. The EOM of ψ reads

$$\dot{\psi} = \left[-\frac{\partial}{\partial \lambda} + \frac{\tan \theta_{F-1}}{2\lambda} \frac{\partial}{\partial \theta_{F-1}} \right] H_C^{(\lambda)}(\boldsymbol{\theta}, \boldsymbol{\phi}; s) \Big|_{\lambda=(1+F)^{\frac{1+s}{2}}}, \quad 133$$

where the extended mapping Hamiltonian function is defined by

$$H_C^{(\lambda)}(\boldsymbol{\theta}, \boldsymbol{\phi}; s) = \text{Tr} \left[\hat{K}_{\text{ele}}^{\text{SU}(F), (\lambda)}(\boldsymbol{\theta}, \boldsymbol{\phi}; s) \hat{H} \right] \quad 134$$

for the extended $\text{SU}(F)$ Stratonovich mapping ‘kernel’

$$\hat{K}_{\text{ele}}^{\text{SU}(F), (\lambda)}(\boldsymbol{\theta}, \boldsymbol{\phi}; s) = \lambda |\boldsymbol{\theta}, \boldsymbol{\phi}\rangle\langle\boldsymbol{\theta}, \boldsymbol{\phi}| + \frac{\hat{I}}{F} \left(1 - (1+F)^{\frac{1+s}{2}} \right). \quad 135$$

In eq 135 λ is treated as an ‘invariant’ variable. The evolution of state $\sqrt{\lambda} e^{i\psi} |\boldsymbol{\theta}, \boldsymbol{\phi}\rangle \equiv |\mathbf{x}, \mathbf{p}\rangle$ generates

$$\begin{cases} \dot{\lambda} = \frac{\partial}{\partial \psi} H_C^{(\lambda)}(\boldsymbol{\theta}, \boldsymbol{\phi}; s) = 0 \\ \dot{\psi} = \left[-\frac{\partial}{\partial \lambda} + \frac{\tan \theta_{F-1}}{2\lambda} \frac{\partial}{\partial \theta_{F-1}} \right] H_C^{(\lambda)}(\boldsymbol{\theta}, \boldsymbol{\phi}; s) \\ \dot{\theta}_i = -\sum_{j=1}^{F-1} \frac{A_{ji}}{\lambda} \frac{\partial}{\partial \phi_j} H_C^{(\lambda)}(\boldsymbol{\theta}, \boldsymbol{\phi}; s) - \delta_{i,F-1} \frac{\tan \theta_{F-1}}{2\lambda} \frac{\partial}{\partial \psi} H_C^{(\lambda)}(\boldsymbol{\theta}, \boldsymbol{\phi}; s) \\ \dot{\phi}_i = +\sum_{j=1}^{F-1} \frac{A_{ij}}{\lambda} \frac{\partial}{\partial \theta_j} H_C^{(\lambda)}(\boldsymbol{\theta}, \boldsymbol{\phi}; s) \end{cases}. \quad 136$$

It is straightforward to show that under the bijection,

$$\begin{pmatrix} \mathbf{x}^{(n)} \\ \mathbf{p}^{(n)} \end{pmatrix} = \sqrt{2\lambda} \begin{pmatrix} \cos \psi & -\sin \psi \\ \sin \psi & \cos \psi \end{pmatrix} \begin{pmatrix} \text{Re}\langle n | \boldsymbol{\theta}, \boldsymbol{\phi} \rangle \\ \text{Im}\langle n | \boldsymbol{\theta}, \boldsymbol{\phi} \rangle \end{pmatrix}, \quad 137$$

between variables $(\lambda, \psi, \boldsymbol{\theta}, \boldsymbol{\phi})$ and (\mathbf{x}, \mathbf{p}) , eq 136 leads to the EOMS of phase variables of (weighted) constraint phase space

$$\begin{aligned} \dot{\mathbf{x}}^{(n)} &= + \frac{\partial H_C}{\partial \mathbf{p}^{(n)}} \\ \dot{\mathbf{p}}^{(n)} &= - \frac{\partial H_C}{\partial \mathbf{x}^{(n)}} \end{aligned} \quad 138$$

by the chain rules, i.e.,

$$\begin{aligned}\mathbf{x}^{(n)} &= \sum_{i=1}^{2F} \frac{\partial \mathbf{x}^{(n)}}{\partial z_i} \mathbf{z}_i \\ \mathbf{p}^{(n)} &= \sum_{i=1}^{2F} \frac{\partial \mathbf{p}^{(n)}}{\partial z_i} \mathbf{z}_i\end{aligned}$$

139

and

$$\frac{\partial H_C}{\partial z_i} = \sum_{n=1}^F \frac{\partial \mathbf{x}^{(n)}}{\partial z_i} \frac{\partial H_C}{\partial \mathbf{x}^{(n)}} + \sum_{n=1}^F \frac{\partial \mathbf{p}^{(n)}}{\partial z_i} \frac{\partial H_C}{\partial \mathbf{p}^{(n)}}, \quad 140$$

where $\{z_i\}$ denote variables $\{\lambda, \psi, \theta, \phi\}$.

4. Marginal distribution functions on symmetrically weighted coordinate-momentum phase space

As demonstrated in Figure 5, the marginal distribution functions on symmetrically weighted constraint coordinate-momentum phase space demonstrate a hollow structure. Equation 51 leads to the marginal functions on symmetrically weighted coordinate-momentum phase space

$$\begin{aligned}K_{\uparrow\uparrow}(x^{(1)}, x^{(2)}) &= \frac{1-2\Delta^2+2\Delta}{4\Delta} \frac{1+(x^{(1)})^2/2-(x^{(2)})^2/2}{2\pi(1+2\Delta)} \Big|_{(x^{(1)})^2+(x^{(2)})^2 \leq 2(1+2\Delta)} \\ &\quad - \frac{1-2\Delta^2-2\Delta}{4\Delta} \frac{1+(x^{(1)})^2/2-(x^{(2)})^2/2}{2\pi(1-2\Delta)} \Big|_{(x^{(1)})^2+(x^{(2)})^2 \leq 2(1-2\Delta)} \\ K_{\uparrow\downarrow}(x^{(1)}, x^{(2)}) &= K_{\downarrow\uparrow}(x^{(1)}, x^{(2)}) = \frac{1-2\Delta^2+2\Delta}{4\Delta} \frac{x^{(1)}x^{(2)}}{2\pi(1+2\Delta)} \Big|_{(x^{(1)})^2+(x^{(2)})^2 \leq 2(1+2\Delta)} \\ &\quad - \frac{1-2\Delta^2-2\Delta}{4\Delta} \frac{x^{(1)}x^{(2)}}{2\pi(1-2\Delta)} \Big|_{(x^{(1)})^2+(x^{(2)})^2 \leq 2(1-2\Delta)} \\ K_{\downarrow\downarrow}(x^{(1)}, x^{(2)}) &= \frac{1-2\Delta^2+2\Delta}{4\Delta} \frac{1-(x^{(1)})^2/2+(x^{(2)})^2/2}{2\pi(1+2\Delta)} \Big|_{(x^{(1)})^2+(x^{(2)})^2 \leq 2(1+2\Delta)} \\ &\quad - \frac{1-2\Delta^2-2\Delta}{4\Delta} \frac{1-(x^{(1)})^2/2+(x^{(2)})^2/2}{2\pi(1-2\Delta)} \Big|_{(x^{(1)})^2+(x^{(2)})^2 \leq 2(1-2\Delta)}.\end{aligned} \quad 141$$

As $\Delta \rightarrow 0^+$, $K_{nm}(x^{(1)}, x^{(2)})$ approaches zero in region $(x^{(1)})^2 + (x^{(2)})^2 \leq 2(1-F\Delta)$, yielding the hollow structure.

References

1. Lee HW, Scully MO. A new approach to molecular-collisions - statistical quasiclassical method. *The Journal of Chemical Physics* 1980, 73:2238-2242.
2. Lee HW, Scully MO. The Wigner phase-space description of collision processes. *Foundations of Physics* 1983, 13:61-72.
3. Heller EJ. Wigner phase space method: Analysis for semiclassical applications. *The Journal of Chemical Physics* 1976, 65:1289.
4. Sun X, Wang H, Miller WH. Semiclassical theory of electronically nonadiabatic dynamics: Results of a linearized approximation to the initial value representation. *The Journal of Chemical Physics* 1998, 109:7064-7074.
5. Wang H, Sun X, Miller WH. Semiclassical approximations for the calculation of thermal rate constants for chemical reactions in complex molecular systems. *The Journal of Chemical Physics* 1998, 108:9726-9736.
6. Pollak E, Liao J-L. A new quantum transition state theory. *The Journal of Chemical Physics* 1998, 108:2733-2743.
7. Shao J, Liao J-L, Pollak E. Quantum transition state theory: Perturbation expansion. *The Journal of Chemical Physics* 1998, 108:9711-9725.
8. Hernandez R, Voth GA. Quantum time correlation functions and classical coherence. *Chemical Physics* 1998, 233:243-255.
9. Liu J, Miller WH. Using the thermal Gaussian approximation for the Boltzmann operator in semiclassical initial value time correlation functions. *The Journal of Chemical Physics* 2006, 125:224104.
10. Liu J, Miller WH. Linearized semiclassical initial value time correlation functions using the thermal Gaussian approximation: applications to condensed phase systems. *The Journal of Chemical Physics* 2007, 127:114506.
11. Liu J, Miller WH. Real time correlation function in a single phase space integral beyond the linearized semiclassical initial value representation. *The Journal of Chemical Physics* 2007, 126:234110.
12. Liu J, Miller WH. Linearized semiclassical initial value time correlation functions with maximum entropy analytic continuation. *The Journal of Chemical Physics* 2008, 129:124111.
13. Liu J, Miller WH. Test of the consistency of various linearized semiclassical initial value time correlation functions in application to inelastic neutron scattering from liquid para-hydrogen. *The Journal of Chemical Physics* 2008, 128:144511.
14. Liu J, Miller WH, Paesani F, Zhang W, Case DA. Quantum dynamical effects in liquid water: A semiclassical study on the diffusion and the infrared absorption spectrum. *The Journal of Chemical Physics* 2009, 131:164509.
15. Liu J, Miller WH. A simple model for the treatment of imaginary frequencies in chemical reaction rates and molecular liquids. *The Journal of Chemical Physics* 2009, 131:074113.
16. Liu J, Alder BJ, Miller WH. A semiclassical study of the thermal conductivity of low temperature liquids. *The Journal of Chemical Physics* 2011, 135:114105.
17. Liu J, Miller WH, Fanourgakis GS, Xantheas SS, Imoto S, Saito S. Insights in quantum dynamical effects in the infrared spectroscopy of liquid water from a semiclassical study with an ab initio-based flexible and polarizable force field. *The Journal of Chemical Physics* 2011, 135:244503.
18. Liu J. Recent advances in the linearized semiclassical initial value representation/classical Wigner model for the thermal correlation function. *International Journal of Quantum Chemistry* 2015, 115:657-670.
19. Liu X, Liu J. Critical role of quantum dynamical effects in the Raman spectroscopy of liquid water. *Molecular Physics* 2018, 116:755-779.
20. Shi Q, Geva E. Semiclassical theory of vibrational energy relaxation in the condensed phase. *Journal of Physical Chemistry A* 2003, 107:9059-9069.
21. Shi Q, Geva E. A relationship between semiclassical and centroid correlation functions. *The Journal of Chemical Physics* 2003, 118:8173-8184.
22. Ka BJ, Geva E. Vibrational energy relaxation of polyatomic molecules in liquid solution via the linearized semiclassical method. *Journal of Physical Chemistry A* 2006, 110:9555-9567.
23. Poulsen JA, Nyman G, Rossky PJ. Practical evaluation of condensed phase quantum correlation functions: A Feynman-Kleinert variational linearized path integral method. *The Journal of Chemical Physics* 2003, 119:12179-12193.
24. Poulsen JA, Nyman G, Rossky PJ. Feynman-Kleinert linearized path integral (FK-LPI) algorithms for quantum molecular dynamics, with application to water and He(4). *Journal of Chemical Theory and Computation* 2006, 2:1482-1491.
25. Shao J, Makri N. Forward-Backward Semiclassical Dynamics with Linear Scaling. *The Journal of Physical Chemistry A* 1999, 103:9479-9486.
26. Shao J, Makri N. Forward-Backward Semiclassical Dynamics without Prefactors. *The Journal of Physical Chemistry A* 1999, 103:7753-7756.
27. Liu J, Nakayama A, Makri N. Long-time behaviour of quantized distributions in forward-backward semiclassical dynamics. *Molecular Physics* 2006, 104:1267-1274.
28. Liu J, Makri N. Symmetries and detailed balance in forward-backward semiclassical dynamics. *Chemical Physics* 2006, 322:23-29.
29. Makri N, Nakayama A, Wright NJ. Forward-backward semiclassical simulation of dynamical properties in liquids. *Journal of Theoretical and Computational Chemistry* 2004, 3:391-417.

- 1
2
3 30. Makri N. Quantum-classical path integral: A rigorous approach to condensed phase dynamics. *International Journal of Quantum Chemistry* 2015, 115:1209-1214.
- 4 31. Walters PL, Makri N. Quantum-Classical Path Integral Simulation of Ferrocene-Ferrocenium Charge Transfer in Liquid Hexane. *Journal of Physical Chemistry Letters* 2015, 6:4959-4965.
- 5 32. Kryvohuz M, Cao JS. Quantum-classical correspondence in response theory. *Physical Review Letters* 2005, 95:180405.
- 6 33. Donoso A, Martens CC. Quantum tunneling using entangled classical trajectories. *Physical Review Letters* 2001, 87:223202.
- 7 34. Donoso A, Zheng Y, Martens CC. Simulation of quantum processes using entangled trajectory molecular dynamics. *Journal of Chemical Physics* 2003, 119:5010-5020.
- 8 35. Wang A, Zheng Y, Martens CC, Ren W. Quantum tunneling dynamics using entangled trajectories: general potentials. *Physical Chemistry Chemical Physics* 2009, 11:1588-1594.
- 9 36. Xu F, Martens CC, Zheng Y. Entanglement dynamics with a trajectory-based formulation. *Physical Review A* 2017, 96:022138.
- 10 37. Liu J, Miller WH. An approach for generating trajectory-based dynamics which conserves the canonical distribution in the phase space formulation of quantum mechanics. I. Theories. *The Journal of Chemical Physics* 2011, 134:104101.
- 11 38. Liu J, Miller WH. An approach for generating trajectory-based dynamics which conserves the canonical distribution in the phase space formulation of quantum mechanics. II. Thermal correlation functions. *The Journal of Chemical Physics* 2011, 134:104102.
- 12 39. Liu J. Two more approaches for generating trajectory-based dynamics which conserves the canonical distribution in the phase space formulation of quantum mechanics. *The Journal of Chemical Physics* 2011, 134:194110.
- 13 40. Liu J. Path integral Liouville dynamics for thermal equilibrium systems. *The Journal of Chemical Physics* 2014, 140:224107.
- 14 41. Liu J, Zhang Z. Path integral Liouville dynamics: Applications to infrared spectra of OH, water, ammonia, and methane. *The Journal of Chemical Physics* 2016, 144:034307.
- 15 42. Liu J, Li D, Liu X. Further study of path integral Liouville dynamics. *Scientia Sinica Chimica* 2016, 46:27-37.
- 16 43. Zhang Z, Chen Z, Liu J. Path integral Liouville dynamics simulations of vibrational spectra of formaldehyde and hydrogen peroxide. *Chinese Journal of Chemical Physics* 2020, 33:613-622.
- 17 44. Liu X, Zhang L, Liu J. Machine learning phase space quantum dynamics approaches. *The Journal of Chemical Physics* 2021, 154:184104.
- 18 45. Smith KKG, Poulsen JA, Nyman G, Cunsolo A, Rossky PJ. Application of a new ensemble conserving quantum dynamics simulation algorithm to liquid para-hydrogen and ortho-deuterium. *Journal of Chemical Physics* 2015, 142:244113.
- 19 46. Smith KKG, Poulsen JA, Nyman G, Rossky PJ. A new class of ensemble conserving algorithms for approximate quantum dynamics: Theoretical formulation and model problems. *Journal of Chemical Physics* 2015, 142:244112.
- 20 47. Willatt MJ, Ceriotti M, Althorpe SC. Approximating Matsubara dynamics using the planetary model: Tests on liquid water and ice. *Journal of Chemical Physics* 2018, 148:102336.
- 21 48. Orr L, de la Pena LH, Roy P-N. Formulation of state projected centroid molecular dynamics: Microcanonical ensemble and connection to the Wigner distribution. *Journal of Chemical Physics* 2017, 146:214116.
- 22 49. Bonella S, Montemayor D, Coker DF. Linearized path integral approach for calculating nonadiabatic time correlation functions. *Proceedings of the National Academy of Sciences* 2005, 102:6715-6719.
- 23 50. Nassimi A, Bonella S, Kapral R. Analysis of the quantum-classical Liouville equation in the mapping basis. *The Journal of Chemical Physics* 2010, 133:134115.
- 24 51. Weinrib J, Ferry DK. Recent advances in Wigner function approaches. *Applied Physics Reviews* 2018, 5:041104.
- 25 52. Pie T, Huppert S, Finocchi F, Depondt P, Bonella S. Sampling the thermal Wigner density via a generalized Langevin dynamics. *Journal of Chemical Physics* 2019, 151:114114.
- 26 53. Kapral R, Ciccotti G. Mixed quantum-classical dynamics. *The Journal of Chemical Physics* 1999, 110:8919-8929.
- 27 54. Kapral R. Quantum dynamics in open quantum-classical systems. *Journal of Physics: Condensed Matter* 2015, 27:073201.
- 28 55. Bai S, Xie W, Zhu L, Shi Q. Calculation of absorption spectra involving multiple excited states: Approximate methods based on the mixed quantum classical Liouville equation. *Journal of Chemical Physics* 2014, 140:084105.
- 29 56. Tao G, Miller WH. Semiclassical Description of Electronic Excitation Population Transfer in a Model Photosynthetic System. *Journal of Physical Chemistry Letters* 2010, 1:891-894.
- 30 57. He X, Wu B, Gong Z, Liu J. Commutator Matrix in Phase Space Mapping Models for Nonadiabatic Quantum Dynamics. *The Journal of Physical Chemistry A* 2021, 125:6845-6863.
- 31 58. Liu J, He X, Wu B. Unified Formulation of Phase Space Mapping Approaches for Nonadiabatic Quantum Dynamics. *Accounts of chemical research* 2021, 54:4215-4228.

- 1
2
3 59. Orioli AP, Safavi-Naini A, Wall ML, Rey AM. Nonequilibrium dynamics of spin-boson models from phase-space methods. *Physical Review A* 2017, 96:033607.
4
5 60. Lang H, Vendrell O, Hauke P. Generalized discrete truncated Wigner approximation for nonadiabatic quantum-classical dynamics. *Journal of Chemical Physics* 2021, 155:024111.
6
7 61. Glauber RJ. Coherent and Incoherent States of Radiation Field. *Physical Review* 1963, 131:2766.
8
9 62. Sudarshan ECG. Equivalence of Semiclassical and Quantum Mechanical Descriptions of Statistical Light Beams. *Physical Review Letters* 1963, 10:277.
10
11 63. Cahill KE, Glauber RJ. Ordered expansions in boson amplitude operators. *Physical Review* 1969, 177:1857.
12
13 64. Cahill KE, Glauber RJ. Density operators and quasiprobability distributions. *Physical Review* 1969, 177:1882.
14
15 65. Arechi FT, Thomas H, Gilmore R, Courtens E. Atomic coherent states in quantum optics. *Physical Review A* 1972, 6:2211.
16
17 66. Drummond PD, Gardiner CW. Generalized P-Representations in Quantum Optics. *Journal of Physics A: Mathematical and General* 1980, 13:2353-2368.
18
19 67. Walls D, Millburn G. *Quantum Optics*. Berlin: Springer-Verlag; 1994.
20
21 68. Gardiner C, Zoller P. *Quantum Noise*. 3rd edition ed. Berlin Heidelberg: Springer-Verlag; 2004.
22
23 69. Schleich WP. Quantum Optics in Phase Space. *Quantum Optics in Phase Space* 2001:716.
24
25 70. Deleglise S, Dotsenko I, Sayrin C, Bernu J, Brune M, Raimond JM, Haroche S. Reconstruction of non-classical cavity field states with snapshots of their decoherence. *Nature* 2008, 455:510-514.
26
27 71. Steel MJ, Olsen MK, Plimak LI, Drummond PD, Tan SM, Collett MJ, Walls DF, Graham R. Dynamical quantum noise in trapped Bose-Einstein condensates. *Physical Review A* 1998, 58:4824-4835.
28
29 72. Sinatra A, Lobo C, Castin Y. The truncated Wigner method for Bose-condensed gases: limits of validity and applications. *Journal of Physics B: Atomic Molecular and Optical Physics* 2002, 35:3599-3631.
30
31 73. Blakie PB, Bradley AS, Davis MJ, Ballagh RJ, Gardiner CW. Dynamics and statistical mechanics of ultra-cold Bose gases using c-field techniques. *Advances in Physics* 2008, 57:363-455.
32
33 74. Polkovnikov A. Phase space representation of quantum dynamics. *Annals of Physics* 2010, 325:1790-1852.
34
35 75. Mukherjee R, Mirasola AE, Hollingsworth J, White IG, Hazzard KRA. Geometric representation of spin correlations and applications to ultracold systems. *Physical Review A* 2018, 97:043606.
36
37 76. Zurek WH. Sub-Planck structure in phase space and its relevance for quantum decoherence. *Nature* 2001, 412:712-717.
38
39 77. Miquel C, Paz JP, Saraceno M. Quantum computers in phase space. *Physical Review A* 2002, 65:062309.
40
41 78. Wootters WK. Picturing Qubits in Phase Space. *IBM Journal of Research and Development* 2004, 48:99-110.
42
43 79. Paz JP, Roncaglia AJ, Saraceno M. Qubits in phase space: Wigner-function approach to quantum-error correction and the mean-king problem. *Physical Review A* 2005, 72:012309.
44
45 80. Braunstein SL, van Loock P. Quantum information with continuous variables. *Reviews of Modern Physics* 2005, 77:513-577.
46
47 81. Delfosse N, Guerin PA, Bian J, Raussendorf R. Wigner function negativity and contextuality in quantum computation on rebits. *Physical Review X* 2015, 5:021003.
48
49 82. Schachenmayer J, Pikovski A, Rey AM. Many-Body Quantum Spin Dynamics with Monte-Carlo Trajectories on a Discrete Phase Space. *Physical Review X* 2015, 5:011022.
50
51 83. Schachenmayer J, Pikovski A, Rey AM. Dynamics of correlations in two-dimensional quantum spin models with long-range interactions: a phase-space Monte-Carlo study. *New Journal of Physics* 2015, 17:065009.
52
53 84. Bermejo-Vega J, Delfosse N, Browne DE, Okay C, Raussendorf R. Contextuality as a resource for models of quantum computation with qubits. *Physical Review Letters* 2017, 119:120505.
54
55 85. Rundle RP, Mills PW, Tilma T, Samson JH, Everitt MJ. Simple procedure for phase-space measurement and entanglement validation. *Physical Review A* 2017, 96:022117.
56
57 86. Zhu B, Rey AM, Schachenmayer J. A generalized phase space approach for solving quantum spin dynamics. *New Journal of Physics* 2019, 21:082001.
58
59 87. Rundle RP, Everitt MJ. Overview of the Phase Space Formulation of Quantum Mechanics with Application to Quantum Technologies. *Advanced Quantum Technologies* 2021, 4:2100016.
60
61 88. Weyl H. Quantum mechanics and Group theory. *Zeitschrift Fur Physik* 1927, 46:1-46.
62
63 89. Wigner E. On the Quantum Correction For Thermodynamic Equilibrium. *Physical Review* 1932, 40:749-759.
64
65 90. Hillery M, Oconnell RF, Scully MO, Wigner EP. Distribution-functions in physics - fundamentals. *Physics Reports-Review Section of Physics Letters* 1984, 106:121-167.

- 1
2
3 91. Lee HW. Theory and Application of the Quantum Phase-Space Distribution Functions. *Physics Reports-Review Section of Physics Letters* 1995,
4 259:147-211.
5 92. Cohen L. Generalized Phase-Space Distribution Functions. *Journal of Mathematical Physics* 1966, 7:781-786.
6 93. Groenewold HJ. On the Principles of Elementary Quantum Mechanics. *Physica* 1946, 12:405-460.
7 94. Moyal JE. Quantum mechanics as a statistical theory. *Mathematical Proceedings of the Cambridge Philosophical Society* 1949, 45:99-124.
8 95. Bopp F. *Werner Heisenberg und die Physik unserer Zeit*. Braunschweig: Vieweg; 1961.
9 96. Miller WH. Quantum dynamics of complex molecular systems. *Proceedings of the National Academy of Sciences* 2005, 102:6660-6664.
10 97. Miller WH. Including quantum effects in the dynamics of complex (i.e., large) molecular systems. *The Journal of Chemical Physics* 2006,
11 125:132305.
12 98. Miller WH. Classical-limit quantum mechanics and the theory of molecular collisions. *Advances in Chemical Physics* 1974, 25:69-177.
13 99. Miller WH. The classical S-matrix in molecular collisions. *Advances in Chemical Physics* 1975, 30:77.
14 100. Stratonovich RL. On distributions in representation space. *Zh. Eksp. Teor. Fiz.* 1956, 31:1012.
15 101. Feynman RP. Negative probability. In: Hiley BJ, Peat D, eds. *Quantum Implications: Essays in Honour of David Bohm*. New York: Routledge;
16 1987, 235-248.
17 102. Wootters WK. A Wigner-function formulation of finite-state quantum mechanics. *Annals of Physics* 1987, 176:1-21.
18 103. Várilly JC, Gracia-Bondía J. The Moyal representation for spin. *Annals of Physics* 1989, 190:107-148.
19 104. Amiet JP, Cibils MB. Description of quantum spin using functions on the sphere S^2 . *Journal of Physics A: Mathematical and General* 1991,
20 24:1515-1535.
21 105. Amiet JP, Weigert S. Discrete Q- and P-symbols for spin s . *Journal of Optics B-Quantum and Semiclassical Optics* 2000, 2:118-121.
22 106. Dowling JP, Agarwal GS, Schleich WP. Wigner distribution of a general angular-momentum state - Applications to a collection of 2-level atoms.
23 *Physical Review A* 1994, 49:4101-4109.
24 107. Brif C, Mann A. Phase-space Formulation of Quantum Mechanics and Quantum-state Reconstruction for Physical Systems with Lie-group
25 Symmetries. *Physical Review A* 1999, 59:971-987.
26 108. Cunha MOT, Man'ko VI, Scully MO. Quasiprobability and probability distributions for spin-1/2 states. *Foundations of Physics Letters* 2001,
27 14:103-117.
28 109. Klimov AB, Espinoza P. Moyal-like form of the star product for generalized $SU(2)$ Stratonovich-Weyl symbols. *Journal of Physics A: Mathematical
29 and General* 2002, 35:8435-8447.
30 110. Klimov AB, Romero JL. A Generalized Wigner Function for Quantum Systems with the $SU(2)$ Dynamical Symmetry Group. *Journal of Physics
31 A: Mathematical and Theoretical* 2008, 41:055303.
32 111. Klimov AB, Romero JL, de Guise H. Generalized $SU(2)$ Covariant Wigner Functions and Some of Their Applications. *Journal of Physics A:
33 Mathematical and Theoretical* 2017, 50:323001.
34 112. Adam P, Andreev VA, Man'ko MA, Man'ko VI, Mechler M. $SU(2)$ Symmetry of Qubit States and Heisenberg-Weyl Symmetry of Systems with
35 Continuous Variables in the Probability Representation of Quantum Mechanics. *Symmetry-Basel* 2020, 12:23.
36 113. Koczor B, Zeier R, Glaser SJ. Continuous Phase-space Representations for Finite-dimensional Quantum States and Their Tomography. *Physical
37 Review A* 2020, 101:022318.
38 114. Tilma T, Nemoto K. $SU(N)$ -symmetric quasi-probability distribution functions. *Journal of Physics A: Mathematical and Theoretical* 2012, 45:14.
39 115. Tilma T, Everitt MJ, Samson JH, Munro WJ, Nemoto K. Wigner Functions for Arbitrary Quantum Systems. *Physical Review Letters* 2016,
40 117:180401.
41 116. Marchiolli MA, Galetti D. On the discrete Wigner function for $SU(N)$. *Journal of Physics A: Mathematical and Theoretical* 2019, 52:405305.
42 117. Rundle RP, Tilma T, Samson JH, Dwyer VM, Bishop RF, Everitt MJ. General Approach to Quantum Mechanics As a Statistical Theory. *Physical
43 Review A* 2019, 99:012115.
44 118. Cohenet O, Combe P, Sirugue M, Siruguecollin M. A stochastic treatment of the dynamics of an integer spin. *Journal of Physics A:
45 Mathematical and General* 1988, 21:2875-2883.
46 119. Leonhardt U. Quantum-state tomography and discrete Wigner function. *Physical Review Letters* 1995, 74:4101-4105.
47 120. Leonhardt U. Discrete Wigner function and quantum-state tomography. *Physical Review A* 1996, 53:2998-3013.
48 121. Gibbons KS, Hoffman MJ, Wootters WK. Discrete phase space based on finite fields. *Physical Review A* 2004, 70:062101.
49 122. Wootters WK. Quantum Measurements and Finite Geometry. *Foundations of Physics* 2006, 36:112-126.
50 123. Ruzzi M, Marchiolli MA, Galetti D. Extended Cahill-Glauber formalism for finite-dimensional spaces: I. Fundamentals. *Journal of Physics A:
51 Mathematical and General* 2005, 38:6239-6251.
52
53
54
55
56
57
58
59
60

- 1
2
3
4
5
6
7
8
9
10
11
12
13
14
15
16
17
18
19
20
21
22
23
24
25
26
27
28
29
30
31
32
33
34
35
36
37
38
39
40
41
42
43
44
45
46
47
48
49
50
51
52
53
54
55
56
57
58
59
60
124. Chaturvedi S, Ercolessi E, Marmo G, Morandi G, Mukunda N, Simon R. Wigner distributions for finite dimensional quantum systems: An algebraic approach. *Pramana* 2005, 65:981-993.
125. Chaturvedi S, Ercolessi E, Marmo G, Morandi G, Mukunda N, Simon R. Wigner-Weyl correspondence in quantum mechanics for continuous and discrete systems-a Dirac-inspired view. *Journal of Physics A: Mathematical and General* 2006, 39:1405-1423.
126. Gross D. Hudson's theorem for finite-dimensional quantum systems. *Journal of Mathematical Physics* 2006, 47:25.
127. Valtierra IF, Romero JL, Klimov AB. TWA versus semiclassical unitary approximation for spin-like systems. *Annals of Physics* 2017, 383:620-634.
128. Valtierra IF, Klimov AB, Leuchs G, Sánchez-Soto LL. Quasiprobability currents on the sphere. *Physical Review A* 2020, 101:033803.
129. Czischek S. Discrete Truncated Wigner Approximation. In: *Springer Theses*: Springer International Publishing; 2020, 85-109.
130. Morales-Hernández GE, Castellanos JC, Romero JL, Klimov AB. Semi-classical Discretization and Long-time Evolution of Variable Spin Systems. *Entropy* 2021, 23:684.
131. Liu J. A unified theoretical framework for mapping models for the multi-state Hamiltonian. *The Journal of Chemical Physics* 2016, 145:204105.
132. He X, Liu J. A new perspective for nonadiabatic dynamics with phase space mapping models. *The Journal of Chemical Physics* 2019, 151:024105.
133. Liu J. Isomorphism between the multi-state Hamiltonian and the second-quantized many-electron Hamiltonian with only 1-electron interactions. *The Journal of Chemical Physics* 2017, 146:024110.
134. He X, Gong Z, Wu B, Liu J. Negative Zero-Point-Energy Parameter in the Meyer-Miller Mapping Model for Nonadiabatic Dynamics. *The journal of physical chemistry letters* 2021, 12:2496-2501.
135. Domcke W, Yarkony DR, Köppel H. *Conical Intersections: Theory, Computation and Experiment*. Singapore: World Scientific; 2011.
136. Yonehara T, Hanasaki K, Takatsuka K. Fundamental Approaches to Nonadiabaticity: Toward a Chemical Theory beyond the Born-Oppenheimer Paradigm. *Chemical Reviews* 2011, 112:499-542.
137. Tully JC. Perspective: Nonadiabatic dynamics theory. *The Journal of Chemical Physics* 2012, 137:22A301.
138. Miller WH, Cotton SJ. Classical molecular dynamics simulation of electronically non-adiabatic processes. *Faraday Discussions* 2016, 195:9-30.
139. Levine BG, Martinez TJ. Isomerization through conical intersections. *Annual Review of Physical Chemistry* 2007, 58:613-634.
140. Martinez TJ. Seaming is believing. *Nature* 2010, 467:412-413.
141. Sisto A, Glowacki DR, Martinez TJ. Ab Initio Nonadiabatic Dynamics of Multichromophore Complexes: A Scalable Graphical-Processing-Unit-Accelerated Exciton Framework. *Accounts of Chemical Research* 2014, 47:2857-2866.
142. Makarov DV, Glover WJ, Martinez TJ, Shalashilin DV. Ab initio multiple cloning algorithm for quantum nonadiabatic molecular dynamics. *The Journal of Chemical Physics* 2014, 141:054110.
143. Mai S, Marquetand P, Gonzalez L. Nonadiabatic dynamics: The SHARC approach. *Wiley Interdisciplinary Reviews-Computational Molecular Science* 2018, 8:e1370.
144. Mai S, Gonzalez L. Molecular Photochemistry: Recent Developments in Theory. *Angewandte Chemie-International Edition* 2020, 59:16832-16846.
145. Subotnik JE, Jain A, Landry B, Petit A, Ouyang W, Bellonzi N. Understanding the Surface Hopping View of Electronic Transitions and Decoherence. In: Johnson MA, Martinez TJ, eds. *Annual Review of Physical Chemistry*, Vol 67. Vol. 67: Annual Reviews; 2016, 387-417.
146. Fang W-H. Ab Initio Determination of Dark Structures in Radiationless Transitions for Aromatic Carbonyl Compounds. *Accounts of Chemical Research* 2008, 41:452-457.
147. Long R, Prezhdo OV, Fang W-H. Nonadiabatic charge dynamics in novel solar cell materials. *Wiley Interdisciplinary Reviews-Computational Molecular Science* 2017, 7:e1305.
148. Feng W, Xu L, Li X-Q, Fang W-H, Yan Y. Nonadiabatic molecular dynamics simulation: An approach based on quantum measurement picture. *AIP Advances* 2014, 4:077131.
149. Lan Z, Shao J. Approximate Theoretical Methods for Nonadiabatic Dynamics of Polyatomic Molecules. *Progress in Chemistry* 2012, 24:1105-1119.
150. Wang Y-C, Ke Y, Zhao Y. The hierarchical and perturbative forms of stochastic Schrödinger equations and their applications to carrier dynamics in organic materials. *Wiley Interdisciplinary Reviews-Computational Molecular Science* 2019, 9:e1375.
151. Nelson T, Fernandez-Alberti S, Roitberg AE, Tretiak S. Nonadiabatic Excited-State Molecular Dynamics: Modeling Photophysics in Organic Conjugated Materials. *Accounts of Chemical Research* 2014, 47:1155-1164.
152. Crespo-Otero R, Barbatti M. Recent Advances and Perspectives on Nonadiabatic Mixed Quantum-Classical Dynamics. *Chemical Reviews* 2018, 118:7026-7068.

- 1
2
3 153. Meyer H-D, Miller WH. A classical analog for electronic degrees of freedom in nonadiabatic collision processes. *The Journal of Chemical Physics* 1979, 70:3214-3223.
- 4 154. Stock G, Thoss M. Semiclassical description of nonadiabatic quantum dynamics. *Physical Review Letters* 1997, 78:578-581.
- 5 155. Wigner EP. *Perspectives in Quantum Theory*. Cambridge: MIT; 1971.
- 6 156. Husimi K. Some Formal Properties of the Density Matrix. *Proceedings of the Physico-Mathematical Society of Japan* 1940, 22:264-314.
- 7 157. Glauber RJ. Optical Coherence and Photon Statistics. In: deWitt C, Blandin A, C. C-T, eds. *Quantum Optics and Electronics*. New York: Gordon and Breach; 1965.
- 8 158. Kirkwood JG. Quantum Statistics of Almost Classical Assemblies. *Physical Review* 1933, 44:31.
- 9 159. Rihaczek AW. Signal Energy Distribution in Time and Frequency. *IEEE Transactions on Information Theory* 1968, 14:369-374.
- 10 160. Mehta CL. Phase-Space Formulation of the Dynamics of Canonical Variables. *Journal of Mathematical Physics* 1964, 5:677-686.
- 11 161. Rivier DC. On a One-to-One Correspondence between Infinitesimal Canonical Transformations and Infinitesimal Unitary Transformations. *Physical Review* 1951, 83:862.
- 12 162. Margenau H, Hill RN. Correlation between Measurements in Quantum Theory. *Progress of Theoretical Physics* 1961, 26:722-738.
- 13 163. Born M, Jordan P. On quantum mechanics. *Zeitschrift fur Physik* 1925, 34:858-888.
- 14 164. Meyer H-D, Miller WH. Classical-Models for Electronic Degrees of Freedom: Derivation Via Spin Analogy and Application to $F^* + H_2 \rightarrow F + H_2$. *The Journal of Chemical Physics* 1979, 71:2156-2169.
- 15 165. Gray SK, Miller WH. Classical model for electronic degrees of freedom: charge transfer in Na + I collisions. *Chemical Physics Letters* 1982, 93:341-344.
- 16 166. Ali DP, Miller WH. Effect of electronic transition dynamics on iodine atom recombination in liquids. *The Journal of Chemical Physics* 1983, 78:6640-6645.
- 17 167. Ali DP, Miller WH. Classical models for electronic degrees of freedom: Quenching of Br*(2P1/2) by collision with H₂ in three dimensions. *Chemical Physics Letters* 1984, 103:470-474.
- 18 168. Stock G, Miller WH. A classical model for time- and frequency-resolved spectroscopy of nonadiabatic excited-state dynamics. *Chemical Physics Letters* 1992, 197:396-404.
- 19 169. Stock G, Miller WH. Classical formulation of the spectroscopy of nonadiabatic excited-state dynamics. *The Journal of Chemical Physics* 1993, 99:1545-1555.
- 20 170. Sun X, Miller WH. Semiclassical initial value representation for electronically nonadiabatic molecular dynamics. *The Journal of Chemical Physics* 1997, 106:6346-6353.
- 21 171. Coronado EA, Batista VS, Miller WH. Nonadiabatic photodissociation dynamics of CN in the A continuum: A semiclassical initial value representation study. *The Journal of Chemical Physics* 2000, 112:5566-5575.
- 22 172. Coronado EA, Xing J, Miller WH. Ultrafast non-adiabatic dynamics of systems with multiple surface crossings: a test of the Meyer-Miller Hamiltonian with semiclassical initial value representation methods. *Chemical Physics Letters* 2001, 349:521-529.
- 23 173. Ananth N, Venkataraman C, Miller WH. Semiclassical description of electronically nonadiabatic dynamics via the initial value representation. *The Journal of Chemical Physics* 2007, 127:084114.
- 24 174. Miller WH. Electronically Nonadiabatic Dynamics via Semiclassical Initial Value Methods. *Journal of Physical Chemistry A* 2009, 113:1405-1415.
- 25 175. Ananth N, Miller TF. Exact quantum statistics for electronically nonadiabatic systems using continuous path variables. *The Journal of Chemical Physics* 2010, 133:234103.
- 26 176. Cotton SJ, Miller WH. Symmetrical Windowing for Quantum States in Quasi-Classical Trajectory Simulations. *Journal of Physical Chemistry A* 2013, 117:7190-7194.
- 27 177. Cotton SJ, Miller WH. Symmetrical windowing for quantum states in quasi-classical trajectory simulations: Application to electronically non-adiabatic processes. *The Journal of Chemical Physics* 2013, 139:234112.
- 28 178. Cotton SJ, Igumenshchev K, Miller WH. Symmetrical windowing for quantum states in quasi-classical trajectory simulations: Application to electron transfer. *The Journal of Chemical Physics* 2014, 141:084104.
- 29 179. Cotton SJ, Miller WH. A Symmetrical Quasi-Classical Spin-Mapping Model for the Electronic Degrees of Freedom in Non-Adiabatic Processes. *Journal of Physical Chemistry A* 2015, 119:12138-12145.
- 30 180. Miller WH, Cotton SJ. Communication: Note on detailed balance in symmetrical quasi-classical models for electronically non-adiabatic dynamics. *The Journal of Chemical Physics* 2015, 142:131103.
- 31 181. Cotton SJ, Miller WH. A new symmetrical quasi-classical model for electronically non-adiabatic processes: Application to the case of weak non-adiabatic coupling. *The Journal of Chemical Physics* 2016, 145:144108.

- 1
2
3
4
5
6
7
8
9
10
11
12
13
14
15
16
17
18
19
20
21
22
23
24
25
26
27
28
29
30
31
32
33
34
35
36
37
38
39
40
41
42
43
44
45
46
47
48
49
50
51
52
53
54
55
56
57
58
59
60
182. Cotton SJ, Miller WH. The Symmetrical Quasi-Classical Model for Electronically Non-Adiabatic Processes Applied to Energy Transfer Dynamics in Site-Exciton Models of Light-Harvesting Complexes. *Journal of Chemical Theory and Computation* 2016, 12:983-991.
183. Miller WH, Cotton SJ. Communication: Wigner functions in action-angle variables, Bohr-Sommerfeld quantization, the Heisenberg correspondence principle, and a symmetrical quasi-classical approach to the full electronic density matrix. *The Journal of Chemical Physics* 2016, 145:081102.
184. Cotton SJ, Liang R, Miller WH. On the adiabatic representation of Meyer-Miller electronic-nuclear dynamics. *The Journal of Chemical Physics* 2017, 147:064112.
185. Liang R, Cotton SJ, Binder R, Hegger R, Burghardt I, Miller WH. The symmetrical quasi-classical approach to electronically nonadiabatic dynamics applied to ultrafast exciton migration processes in semiconducting polymers. *The Journal of Chemical Physics* 2018, 149:044101.
186. Cotton SJ, Miller WH. A symmetrical quasi-classical windowing model for the molecular dynamics treatment of non-adiabatic processes involving many electronic states. *The Journal of Chemical Physics* 2019, 150:104101.
187. Cotton SJ, Miller WH. Trajectory-adjusted electronic zero point energy in classical Meyer-Miller vibronic dynamics: Symmetrical quasiclassical application to photodissociation. *The Journal of Chemical Physics* 2019, 150:194110.
188. Muller U, Stock G. Flow of zero-point energy and exploration of phase space in classical simulations of quantum relaxation dynamics. II. Application to nonadiabatic processes. *Journal of Chemical Physics* 1999, 111:77-88.
189. Stock G, Muller U. Flow of zero-point energy and exploration of phase space in classical simulations of quantum relaxation dynamics. *Journal of Chemical Physics* 1999, 111:65-76.
190. Stock G, Muller U. Flow of zero-point energy and exploration of phase space in classical simulations of quantum relaxation dynamics. II. application to nonadiabatic processes. *The Journal of Chemical Physics* 1999, 111:77-88.
191. Stock G, Thoss M. Classical Description of Nonadiabatic Quantum Dynamics. In: Rice SA, ed. *Advances in Chemical Physics*. Vol. 131: John Wiley and Sons, Inc.; 2005, 243-375.
192. Thoss M, Miller WH, Stock G. Semiclassical description of nonadiabatic quantum dynamics: Application to the S1-S2 conical intersection in pyrazine. *The Journal of Chemical Physics* 2000, 112:10282-10292.
193. Thoss M, Stock G. Mapping approach to the semiclassical description of nonadiabatic quantum dynamics. *Physical Review A* 1999, 59:64-79.
194. Golosov AA, Reichman DR. Classical mapping approaches for nonadiabatic dynamics: Short time analysis. *The Journal of Chemical Physics* 2001, 114:1065-1074.
195. Saller MAC, Kelly A, Richardson JO. On the identity of the identity operator in nonadiabatic linearized semiclassical dynamics. *The Journal of Chemical Physics* 2019, 150:071101.
196. Saller MAC, Kelly A, Richardson JO. Improved population operators for multi-state nonadiabatic dynamics with the mixed quantum-classical mapping approach. *Faraday Discussions* 2020, 221:150-167.
197. Runeson JE, Richardson JO. Generalized spin mapping for quantum-classical dynamics. *The Journal of Chemical Physics* 2020, 152:084110.
198. Kananenka AA, Hsieh CY, Cao JS, Geva E. Nonadiabatic Dynamics via the Symmetrical Quasi-Classical Method in the Presence of Anharmonicity. *Journal of Physical Chemistry Letters* 2018, 9:319-326.
199. Mulvihill E, Gao X, Liu Y, Schubert A, Dunietz BD, Geva E. Combining the mapping Hamiltonian linearized semiclassical approach with the generalized quantum master equation to simulate electronically nonadiabatic molecular dynamics. *The Journal of Chemical Physics* 2019, 151:074103.
200. Gao X, Geva E. Improving the Accuracy of Quasiclassical Mapping Hamiltonian Methods by Treating the Window Function Width as an Adjustable Parameter. *Journal of Physical Chemistry A* 2020, 124:11006-11016.
201. Gao X, Lai Y, Geva E. Simulating Absorption Spectra of Multiexcitonic Systems via Quasiclassical Mapping Hamiltonian Methods. *Journal of Chemical Theory and Computation* 2020, 16:6465-6480.
202. Gao X, Sailer MAC, Liu Y, Kelly A, Richardson JO, Geva E. Benchmarking Quasiclassical Mapping Hamiltonian Methods for Simulating Electronically Nonadiabatic Molecular Dynamics. *Journal of Chemical Theory and Computation* 2020, 16:2883-2895.
203. Liu Y, Gao X, Lai Y, Mulvihill E, Geva E. Electronic Dynamics through Conical Intersections via Quasiclassical Mapping Hamiltonian Methods. *Journal of Chemical Theory and Computation* 2020, 16:4479-4488.
204. Saller MAC, Kelly A, Geva E. Benchmarking Quasiclassical Mapping Hamiltonian Methods for Simulating Cavity-Modified Molecular Dynamics. *Journal of Physical Chemistry Letters* 2021, 12:3163-3170.
205. Bonella S, Coker DF. A semiclassical limit for the mapping Hamiltonian approach to electronically nonadiabatic dynamics. *The Journal of Chemical Physics* 2001, 114:7778-7789.
206. Bonella S, Coker DF. Semiclassical implementation of the mapping Hamiltonian approach for nonadiabatic dynamics using focused initial distribution sampling. *The Journal of Chemical Physics* 2003, 118:4370-4385.

- 1
2
3 207. Bonella S, Coker DF. LAND-map, a linearized approach to nonadiabatic dynamics using the mapping formalism. *The Journal of Chemical Physics* 2005, 122:194102.
4
5 208. Huo PF, Coker DF. Semi-classical path integral non-adiabatic dynamics: a partial linearized classical mapping Hamiltonian approach. *Molecular Physics* 2012, 110:1035-1052.
6
7 209. Tang D, Fang W-H, Shen L, Cui G. Combining Meyer-Miller Hamiltonian with electronic structure methods for on-the-fly nonadiabatic dynamics
8 simulations: implementation and application. *Physical Chemistry Chemical Physics* 2019, 21:17109-17117.
9
10 210. Zheng J, Xie Y, Jiang S, Long Y, Ning X, Lan Z. Ultrafast Electron Transfer with Symmetrical Quasi-classical Dynamics based on Mapping
11 Hamiltonian and Quantum Dynamics based on ML-MCTDH. *Chinese Journal of Chemical Physics* 2017, 30:800-810.
12
13 211. Xie Y, Zheng J, Lan Z. Performance evaluation of the symmetrical quasi-classical dynamics method based on Meyer-Miller mapping Hamiltonian
14 in the treatment of site-exciton models. *The Journal of Chemical Physics* 2018, 149:174105.
15
16 212. Zheng J, Xie Y, Jiang S, Long Y, Ning X, Lan Z. Initial sampling in symmetrical quasiclassical dynamics based on Li-Miller mapping Hamiltonian.
17 *Physical Chemistry Chemical Physics* 2019, 21:26502-26514.
18
19 213. Zheng J, Peng J, Xie Y, Long Y, Ning X, Lan Z. Study of the exciton dynamics in perylene bisimide (PBI) aggregates with symmetrical
20 quasiclassical dynamics based on the Meyer-Miller mapping Hamiltonian. *Physical Chemistry Chemical Physics* 2020, 22:18192-18204.
21
22 214. Peng J, Xie Y, Hu D, Lan Z. Analysis of bath motion in MM-SQC dynamics via dimensionality reduction approach: Principal component analysis.
23 *The Journal of Chemical Physics* 2021, 154:094122.
24
25 215. Hu D, Xie Y, Peng J, Lan Z. On-the-Fly Symmetrical Quasi-Classical Dynamics with Meyer-Miller Mapping Hamiltonian for the Treatment of
26 Nonadiabatic Dynamics at Conical Intersections. *Journal of Chemical Theory and Computation* 2021, 17:3267-3279.
27
28 216. Tao G. A multi-state trajectory method for non-adiabatic dynamics simulations. *The Journal of Chemical Physics* 2016, 144:094108.
29
30 217. Tao G. Coherence-Controlled Nonadiabatic Dynamics via State-Space Decomposition: A Consistent Way To Incorporate Ehrenfest and Born-
31 Oppenheimer-Like Treatments of Nuclear Motion. *Journal of Physical Chemistry Letters* 2016, 7:4335-4339.
32
33 218. Tao G. Multi-state trajectory approach to non-adiabatic dynamics: General formalism and the active state trajectory approximation. *The Journal
34 of Chemical Physics* 2017, 147:044107.
35
36 219. Schwinger J. In: Biedenharn LC, VanDam H, eds. *Quantum Theory of Angular Momentum*. New York: Academic; 1965.
37
38 220. Sakurai JJ. *Modern Quantum Mechanics*. New York: Addison-Wesley; 1994.
39
40 221. Flammia ST, Liu Y-K. Direct Fidelity Estimation from Few Pauli Measurements. *Physical Review Letters* 2011, 106:230501.
41
42 222. Sperling J, Walmsley IA. Quasiprobability representation of quantum coherence. *Physical Review A* 2018, 97:062327.
43
44 223. Bohmann M, Agudelo E, Sperling J. Probing nonclassicality with matrices of phase-space distributions. *Quantum* 2020, 4:16.
45
46 224. Bohmann M, Agudelo E. Phase-space inequalities beyond negativities. *Physical Review Letters* 2020, 124:133601.
47
48 225. Lutterbach LG, Davidovich L. Method for direct measurement of the Wigner function in cavity QED and ion traps. *Physical Review Letters* 1997,
49 78:2547-2550.
50
51 226. Signoles A, Facon A, Grosso D, Dotsenko I, Haroche S, Raimond JM, Brune M, Gleyzes S. Confined quantum Zeno dynamics of a watched
52 atomic arrow. *Nature Physics* 2014, 10:715-719.
53
54 227. Leiner D, Glaser SJ. Wigner process tomography: Visualization of spin propagators and their spinor properties. *Physical Review A* 2018,
55 98:012112.
56
57 228. Tian Y, Wang Z, Zhang P, Li G, Li J, Zhang T. Measurement of complete and continuous Wigner functions for discrete atomic systems. *Physical
58 Review A* 2018, 97:013840.
59
60 229. Chen B, Geng J, Zhou F, Song L, Shen H, Xu N. Quantum state tomography of a single electron spin in diamond with Wigner function
reconstruction. *Applied Physics Letters* 2019, 114:041102.
230. Jing Y, Fadel M, Ivannikov V, Byrnes T. Split spin-squeezed Bose-Einstein condensates. *New Journal of Physics* 2019, 21:093038.
231. Song C, Xu K, Li H, Zhang Y-R, Zhang X, Liu W, Guo Q, Wang Z, Ren W, Hao J, et al. Generation of multicomponent atomic Schrodinger cat
states of up to 20 qubits. *Science* 2019, 365:574-577.
232. Eichler C, Lang C, Fink JM, Govenius J, Filipp S, Wallraff A. Observation of Entanglement between Itinerant Microwave Photons and a
Superconducting Qubit. *Physical Review Letters* 2012, 109:240501.
233. Morin O, Huang K, Liu J, Le Jeannic H, Fabre C, Laurat J. Remote creation of hybrid entanglement between particle-like and wave-like optical
qubits. *Nature Photonics* 2014, 8:570-574.
234. Agudelo E, Sperling J, Costanzo LS, Bellini M, Zavatta A, Vogel W. Conditional Hybrid Nonclassicality. *Physical Review Letters* 2017,
119:120403.
235. Banaszek K, Radzewicz C, Wodkiewicz K, Krasinski JS. Direct measurement of the Wigner function by photon counting. *Physical Review A*
1999, 60:674-677.

- 1
2
3 236. Garon A, Zeier R, Glaser SJ. Visualizing operators of coupled spin systems. *Physical Review A* 2015, 91:042122.
4 237. Koczor B, Zeier R, Glaser SJ. Time evolution of coupled spin systems in a generalized Wigner representation. *Annals of Physics* 2019, 408:1-
5 50.
6 238. Davies BI, Rundle RP, Dwyer VM, Samson JH, Tilma T, Everitt MJ. Visualizing spin degrees of freedom in atoms and molecules. *Physical Review*
7 A 2019, 100:042102.
8 239. Rundle RP, Davies BI, Dwyer VM, Tilma T, Everitt MJ. Visualization of correlations in hybrid discrete-continuous variable quantum systems.
9 *Journal of Physics Communications* 2020, 4:025002.
10 240. Ehrenfest P. Bemerkung über die angenäherte Gültigkeit der klassischen Mechanik innerhalb der Quantenmechanik. *Zeitschrift für Physik* 1927,
11 45:455-457.
12 241. Li X, Tully JC, Schlegel HB, Frisch MJ. Ab initio Ehrenfest dynamics. *The Journal of Chemical Physics* 2005, 123:084106.
13 242. Tully JC. Molecular dynamics with electronic transitions. *The Journal of Chemical Physics* 1990, 93:1061-1071.
14 243. Wang LJ, Akimov A, Prezhdo OV. Recent Progress in Surface Hopping: 2011-2015. *Journal of Physical Chemistry Letters* 2016, 7:2100-2112.
15 244. Peng J, Xie Y, Hu D, Du L, Lan Z. Treatment of Nonadiabatic Dynamics by On-The-Fly Trajectory Surface Hopping Dynamics. *Acta Physico-*
16 *Chimica Sinica* 2019, 35:28-48.
17 245. Meyer KR, Offin DC. *Introduction to Hamiltonian Dynamical Systems and the N-Body Problem*. New York: Springer Science+Business Media,
18 LLC; 1992.
19 246. Yarkony DR. Conical Intersections: Diabolical and Often Misunderstood. *Accounts of Chemical Research* 1998, 31:511-518.
20 247. Paterson MJ, Bearpark MJ, Robb MA, Blancafort L, Worth GA. Conical intersections: A perspective on the computation of spectroscopic Jahn-
21 Teller parameters and the degenerate 'intersection space'. *Physical Chemistry Chemical Physics* 2005, 7:2100-2115.
22 248. Matsika S, Krause P. Nonadiabatic Events and Conical Intersections. In: Leone SR, Cremer PS, Groves JT, Johnson MA, eds. *Annual Review*
23 *of Physical Chemistry*, Vol 62. Vol. 62: Annual Reviews; 2011, 621-643.
24 249. Makarov DE, Makri N. Path-Integrals for Dissipative Systems by Tensor Multiplication - Condensed-Phase Quantum Dynamics for Arbitrarily
25 Long-Time. *Chemical Physics Letters* 1994, 221:482-491.
26 250. Makri N, Makarov DE. Tensor Propagator for Iterative Quantum Time Evolution of Reduced Density-Matrices .2. Numerical Methodology. *Journal*
27 *of Chemical Physics* 1995, 102:4611-4618.
28 251. Makri N, Makarov DE. Tensor Propagator for Iterative Quantum Time Evolution of Reduced Density-Matrices .1. Theory. *Journal of Chemical*
29 *Physics* 1995, 102:4600-4610.
30 252. Topaler M, Makri N. Path integral calculation of quantum nonadiabatic rates in model condensed phase reactions. *Journal of Physical Chemistry*
31 1996, 100:4430-4436.
32 253. Tanimura Y, Kubo R. Time Evolution of a Quantum System in Contact with a Nearly Gaussian-Markoffian Noise Bath. *Journal of the Physical*
33 *Society of Japan* 1989, 58:101-114.
34 254. Yan Y-A, Yang F, Liu Y, Shao J. Hierarchical approach based on stochastic decoupling to dissipative systems. *Chemical Physics Letters* 2004,
35 395:216-221.
36 255. Xu R-X, Cui P, Li X-Q, Mo Y, Yan Y. Exact quantum master equation via the calculus on path integrals. *The Journal of Chemical Physics* 2005,
37 122:041103.
38 256. Shao J. Stochastic description of quantum open systems: Formal solution and strong dissipation limit. *Chemical Physics* 2006, 322:187-192.
39 257. Moix JM, Cao J. A hybrid stochastic hierarchy equations of motion approach to treat the low temperature dynamics of non-Markovian open
40 quantum systems. *The Journal of Chemical Physics* 2013, 139:134106.
41 258. Tanimura Y. Reduced hierarchical equations of motion in real and imaginary time: Correlated initial states and thermodynamic quantities. *The*
42 *Journal of Chemical Physics* 2014, 141:044114.
43 259. Yan Y. Theory of open quantum systems with bath of electrons and phonons and spins: Many-dissipation density matrixes approach. *The*
44 *Journal of Chemical Physics* 2014, 140:054105.
45 260. Tang Z, Ouyang X, Gong Z, Wang H, Wu J. Extended hierarchy equation of motion for the spin-boson model. *The Journal of Chemical Physics*
46 2015, 143:224112.
47 261. Tanimura Y. Real-time and imaginary-time quantum hierarchical Fokker-Planck equations. *The Journal of Chemical Physics* 2015, 142:144110.
48 262. Meyer H-D, Manthe U, Cederbaum LS. The multi-configurational time-dependent Hartree approach. *Chemical Physics Letters* 1990, 165:73-
49 78.
50 263. Thoss M, Wang H, Miller WH. Self-consistent hybrid approach for complex systems: Application to the spin-boson model with Debye spectral
51 density. *The Journal of Chemical Physics* 2001, 115:2991-3005.

- 1
2
3 264. Wang H, Thoss M, Miller WH. Systematic convergence in the dynamical hybrid approach for complex systems: A numerically exact
4 methodology. *The Journal of Chemical Physics* 2001, 115:2979-2990.
5 265. Wang H, Thoss M. Multilayer formulation of the multiconfiguration time-dependent Hartree theory. *The Journal of Chemical Physics* 2003,
6 119:1289-1299.
7 266. Wang H, Thoss M. From coherent motion to localization: dynamics of the spin-boson model at zero temperature. *New Journal of Physics* 2008,
8 10:115005.
9 267. Worth GA, Meyer H-D, Köppel H, Cederbaum LS, Burghardt I. Using the MCTDH wavepacket propagation method to describe multimode non-
10 adiabatic dynamics. *International Reviews in Physical Chemistry* 2008, 27:569-606.
11 268. Wang H, Thoss M. From coherent motion to localization: II. Dynamics of the spin-boson model with sub-Ohmic spectral density at zero
12 temperature. *Chemical Physics* 2010, 370:78-86.
13 269. Craig IR, Thoss M, Wang H. Proton transfer reactions in model condensed-phase environments: Accurate quantum dynamics using the
14 multilayer multiconfiguration time-dependent Hartree approach. *The Journal of Chemical Physics* 2007, 127:144503.
15 270. Wang H. Iterative Calculation of Energy Eigenstates Employing the Multi layer Multiconfiguration Time-Dependent Hartree Theory. *Journal of
16 Physical Chemistry A* 2014, 118:9253-9261.
17 271. Purcell EM. Spontaneous Emission Probabilities at Radio Frequencies. In: Burstein E, Weisbuch C, eds. *Confined Electrons and Photons: New
18 Physics and Applications*. Boston, MA: Springer US; 1995, 839-839.
19 272. Krasnok AE, Slobozhanyuk AP, Simovski CR, Tretyakov SA, Poddubny AN, Miroshnichenko AE, Kivshar YS, Belov PA. An antenna model for
20 the Purcell effect. *Scientific Reports* 2015, 5:12956.
21 273. Rybin MV, Mingaleev SF, Limonov MF, Kivshar YS. Purcell effect and Lamb shift as interference phenomena. *Scientific Reports* 2016, 6:20599.
22 274. Holsteen AL, Raza S, Fan P, Kik PG, Brongersma ML. Purcell effect for active tuning of light scattering from semiconductor optical antennas.
23 *Science* 2017, 358:1407-1410.
24 275. Alagappan G, Krivitsky LA, Png CE. Diamond in a Nanopocket: A New Route to a Strong Purcell Effect. *ACS Omega* 2018, 3:4733-4742.
25 276. Gallego J, Alt W, Macha T, Martinez-Dorantes M, Pandey D, Meschede D. Strong Purcell Effect on a Neutral Atom Trapped in an Open Fiber
26 Cavity. *Physical Review Letters* 2018, 121:173603.
27 277. Ren T, Dong Y, Xu S, Gong X. Strong Purcell effect in deep subwavelength coaxial cavity with GeSn active medium. *Optics Letters* 2021,
28 46:3889-3892.
29 278. Carmichael HJ, Brecha RJ, Raizen MG, Kimble HJ, Rice PR. Subnatural linewidth averaging for coupled atomic and cavity-mode oscillators.
30 *Physical Review A* 1989, 40:5516-5519.
31 279. Zhu Y, Gauthier DJ, Morin SE, Wu Q, Carmichael HJ, Mossberg TW. Vacuum Rabi splitting as a feature of linear-dispersion theory: Analysis
32 and experimental observations. *Physical Review Letters* 1990, 64:2499-2502.
33 280. Field JE. Vacuum-Rabi-splitting-induced transparency. *Physical Review A* 1993, 47:5064-5067.
34 281. Abram II, Oudar JL. Spontaneous emission in planar semiconductor microcavities displaying vacuum Rabi splitting. *Physical Review A* 1995,
35 51:4116-4122.
36 282. Li K, Wang W, Chen Z, Gao N, Yang W, Li W, Chen H, Li S, Li H, Jin P, et al. Vacuum Rabi splitting of exciton-polariton emission in an AlN film.
37 *Scientific Reports* 2013, 3:3551.
38 283. Toida H, Nakajima T, Komiyama S. Vacuum Rabi splitting in a semiconductor circuit QED system. *Physical Review Letters* 2013, 110:066802.
39 284. Guerin W, Santo T, Weiss P, Cipris A, Schachenmayer J, Kaiser R, Bachelard R. Collective Multimode Vacuum Rabi Splitting. *Physical Review
40 Letters* 2019, 123:243401.
41 285. Yan Y, Ergogo TT, Lu Z, Chen L, Luo J, Zhao Y. Lamb Shift and the Vacuum Rabi Splitting in a Strongly Dissipative Environment. *The Journal
42 of Physical Chemistry Letters* 2021, 12:9919-9925.
43 286. Meystre P. *Elements of Quantum Optics*. Berlin New York: Springer; 2007.
44 287. Hoffmann NM, Schafer C, Rubio A, Kelly A, Appel H. Capturing vacuum fluctuations and photon correlations in cavity quantum electrodynamics
45 with multitrajectory Ehrenfest dynamics. *Physical Review A* 2019, 99:063819.
46 288. Hoffmann NM, Schäfer C, Säkkinen N, Rubio A, Appel H, Kelly A. Benchmarking semiclassical and perturbative methods for real-time
47 simulations of cavity-bound emission and interference. *The Journal of Chemical Physics* 2019, 151:244113.
48 289. Li TE, Chen HT, Nitzan A, Subotnik JE. Quasiclassical modeling of cavity quantum electrodynamics. *Physical Review A* 2020, 101:033831.
49 290. Levine BG, Ko C, Quenneville J, Martinez TJ. Conical intersections and double excitations in time-dependent density functional theory.
50 *Molecular Physics* 2006, 104:1039-1051.
51 291. Halcrow MA. Jahn-Teller distortions in transition metal compounds, and their importance in functional molecular and inorganic materials.
52 *Chemical Society Reviews* 2013, 42:1784-1795.

- 1
2
3 292. Bersuker IB. The Jahn-Teller and Pseudo-Jahn-Teller Effects: A Unique and Only Source of Spontaneous Symmetry Breaking in Atomic Matter.
4 *Symmetry* 2021, 13:1577.
5
6 293. Qin A, Lam JYW, Tang BZ. Luminogenic polymers with aggregation-induced emission characteristics. *Progress in Polymer Science* 2012,
7 37:182-209.
8
9 294. Schneider R, Domcke W. S1-S2 Conical intersection and ultrafast S2->S1 Internal conversion in pyrazine. *Chemical Physics Letters* 1988,
10 150:235-242.
11
12 295. Hacker B, Welte S, Daiss S, Shaukat A, Ritter S, Li L, Rempe G. Deterministic creation of entangled atom-light Schrodinger-cat states. *Nature*
13 *Photonics* 2019, 13:110–115.
14
15 296. Vlastakis B, Petrenko A, Ofek N, Sun L, Leghtas Z, Sliwa K, Liu Y, Hatridge M, Blumoff J, Frunzio L, et al. Characterizing entanglement of an
16 artificial atom and a cavity cat state with Bell's inequality. *Nature Communications* 2015, 6:8970.
17
18 297. Isserlis L. On a formula for the product-moment coefficient of any order of a normal frequency distribution in any number of variables. *Biometrika*
19 1918, 12:134-139.
20
21 298. Wang MC, Uhlenbeck GE. On the theory of the Brownian motion-II. *Reviews of Modern Physics* 1945, 17:323-342.
22
23 299. Fano U. Geometrical characterization of nuclear states and the theory of angular correlations. *Physical Review* 1953, 90:577-579.
24
25 300. Tilma T, Sudarshan ECG. Generalized Euler angle parameterization for U(N) with applications to SU(N) coset volume measures. *Journal of*
26 *Geometry and Physics* 2004, 52:263-283.
27
28 301. Tilma T, Sudarshan ECG. Generalized Euler angle parametrization for SU(N). *Journal of Physics A: Mathematical and General* 2002, 35:10467-
29 10501.
30
31 302. Klimov AB. Exact evolution equations for SU(2) quasidistribution functions. *Journal of Mathematical Physics* 2002, 43:2202-2213.
32
33 303. Bóna P. Classical Mechanical Projections of QM. In: Bóna P, ed. *Classical Systems in Quantum Mechanics*. Cham: Springer International
34 Publishing; 2020.
- 35
36
37
38
39
40
41
42
43
44
45
46
47
48
49
50
51
52
53
54
55
56
57
58
59
60

New Phase Space Formulations and Quantum Dynamics Approaches

Article Type:

- OPINION
- PRIMER
- OVERVIEW
- ADVANCED REVIEW
- FOCUS ARTICLE
- SOFTWARE FOCUS

Authors:

Xin He (co-first author)

Beijing National Laboratory for Molecular Sciences, Institute of Theoretical and Computational Chemistry, College of Chemistry and Molecular Engineering, Peking University, Beijing 100871, China

ORCID ID: 0000-0002-5189-7204

Baihua Wu (co-first author)

Beijing National Laboratory for Molecular Sciences, Institute of Theoretical and Computational Chemistry, College of Chemistry and Molecular Engineering, Peking University, Beijing 100871, China

ORCID ID: 0000-0002-1256-6859

Youhao Shang

Beijing National Laboratory for Molecular Sciences, Institute of Theoretical and Computational Chemistry, College of Chemistry and Molecular Engineering, Peking University, Beijing 100871, China

ORCID ID: 0000-0002-9297-6654

Bingqi Li

Beijing National Laboratory for Molecular Sciences, Institute of Theoretical and Computational Chemistry, College of Chemistry and Molecular Engineering, Peking University, Beijing 100871, China

ORCID ID: 0000-0001-7273-8299

Xiangsong Cheng

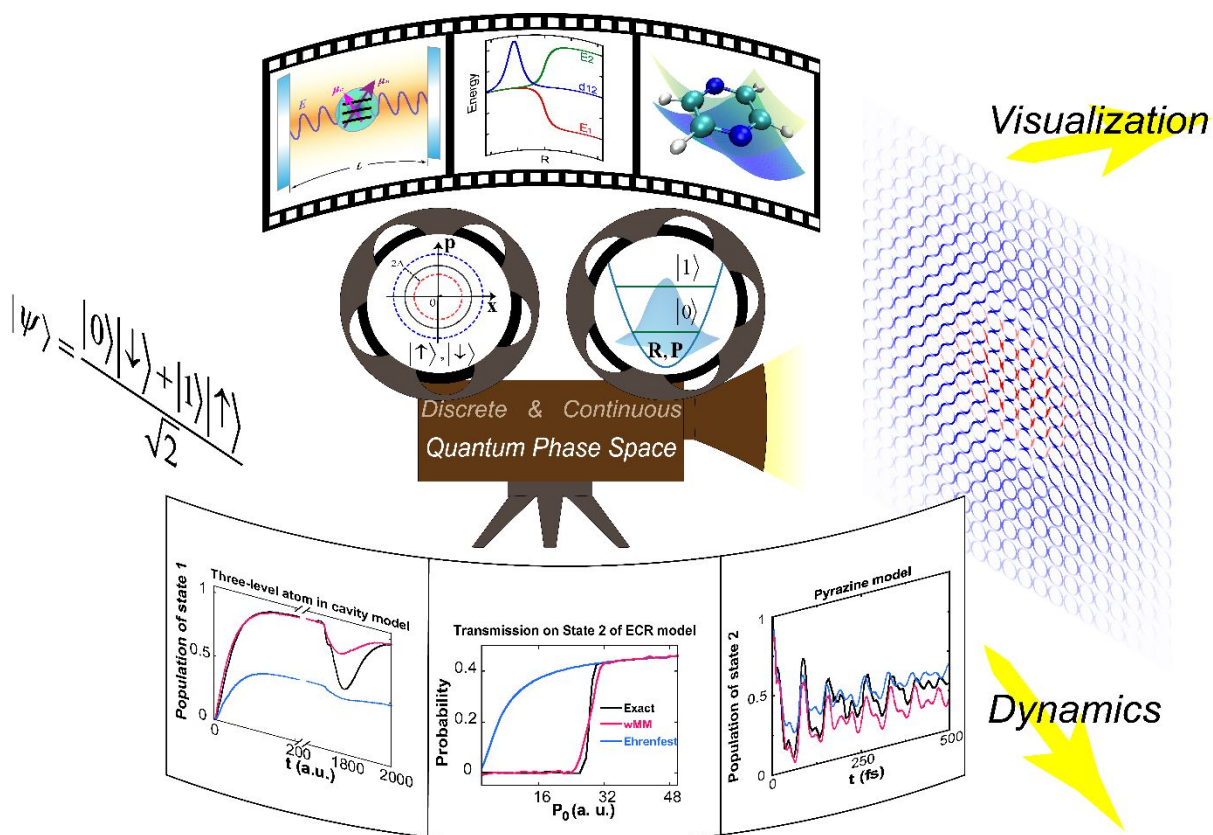
1
2
3 Beijing National Laboratory for Molecular Sciences, Institute of Theoretical and Computational
4 Chemistry, College of Chemistry and Molecular Engineering, Peking University, Beijing 100871,
5 China
6
7
8
9 ORCID ID: 0000-0001-8793-5092
10
11

12 **Jian Liu*** (Corresponding author)
13
14 Beijing National Laboratory for Molecular Sciences, Institute of Theoretical and Computational
15 Chemistry, College of Chemistry and Molecular Engineering, Peking University, Beijing 100871,
16 China
17
18 ORCID ID: 0000-0002-2906-5858
19
20 Email: jianliupku@pku.edu.cn
21
22

23 Abstract

24 We report recent progress on the phase space formulation of quantum mechanics with coordinate-momentum
25 variables, focusing more on new theory of (weighted) constraint coordinate-momentum phase space for discrete-
26 variable quantum systems. This leads to a general coordinate-momentum phase space formulation of composite
27 quantum systems, where conventional representations on infinite phase space are employed for continuous
28 variables. It is convenient to utilize (weighted) constraint coordinate-momentum phase space for representing
29 the quantum state and describing nonclassical features. Various numerical tests demonstrate that new trajectory-
30 based quantum dynamics approaches derived from the (weighted) constraint phase space representation are useful
31 and practical for describing dynamical processes of composite quantum systems in gas phase as well as in
32 condensed phase.
33
34
35
36
37
38
39
40
41
42
43
44
45
46
47
48
49
50
51
52
53
54
55
56
57
58
59
60

Graphical/Visual Abstract and Caption



Schematic representation of dynamics of composite quantum systems *via* phase space formulations.

1. INTRODUCTION

Phase space with coordinate-momentum variables is a fundamental concept and offers a convenient tool to describe statistics as well as dynamics in classical mechanics. In comparison to other equivalent interpretations of quantum mechanics, phase space formulations offer more insight and understanding between quantum and classical counterpart concepts, which are widely used in chemical and biological dynamics and spectroscopy¹⁻⁶⁰, quantum optics^{51, 61-70}, cryogenic physics/chemistry⁷¹⁻⁷⁵, quantum information and computation⁷⁶⁻⁸⁷, etc.

Phase space formulations of quantum mechanics have been developed since two important pioneering works, the Weyl transform in 1927, of which the original formulation converted a Hamiltonian on classical phase space into a quantum mechanical operator⁸⁸, and the Wigner function in 1932 that in principle depicts the inverse transform although a pure state was used for demonstration⁸⁹. The most essential element is the one-to-one correspondence mapping between quantum operators and classical functions often defined on a smooth manifold, namely, phase space. Because of the commutation relation of conjugate operators, the mapping is not unique in quantum mechanics^{90, 91}.

When infinite phase space is employed for a continuous-variable quantum system, most phase space formulations can be described by Cohen's generalized form⁹² in 1966. Quantum dynamics with phase space variables is expressed by the Moyal or Moyal-like bracket as first proposed by Groenewold⁹³ in 1946 and Moyal⁹⁴ in 1949. The Wigner and Husimi representations are most often used for the continuous-variable system. When the Moyal bracket is approximated by the Poisson bracket in the Wigner phase space expression of the quantum Liouville theorem, which was also derived as the linearized semiclassical initial value representation (LSC-IVR) or classical Wigner model^{4-8, 11, 20, 23} for the quantum correlation function, it reproduces exact quantum correlation functions even of nonlinear operators (i.e., nonlinear functions of the coordinate or momentum operator) in the harmonic or classical limit. The truncated Wigner approximation⁷⁴ with the time-dependent generalization of the Bopp representation^{90, 95} is similar to the LSC-IVR, but the former requests more demanding evaluation of the stability matrix elements along the trajectory when nonlinear operators are involved in the correlation function. Ref. ¹⁵ suggests a practical way to implement the imaginary time path integral treatment of the Boltzmann density operator in the LSC-IVR for general molecular systems that often contain imaginary frequencies. Its recent application illustrates that quantum dynamical effects play a critical role in reproducing the peaks in the intermediate region between the librational and bending bands, those between the bending and stretching bands, and the double-peak in the stretching band in the experimental isotropic Raman spectrum of liquid water¹⁹ (as shown in Figure 1). In addition that more advanced versions of SC-IVR⁹⁶⁻⁹⁹ are capable of

improving over the LSC-IVR, in ref¹¹ we first employed the quantum Liouville theorem in the phase space formulation to develop trajectory-based approaches to satisfy the two fundamental criteria: conservation of the quantum Boltzmann distribution for the thermal equilibrium system and being exact for any quantum thermal correlation functions in the classical and harmonic limits. Such trajectory-based approaches can in principle be further improved by higher order corrections of the exact series expansion of the phase space propagator as demonstrated in ref⁴⁴. More progress along this line can be found in refs³⁷⁻⁴⁷. (Figure 2 shows molecular vibrational spectra produced by the new phase space quantum dynamics methods.)

Phase space representations of a finite discrete F -state quantum system were first independently described by Stratonovich¹⁰⁰ in 1956, Feynman¹⁰¹ in 1987, and Wootters¹⁰² in 1987. Further developments of Stratonovich's formulation have focused on an SU(2) or SU(F) structure of phase space¹⁰³⁻¹¹⁷, while those on the construction of a discrete phase space are described in Refs^{78, 118-126}. Other than the 2-state (or spin 1/2) system, the exact equations of motion (EOMs) of phase variables (expressed by the Moyal-like bracket) involved in these approaches for the finite discrete multi-state system are often tedious (and nonlinear)^{109, 127-130}. Recent theoretical progress on exactly mapping the finite discrete F -state quantum system onto *constraint* coordinate-momentum phase space suggests that there exists a novel unified framework to derive comprehensive exact mapping Hamiltonians^{44, 57, 131, 132}, of which the quantum EOMs of mapping coordinate-momentum variables are simply linear^{44, 57, 131-134}.

The unified mapping formulation on coordinate-momentum phase space^{44, 57, 131-134} then offers a useful tool to treat dynamics of a composite quantum system, in which both continuous and finite discrete degrees of freedom (DOFs) are involved and coupled with one another. Because a typical molecular system has vibrational, rotational, and translational motion, it is often much more convenient to employ continuous coordinate space rather than Hilbert space with dense states to describe the nuclear DOFs. On the other hand, the energy gap between different electronic states of interest is often significantly larger such that the (adiabatic or diabatic) state representation is more useful to depict the electronic DOFs. It is evident that a general description of the molecular system leads to a composite quantum system, especially in the nonadiabatic region¹³⁵⁻¹⁵². A comprehensive version of the Meyer-Miller mapping Hamiltonian model^{153, 154} can rigorously be formulated in the general coordinate-momentum phase space formulation^{44, 57, 131-134}.

In the Focus Article we focus on novel developments on the phase space formulation of quantum mechanics with coordinate-momentum variables for discrete-variable systems as well as for composite systems^{44, 57, 131-134}. In Section 2 we first review the general coordinate-momentum phase space formulation, where infinite space is

used for describing continuous variables and constraint space is employed for mapping discrete variables. We then propose a weighted constraint phase space representation that is also an exact formulation for mapping discrete-variable quantum systems. Section 3 demonstrates several examples and discusses implications of the (weighted) constraint coordinate-momentum phase space for studying and illustrating discrete-variable or composite quantum systems. When we use the weighted constraint phase space representation for mapping composite quantum systems, the mapping Hamiltonian (we use the Meyer-Miller mapping Hamiltonian for demonstration throughout the article, albeit that other mapping Hamiltonians are also available^{57, 58, 131, 132}) yields a novel trajectory-based approximate approach for composite systems. Such a new method satisfies the frozen nuclei limit [i.e., the dynamics reproduces the exact evolution when only finite discrete (electronic) DOFs are involved]. In Section 4 the performance of new trajectory-based quantum dynamics approaches on (weighted) constraint phase space is extensively tested for a few typical benchmark composite systems in gas phase as well as in condensed phase. Finally, conclusion remarks are presented in Section 5.

2. GENERAL COORDINATE-MOMENTUM PHASE SPACE FORMULATION OF QUANTUM MECHANICS

Consider a (molecular) system with N continuous (nuclear) DOFs and F discrete (electronic) states, of which the Hamiltonian reads

$$\hat{H} = \sum_{n,m=1}^F H_{nm}(\hat{\mathbf{R}}, \hat{\mathbf{P}}) |n\rangle\langle m| = \sum_{n,m=1}^F \left[\frac{1}{2} \hat{\mathbf{P}}^T \mathbf{M}^{-1} \hat{\mathbf{P}} \delta_{nm} + V_{nm}(\hat{\mathbf{R}}) \right] |n\rangle\langle m| , \quad 2$$

where \mathbf{R} and \mathbf{P} are the nuclear coordinate and momentum variables, respectively, \mathbf{M} is the diagonal mass matrix, and the F states form an orthonormal complete basis sets, i.e.,

$$\langle m | n \rangle = \delta_{mn}, \quad \hat{I}_{\text{ele}} = \sum_{n=1}^F |n\rangle\langle n| . \quad 3$$

\hat{I}_{ele} and \hat{I}_{nuc} stand for the identity operator of the discrete (electronic) DOFs and that of the continuous (nuclear) DOFs. For simplicity, eq 2 employs the (electronically) diabatic representation, where the Hermitian potential matrix $\mathbf{V}(\mathbf{R})$ is a function of only the coordinate vector. (In applications $\mathbf{V}(\mathbf{R})$ is often a real symmetric matrix.) More discussion on the adiabatic representation of discrete (electronic) DOFs is available in Section-4.1.

The unified formulation of mapping phase space with coordinate-momentum variables offers a useful exact approach to describe the composite system. The trace of a product of two quantum operators is expressed as an integral of two functions on mapping phase space, *i.e.*,

$$\text{Tr}_{n,e} [\hat{A}\hat{B}] = \int d\mu_{\text{nuc}}(\mathbf{R}, \mathbf{P}) \int_{S(x,p)} d\mu_{\text{ele}}(\mathbf{x}, \mathbf{p}) A_C(\mathbf{R}, \mathbf{P}; \mathbf{x}, \mathbf{p}) \mathcal{B}_C^o(\mathbf{R}, \mathbf{P}; \mathbf{x}, \mathbf{p}) \quad 4$$

with

$$A_C(\mathbf{R}, \mathbf{P}; \mathbf{x}, \mathbf{p}) = \text{Tr}_{n,e} [\hat{A} \hat{K}_{\text{nuc}}(\mathbf{R}, \mathbf{P}) \otimes \hat{K}_{\text{ele}}(\mathbf{x}, \mathbf{p})] \quad 5$$

$$\mathcal{B}_C^o(\mathbf{R}, \mathbf{P}; \mathbf{x}, \mathbf{p}) = \text{Tr}_{n,e} [\hat{K}_{\text{nuc}}^{-1}(\mathbf{R}, \mathbf{P}) \otimes \hat{K}_{\text{ele}}^{-1}(\mathbf{x}, \mathbf{p}) \hat{B}] \quad 6$$

$d\mu_{\text{nuc}}(\mathbf{R}, \mathbf{P}) = (2\pi\hbar)^{-N} d\mathbf{R} d\mathbf{P}$ and $d\mu_{\text{ele}}(\mathbf{x}, \mathbf{p}) = F d\mathbf{x} d\mathbf{p}$ as the integration measure on nuclear phase space and that on electronic phase space, respectively, and $\text{Tr}_{n,e}$ represents the trace over the corresponding nuclear and electronic Hilbert space. The integral over the mapping phase space variables for the finite discrete (electronic) DOFs in eq 4 is performed as

$$\int_{S(x,p)} F d\mathbf{x} d\mathbf{p} g(\mathbf{x}, \mathbf{p}) = \int F d\mathbf{x} d\mathbf{p} \frac{1}{\Omega} S(\mathbf{x}, \mathbf{p}) g(\mathbf{x}, \mathbf{p}) = \int F d\mathbf{x} d\mathbf{p} \bar{S}(\mathbf{x}, \mathbf{p}) g(\mathbf{x}, \mathbf{p}) \quad 7$$

where the area of constraint space $S(\mathbf{x}, \mathbf{p})$

$$\Omega = \int d\mathbf{x} d\mathbf{p} S(\mathbf{x}, \mathbf{p}) \quad 8$$

is the normalization constant, and $\bar{S}(\mathbf{x}, \mathbf{p})$ is the normalized constraint space.

The normalization of the (inverse) mapping kernel reads

$$\text{Tr}_n [\hat{K}_{\text{nuc}}(\mathbf{R}, \mathbf{P})] = \text{Tr}_n [\hat{K}_{\text{nuc}}^{-1}(\mathbf{R}, \mathbf{P})] = 1 \quad 9$$

$$\text{Tr}_e [\hat{K}_{\text{ele}}(\mathbf{x}, \mathbf{p})] = \text{Tr}_e [\hat{K}_{\text{ele}}^{-1}(\mathbf{x}, \mathbf{p})] = 1 \quad 10$$

and

$$\int d\mu_{\text{nuc}}(\mathbf{R}, \mathbf{P}) \hat{K}_{\text{nuc}}(\mathbf{R}, \mathbf{P}) = \int d\mu_{\text{nuc}}(\mathbf{R}, \mathbf{P}) \hat{K}_{\text{nuc}}^{-1}(\mathbf{R}, \mathbf{P}) = \hat{I}_{\text{nuc}} \quad 11$$

$$\int_{S(x,p)} d\mu_{\text{ele}}(\mathbf{x}, \mathbf{p}) \hat{K}_{\text{ele}}(\mathbf{x}, \mathbf{p}) = \int_{S(x,p)} d\mu_{\text{ele}}(\mathbf{x}, \mathbf{p}) \hat{K}_{\text{ele}}^{-1}(\mathbf{x}, \mathbf{p}) = \hat{I}_{\text{ele}} \quad 12$$

The one-to-one correspondence mapping from phase space function $A_C(\mathbf{R}, \mathbf{P}; \mathbf{x}, \mathbf{p})$ or $\beta_C^0(\mathbf{R}, \mathbf{P}; \mathbf{x}, \mathbf{p})$ of Eq 5 back to operator \hat{A} or \hat{B} is

$$\begin{aligned}\hat{A} &= \int d\mu_{\text{nuc}}(\mathbf{R}, \mathbf{P}) \int_{S(x, p)} d\mu_{\text{ele}}(\mathbf{x}, \mathbf{p}) A_C(\mathbf{R}, \mathbf{P}; \mathbf{x}, \mathbf{p}) \hat{K}_{\text{nuc}}^{-1}(\mathbf{R}, \mathbf{P}) \otimes \hat{K}_{\text{ele}}^{-1}(\mathbf{x}, \mathbf{p}) \\ \hat{B} &= \int d\mu_{\text{nuc}}(\mathbf{R}, \mathbf{P}) \int_{S(x, p)} d\mu_{\text{ele}}(\mathbf{x}, \mathbf{p}) \beta_C^0(\mathbf{R}, \mathbf{P}; \mathbf{x}, \mathbf{p}) \hat{K}_{\text{nuc}}(\mathbf{R}, \mathbf{P}) \otimes \hat{K}_{\text{ele}}(\mathbf{x}, \mathbf{p})\end{aligned}. \quad 13$$

The nuclear or electronic kernel should satisfy five criteria, namely, linearity, reality, standardization (normalization), traciality, and covariance^{93, 94, 100, 115}.

2.1 Mapping kernel for continuous (nuclear) degrees of freedom

The integrals for (\mathbf{R}, \mathbf{P}) in eqs 4, 11, and 13 are over infinite (nuclear) phase space. The mapping kernel and its inverse for the nuclear DOFs are

$$\begin{aligned}\hat{K}_{\text{nuc}}(\mathbf{R}, \mathbf{P}) &= \left(\frac{\hbar}{2\pi} \right)^N \int d\zeta \int d\eta e^{i\zeta \cdot (\hat{\mathbf{R}} - \mathbf{R}) + i\eta \cdot (\hat{\mathbf{P}} - \mathbf{P})} f(\zeta, \eta) \\ \hat{K}_{\text{nuc}}^{-1}(\mathbf{R}, \mathbf{P}) &= \left(\frac{\hbar}{2\pi} \right)^N \int d\zeta \int d\eta e^{i\zeta \cdot (\hat{\mathbf{R}} - \mathbf{R}) + i\eta \cdot (\hat{\mathbf{P}} - \mathbf{P})} [f(-\zeta, -\eta)]^{-1}\end{aligned}, \quad 14$$

where $f(\zeta, \eta)$ is a scalar function. E.g., we have the Wigner function^{89, 155}

$$f(\zeta, \eta) = 1, \quad 15$$

the Husimi function¹⁵⁶

$$f(\zeta, \eta) = \exp \left(-\frac{\zeta^T \Gamma^{-1} \zeta}{4} - \frac{\hbar^2}{4} \eta^T \Gamma \eta \right), \quad 16$$

the anti-Husimi function

$$f(\zeta, \eta) = \exp \left(\frac{\zeta^T \Gamma^{-1} \zeta}{4} + \frac{\hbar^2}{4} \eta^T \Gamma \eta \right), \quad 17$$

the Glauber-Sudarshan P function^{61, 62, 66} (with the characteristic frequency matrix ω of the system)

$$f(\zeta, \eta) = \exp \left[\frac{\hbar}{4} \zeta^T \mathbf{M}^{-1/2} \omega^{-1} \mathbf{M}^{-1/2} \zeta + \frac{\hbar}{4} \eta^T \mathbf{M}^{1/2} \omega \mathbf{M}^{1/2} \eta \right] \quad 18$$

and its generalized versions⁶⁶, the Glauber Q function¹⁵⁷

$$f(\zeta, \eta) = \exp \left[-\frac{\hbar}{4} \zeta^T \mathbf{M}^{-1/2} \boldsymbol{\omega}^{-1} \mathbf{M}^{-1/2} \zeta - \frac{\hbar}{4} \eta^T \mathbf{M}^{1/2} \boldsymbol{\omega} \mathbf{M}^{1/2} \eta \right] , \quad 19$$

the normal-antinormal ordered function⁹¹

$$f(\zeta, \eta) = \cosh \left[\frac{\hbar}{4} \zeta^T \mathbf{M}^{-1/2} \boldsymbol{\omega}^{-1} \mathbf{M}^{-1/2} \zeta + \frac{\hbar}{4} \eta^T \mathbf{M}^{1/2} \boldsymbol{\omega} \mathbf{M}^{1/2} \eta \right] , \quad 20$$

the Kirkwood antistandard-ordered function^{158, 159}

$$f(\zeta, \eta) = e^{i \hbar \zeta^T \eta / 2} , \quad 21$$

the Mehta standard-ordered function¹⁶⁰

$$f(\zeta, \eta) = e^{-i \hbar \zeta^T \eta / 2} , \quad 22$$

the Rivier function^{161, 162}

$$f(\zeta, \eta) = \cos \left[\frac{1}{2} \hbar \zeta^T \eta \right] , \quad 23$$

and the distribution function of Born and Jordan¹⁶³

$$f(\zeta, \eta) = \frac{\sin \left[\frac{1}{2} \hbar \zeta^T \eta \right]}{\frac{1}{2} \hbar \zeta^T \eta} , \quad 24$$

etc.

When operator \hat{A} is a function of only the nuclear DOFs, its phase space function from Eq 5 and the dual function from eq 6 become

$$A_{\text{nuc}}(\mathbf{R}, \mathbf{P}) = \text{Tr}_n \left[\hat{A} \hat{K}_{\text{nuc}}(\mathbf{R}, \mathbf{P}) \right] \quad 25$$

and

$$\%_{\text{nuc}}(\mathbf{R}, \mathbf{P}) = \text{Tr}_n \left[\hat{K}_{\text{nuc}}^{-1}(\mathbf{R}, \mathbf{P}) \hat{A} \right] . \quad 26$$

When the Wigner function eq 15 is used, the mapping kernel and its inverse are the same, i.e., $\hat{K}_{\text{nuc}}(\mathbf{x}, \mathbf{p}) = \hat{K}_{\text{nuc}}^{-1}(\mathbf{x}, \mathbf{p})$. The Wigner phase space function of operator \hat{A} (from eq 25) is identical to its dual (from eq 26),

$$A_{\text{nuc}}^W(\mathbf{R}, \mathbf{P}) = A_{\text{nuc}}^{\mathcal{H}}(\mathbf{R}, \mathbf{P}) . \quad 27$$

When the Husimi phase space (eq 16) is employed, it is straightforward to show the relation between the Wigner and Husimi phase space functions (obtained from eq 25)

$$A_{\text{nuc}}^H(\mathbf{R}, \mathbf{P}) = \exp \left[\frac{1}{4} \left(\frac{d}{d\mathbf{R}} \right)^T \Gamma^{-1} \left(\frac{d}{d\mathbf{R}} \right) + \frac{\hbar^2}{4} \left(\frac{d}{d\mathbf{P}} \right)^T \Gamma \left(\frac{d}{d\mathbf{P}} \right) \right] A_{\text{nuc}}^W(\mathbf{R}, \mathbf{P}) , \quad 28$$

and the relation between the dual function of Husimi phase space $A_{\text{nuc}}^{\mathcal{H}}(\mathbf{R}, \mathbf{P})$ and the Wigner phase space function $A_{\text{nuc}}^W(\mathbf{R}, \mathbf{P})$

$$A_{\text{nuc}}^{\mathcal{H}}(\mathbf{R}, \mathbf{P}) = \exp \left[-\frac{1}{4} \left(\frac{d}{d\mathbf{R}} \right)^T \Gamma^{-1} \left(\frac{d}{d\mathbf{R}} \right) - \frac{\hbar^2}{4} \left(\frac{d}{d\mathbf{P}} \right)^T \Gamma \left(\frac{d}{d\mathbf{P}} \right) \right] A_{\text{nuc}}^W(\mathbf{R}, \mathbf{P}) . \quad 29$$

Because any choice of $f(\zeta, \eta)$ in eq 14 leads to an informationally complete representation of the continuous-variable quantum system, it is not difficult to establish the relation between different (dual) phase space functions in addition to eq 28 and eq 29.

2.2 Mapping kernel on constraint space for discrete (electronic) degrees of freedom

As derived first in Appendix A of ref¹³² in the spirit of Ref¹³¹ and then in the Supporting Information of ref¹³⁴, the kernel that maps a set of F states onto constraint phase space $\mathbf{S}(\mathbf{x}, \mathbf{p})$ reads

$$\hat{K}_{\text{ele}}(\mathbf{x}, \mathbf{p}) = \sum_{n,m=1}^F \left[\frac{1}{2} (x^{(n)} + ip^{(n)}) (x^{(m)} - ip^{(m)}) - \gamma \delta_{nm} \right] |n\rangle\langle m| \quad 30$$

and the corresponding inverse kernel is

$$\hat{K}_{\text{ele}}^{-1}(\mathbf{x}, \mathbf{p}) = \sum_{n,m=1}^F \left[\frac{1+F}{2(1+F\gamma)^2} (x^{(n)} + ip^{(n)}) (x^{(m)} - ip^{(m)}) - \frac{1-\gamma}{1+F\gamma} \delta_{nm} \right] |n\rangle\langle m| . \quad 31$$

As naturally required by eq 10, constraint phase space $\mathbf{S}(\mathbf{x}, \mathbf{p})$ is defined by

$$\delta \left(\sum_{n=1}^F \frac{(x^{(n)})^2 + (p^{(n)})^2}{2} - (1+F\gamma) \right) , \quad 32$$

of which the area is

$$\Omega(\gamma) = \int d\mathbf{x}d\mathbf{p} \delta \left(\sum_{n=1}^F \frac{(x^{(n)})^2 + (p^{(n)})^2}{2} - (1+F\gamma) \right) . \quad 33$$

The normalized constraint phase space is $\bar{\mathbb{S}}(\mathbf{x}, \mathbf{p}) = \mathbb{S}(\mathbf{x}, \mathbf{p})/\Omega(\gamma)$.

Equations 30-33 define the mapping kernel and inverse kernel as well as constraint phase space, which are the key elements of the coordinate-momentum phase space formulation of the discrete-variable quantum system that we first established in refs^{131, 132} and further developed in refs^{57, 58, 134}. As yielded from eq 5, when the Wigner function eq 15 is used for the nuclear DOFs, the mapping Hamiltonian for the quantum Hamiltonian operator eq 2 reads

$$H_C(\mathbf{R}, \mathbf{P}; \mathbf{x}, \mathbf{p}; \gamma) = \frac{1}{2} \mathbf{P}^T \mathbf{M}^{-1} \mathbf{P} + \sum_{n,m=1}^F V_{mn}(\mathbf{R}) \left[\frac{1}{2} (x^{(n)} + ip^{(n)}) (x^{(m)} - ip^{(m)}) - \gamma \delta_{nm} \right] . \quad 34$$

Because $\mathbf{V}(\mathbf{R})$ is Hermitian, the mapping Hamiltonian is real. As $\mathbf{V}(\mathbf{R})$ is often a real symmetric matrix, eq 34 becomes

$$H_C(\mathbf{R}, \mathbf{P}; \mathbf{x}, \mathbf{p}; \gamma) = \frac{1}{2} \mathbf{P}^T \mathbf{M}^{-1} \mathbf{P} + \sum_{n,m=1}^F \left[\frac{1}{2} (x^{(n)} x^{(m)} + p^{(n)} p^{(m)}) - \gamma \delta_{nm} \right] V_{mn}(\mathbf{R}) , \quad 35$$

which is the seminal Meyer-Miller Hamiltonian¹⁵³ that has extensively been implemented for nonadiabatic dynamics in the literature^{4, 56, 60, 138, 154, 164-218}. In refs^{58, 131, 132} it is shown that there also exist other comprehensive mapping Hamiltonian models in the general coordinate-momentum phase space formulation of quantum mechanics. When the mapping Hamiltonian is employed to generate trajectory-based dynamics in the phase space formulation for a composite quantum system, we denote it the classical mapping model (CMM) approach. It satisfies the frozen nuclei limit. We use the Meyer-Miller Hamiltonian for demonstration throughout the Focus Article.

When Meyer and Miller proposed the conventional Meyer-Miller mapping Hamiltonian model for the nonadiabatic system in 1979, they did not invoke the phase space formulation. In 1997 Stock and Thoss¹⁵⁴ utilized the Schwinger oscillator theory of angular momentum^{219, 220} to derive the Meyer-Miller mapping Hamiltonian¹⁵³. Its LSC-IVR approximation⁴ in principle includes *infinite* Wigner phase space for the finite set of (electronic) states. The applications, however, suggest that the LSC-IVR approximation in the framework of

refs^{4, 154, 170} is not good^{172, 177, 181, 187, 195, 200, 202}. More advanced semiclassical approaches^{96, 97} improve the performance but request more computational effort^{172, 173}. The symmetric-window-function and other techniques have been introduced to practically overcome the drawbacks^{177, 181, 187, 195, 200, 202}. Recent progress along this line is briefly summarized in ref¹³⁸.

Equation 32 indicates that parameter γ lies in region $(-1/F, \infty)$. It is shown that parameter γ can be either positive or negative^{131, 134} and should be interpreted as a special case of the commutator matrix^{57, 58, 131, 134} rather than the conventional zero-point-energy parameter^{153, 154}. There exist three key elements for a trajectory-based quantum dynamics method to evaluate the evolution of the expectation/ensemble average of a physical property, namely,

- 1) the EOMs of the trajectory,
- 2) the initial condition of the trajectory, and
- 3) the integral expression for the expectation/ensemble average of the physical property of interest.

In the frozen-nuclei limit, Hamilton's EOMs governed by the Meyer-Miller mapping Hamiltonian is isomorphic to exact dynamics. While it is reasonable to employ the mapping Hamiltonian to define the EOMs of the trajectory, the left two elements are also important to consider such that the trajectory-based dynamics method is consistent. The constraint coordinate-momentum phase space formulation then offers a more advanced platform to consider all the three key elements.

It is evident that eq 32 is a special choice of constraint phase space $S(x, p)$. The interpretation of parameter γ in refs^{57, 58, 131, 134} hints that a more comprehensive choice of normalized constraint phase space $\bar{S}(x, p)$ is

$$\int_{-1/F}^{\infty} d\gamma w(\gamma) \frac{1}{\Omega(\gamma)} \delta\left(\sum_{n=1}^F \frac{(x^{(n)})^2 + (p^{(n)})^2}{2} - (1+F\gamma)\right) , \quad 36$$

with the *quasi*-probability distribution function

$$\int_{-1/F}^{\infty} d\gamma w(\gamma) = 1 . \quad 37$$

Equation 7, the integral over the mapping phase space variables for the finite discrete (electronic) DOFs then becomes

$$\int_{S(x,p)} F dx dp g(x,p) = \int_{-1/F}^{\infty} d\gamma w(\gamma) \int F dx dp \frac{1}{\Omega(\gamma)} \delta \left(\sum_{n=1}^F \frac{(x^{(n)})^2 + (p^{(n)})^2}{2} - (1+F\gamma) \right) g(x,p) . \quad 38$$

If we require that the kernel is the same as its inverse, i.e.,

$$\hat{K}_{\text{ele}}(x,p) = \hat{K}_{\text{ele}}^{-1}(x,p) = \sum_{n,m=1}^F \left[\frac{1}{2} (x^{(n)} + ip^{(n)}) (x^{(m)} - ip^{(m)}) - \gamma \delta_{nm} \right] |n\rangle \langle m| , \quad 39$$

it is then not difficult to obtain

$$\int_{-1/F}^{\infty} d\gamma w(\gamma) \chi(\gamma) = 1 \quad 40$$

with

$$\chi(\gamma) = F\gamma^2 + 2\gamma . \quad 41$$

(See Appendix 1 of Supporting Information for more discussion.) Equations 36-41 define normalized constraint phase space $\bar{S}(x,p)$, the mapping kernel and inverse kernel, and the *quasi*-probability distribution function $w(\gamma)$ of parameter γ . The weighted constraint phase space formulation for the discrete-variable quantum system is the key new theoretical result of the Focus Article. When the Wigner function eq 15 is used for the nuclear DOFs, where $\hat{K}_{\text{nuc}}(x,p) = \hat{K}_{\text{nuc}}^{-1}(x,p)$, eq 5 is then identical to eq 6 when $\hat{A} = \hat{B}$. The mapping Hamiltonian for the quantum Hamiltonian operator eq 2 produced by either of eq 5 and eq 6 leads to the same expression as eq 35. When the mapping Hamiltonian is utilized to produce the trajectory-based dynamics for a composite system, it is denoted the weighted mapping model (wMM) approach. The frozen nuclei limit is satisfied in wMM.

Many choices are possible for the discrete or continuous version of the normalized quasi-probability distribution function $w(\gamma)$ in the weighted constraint phase space mapping theory. In the Focus Article we consider only the simplest cases of the discrete version. When but a single value of parameter γ is chosen in eq 40, i.e., $w(\gamma) = \delta(\gamma - \gamma_1)$, we obtain

$$F\gamma^2 + 2\gamma = 1 , \quad 42$$

of which the non-trivial solution is

$$\gamma = \frac{\sqrt{1+F} - 1}{F} \quad . \quad 43$$

In this case, the weighted constraint phase space formulation is identical to the constraint phase space formulation, and wMM becomes CMM when trajectory-based dynamics is considered. When only two values of parameter γ are selected, i.e.,

$$w(\gamma) = \sum_{j=1}^2 w(\gamma_j) \delta(\gamma - \gamma_j) \quad , \quad 44$$

eq 37 and eq 40 lead to

$$\begin{aligned} w(\gamma_1) &= \frac{1 - \chi(\gamma_2)}{\chi(\gamma_1) - \chi(\gamma_2)} \\ w(\gamma_2) &= \frac{\chi(\gamma_1) - 1}{\chi(\gamma_1) - \chi(\gamma_2)} \end{aligned} \quad . \quad 45$$

When the values of parameter γ are close to zero or smaller than zero in region $(-1/F, \infty)$, trajectories produced by the Meyer-Miller mapping Hamiltonian eq 35 for nonadiabatic molecular dynamics are stable. For demonstration in the paper we choose

$$\gamma_1 = -\gamma_2 = \Delta \quad 46$$

with Δ a reasonably small positive real number in region $(0, 1/F)$. Figure 3 presents the constraint coordinate-momentum phase space formulation when a single value of parameter γ is used (Figure 3a) as well as the weighted formulation when two values of parameter γ suggested by eq 46 are used (Figure 3b).

3. PHASE SPACE REPRESENTATION OF THE NONCLASSICAL FEATURE OF QUANTUM SYSTEMS

Recent advance on quantum technologies makes it possible to control and manipulate quantum states in experiment. Because the phase space formulation offers an informationally complete description of the density matrix, direct measurements of phase space of the quantum system with continuous DOFs, those of the quantum system with discrete DOFs, and those of the composite quantum system have been realized in experiment^{70, 85, 221-234}. While the celebrated Wigner phase space has long been used for illustration of the negative *quasi*-probability for continuous-variable systems^{225, 235}, Stratonovich phase space has recently been proposed for visualization and tomography of discrete-variable systems^{85, 113, 227-229, 231, 236, 237}. A combination of these two spaces has been used for illustration of nonclassical correlations or entanglement between the discrete DOF and the continuous DOF of

the composite system^{238, 239}. (In Appendix 3 of Supporting Information, we briefly review Stratonovich phase space with an either SU(2) or SU(F) structure, as well as the relationship between Stratonovich phase space and constraint coordinate-momentum phase space as already pointed out in refs^{57, 58}.)

As coordinate-momentum phase space is well-established in classical mechanics, the formulation of (weighted) constraint coordinate-momentum phase space described in Section 2 offers a potentially useful approach for describing correlations and dynamics in the discrete-variable system as well as the composite system in quantum mechanics. When (weighted) constraint coordinate-momentum phase space is used for mapping an F -state system, the phase space distribution is

$$\rho_C(\mathbf{x}, \mathbf{p}) = \sum_{m,n=1}^F \rho_{mn} K_{nm}(\mathbf{x}, \mathbf{p}), \quad 47$$

where $\rho_{mn} = \langle m | \hat{\rho} | n \rangle$ and $K_{nm}(\mathbf{x}, \mathbf{p}) = \langle n | \hat{K}_{\text{ele}}(\mathbf{x}, \mathbf{p}) | m \rangle$ with $\hat{K}_{\text{ele}}(\mathbf{x}, \mathbf{p})$ defined in eq 39. For the sake of visualization, it is convenient to further reduce constraint phase space variables (\mathbf{x}, \mathbf{p}) to two relevant variables, $(x^{(n)}, x^{(m)})$ or $(x^{(n)}, p^{(m)})$ for describing the correlation on arbitrary two states $|n\rangle$ and $|m\rangle$. We define the marginal function, $K_{(n,m)}(x^{(n)}, x^{(m)})$, on constraint coordinate-momentum phase space (Figure 4),

$$K_{(n,m)}(x^{(n)}, x^{(m)}) = \int F d\mathbf{x}_\perp d\mathbf{p} \frac{1}{\Omega(\gamma)} \delta \left(\sum_{j=1}^F \frac{(x^{(j)})^2 + (p^{(j)})^2}{2} - (1+F\gamma) \right) K_{nm}(\mathbf{x}, \mathbf{p}; \gamma), \quad 48$$

where \mathbf{x}_\perp represents all $x^{(i)}$ other than $\{x^{(n)}, x^{(m)}\}$, and that on weighted constraint phase space,

$$K_{(n,m)}(x^{(n)}, x^{(m)}) = \int_{-1/F}^{\infty} d\gamma w(\gamma) \frac{1}{\Omega(\gamma)} \int F d\mathbf{x}_\perp d\mathbf{p} \delta \left(\sum_{j=1}^F \frac{(x^{(j)})^2 + (p^{(j)})^2}{2} - (1+F\gamma) \right) K_{nm}(\mathbf{x}, \mathbf{p}; \gamma). \quad 49$$

Figure 5 demonstrates the case of eq 49 when the quasi-probability distribution function $w(\gamma)$ is defined by eqs 44-46 where two symmetrical values of parameter γ are used. Similar definitions also apply for $K_{(n,m)}(x^{(n)}, p^{(m)})$. The explicit formula of these marginal functions can be derived by using the integral techniques in Appendix 1 of Supporting Information.

Figures 4-5 demonstrate a composite system that consists of a discrete DOF for spin-1/2 and a continuous DOF for a harmonic oscillator. The marginal joint distribution function of the composite system reads

$$\rho_C^{(n,m)}(\mathbf{R}, \mathbf{P}; x^{(n)}, x^{(m)}) = \text{Tr}_{n,e} \left[\hat{\rho} \hat{K}_{\text{nuc}}(\mathbf{R}, \mathbf{P}) \otimes |n\rangle \langle m| K_{(n,m)}(x^{(n)}, x^{(m)}) \right]. \quad 50$$

The marginal quasi-probability distribution functions of the continuous variable for both the pure state and the mixed state are presented in Figure 4a, where infinite Wigner phase space is employed. The marginal functions of the discrete variables (based on eq 48) of the spin-1/2 system read

$$\begin{aligned} & \begin{pmatrix} K_{\uparrow\uparrow}(x^{(1)}, x^{(2)}) & K_{\uparrow\downarrow}(x^{(1)}, x^{(2)}) \\ K_{\downarrow\uparrow}(x^{(1)}, x^{(2)}) & K_{\downarrow\downarrow}(x^{(1)}, x^{(2)}) \end{pmatrix} \\ &= \frac{1}{2\pi(1+2\gamma)} \begin{pmatrix} 1 + \frac{1}{2}(x^{(1)})^2 - \frac{1}{2}(x^{(2)})^2 & x^{(1)}x^{(2)} \\ x^{(1)}x^{(2)} & 1 - \frac{1}{2}(x^{(1)})^2 + \frac{1}{2}(x^{(2)})^2 \end{pmatrix}, \end{aligned} \quad 51$$

where notations \uparrow, \downarrow are used to represent the two discrete states.

The marginal functions for the discrete variable are demonstrated on constraint coordinate-momentum phase space in Figure 4b and on weighted constraint space in Figure 5b. More interestingly, the identical angular behaviour and the radial cancellation behaviour of two weighted components lead to a hollow ring structure on weighted constraint phase space (Figure 5a, also see Appendix 4 of Supporting Information). The difference between the Schrodinger cat state and the mixed state is distinct in either Figure 4b on constraint space or Figure 5b on weighted constraint space.

The marginal joint function of a pure Bell entangled state, $(|0\rangle|\downarrow\rangle + |1\rangle|\uparrow\rangle)/2$, of the composite system is demonstrated in Figure 4c (by adopting the similar strategy of refs ^{238, 239}), where constraint coordinate-momentum phase space is used for the discrete DOF at each grid, as well as in Figure 5c where weighted constraint space is employed for the discrete DOF at each grid. The two-dimensional grids represent variables (R, P) of infinite Wigner phase space for the continuous DOF in either of Figure 4c and Figure 5c. When the pure Bell entangled state is studied, both Figure 4c and Figure 5c clearly demonstrate a Gaussian decay of the joint marginal function against Wigner phase space variables (R, P) of the continuous DOF. Either Figure 4c or Figure 5c also shows the pattern of the correlation between the continuous DOF and the discrete DOF. It is convenient to distinguish the pure Bell entangled state, $(|0\rangle|\downarrow\rangle + |1\rangle|\uparrow\rangle)/2$, from the direct product of the Schrodinger cat states, $(|0\rangle + |1\rangle) \otimes (|\uparrow\rangle + |\downarrow\rangle)/2$, when the hybrid representation of the general coordinate-momentum phase space is used.

4. DYNAMICS OF COMPOSITE QUANTUM SYSTEMS

The quantum Liouville theorem can be expressed as a generalized Moyal bracket on hybrid coordinate-momentum phase space. When the Poisson bracket for classical Hamilton's EOMs governed by the mapping Hamiltonian, eq 35, is used to approximate the generalized Moyal bracket on phase space, we have CMM when constraint space is used, and wMM when weighted constraint space is employed. We compare the new wMM and CMM approaches to Ehrenfest dynamics^{240, 241} as well as the fewest-switches surface hopping (FSSH) method²⁴²⁻²⁴⁴, two prevailing trajectory-based dynamics methods for a few typical composite quantum systems. (In this section we set $\hbar = 1$ for simplicity if it is not specifically stated).

4.1 Equations of motion governed by the mapping Hamiltonian

In eq 2, the 'complete' set of diabatic states $\{|n\rangle\}$ is independent of nuclear coordinate/configuration \mathbf{R} . The mapping variables for discrete (electronic) DOFs, (\mathbf{x}, \mathbf{p}) , are independent of \mathbf{R} . Define $\mathbf{g} = \mathbf{x} + i\mathbf{p}$. The EOMs governed by eq 34, the mapping Hamiltonian of eq 2, then read,

$$\dot{\mathbf{g}} = -i\mathbf{V}(\mathbf{R})\mathbf{g} \quad . \quad 52$$

$$\dot{\mathbf{R}} = \mathbf{M}^{-1}\mathbf{P} \quad 53$$

$$\dot{\mathbf{P}} = -\sum_{n,m=1}^F (\nabla_{\mathbf{R}} V_{mn}(\mathbf{R})) \left(\frac{1}{2} (x^{(n)} + ip^{(n)}) (x^{(m)} - ip^{(m)}) - \gamma \delta_{nm} \right) \quad . \quad 54$$

Diabatic potential matrix $\mathbf{V}(\mathbf{R})$ is Hermitian, so is the force matrix, $\{\nabla_{\mathbf{R}} V_{mn}(\mathbf{R})\}$. It is trivial to verify that the mean force of the right-hand side (RHS) of eq 54 is always real. When $\mathbf{V}(\mathbf{R})$ is a real symmetric matrix, the EOMs become

$$\begin{aligned} \dot{\mathbf{x}} &= \mathbf{V}(\mathbf{R})\mathbf{p} \\ \dot{\mathbf{p}} &= -\mathbf{V}(\mathbf{R})\mathbf{x} \\ \dot{\mathbf{R}} &= \mathbf{M}^{-1}\mathbf{P} \end{aligned} \quad . \quad 55$$

$$\dot{\mathbf{P}} = -\sum_{n,m=1}^F (\nabla_{\mathbf{R}} V_{mn}(\mathbf{R})) \left[\frac{1}{2} (x^{(n)}x^{(m)} + p^{(n)}p^{(m)}) - \gamma \delta_{nm} \right]$$

Consider the full Hamiltonian of nuclei and electrons of the molecular system,

$$\hat{H} = \frac{1}{2} \hat{\mathbf{P}}^T \mathbf{M}^{-1} \hat{\mathbf{P}} + \hat{H}_{el}(\hat{\mathbf{R}}) \quad , \quad 56$$

where $\hat{H}_{el}(\hat{\mathbf{R}})$ is the electronic Hamiltonian. Its representation in the diabatic basis reads

$$\hat{H}_{el}(\mathbf{R}) = \sum_{n,m} V_{nm}(\mathbf{R}) |n\rangle \langle m| \quad 57$$

and that in the adiabatic basis is

$$\hat{H}_{el}(\mathbf{R}) = \sum_k E_k(\mathbf{R}) |\phi_k(\mathbf{R})\rangle\langle\phi_k(\mathbf{R})| , \quad 58$$

where $E_k(\mathbf{R})$ denotes the adiabatic potential energy surface of the k -th adiabatic electronic state. Assume that the unitary transformation between a set of diabatic basis states, $\{|m\rangle\}$, and a set of adiabatic basis states, $\{|\phi_k(\mathbf{R})\rangle\}$, is

$$|\phi_k(\mathbf{R})\rangle = \sum_m U_{mk}(\mathbf{R}) |m\rangle , \quad 59$$

$$|n\rangle = \sum_k U_{nk}^*(\mathbf{R}) |\phi_k(\mathbf{R})\rangle$$

where $U_{mk}(\mathbf{R}) = \langle m | \phi_k(\mathbf{R}) \rangle$. This states the diagonalization of the diabatic potential matrix,

$$\sum_{n,m} U_{nj}^*(\mathbf{R}) V_{nm}(\mathbf{R}) U_{mk}(\mathbf{R}) = E_k(\mathbf{R}) \delta_{kj} , \quad 60$$

or equivalently,

$$V_{mn}(\mathbf{R}) = \sum_k U_{mk}(\mathbf{R}) E_k(\mathbf{R}) U_{nk}^*(\mathbf{R}) . \quad 61$$

Define the nonadiabatic coupling vector,

$$\mathbf{d}_{mn}(\mathbf{R}) = \left\langle \phi_m(\mathbf{R}) \left| \frac{\partial \phi_n(\mathbf{R})}{\partial \mathbf{R}} \right. \right\rangle . \quad 62$$

It is trivial to show

$$\mathbf{d}_{mn}(\mathbf{R}) = -\mathbf{d}_{nm}^*(\mathbf{R}) \quad 63$$

because of the orthonormality of the basis set, i.e., $\langle \phi_m(\mathbf{R}) | \phi_n(\mathbf{R}) \rangle = \delta_{mn}$. We then obtain

$$\nabla_{\mathbf{R}} U_{mk}^*(\mathbf{R}) = \langle \nabla_{\mathbf{R}} \phi_k(\mathbf{R}) | m \rangle = \sum_n \langle \nabla_{\mathbf{R}} \phi_k(\mathbf{R}) | \phi_n \rangle \langle \phi_n | m \rangle$$

$$= \sum_n \mathbf{d}_{nk}^*(\mathbf{R}) U_{mn}^*(\mathbf{R}) = -\sum_n \mathbf{d}_{kn}(\mathbf{R}) U_{mn}^*(\mathbf{R}) \quad 64$$

and

$$\nabla_{\mathbf{R}} U_{mk}(\mathbf{R}) = -\sum_n \mathbf{d}_{kn}^*(\mathbf{R}) U_{mn}(\mathbf{R}) = \sum_n U_{mn}(\mathbf{R}) \mathbf{d}_{nk}(\mathbf{R}) . \quad 65$$

Below we show the explicit form of the EOMs, eqs 52-54, under the diabatic-to-adiabatic transformation, eq 59.

The covariant transformation for mapping variables corresponding to the diabatic-to-adiabatic transformation, eq 59, reads

$$\mathcal{X}_0^{(m)}(\mathbf{R}) + i\mathcal{P}_0^{(m)}(\mathbf{R}) = \sum_m U_{mn}^*(\mathbf{R}) (x^{(m)} + ip^{(m)}) \quad 66$$

or

$$x^{(n)} + ip^{(n)} = \sum_m U_{nm}(\mathbf{R}) (\mathcal{X}_0^{(m)}(\mathbf{R}) + i\mathcal{P}_0^{(m)}(\mathbf{R})) \quad 67$$

Denote $\mathbf{g}(\mathbf{R}) = \mathcal{X}_0(\mathbf{R}) + i\mathcal{P}_0(\mathbf{R})$. Equations 66-67 become

$$\begin{aligned} \mathcal{X}_0(\mathbf{R}) &= \mathbf{U}^\dagger(\mathbf{R}) \mathbf{g} \\ \mathbf{g} &= \mathbf{U}(\mathbf{R}) \mathcal{X}_0(\mathbf{R}) \end{aligned} \quad 68$$

The electronic mapping kernel, eq 30, is

$$\hat{K}_{\text{ele}} = \sum_{n,m} \left[\frac{1}{2} \left(\mathcal{X}_0^{(m)} + i\mathcal{P}_0^{(m)} \right) \left(\mathcal{X}_0^{(n)} - i\mathcal{P}_0^{(n)} \right) - \gamma \delta_{nm} \right] |\phi_n\rangle \langle \phi_m|, \quad 69$$

under the transformation for a specific nuclear configuration, \mathbf{R} . Substitution of eq 64 into eq 66 yields

$$\nabla_{\mathbf{R}} (\mathcal{X}_0^{(n)}(\mathbf{R}) + i\mathcal{P}_0^{(n)}(\mathbf{R})) = - \sum_k \mathbf{d}_{nk}(\mathbf{R}) (\mathcal{X}_0^{(k)}(\mathbf{R}) + i\mathcal{P}_0^{(k)}(\mathbf{R})) \quad 70$$

The total time derivative of $\mathcal{X}_0^{(n)} + i\mathcal{P}_0^{(n)}$ reads

$$\begin{aligned} \frac{d}{dt} (\mathcal{X}_0^{(n)} + i\mathcal{P}_0^{(n)}) &= \sum_m U_{mn}^*(\mathbf{R}) \left(\frac{d}{dt} (x^{(m)} + ip^{(m)}) \right) + \sum_m \left(\frac{d}{dt} U_{mn}^*(\mathbf{R}) \right) (x^{(m)} + ip^{(m)}) \\ &= -i \sum_k \delta_{nk} E_k(\mathbf{R}) (\mathcal{X}_0^{(k)} + i\mathcal{P}_0^{(k)}) - \sum_k \mathbf{R} \cdot \mathbf{d}_{nk}(\mathbf{R}) (\mathcal{X}_0^{(k)} + i\mathcal{P}_0^{(k)}) \\ &= -i \sum_k [E_k(\mathbf{R}) \delta_{nk} - i \mathbf{R} \cdot \mathbf{d}_{nk}(\mathbf{R})] (\mathcal{X}_0^{(k)} + i\mathcal{P}_0^{(k)}) \end{aligned} \quad 71$$

Equation 71 is the EOMs for mapping variables of electronic DOFs in the adiabatic representation.

We then consider the EOMs of nuclear mapping variables under the transformation eq 59. Equation 53 remains invariant under the transformation. Substitution of eqs 61, 64, 65, and 69 into eq 54 produces

$$\begin{aligned}
& \dot{\mathbf{P}} = - \sum_{n,m=1}^F (\nabla_{\mathbf{R}} V_{mn}(\mathbf{R})) \left[\frac{1}{2} (x^{(n)} + ip^{(n)}) (x^{(m)} - ip^{(m)}) - \gamma \delta_{nm} \right] \\
& = - \sum_{n,m} \nabla_{\mathbf{R}} \left(\sum_k U_{mk}(\mathbf{R}) E_k(\mathbf{R}) U_{nk}^*(\mathbf{R}) \right) \left[\frac{1}{2} (x^{(n)} + ip^{(n)}) (x^{(m)} - ip^{(m)}) - \gamma \delta_{nm} \right] \\
& = \sum_{k,l} \mathbf{d}_{lk}(\mathbf{R}) (E_l(\mathbf{R}) - E_k(\mathbf{R})) \left[\frac{1}{2} (\mathcal{X}_0^{(k)} + i\beta_0^{(k)}) (\mathcal{X}_0^{(l)} - i\beta_0^{(l)}) - \gamma \delta_{kl} \right] \\
& \quad - \sum_{k,l} \nabla_{\mathbf{R}} E_k(\mathbf{R}) \delta_{kl} \left[\frac{1}{2} (\mathcal{X}_0^{(k)} + i\beta_0^{(k)}) (\mathcal{X}_0^{(l)} - i\beta_0^{(l)}) - \gamma \delta_{kl} \right]
\end{aligned} \tag{72}$$

Since force matrix $\{\mathbf{F}_{kl} = \nabla_{\mathbf{R}} E_k(\mathbf{R}) \delta_{kl} + (E_k(\mathbf{R}) - E_l(\mathbf{R})) \mathbf{d}_{lk}(\mathbf{R})\}$ is Hermitian, the mean force of the RHS of eq 72 stays real. Under the diabatic-to-adiabatic transformation, eq 59, the EOMs of nuclear phase variables (eqs 53-54) are then recast into

$$\begin{aligned}
& \dot{\mathbf{R}} = \mathbf{M}^{-1} \mathbf{P} \\
& \dot{\mathbf{P}} = - \sum_{k,l} \left[\nabla_{\mathbf{R}} E_k(\mathbf{R}) \delta_{kl} + (E_k(\mathbf{R}) - E_l(\mathbf{R})) \mathbf{d}_{lk}(\mathbf{R}) \right] \left[\frac{1}{2} (\mathcal{X}_0^{(k)} + i\beta_0^{(k)}) (\mathcal{X}_0^{(l)} - i\beta_0^{(l)}) - \gamma \delta_{kl} \right].
\end{aligned} \tag{73}$$

Define the effective potential matrix, $\mathbf{V}^{(\text{eff})}$, whose element is a function of the nuclear phase variables,

$$V_{nk}^{(\text{eff})}(\mathbf{R}, \mathbf{P}) = E_n(\mathbf{R}) \delta_{nk} - i \dot{\mathbf{R}} \cdot \mathbf{d}_{nk}(\mathbf{R}) = E_n(\mathbf{R}) \delta_{nk} - i \mathbf{M}^{-1} \mathbf{P} \cdot \mathbf{d}_{nk}(\mathbf{R}). \tag{74}$$

A more compact form of eq 71 for the electronic phase variables becomes

$$\dot{\mathbf{g}} = -i \mathbf{V}^{(\text{eff})}(\mathbf{R}, \mathbf{P}) \mathbf{g}. \tag{75}$$

Equations 73 and 75 are the final EOMs under the covariant transformation eq 66.

When the electronic wavefunction of the basis set is always real, i.e., $\langle r | \phi_n(\mathbf{R}) \rangle$ is real for any n , which is often the case for molecular systems, eq 63 leads to

$$\mathbf{d}_{mn}(\mathbf{R}) = -\mathbf{d}_{nm}(\mathbf{R}). \tag{76}$$

Equation 73 is simplified to

$$\begin{aligned}
& \dot{\mathbf{R}} = \mathbf{M}^{-1} \mathbf{P} \\
& \dot{\mathbf{P}} = - \sum_{k,l} \left[\nabla_{\mathbf{R}} E_k(\mathbf{R}) \delta_{kl} + (E_k(\mathbf{R}) - E_l(\mathbf{R})) \mathbf{d}_{lk}(\mathbf{R}) \right] \left[\frac{1}{2} (\mathcal{X}_0^{(k)} \mathcal{X}_0^{(l)} + \beta_0^{(k)} \beta_0^{(l)}) - \gamma \delta_{kl} \right].
\end{aligned} \tag{77}$$

Note that the mapping Hamiltonian of eq 34 (obtained in the diabatic representation) becomes

$$H_C(\mathbf{R}, \mathbf{P}, \mathbf{x}(\mathcal{X}_0 \mathcal{P}_0), \mathbf{p}(\mathcal{X}_0 \mathcal{P}_0)) = \frac{1}{2} \mathbf{P}^T \mathbf{M}^{-1} \mathbf{P} + \sum_{n=1}^F E_n(\mathbf{R}) \left(\frac{1}{2} \left((\mathcal{X}_0^{(n)}(\mathbf{R}))^2 + (\beta_0^{(n)}(\mathbf{R}))^2 \right) - \gamma \right) \tag{78}$$

under the transformation defined by eq 61 and eq 66. The new EOMs, eq 73 and eq 75, conserve the mapping Hamiltonian of eq 78. The diabatic-to-adiabatic transformation depends on nuclear coordinate \mathbf{R} , which is also a time-dependent variable of the evolution. The time-dependent canonical transformation for the Hamiltonian system yields a new set of EOMs by the chain rule²⁴⁵.

In eqs 72-75 and eqs 77-78 \mathbf{P} corresponds to the mapping momentum in the diabatic representation, but *not* the canonical momentum in the adiabatic representation because eq 72 is *not* generated from Hamilton's equations of motion. Equations 75 and 77 share a similar form to the EOMs proposed by Cotton *et al* in ref¹⁸⁴ and discussed in the Supporting Information of ref⁵⁷. Define the covariant transformation for nuclear phase variables,

$$\mathbf{R}^0 = \mathbf{R} \quad 79$$

$$\dot{\mathbf{P}}^0 = \mathbf{P} + i \sum_{m,n} \left[\frac{1}{2} (\dot{\mathbf{R}}_0^{(n)} + i \dot{\mathbf{P}}_0^{(n)}) (\mathbf{R}_0^{(m)} - i \mathbf{P}_0^{(m)}) - \gamma \delta_{nm} \right] \mathbf{d}_{mn}(\mathbf{R})$$

The Hamiltonian of eq 78 becomes

$$H_C(\mathbf{R}^0, \mathbf{P}^0, \dot{\mathbf{R}}^0, \dot{\mathbf{P}}^0) = \frac{1}{2} \mathbf{P}^0 \mathbf{M}^{-1} \mathbf{P}^0 + \sum_{n=1}^F E_n(\mathbf{R}^0) \left(\frac{1}{2} \left((\dot{\mathbf{R}}_0^{(n)}(\mathbf{R}^0))^2 + (\dot{\mathbf{P}}_0^{(n)}(\mathbf{R}^0))^2 \right) - \gamma \right) \quad 80$$

of which the canonical variables are $\{\mathbf{R}^0, \mathbf{P}^0, \dot{\mathbf{R}}^0, \dot{\mathbf{P}}^0\}$ instead of $\{\mathbf{R}, \mathbf{P}, \dot{\mathbf{R}}, \dot{\mathbf{P}}\}$. (See more discussions in Appendix 2 of Supporting Information). The mapping diabatic momentum, \mathbf{P} , is related to the kinematic momentum of the adiabatic representation. Although we can directly use Hamilton's EOMs for $\{\mathbf{R}^0, \mathbf{P}^0, \dot{\mathbf{R}}^0, \dot{\mathbf{P}}^0\}$, it is more convenient to employ the EOMs for $\{\mathbf{R}, \mathbf{P}, \dot{\mathbf{R}}, \dot{\mathbf{P}}\}$ instead to avoid the derivative of nonadiabatic coupling terms. This is indeed the strategy suggested by Cotton *et al* in ref¹⁸⁴. When the initial condition does not involve nonadiabatic coupling terms, the sampling of \mathbf{P} in the diabatic representation is the same for that of \mathbf{P}^0 in the adiabatic representation. This is the case in the following applications, where FSSH has to be used in the adiabatic representation. By applying the covariance relation under the diabatic-to-adiabatic transformation, the EOMs on mapping phase space are independent of the representation of the (electronic) basis set, which is also the merit of Ehrenfest dynamics.

We note that either eq 52 or eq 75 can analytically be solved by a symplectic approach that employs an exact propagator on electronic phase space at each nuclear phase point. For example, for eq 75 we use

$$\mathbf{U}(\mathbf{R}, \mathbf{P}; \Delta t) = \exp[-i\Delta t \mathbf{V}^{(\text{eff})}]$$

81

such that the evolution of electronic phase variables follows $\mathbf{g}(t + \Delta t) = \mathbf{U}(\mathbf{R}, \mathbf{P}; \Delta t)\mathbf{g}(t)$.

We then test a range of benchmark systems, including two-site dissipative models, Tully's scattering models, atomic systems in cavity interacted with a number of field modes, and linear vibronic coupling model systems that involve the conical intersection^{135, 246-248}. They are typical composite quantum systems in chemistry, physics, condensed matter science, quantum optics, and quantum information.

4.2 Spin-boson models at low-temperature in condensed phase

The first model illustrated is the spin-boson model, which describes a two-site system interacted with an environmental bath in condense phase. It is also a simplified model for electron transfer and energy transfer in chemical and biological reactions. Several numerically exact benchmark methods for solving the spin-boson model include quasi-adiabatic propagator path integral (QuAPI)²⁴⁹⁻²⁵², hierarchy equations of motion (HEOM)²⁵³⁻²⁶¹, (multi-layer) multi-configuration time-dependent Hartree [(ML-)MCTDH]²⁶²⁻²⁶⁸, but their numerical costs typically increase exponentially as the number of DOFs increases. Quantum dynamics of the spin-boson model exhibits interesting dissipative characters, of which the asymptotic behaviours are often missed by either of Ehrenfest dynamics and FSSH in the low temperature regime⁵⁸. Spin-boson models with strong coupling in the low temperature regime presents challenging tests for trajectory-based dynamics methods.

The Hamiltonian of the spin-boson model is divided to three parts, $\hat{H} = \hat{H}_s + \hat{H}_b + \hat{H}_{sb}$. Here $\hat{H}_s = \varepsilon \hat{\sigma}_z + \Delta_c \hat{\sigma}_x$ describes a two-site system with the bias ε and tunneling Δ_c , while the bath part of the Hamiltonian is discretized into a combination of a number of quantum harmonic oscillators $\hat{H}_b = \sum_{j=1}^{N_b} (\hat{P}_j^2 + \omega_j^2 \hat{R}_j^2)/2$. The system-bath coupling adopts a bilinear interaction, $\hat{H}_{sb} = -\sum_{j=1}^{N_b} c_j \hat{R}_j \hat{\sigma}_z$. Here we use an Ohmic bath spectral density $J(\omega) = (\pi/2)\alpha \omega e^{-\omega/\omega_c}$, where α is the Kondo parameter and ω_c is the cut-off frequency. Its discrete frequencies and coupling strengths $\{\omega_j, c_j\}$ are sampled^{269, 270} from

$$\begin{cases} \omega_j = -\omega_c \ln[1 - j/(1+N_b)] \\ c_j = \omega_j \sqrt{\alpha \omega_c / (1+N_b)} \end{cases}, \quad j = 1, L, N_b$$

82

The initial density is set as $|1\rangle_s\langle 1|_s \otimes \hat{\rho}_b$, where the system is in excited state $|1\rangle_s$ while all bath modes are at thermal equilibrium with $\hat{\rho}_b = e^{-\beta\hat{H}_b} / Z_b$. Initial nuclear DOFs are sampled from the Wigner distribution of $\hat{\rho}_b$, while initial electronic DOFs are sampled from (weighted) constraint coordinate-momentum phase space $S(\mathbf{x}, \mathbf{p})$. The continuous spectral density is discretized into $N_b = 300$ effective bath modes to guarantee numerical convergence in simulations.

In Figure 6, we demonstrate results produced by wMM with parameter $\Delta = 0.05$, by wMM with $\Delta = 0.1$, and by CMM with $\gamma = (\sqrt{F+1} - 1) / F = 0.366$ that is a special case of CMM of ref.¹³⁴. Numerically exact results, as well as results yielded by Ehrenfest dynamics and FSSH, are also shown for comparison. Figure 6 indicates that wMM, as well as CMM, outperforms both Ehrenfest dynamics and FSSH dynamics, either for short-time coherences or for long-time dissipations.

4.3 Tully's gas phase scattering models

Tully's scattering models²⁴² mimic different intersection types of molecular systems, which have widely been tested for various nonadiabatic dynamics methods. They describe a two-state Hamiltonian with a central coupling area and asymptotic plateau regions where diabatic potential function $V_{nn}(R \rightarrow \pm\infty)$ is flat. All the three models, including the single avoided crossing (SAC), dual avoided crossing (DAC), and extended coupling region (ECR) problems, are used in our numerical tests.

Atomic units are used in the simulations of the Tully models. The SAC model (Panel (a1) of Figure 7) describes the simplest but essential surface crossing in molecular systems. In the diabatic representation, its diagonal potential energy surfaces (PESes) are $V_{11} = -V_{22} = A(1 - e^{-B|R|})\text{sgn}(R)$ and off-diagonal coupling terms are $V_{12} = V_{21} = Ce^{-DR^2}$. Here, the parameters are $A = 0.01$, $B = 1.6$, $C = 0.005$, and $D = 1.0$. The DAC model (Panel (b1) of Figure 7) includes two crossing points, thus different (electronic) paths are interfered with the dependence on the initial momentum. Its diagonal PESes are $V_{11} = 0$ and $V_{22} = -Ae^{-BR^2} + E_0$, and off-diagonal coupling terms are $V_{12} = V_{21} = Ce^{-DR^2}$ in the diabatic representation with parameters $A = 0.10$, $B = 0.28$, $E_0 = 0.05$, $C = 0.015$ and $D = 0.06$. The ECR model in the diabatic representation (Panel (c1) of Figure 7) has diagonal PESes $V_{11} = -V_{22} = E_0$ and coupling terms $V_{12} = V_{21} = C[e^{BR}\Theta(-R) + (2 - e^{-BR})\Theta(R)]$, with $E_0 = -0.0006$, $B = 0.9$, $C = 0.1$. Here

1
2
3 $\Theta(R)$ is the Heaviside function of coordinate R . The adiabatic PESes and nonadiabatic coupling vector of
4
5 the ECR model are also illustrated in Panel (c2) of Figure 7.
6

7 We investigate the transmission and reflection coefficients of each state. In the simulations, the initial
8 condition is a nuclear wavepacket, $\Psi(R; t = 0) \propto \exp[-\alpha(R - R_0)^2/2 + i(R - R_0)P_0]$ (here we adopt
9
10 $\hbar = 1$), occupied in state 1, where $\alpha = 1$ is the Gaussian width parameter, and R_0 and P_0 are the initial
11 average coordinate and momentum. The initial average coordinate is set at $R_0 = -3.8$, -10 , and -13
12
13 for the SAC, DAC and ECR models, respectively. The initial Wigner distribution for the nuclear DOF is then
14
15 $\rho_W^{\text{nuc}}(R, P) \propto \exp[-\alpha(R - R_0)^2 - (P - P_0)^2 / \alpha]$.
16
17

18 Figure 7a shows that all methods are capable of quantitatively describing transmission coefficients in
19 (diabatic) state 1 and state 2 of the SAC model. Figure 7b demonstrates that either wMM or CMM outperforms
20
21 Ehrenfest dynamics and FSSH in predicting the peak shape when the initial momentum is relatively high, e.g.,
22
23 $P_0 \geq 15$ au. This indicates that the trajectory-based approximate dynamics approaches in the mapping phase
24
25 space formulation are good for fast processes in the gas phase composite/nonadiabatic system. However, the
26
27 performance of either wMM or CMM in the low initial momentum region should be improved. It is important
28
29 to note that the EOMs of wMM/CMM are invariant with the representation of the electronic state, as described in
30
31 the Supporting Information of ref⁵⁷. (More discussion is also available in Appendix 2 of Supporting
32
33 Information.) That is, both the diabatic and adiabatic representations produce the same results for wMM or
34
35 CMM, which is often not satisfied in FSSH and other nonadiabatic dynamics approaches.
36
37

38 For the ECR model of Figure 7c, the numerically exact DVR solution indicates an energy threshold for a
39 bifurcation. Ehrenfest dynamics totally misses the step-like behaviours for the transmission coefficient in state
40
41 1, and for the reflection coefficient in either state 1 or state 2. CMM greatly improves over Ehrenfest dynamics.
42
43 It is more encouraging that wMM is capable of faithfully describing such step-like behaviours. Tully's original
44
45 FSSH algorithm is not able to well describe the ECR model²⁴², but a modified version for treating frustrated
46
47 hopping of FSSH (e.g., see ref.²⁴⁴) is capable of qualitatively capturing the step-like behaviours. As shown in
48
49 Figure 7c, in comparison to the traditional FSSH approach^{242, 244}, the overall performance of wMM for the ECR
50
51 model is better.
52
53
54

55 4.4 Atom/molecule-in-cavity models of quantum electrodynamic light-matter systems

56
57 The cavity quantum electrodynamics (cQED) focuses on studying the interaction between light and a multi-
58
59 level system (e.g., an atom or a molecule) in an optical cavity, which has many applications in the field of quantum
60

information and quantum computation. There exist many interesting and important phenomena in cQED, e.g., the Purcell effect when coupling is weak and the vacuum Rabi splitting when coupling becomes strong²⁷¹⁻²⁸⁵. When the general atomic/molecular system is coupled to multi-cavity modes, it is often intractable to solve the exact evolution in real time due to the curse of dimensionality. We test wMM for two typical models that describe an imprisoned multi-level atom coupled with a series of optical modes in a one-dimensional lossless cavity^{57, 204, 286-289}.

The total Hamiltonian consists of three parts. The optical field is depicted by N effective modes

$$\hat{H}_p = \sum_{j=1}^N \frac{1}{2} (\hat{P}_j^2 + \omega_j^2 \hat{R}_j^2) , \quad 83$$

where $\{\hat{R}_j, \hat{P}_j\}$ denote the canonical coordinate-momentum variables of j -th optical field mode with the corresponding photonic frequency ω_j . The atomic system is described by $\hat{H}_a = \sum_{n=1}^F \varepsilon_n |n\rangle\langle n|$ with ε_n representing the n -th atomic energy level. Employing the dipole approximation, one can formulate the interaction between atom and optical field as

$$\hat{H}_c = \sum_{n \neq m}^F \left(\sum_{j=1}^N \omega_j \lambda_j(r_0) \hat{R}_j \right) \mu_{nm} |n\rangle\langle m| . \quad 84$$

Here μ_{nm} denotes the transitional dipole moment between the n -th and m -th atomic levels, and the coupling between the j -th mode and the atom is

$$\lambda_j(r_0) = \sqrt{\frac{2}{\varepsilon_0 L}} \sin\left(\frac{j\pi r_0}{L}\right) , \quad 85$$

where L is the volume length of cavity, ε_0 denotes the vacuum permittivity, and r_0 represents the location of the atom. In the simulation, the volume length of the cavity is set to 236200 au and the atom is frozen at the central location, i.e., $r_0 = L / 2$. The optical field is depicted by 400 standing-wave modes in cavity, of which the j -th frequency is $\omega_j = j\pi c / L$ with c the light speed in vacuum. We use two benchmark models for studying cQED processes, a three-level model with $\varepsilon_1 = -0.6738$, $\varepsilon_2 = -0.2798$, $\varepsilon_3 = -0.1547$, $\mu_{12} = -1.034$, $\mu_{23} = -2.536$ (all in atomic units), and a reduced two-level model where only the two lowest atomic levels are employed.

The highest atomic level of each model is initially occupied with no photon in cavity, i.e., all cavity modes are in the corresponding vacuum state. The spontaneous emission occurs at the beginning, the released photon evolves in the cavity, and the re-absorption and re-emission happen later when the photon is reflected to meet the atom. Figure 8 shows the population transfer of each atomic level of the two models. The wMM results are compared with CMM, Ehrenfest dynamics, FSSH, and exact results^{287, 288}. Results of Ehrenfest dynamics and of FSSH significantly deviate from exact results even since very short time, while CMM and wMM yield much more reasonable descriptions for all energy levels, including the transfer behaviour at short time and the revival at around $t = 1800$ au. The wMM approach shows overall better performance than CMM in most of the cases. Figure 8 implies that the trajectory-based methods in the general coordinate-momentum phase space formulation will be useful for studying cQED phenomena in the field of quantum optics and quantum information.

4.5 Linear vibronic coupling model for the molecular system involving the conical intersection

The conical intersection widely exists in molecular systems and plays a central role in many photophysical and photochemical phenomena^{135, 139, 214, 246, 247, 290-293}. The linear vibronic coupling model (LVCM) is the simplest but effective model widely used to describe dynamic properties around the conical intersection region, of which Hamiltonian in the diabatic representation is

$$\hat{H} = \hat{H}_0 + \hat{H}_l + \hat{H}_c \quad . \quad 86$$

Here, $\hat{H}_0 = \sum_{k=1}^N \omega_k (\hat{P}_k^2 + \hat{R}_k^2)/2$ is the zeroth-order harmonic oscillator Hamiltonian in normal-mode space of the electronic ground state, where $\hat{P}_k, \hat{R}_k (k=1, \dots, N)$ denote the k -th effective weighted normal-mode variables with frequency ω_k (i.e., $P_k = p_k / \sqrt{\omega_k}$, $R_k = \sqrt{\omega_k} r_k$, where p_k, r_k are the canonical momentum, and canonical coordinate of k -th normal-mode). In eq 86, $\hat{H}_l = \sum_{n=1}^F \left(E_n + \sum_{k=1}^N \kappa_k^{(n)} \hat{R}_k \right) |n\rangle\langle n|$ contains the vertical excitation energy, $E_n (n=1, \dots, F)$ of F electronic states, and the linear coupling term $\kappa_k^{(n)}$ of each nuclear DOF for diagonal Hamiltonian elements, while $\hat{H}_c = \sum_{n \neq m}^F \left(\sum_{k=1}^N \lambda_k^{(nm)} \hat{R}_k \right) |n\rangle\langle m|$ includes linear coupling $\lambda_k^{(nm)}$ for each normal-mode between two different electronic states, $|n\rangle$ and $|m\rangle$.

A typical two-level 3-mode LVCM describes the S1/S2 conical intersection of the pyrazine molecule. The parameters of this model are fitted from semi-empirical electronic structure calculations by Schneiders and

Domcke in ref²⁹⁴. The excitation energies for the two electronic states are $E_1 = 3.94$ eV and $E_2 = 4.84$ eV. The diagonal linear coupling terms of first two modes $\{\hat{R}_1, \hat{R}_2\}$ are $\kappa_1^{(1)} = 0.037$ eV, $\kappa_2^{(1)} = -0.105$ eV for the first electronic state, and $\kappa_1^{(2)} = -0.254$ eV, $\kappa_2^{(2)} = 0.149$ eV for the second electronic state, respectively. The off-diagonal linear coupling of third mode \hat{R}_3 is $\lambda_3^{(12)} = \lambda_3^{(21)} = 0.262$ eV. The normal-mode vibronic frequency of each mode is $\omega_1 = 0.126$ eV, $\omega_2 = 0.074$ eV, and $\omega_3 = 0.118$ eV, respectively. Initial conditions of nuclear DOFs are sampled from the corresponding Wigner function of the vibronic ground state while the second electronic state is occupied. All simulations employ 10^5 trajectories and time stepsize $\Delta t = 0.01$ fs for fully converged results. Numerically exact result of this model calculated by ML-MCTDH are available in ref²¹².

Figure 9 shows population dynamics of state 2 yielded by wMM, CMM, Ehrenfest dynamics, FSSH and ML-MCTDH. It is evident that Ehrenfest dynamics performs poorly even for the short-time behaviour (before 100 fs). In comparison, wMM, CMM, and FSSH more reasonably describe the radiationless energy transfer process at short time. Interestingly, wMM describes the oscillating behaviours in the long-time region (after 300 fs) better than other approximate methods. Such oscillating behaviour in population dynamics indicates the molecular system passes through the “slopped” conical intersection region²⁹⁴.

Figures 6-9 demonstrate that the overall performance of wMM is better than CMM, especially in the gas phase scattering case of Figure 7c and the quantum electrodynamic light-matter systems of Figure 8. Both wMM and CMM approaches are able to outperform Ehrenfest dynamics as well as FSSH for condensed phase systems (e.g., in Figure 6 and Figure 8).

5. CONCLUSION REMARKS

The phase space formulation of quantum mechanics not only presents a type of convenient interpretation to describe quantum-classical correspondences as well as nonclassical correlations/entanglement, but also sets the insightful scene for developing practical and useful trajectory-based quantum dynamics approaches.

In the Focus Article we show that the constraint coordinate-momentum phase space formulation for the discrete-variable system which we have recently developed, and the weighted representation that we propose in the Focus Article are useful approaches for illustration of nonclassical features of quantum systems. The novel formulation is expected to have potential use for illustration of nonclassical features of quantum states, as well as for future phase point measurement experiment^{70, 85, 221-234}.

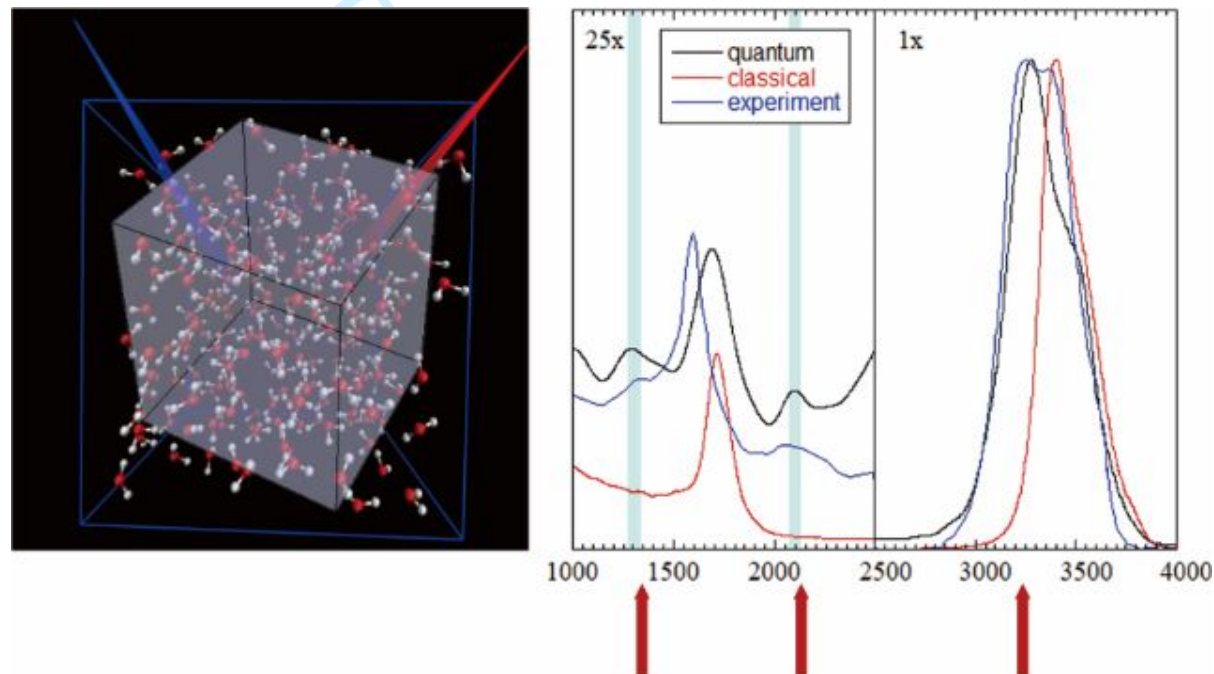
1
2
3 It is straightforward to show the relation between the $SU(F)/U(F-1)$ Stratonovich phase space¹¹⁴ and
4 constraint coordinate-momentum phase space, which is diffeomorphic to $U(F)/U(F-1)$. When $F > 2$, it is
5 inevitable to meet singularities in dynamics for discrete-variable systems when Stratonovich phase space is used.
6 In comparison, (weighted) constraint coordinate-momentum phase space does not cause any singularities in
7 trajectory-based exact dynamics, which is much more numerically favourable. (See more discussion in
8 Appendix 3 of Supporting Information).

9
10
11 When the general Moyal bracket of the quantum Liouville theorem is approximated by the corresponding
12 Poisson bracket on (weighted) constraint phase space, it reproduces the correct frozen-nuclei limit of
13 composite/nonadiabatic systems. Such trajectory-based EOMs on (weighted) constraint coordinate-momentum
14 phase space do not rely on the choice of representation of electronic states and are straightforward to obtain the
15 form under covariant transformations. Because second-order nonadiabatic coupling terms are avoided in the
16 EOMs of the adiabatic representation, it is especially useful for applications to realistic molecular systems.
17 Various benchmark model tests of from gas phase to condensed phase quantum systems (as shown in Figures 6-
18 9) indicate that wMM, the new trajectory-based approximate approach with the weighted constraint coordinate-
19 momentum phase space representation, demonstrates overall better performance than FSSH as well as Ehrenfest
20 dynamics. It is expected that more investigations on the (weighted) constraint phase space formulation will shed
21 light on more numerically favourable dynamics approaches with the Meyer-Miller mapping Hamiltonian or other
22 mapping Hamiltonians (e.g., those of ref¹³¹ and discussed in ref⁵⁸).

23
24 We note that the (weighted) constraint coordinate-momentum phase space formulation is established for any
25 systems with a finite set of states, not only limited to discrete electronic states, but also for finite discrete nuclear
26 states. The weighted phase space strategy that we propose can also be applied to other types of phase space
27 formulations of the discrete-variable system, such as Stratonovich phase space, and Wootters phase space, albeit
28 that the general coordinate-momentum phase space formulation presented in the Focus Article will be more
29 convenient, for experimental measurements, tomography, or characterizations of fidelity, coherence, inequalities,
30 displaced parity, atomic/molecular/optical Schrodinger cat states, and entanglement in quantum information and
31 computation^{70, 85, 221-234, 295, 296} as well as for studying dynamic processes of composite systems in physics,
32 chemistry, materials, biology, and environmental science.

1
2
3
4
5
6
7
8
9
10
11
12
13
14
15
16
17
18
19

20 **Figures and Tables**

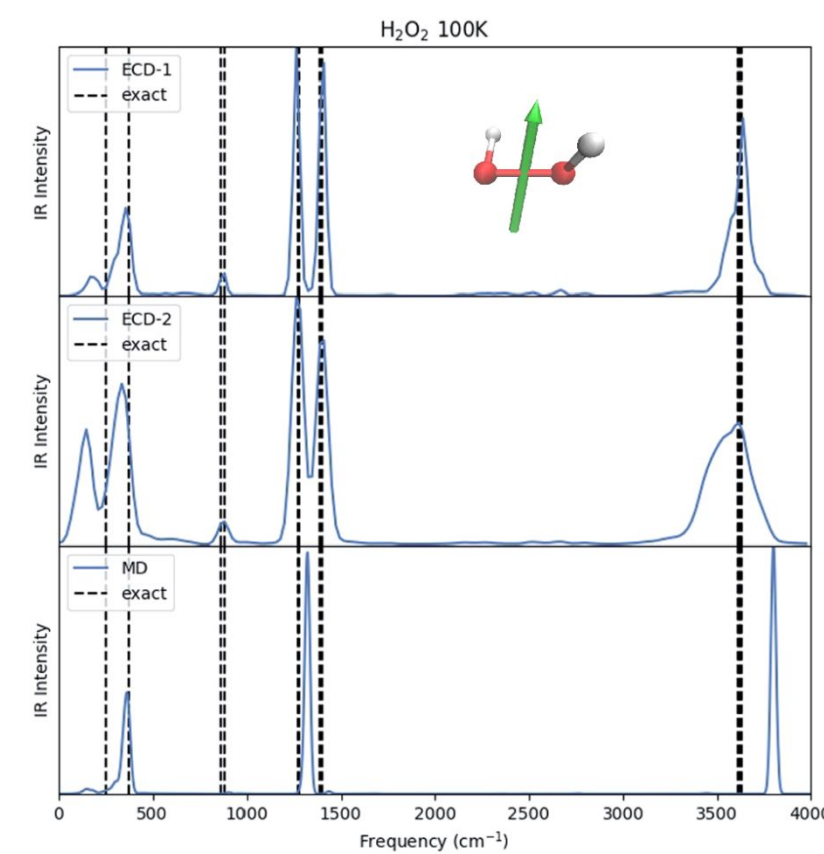
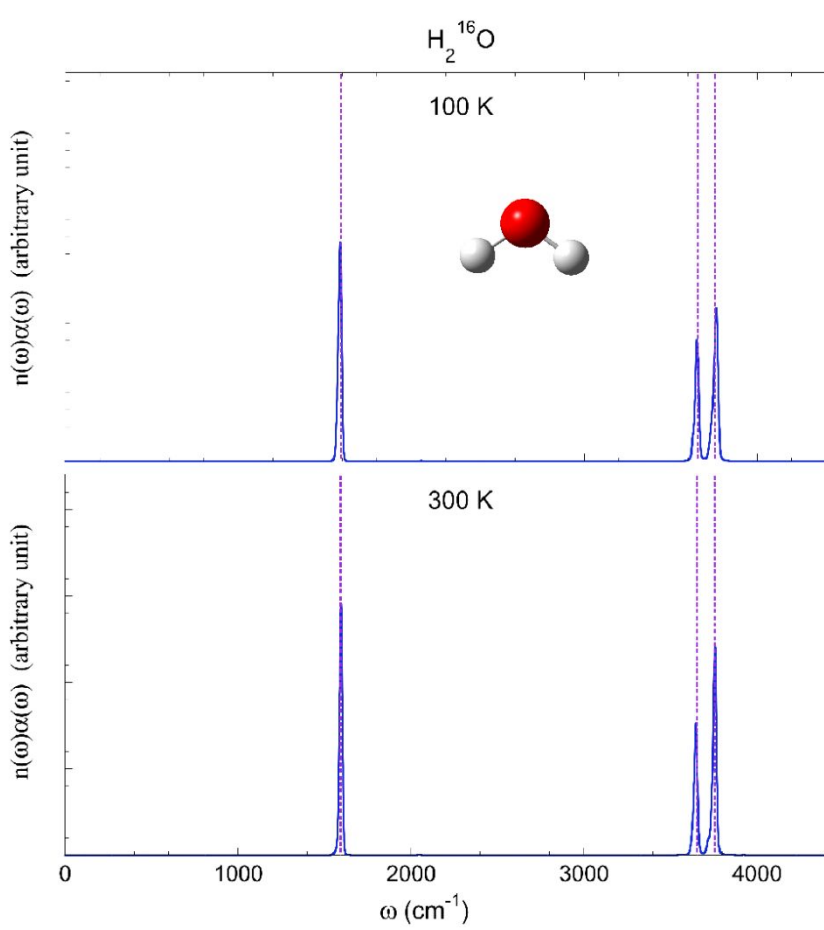


43 **Figure 1.** Quantum dynamical effects are decisive in reproducing the experimental isotropic Raman spectrum
44 of liquid water at room temperature, as illustrated by the LSC-IVR simulation where infinite (Wigner) phase space
45 for nuclear DOFs is used. Converged results were obtained with 216 water molecules in a box with periodic
46 boundary conditions. (Reprinted with permission from ref¹⁹. Copyright 2018 Taylor & Francis.)

51
52
53
54
55
56
57
58
59
60

For Peer Review

1
2
3
4
5
6
7
8
9
10
11
12
13
14
15
16
17
18
19
20
21
22
23
24
25
26
27
28
29
30
31
32
33
34
35
36
37
38
39
40
41
42
43
44
45
46
47
48
49
50
51
52
53
54
55
56
57
58
59
60



1
2
3 **Figure 2.** Molecular vibrational spectra produced by more advanced trajectory-based dynamics methods with
4 infinite (Wigner) phase space used for nuclear DOFs, which satisfy the two fundamental criteria: conservation of
5 the quantum Boltzmann distribution for the thermal equilibrium system and being exact for any quantum thermal
6 correlation functions in the classical and harmonic limits. (a) Vibrational spectrum of the H_2O molecule at
7 100K and that at 300K. Adapted with permission from ref⁴¹. Copyright 2016 American Institute of Physics
8 Publishing. (b) Vibrational spectrum of the H_2O_2 molecule at 100K. Adapted with permission from ref⁴⁴.
9 Copyright 2021 American Institute of Physics Publishing.
10
11
12
13
14
15
16
17
18
19
20
21
22
23
24
25
26
27
28
29
30
31
32
33
34
35
36
37
38
39
40
41
42
43
44
45
46
47
48
49
50
51
52
53
54
55
56
57
58
59
60

For Peer Review

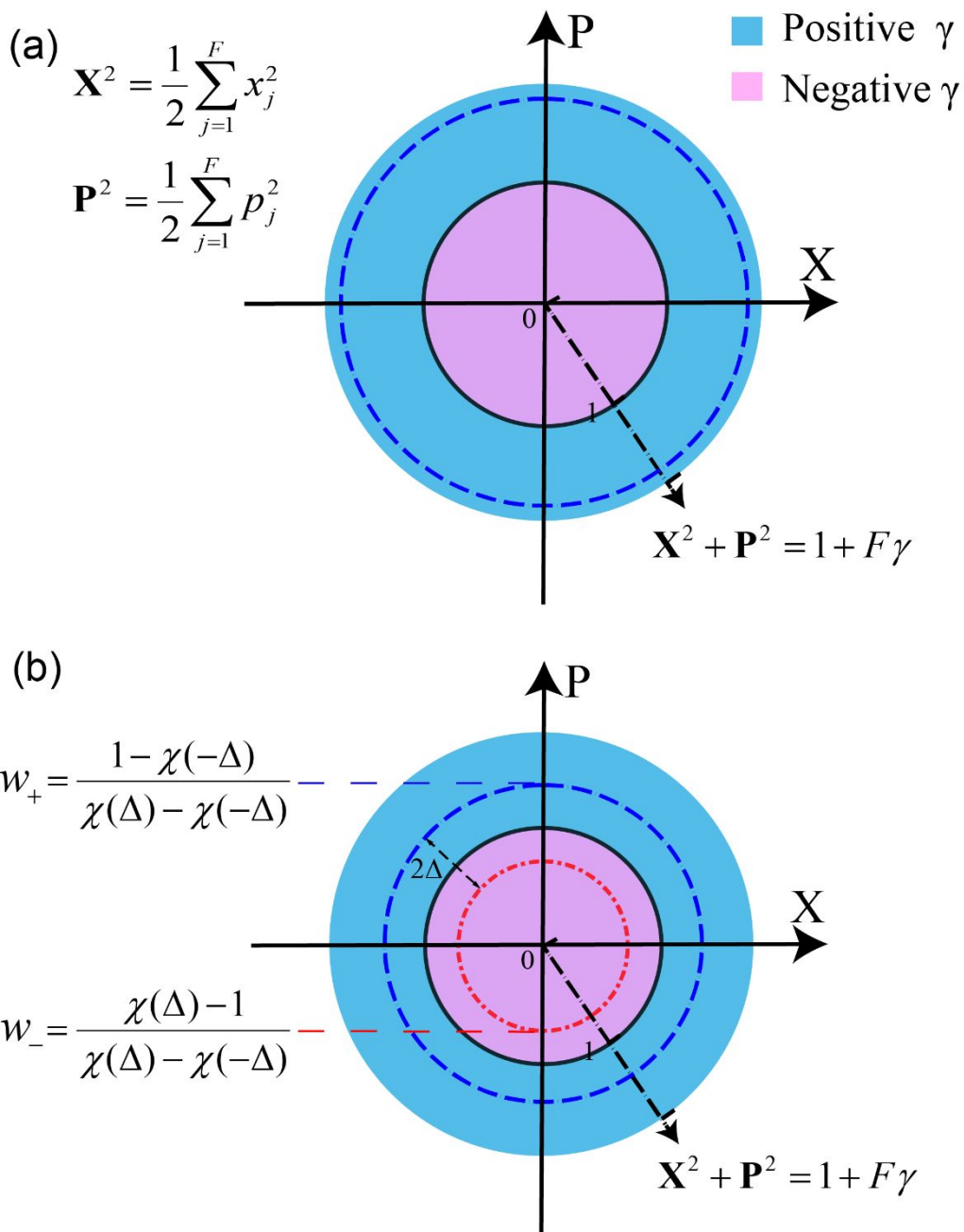
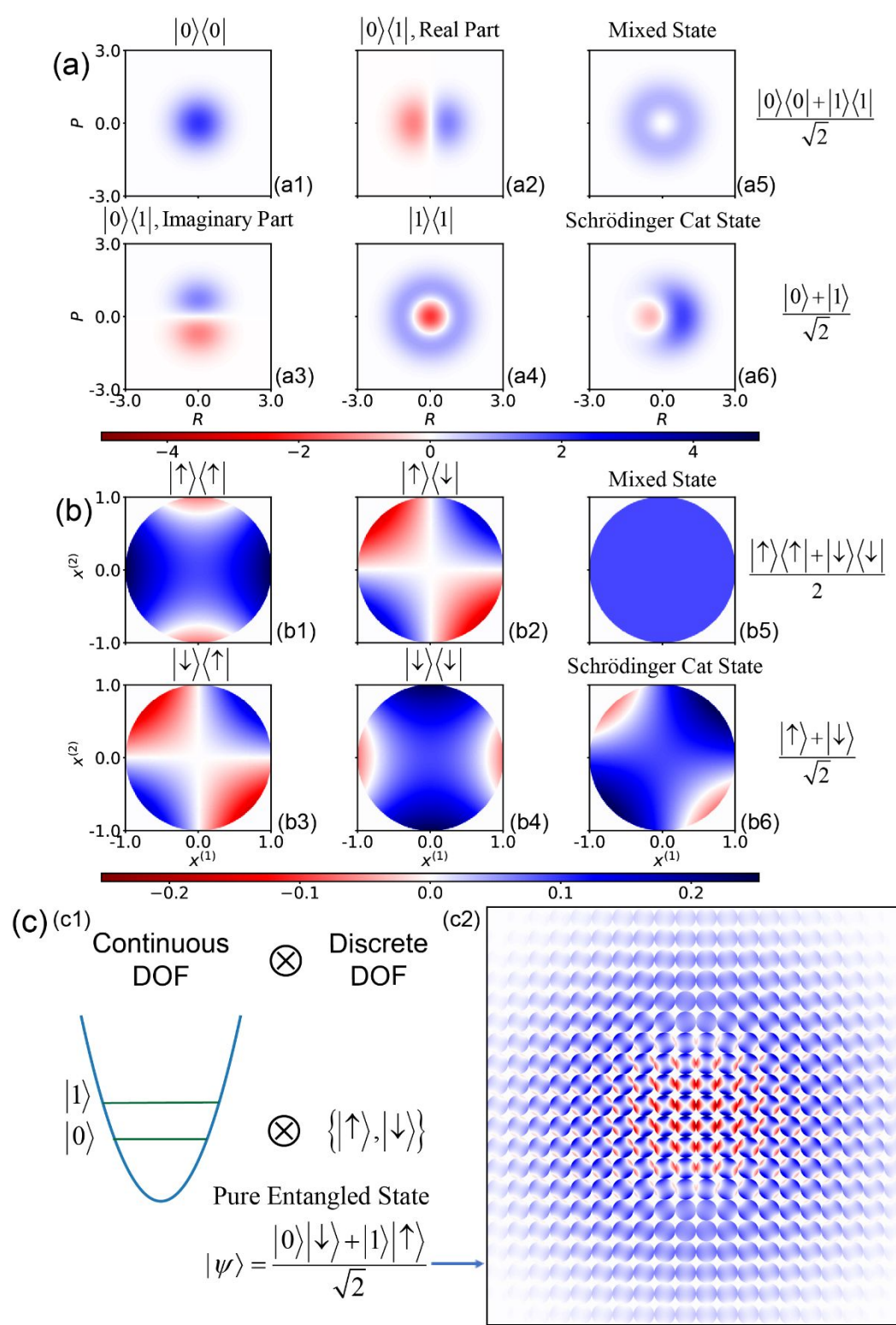


Figure 3: Illustration of the exact mapping formulation with constraint coordinate-momentum phase space. Panel (a) presents constraint phase space with only a single value of parameter γ . Panel (b) demonstrates weighted constraint phase space with two values of parameter γ , where the quasi-probability distribution function is $w(\gamma) = w_+ \delta(\gamma - \Delta) + w_- \delta(\gamma + \Delta)$. Constraint phase space with the positive weight is blue-dashed, while that with the negative weight is red dot-dashed. (Panel (a) is adapted with permission from ref¹³⁴. Copyright 2021 American Chemical Society.)

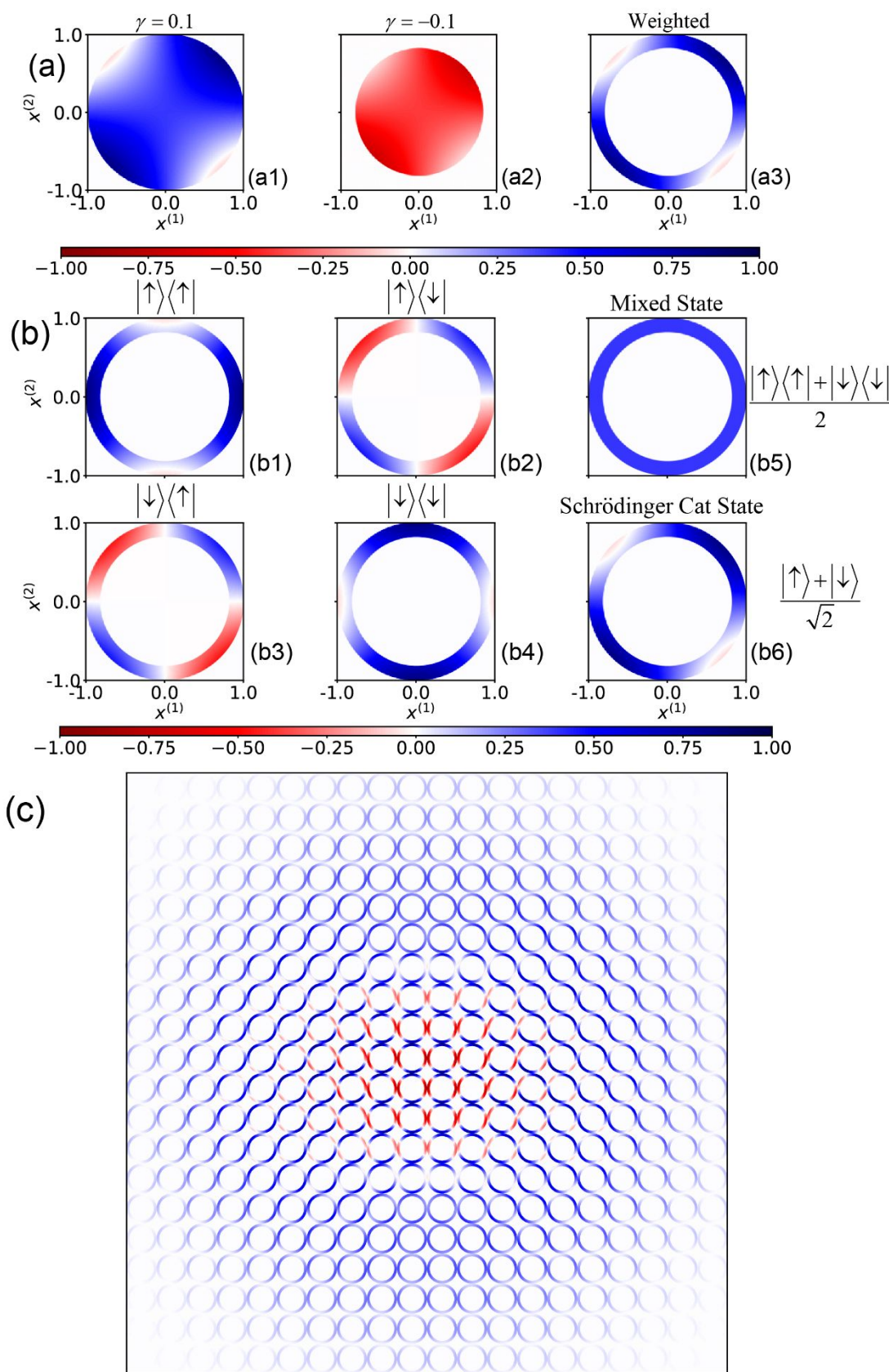


1
2
3 **Figure 4:** Illustrations of (a) Wigner representation of a continuous-variable system, (b) constraint phase space
4 representation of a discrete-variable system, and (c) hybrid coordinate-momentum phase space representation of
5 a composite system with both discrete and continuous DOFs.
6
7

8 (a) Wigner distribution for $|0\rangle\langle 0|$ (Panel a1), that for $|1\rangle\langle 1|$ (Panel a4), real part (Panel a2) and imaginary
9 part (Panel a3) of the Wigner distribution for $|0\rangle\langle 1|$, Wigner distribution for mixed state
10 $(|0\rangle\langle 0|+|1\rangle\langle 1|)/2$ (Panel a5), and that for Schrödinger cat state $(|0\rangle+|1\rangle)/\sqrt{2}$ (Panel a6). Here,
11
12 $|0\rangle$ and $|1\rangle$ are two energy levels of a continuous-variable system.
13
14

15 (b) Marginal distribution of constraint phase space coordinates $(x^{(1)}, x^{(2)})$ for $|\uparrow\rangle\langle \uparrow|$ (Panel b1), $|\downarrow\rangle\langle \downarrow|$
16 (Panel b4), that for $|\uparrow\rangle\langle \downarrow|$ (Panel b2), that for $|\downarrow\rangle\langle \uparrow|$ (Panel b3), that for mixed state
17 $(|\uparrow\rangle\langle \uparrow|+|\downarrow\rangle\langle \downarrow|)/2$ (Panel b5), and that for Schrödinger cat state $(|\uparrow\rangle+|\downarrow\rangle)/\sqrt{2}$ (Panel b6). Here,
18
19 $|\uparrow\rangle$ and $|\downarrow\rangle$ represent two discrete states of a discrete-variable system.
20
21

22 (c) Panel c1: Schematic representaton of the composite system and the pure entangled state
23 $(|0\rangle|\downarrow\rangle+|1\rangle|\uparrow\rangle)/2$; Panel c2: hybrid coordinate-momentum phase space representation of the entangled
24 state. The grid is on the Wigner phase space (R, P) for the continous DOF, and each circle of a grid stands
25 for the local marginal distribution function of constraint phase space variables $(x^{(1)}, x^{(2)})$. The notations
26 are identical to those in Panels (a)-(b).
27
28
29
30
31
32
33
34
35
36
37
38
39
40
41
42
43
44
45
46
47
48
49
50
51
52
53
54
55
56
57
58
59
60



1
2
3 **Figure 5:** Illustrations of (a) components and (b) marginal distribution functions of the weighted constraint phase
4 space representation of a discrete-variable system, and (c) weighted hybrid representation of the same composite
5 system as that of Figure 4(c).
6
7

- 8
9 (a) Marginal distribution of constraint phase space coordinates $(x^{(1)}, x^{(2)})$ for Schrödinger cat state
10
11 $(|\uparrow\rangle + |\downarrow\rangle)/\sqrt{2}$ with $\gamma = \Delta$ weighted by w_+ (Panel a1), with $\gamma = -\Delta$ weighted by w_- (Panel
12
13 a2). The sum of the two components yields the marginal distribution of constraint phase space coordinates
14
15 (x_1, x_2) of the weighted representation with two values of parameter γ for the Schrödinger cat state
16
17 (Panel a3). Coordinates are scaled by the larger radius $\sqrt{2(1+F\Delta)}$.
18
19
20
21 (b) Weighted marginal distribution of constraint phase space coordinates $(x^{(1)}, x^{(2)})$ for the same properties
22
23 as those in Figure 4(b).
24
25
26 (c) Same as Figure 4(c), but using weighted marginal distribution for the discrete DOF.
27
28
29
30
31
32
33
34
35
36
37
38
39
40
41
42
43
44
45
46
47
48
49
50
51
52
53
54
55
56
57
58
59
60

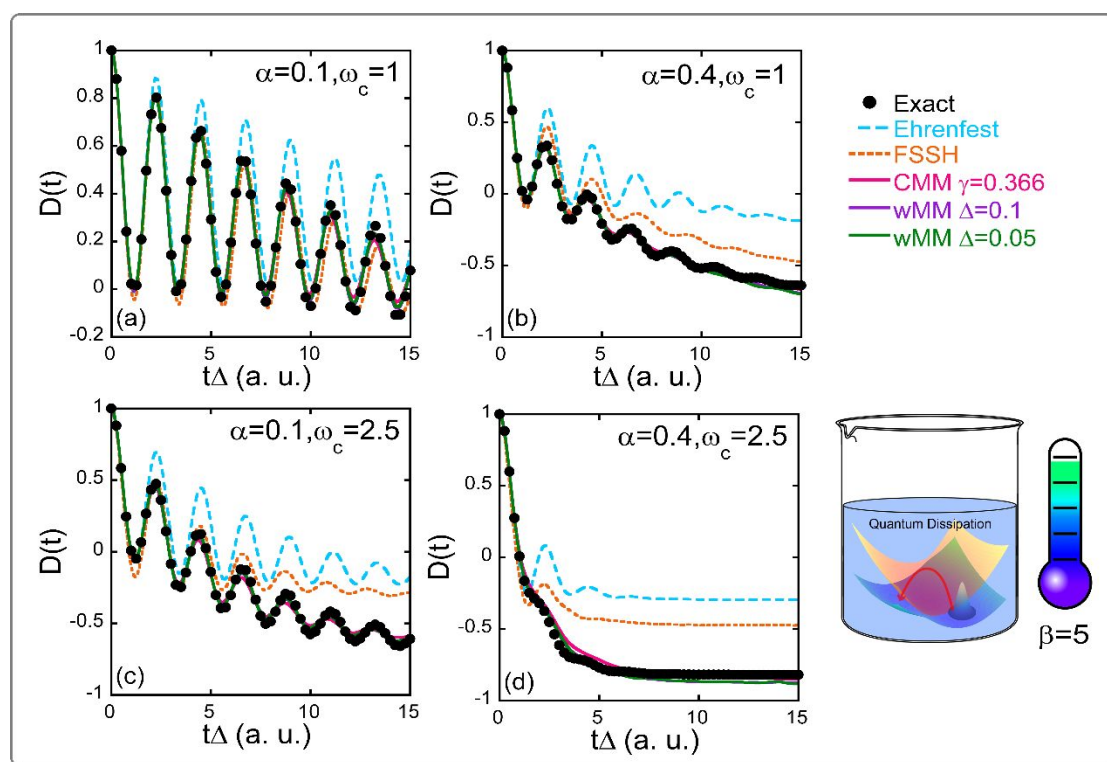
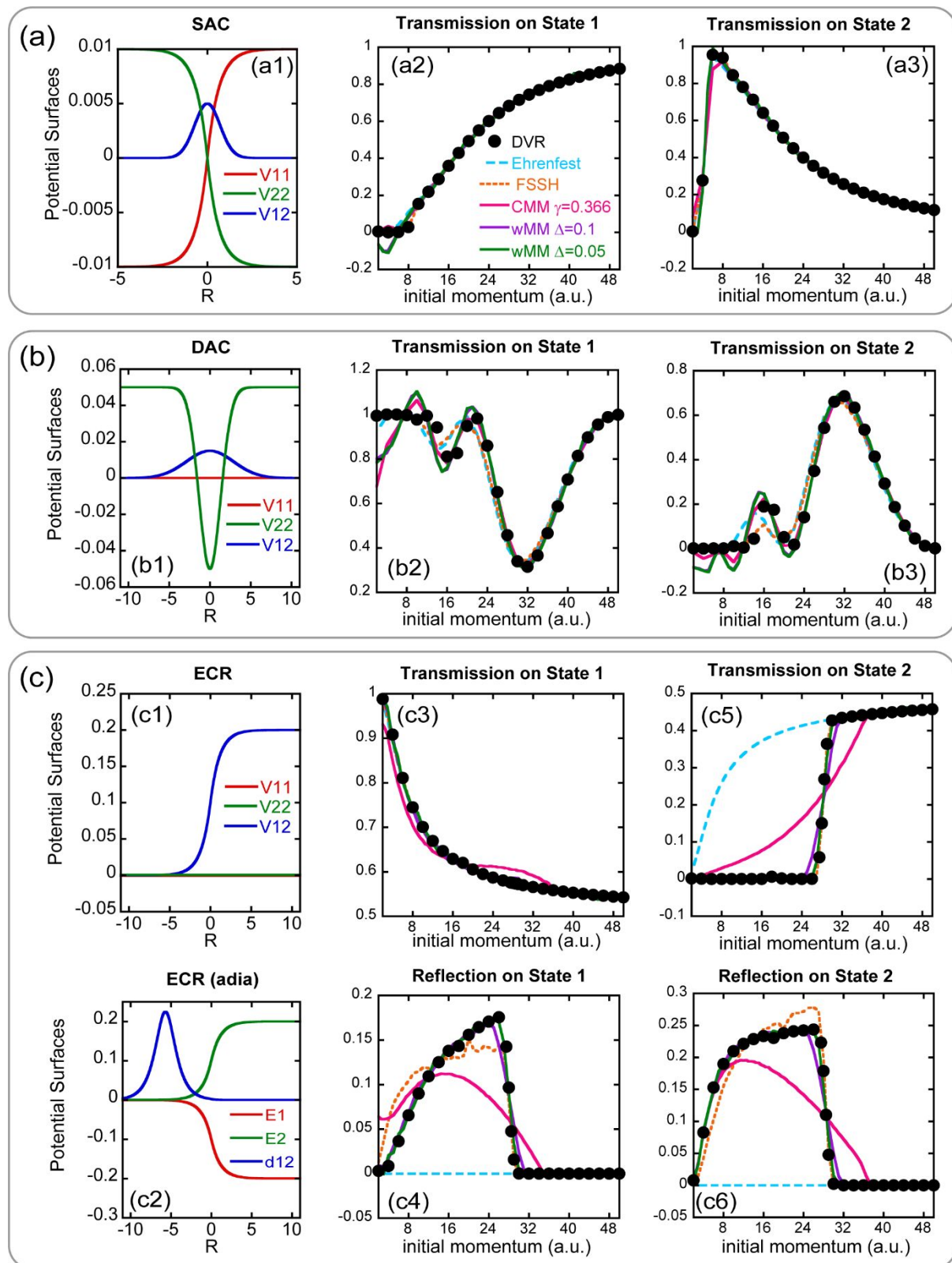


Figure 6: Results of population difference $D(t) = P_1(t) - P_0(t)$ between two states for the spin-boson model at low-temperature ($\beta = 1 / (k_B T) = 5$) with the Ohmic bath. Panel (a) reports the population dynamics of the spin-boson model with parameters $\varepsilon = \Delta_c = 1$, $\beta = 5$, $\omega_c = 1$, $\alpha = 0.1$ in Panel (a). Solid circles: Exact results produced by eHEOM reported in ref¹³⁴. Cyan dashed lines: Ehrenfest dynamics. Orange dashed lines: FSSH. Magenta solid lines: CMM with $\gamma = 0.366$. Purple and green solid lines: wMM with $\Delta = 0.1$ and 0.05, respectively. Panel (b) is similar to Panel (a) but for $\alpha = 0.4$; Panel (c) is similar to Panel (a) but for $\omega_c = 2.5$; Panel (d) is similar to Panel (a) but for $\omega_c = 2.5$, $\alpha = 0.4$. In each model 300 continuous DOFs (i.e., effective bath modes) are used.



1
2
3 **Figure 7:** Illustration of three Tully models and simulation results. Panel (a1) denotes diabatic PESes $V_{11}(R)$
4 and $V_{22}(R)$, as well as coupling term $V_{12}(R)$ for the SAC model; Panel (b1) does so for the DAC model;
5
6 Panel (c1) does so for the ECR model. Panel (c2) demonstrates adiabatic PESes $E_1(R)$ and $E_2(R)$, as well
7
8 as nonadiabatic coupling vector $d_{12}(R)$.
9

10
11 Panels (a2)-(a3): transmission coefficients on diabatic state 1, and those on diabatic state 2 of the SAC model,
12 respectively. Panels (b2)-(b3): similar to Panels (a2)-(a3), but for the DAC model. Panels (c3) and (c4):
13 transmission/reflection coefficients on adiabatic state 1 of the ECR model; Panels (c5) and (c6): those on adiabatic
14 state 2.
15

16
17 In Panels (a2)-(a3), (b2)-(b3), and (c3)-(c6), magenta, purple and green lines stand for transmission coefficients
18 results for CMM with $\gamma = 0.366$, wMM with $\Delta = 0.1$, and wMM with $\Delta = 0.05$, respectively. Long-
19 dashed blue lines: Ehrenfest dynamics; Short-dashed orange lines: FSSH; Black points: exact DVR benchmarks.
20
21
22
23
24
25
26
27
28
29
30
31
32
33
34
35
36
37
38
39
40
41
42
43
44
45
46
47
48
49
50
51
52
53
54
55
56
57
58
59
60

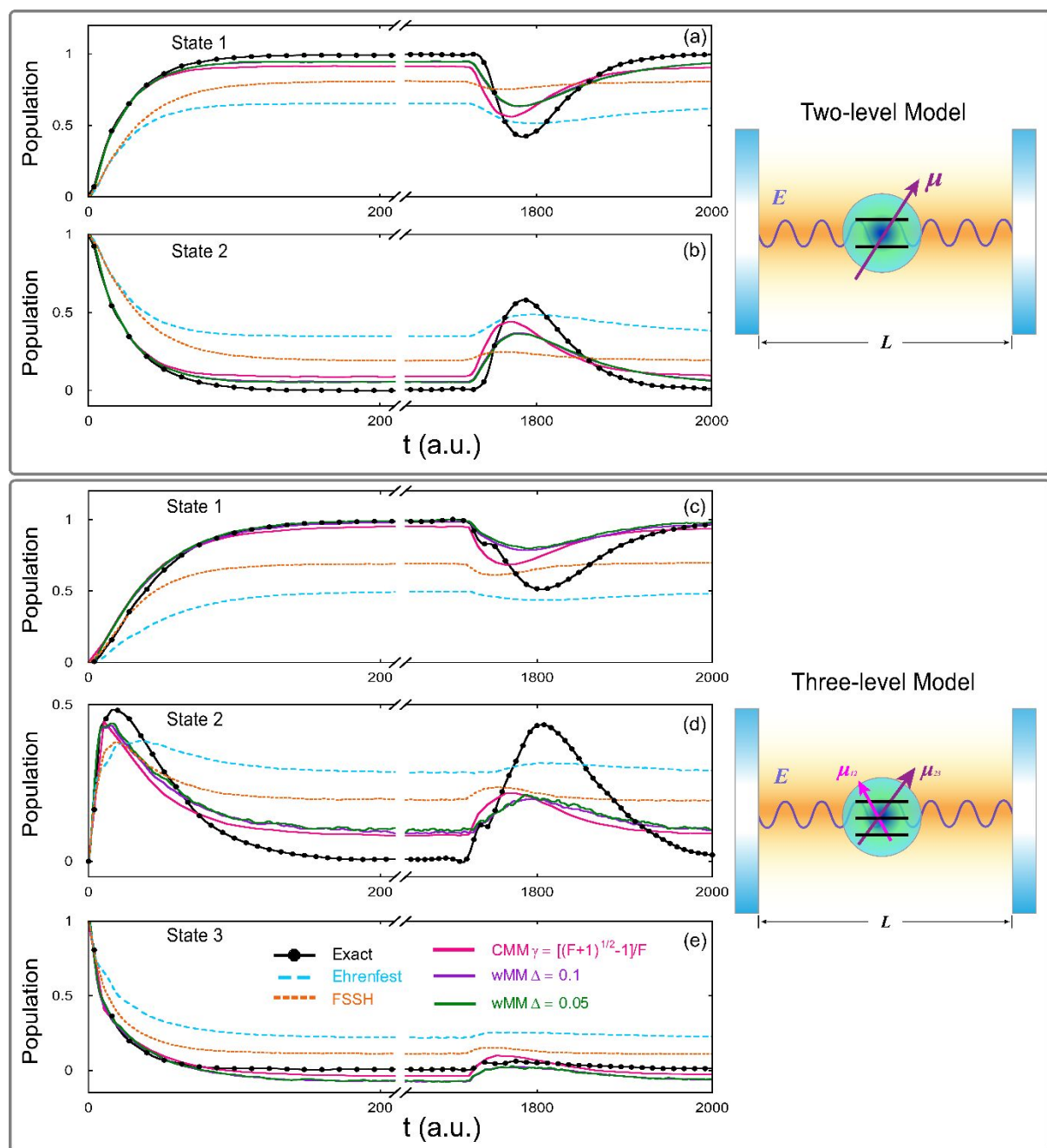


Figure 8: Results of population dynamics for the atom-in-cavity models. Panels (a)-(b) represent data of the first and second states of the two-level model, respectively. Panels (c)-(e) denote data of the first, second and third states of the three-level model, respectively. Magenta solid lines: CMM with $\gamma = (\sqrt{F+1} - 1)/F$; Purple solid lines: wMM with $\Delta = 0.1$; Green solid lines: wMM with $\Delta = 0.05$; Cyan long-dashed lines: Ehrenfest dynamics; Orange short-dashed lines: FSSH; Black solid-dotted lines: exact results from refs^{287, 288}. In each model 400 continuous DOFs (i.e., standing-wave modes) are involved.

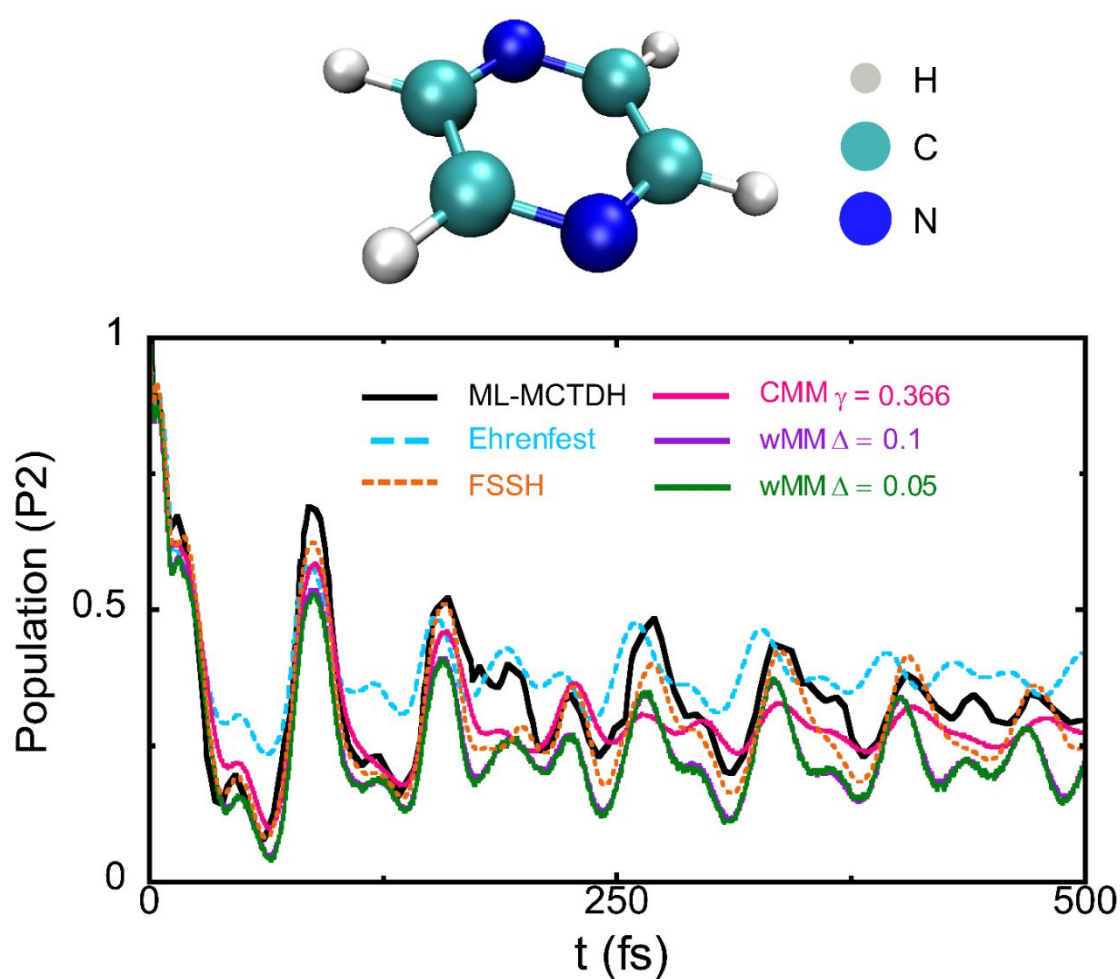


Figure 9: Results of population dynamics of the second electronic state of the 2-level 3-mode pyrazine model.

Magenta solid lines: CMM with $\gamma = (\sqrt{F+1} - 1) / F \approx 0.366$; Purple solid lines: wMM with $\Delta = 0.1$; Green solid lines: wMM with $\Delta = 0.05$. Cyan dashed lines: Ehrenfest dynamics; Orange short-dashed lines: FSSH; Black solid lines: ML-MCTDH results of ref²¹².

Funding Information

National Natural Science Foundation of China (NSFC) Grant No. 21961142017; Ministry of Science and Technology of China (MOST) Grant No. 2017YFA0204901

Research Resources

High-performance Computing Platform of Peking University, Beijing PARATERA Tech CO., Ltd., and Guangzhou supercomputer center

Acknowledgments

This work was supported by the National Natural Science Foundation of China (NSFC) Grant No. 21961142017, and by the Ministry of Science and Technology of China (MOST) Grant No. 2017YFA0204901. We acknowledge the High-performance Computing Platform of Peking University, Beijing PARATERA Tech CO., Ltd., and Guangzhou supercomputer center for providing computational resources.

Notes

The authors declare no competing financial interest.

Further Reading**Appendices****1. Derivation of the formulation of (weighted) constraint coordinate-momentum phase space.**

In this appendix, we introduce the techniques for performing integrals on constraint coordinate-momentum phase space, and show the brief derivation of the formulation of (weighted) constraint coordinate-momentum phase space. Such techniques have been expressed in Appendix A of ref¹³² as well as in Section S1 of the Supporting Information of ref¹³⁴.

Consider the expectation of any function $f(X_1, X_2, \dots, X_L)$ under the L -dimensional independent standard normal distribution (i.e., $\{X_i\} : N^{(L)}(0, 1)$). It is closely related to that under the uniform distribution on the $(L-1)$ -dimensional constraint space, i.e.,

$$\begin{aligned}
 \langle f \rangle_{N^{(L)}(0,1)} &= \frac{1}{(2\pi)^{L/2}} \int dX_1 dX_2 \dots dX_L e^{-\frac{1}{2} \sum_{k=1}^L X_k^2} f(X_1, X_2, \dots, X_L) \\
 &= \frac{1}{(2\pi)^{L/2}} \int_0^\infty d\xi \int dX_1 dX_2 \dots dX_L e^{-\xi} \delta\left(\frac{1}{2} \sum_{k=1}^L X_k^2 - \xi\right) f(X_1, X_2, \dots, X_L) . \quad 87 \\
 &= \frac{1}{(2\pi)^{L/2}} \int_0^\infty d\xi e^{-\xi} S_{L-1}(\sqrt{\xi}) \langle f \rangle_{S_{L-1}(\sqrt{\xi})}
 \end{aligned}$$

Here,

$$S_{L-1}(R) = \int dX_1 dX_2 \dots dX_L \delta\left(\frac{1}{2} \sum_{k=1}^L X_k^2 - R^2\right) \quad 88$$

denotes the area of the constraint space with radius R , and the expectation under the uniform distribution on the $(L-1)$ -dimensional constraint space, $\langle L \rangle_{S_{L-1}(R)}$, is given by

$$\langle f \rangle_{S_{L-1}(R)} = \frac{1}{S_{L-1}(R)} \int dX_1 dX_2 \dots dX_L \delta\left(\frac{1}{2} \sum_{k=1}^L X_k^2 - R^2\right) f(X_1, X_2, \dots, X_L) . \quad 89$$

(Note that the constraint space with radius R defined in eq 88 is slightly different from the $(L-1)$ -sphere in mathematics.) It is trivial to verify that $S_{L-1}(R) = R^{L-2} S_{L-1}(1)$ is the scaling relation of $S_{L-1}(R)$. We can calculate $S_{L-1}(1)$ by setting $f(X_1, X_2, \dots, X_L) \equiv 1$ in eq 87, i.e.,

$$1 = \frac{1}{(2\pi)^{L/2}} \int_0^\infty d\xi e^{-\xi} S_{L-1}(\sqrt{\xi}) = \frac{1}{(2\pi)^{L/2}} S_{L-1}(1) \int_0^\infty d\xi e^{-\xi} \xi^{\frac{L-2}{2}} . \quad 90$$

Equation 90 yields

$$S_{L-1}(1) = \frac{(2\pi)^{L/2}}{\Gamma(L/2)} \quad 91$$

after we use the equality $\int_0^\infty de^{-x} x^\alpha = \Gamma(\alpha+1)$ for $\alpha > -1$, where the Gamma function is defined by

$$\Gamma(s) = \int_0^\infty dt e^{-t} t^{s-1} \quad (s > 0).$$

The k -th order moment of the uniform distribution on the $(L-1)$ -dimensional constraint space has the scaling relation,

$$\begin{aligned} \langle X_{n_1} X_{n_2} \perp \! X_{n_k} \rangle_{S_{L-1}(\sqrt{\xi})} &= \frac{1}{S_{L-1}(\sqrt{\xi})} \int dX_1 dX_2 \perp \! dX_L \delta\left(\frac{1}{2} \sum_{l=1}^L X_l^2 - \xi\right) X_{n_1} X_{n_2} \perp \! X_{n_k} \\ &= \xi^{k/2} \langle X_{n_1} X_{n_2} \perp \! X_{n_k} \rangle_{S_{L-1}(1)} \end{aligned} \quad 92$$

Substitution of eq 92 into eq 87 produces

$$\begin{aligned} \langle X_{n_1} X_{n_2} \perp \! X_{n_k} \rangle_{N^{(L)}(0,1)} &= \frac{\Gamma\left(\frac{L+k}{2}\right)}{\Gamma(L/2)} \langle X_{n_1} X_{n_2} \perp \! X_{n_k} \rangle_{S_{L-1}(1)} \\ &= \frac{\Gamma\left(\frac{L+k}{2}\right)}{\xi^{k/2} \Gamma(L/2)} \langle X_{n_1} X_{n_2} \perp \! X_{n_k} \rangle_{S_{L-1}(\sqrt{\xi})} \end{aligned} \quad 93$$

The well-known Wick theorem (also called Isserlis's theorem)^{297, 298} for the independent and identical standard normal distribution reads

$$\langle X_{n_1} X_{n_2} \perp \! X_{n_k} \rangle_{N^{(L)}(0,1)} = \begin{cases} 0, & k \text{ is odd} \\ \sum \left(\prod \langle X_{n_i} X_{n_j} \rangle_{N^{(L)}(0,1)} \right), & k \text{ is even} \end{cases} \quad 94$$

Here, the notation $\sum(\prod \perp \!)$ stands for the summation of the products over all possible pair partitions of $\{X_{n_1}, X_{n_2}, \perp \! , X_{n_k}\}$. It is straightforward to obtain the second order moment and fourth order moment of $N^{(L)}(0,1)$,

$$\begin{aligned} \langle X_i X_j \rangle_{N(0,1)} &= \delta_{ij} \\ \langle X_i X_j X_k X_l \rangle_{N(0,1)} &= \delta_{ij} \delta_{kl} + \delta_{ik} \delta_{jl} + \delta_{il} \delta_{jk} \end{aligned} \quad 95$$

Substitution of eq 95 into eq 93 leads to

$$\begin{aligned} \langle X_i X_j \rangle_{S_{L-1}(\sqrt{\xi})} &= \frac{\xi}{L/2} \delta_{ij} \\ \langle X_i X_j X_k X_l \rangle_{S_{L-1}(\sqrt{\xi})} &= \frac{\xi^2}{\frac{L}{2} \left(\frac{L}{2} + 1 \right)} (\delta_{ij} \delta_{kl} + \delta_{ik} \delta_{jl} + \delta_{il} \delta_{jk}) \end{aligned} \quad 96$$

We then set $L = 2F$ as well as $\xi = 1 + F\gamma$ and relabel the constraint space (defined by eq 32) as $S_\gamma(\mathbf{x}, \mathbf{p})$ parameterized by γ . The comparison between eq 33 and eq 88 states that the area of constraint phase space is

$$\Omega(\gamma) = S_{2F-1} \left(R = \sqrt{1+F\gamma} \right) = \frac{(2\pi)^F}{\Gamma(F)} (1+F\gamma)^{F-1} . \quad 97$$

We then obtain

$$\begin{aligned} \langle g(\mathbf{x}, \mathbf{p}) \rangle_{S_{L-1}(\sqrt{\xi})} &= \int_{S_\gamma(\mathbf{x}, \mathbf{p})} d\mathbf{X} g(\mathbf{x}, \mathbf{p}) \\ &= \int F d\mathbf{x} d\mathbf{p} \frac{1}{\Omega(\gamma)} \delta \left(\sum_{n=1}^F \frac{(x^{(n)})^2 + (p^{(n)})^2}{2} - (1+F\gamma) \right) g(\mathbf{x}, \mathbf{p}) , \end{aligned} \quad 98$$

where $\mathbf{X} = (\mathbf{x}, \mathbf{p})$. The second order moment and fourth order moment on the constraint space of eq 32 read

$$\begin{aligned} \int_{S_\gamma(\mathbf{x}, \mathbf{p})} d\mathbf{X} (X_i X_j) &= \frac{1+F\gamma}{F} \delta_{ij} \\ \int_{S_\gamma(\mathbf{x}, \mathbf{p})} d\mathbf{X} (X_i X_j X_k X_l) &= \frac{(1+F\gamma)^2}{F(F+1)} (\delta_{ij}\delta_{kl} + \delta_{ik}\delta_{jl} + \delta_{il}\delta_{jk}) \end{aligned} . \quad 99$$

Consider $\hat{A} = |m\rangle\langle n|$ and $\hat{B} = |k\rangle\langle l|$. We have

$$\text{Tr}[\hat{A}\hat{B}] = \delta_{nk}\delta_{ml} . \quad 100$$

The constraint phase space expression (i.e., eqs 4-6 when only discrete electronic DOFs exist) of the left-hand side (LHS) of eq 100 is equivalent to

$$\begin{aligned} \text{Tr}[\hat{A}\hat{B}] &= F \int_{S_\gamma(\mathbf{x}, \mathbf{p})} d\mathbf{X} \langle n | \hat{K}_{\text{ele}}(\mathbf{x}, \mathbf{p}) | m \rangle \langle l | K_{\text{ele}}^{-1}(\mathbf{x}, \mathbf{p}) | k \rangle \\ &= F \int_{S_\gamma(\mathbf{x}, \mathbf{p})} d\mathbf{X} K_{nm}^{(\text{ele})}(\mathbf{x}, \mathbf{p}) K_{(ele), lk}^{-1}(\mathbf{x}, \mathbf{p}) \end{aligned} . \quad 101$$

In eq 101, $K_{nm}^{(\text{ele})}(\mathbf{x}, \mathbf{p})$ is the element of operator $\hat{K}_{\text{ele}}(\mathbf{x}, \mathbf{p})$, and $K_{(ele), lk}^{-1}(\mathbf{x}, \mathbf{p})$ is the element of operator $K_{\text{ele}}^{-1}(\mathbf{x}, \mathbf{p})$. When the mapping kernel is given by eq 30, it is straightforward to derive that its corresponding inverse kernel is eq 31 by employing eqs 99-101. Specifically, when the mapping kernel is identical to its inverse (i.e., eq 39), the element of the (inverse) kernel operator is

$$K_{nm}(\mathbf{x}, \mathbf{p}) = K_{nm}^{-1}(\mathbf{x}, \mathbf{p}) = \frac{1}{2} (x^{(n)} + ip^{(n)}) (x^{(m)} - ip^{(m)}) - \gamma \delta_{nm} . \quad 102$$

It is trivial to use eq 99 and eq 102 to achieve the equality

$$F \int_{S_\gamma(\mathbf{x}, \mathbf{p})} d\mathbf{X} K_{nm}(\mathbf{x}, \mathbf{p}) K_{lk}^{-1}(\mathbf{x}, \mathbf{p}) = \frac{(1+F\gamma)^2}{(F+1)} \delta_{nk}\delta_{ml} + \left[\frac{(1+F\gamma)^2}{(F+1)} - 2\gamma - F\gamma^2 \right] \delta_{lk}\delta_{nm} . \quad 103$$

After employing eqs 100-101, we obtain $\gamma = (\sqrt{F+1} - 1) / F$ from eq 103 where the mapping kernel is identical to its inverse (i.e., eq 39).

Similarly, the weighting constraint phase space formulation (eqs 4-6 when only discrete electronic DOFs exist, and eq 38) leads to

$$\begin{aligned}\text{Tr}_e [\hat{A}\hat{B}] &= \int_{S(x,p)} F dxdp A_C(x,p) \hat{B}_C^0(x,p) \\ &= \int_{-1/F}^{\infty} d\gamma w(\gamma) \int F dxdp \frac{1}{\Omega(\gamma)} \delta\left(\sum_{n=1}^F \frac{(x^{(n)})^2 + (p^{(n)})^2}{2} - (1+F\gamma)\right) A_C(x,p) \hat{B}_C^0(x,p) \quad 104 \\ &= \int_{-1/F}^{\infty} d\gamma w(\gamma) \langle A_C(x,p) \hat{B}_C^0(x,p) \rangle_{S_{L-1}(\sqrt{\xi})}\end{aligned}$$

Employing eq 100, we obtain an equation similar to eq 101

$$F \int d\gamma w(\gamma) \int_{S_\gamma(x,p)} dX K_{nm}(x,p) K_{lk}^{-1}(x,p) = \delta_{nk} \delta_{ml} \quad . \quad 105$$

Because we request eq 39 that the mapping kernel is identical to its inverse in the weighted constraint phase space formulation, eqs 102-103 also hold. Substitution of eq 103 into eq 105 generates

$$\int d\gamma w(\gamma) (F\gamma^2 + 2\gamma) = \int d\gamma w(\gamma) \chi(\gamma) = 1 \quad , \quad 106$$

which is eq 40 of the main text. When $w(\gamma)$, the quasi-probability distribution function of parameter γ , is a single Dirac delta function, the constraint coordinate-momentum phase space formulation with $\gamma = (\sqrt{F+1} - 1) / F$ is a special case of eq 106, or of eq 40 of the main text. When in eq 106 or eq 40 $w(\gamma)$ is represented by a linear combination of two symmetrical delta functions (i.e., eqs 44-46), we achieve the symmetrically weighted constraint phase space formulation employed in wMM of the Focus Article. Apparently, various other choices for quasi-probability distribution function $w(\gamma)$ are also available and can be investigated in the future.

2. More discussion on the equations of motion in the adiabatic representation

Below we will show that eq 75 and eq 77, the equations of motion (EOMs) under the diabatic-to-adiabatic transformation are intrinsically equivalent to Hamilton's EOMs generated by the Hamiltonian, eq 80, when (nuclear) canonical phase variables $(\mathbf{R}; \mathbf{P})$ are defined by eq 79. For simplicity, assume that all nonadiabatic coupling terms $\{\mathbf{d}_{mn}^{(I)}(\mathbf{R})\}$ are real. It leads to a simplified relation

$$\mathbf{P}_0 = \mathbf{P} + h \sum_{n,m=1}^F \mathbf{x}_0^{(m)} \beta_0^{(m)} \mathbf{d}_{mn}(\mathbf{R})$$

107

in eq 79. In the adiabatic representation, $\mathbf{P} = \mathbf{P}_0 - h \sum_{n,m=1}^F \mathbf{x}_0^{(m)} \beta_0^{(m)} \mathbf{d}_{mn}(\mathbf{R})$ is denoted the kinematic momentum (e.g., in ref¹⁸⁴), which is different from canonical momentum \mathbf{P} . The Hamiltonian, eq 80, is recast into

$$H_C(\mathbf{R}, \mathbf{P}, \mathbf{x}, \mathbf{p}) = \sum_{I=1}^N \frac{\left(\dot{\mathbf{P}}_I - h \sum_{n,m=1}^F \mathbf{x}_0^{(m)} \beta_0^{(m)} d_{mn}^{(I)}(\mathbf{R}) \right)^2}{2M_I} + \sum_{k=1}^F E_k(\mathbf{R}) \left(\frac{1}{2} \left((\mathbf{x}_0^{(k)})^2 + (\beta_0^{(k)})^2 \right) - \gamma \right) . \quad 108$$

Here, $d_{mn}^{(I)}(\mathbf{R})$ and $\dot{\beta}_I^k$ are the the I -th DOF component of $\mathbf{d}_{mn}(\mathbf{R})$ and that of \mathbf{P} , respectively. Note that canonical variables $(\mathbf{R}, \mathbf{P}, \mathbf{x}, \mathbf{p})$ are independent of one another. Hamilton's EOMs produced by eq 108 are

$$\begin{aligned} \dot{\mathbf{x}}_0^{(m)} &= \frac{1}{h} \frac{\partial}{\partial \dot{\beta}_0^{(m)}} H_C(\mathbf{R}, \mathbf{P}, \mathbf{x}, \mathbf{p}) \\ &= - \sum_{J=1}^N \sum_{n=1}^F \frac{\dot{\beta}_J^{(k)} - h \sum_{l=1}^F \mathbf{x}_0^{(k)} \beta_0^{(l)} d_{lk}^{(J)}(\mathbf{R})}{M_J} \mathbf{x}_0^{(n)} d_{mn}^{(J)}(\mathbf{R}) + \frac{1}{h} E_m(\mathbf{R}) \beta_0^{(m)}, \end{aligned} \quad 109$$

$$\begin{aligned} \dot{\beta}_0^{(m)} &= - \frac{1}{h} \frac{\partial}{\partial \dot{\mathbf{x}}_0^{(m)}} H_C(\mathbf{R}, \mathbf{P}, \mathbf{x}, \mathbf{p}) \\ &= \sum_{J=1}^N \sum_{n=1}^F \frac{\dot{\beta}_J^{(k)} - h \sum_{l=1}^F \mathbf{x}_0^{(k)} \beta_0^{(l)} d_{lk}^{(J)}(\mathbf{R})}{M_J} \beta_0^{(n)} d_{nm}^{(J)}(\mathbf{R}) - \frac{1}{h} E_m(\mathbf{R}) \mathbf{x}_0^{(m)}, \end{aligned} \quad 110$$

$$\dot{\beta}_I^k = \frac{\partial}{\partial \dot{\beta}_I^k} H_C(\mathbf{R}, \mathbf{P}, \mathbf{x}, \mathbf{p}) = \frac{\dot{\beta}_I^{(k)} - h \sum_{n,m=1}^F \mathbf{x}_0^{(m)} \beta_0^{(n)} d_{mn}^{(I)}(\mathbf{R})}{M_I}, \quad 111$$

$$\begin{aligned} \dot{\beta}_I^k &= - \frac{\partial}{\partial \dot{\beta}_I^k} H_C(\mathbf{R}, \mathbf{P}, \mathbf{x}, \mathbf{p}) \\ &= h \sum_{J=1}^N \sum_{n,m=1}^F \frac{\dot{\beta}_J^{(k)} - h \sum_{l=1}^F \mathbf{x}_0^{(k)} \beta_0^{(l)} d_{lk}^{(J)}(\mathbf{R})}{M_J} \mathbf{x}_0^{(n)} \beta_0^{(m)} \frac{\partial d_{mn}^{(J)}(\mathbf{R})}{\partial \dot{\beta}_I^k} \\ &\quad - \sum_{k=1}^F \frac{\partial E_k(\mathbf{R})}{\partial \dot{\beta}_I^k} \left(\frac{1}{2} \left((\mathbf{x}_0^{(k)})^2 + (\beta_0^{(k)})^2 \right) - \gamma \right) . \end{aligned} \quad 112$$

It is evident that eqs 109-110 are identical to eq 71 and that eq 111 is the same as the first equation of eq 77.

We will then prove that eq 112 is equivalent to the second equation of eq 77.

Consider the full time-derivative of canonical momentum \dot{P}_I^0 ,

$$\begin{aligned} \dot{P}_I^0 &= \dot{P}_I^0(R^0, P^0, \dot{R}^0, \dot{P}^0) + \hbar \frac{d}{dt} \sum_{n,m=1}^F \dot{\psi}_0^{(m)} \dot{p}_0^{(n)} d_{nm}^{(I)}(R^0) \\ &= \dot{P}_I^0 + \hbar \sum_{n,m=1}^F \dot{\psi}_0^{(m)} \dot{p}_0^{(n)} d_{nm}^{(I)}(R^0) + \hbar \sum_{n,m=1}^F \dot{\psi}_0^{(m)} \dot{p}_0^{(n)} d_{nm}^{(I)}(R^0) + \hbar \sum_{n,m=1}^F \dot{\psi}_0^{(m)} \dot{p}_0^{(n)} \sum_{J=1}^N \frac{\partial d_{nm}^{(I)}(R^0)}{\partial R_J^0} \dot{R}_J^0 . \end{aligned} \quad 113$$

Substitution of eqs 109-112 into eq 113 yields,

$$\begin{aligned} \dot{P}_I^0(R^0, P^0, \dot{R}^0, \dot{P}^0) &= \hbar \sum_{J=1}^N \sum_{n,m=1}^F \frac{P_J(R^0, P^0, \dot{R}^0, \dot{P}^0) \dot{\psi}_0^{(m)} \dot{p}_0^{(n)}}{M_J} \left(\frac{\partial d_{mn}^{(J)}(R^0)}{\partial R_I^0} - \frac{\partial d_{mn}^{(I)}(R^0)}{\partial R_J^0} \right) \\ &\quad - \sum_{k=1}^F \frac{\partial E_k(R^0)}{\partial R_I^0} \left(\frac{1}{2} \left((\dot{\psi}_0^{(k)})^2 + (\dot{p}_0^{(k)})^2 \right) - \gamma \right) \\ &\quad + \hbar \sum_{n,m=1}^F \sum_{J=1}^N \sum_{k=1}^F \frac{P_J(R^0, P^0, \dot{R}^0, \dot{P}^0) d_{nk}^{(I)}(R^0) d_{km}^{(J)}(R^0) (\dot{\psi}_0^{(m)} \dot{p}_0^{(n)} - \dot{\psi}_0^{(n)} \dot{p}_0^{(m)})}{M_J} \\ &\quad + \sum_{n,m=1}^F \left(E_n(R^0) \dot{\psi}_0^{(m)} \dot{\psi}_0^{(n)} - E_m(R^0) \dot{p}_0^{(m)} \dot{p}_0^{(n)} \right) d_{nm}^{(I)}(R^0) . \end{aligned} \quad 114$$

Since the derivative of the first-order nonadiabatic coupling is

$$\begin{aligned} \frac{\partial d_{mn}^{(J)}}{\partial R_I^0} &= \frac{\partial}{\partial R_I^0} \left\langle \phi_m \left| \frac{\partial}{\partial R_J^0} \phi_n \right. \right\rangle = \left\langle \frac{\partial}{\partial R_I^0} \phi_m \left| \frac{\partial}{\partial R_J^0} \phi_n \right. \right\rangle + \left\langle \phi_m \left| \frac{\partial^2}{\partial R_I^0 \partial R_J^0} \phi_n \right. \right\rangle , \\ &= \sum_{k=1}^F d_{km}^{(I)} d_{kn}^{(J)} + D_{mn}^{(IJ)} \end{aligned} \quad 115$$

where $D_{mn}^{(IJ)} = \left\langle \phi_m \left| \frac{\partial^2}{\partial R_I^0 \partial R_J^0} \phi_n \right. \right\rangle$ is a symmetric tensor of nuclear index, i.e., $D_{mn}^{(IJ)} = D_{mn}^{(JI)}$, the first term of

the RHS of eq 114 becomes

$$\begin{aligned} &\hbar \sum_{J=1}^N \sum_{n,m=1}^F \frac{P_J(R^0, P^0, \dot{R}^0, \dot{P}^0) \dot{\psi}_0^{(m)} \dot{p}_0^{(n)}}{M_J} \left(\frac{\partial d_{mn}^{(J)}(R^0)}{\partial R_I^0} - \frac{\partial d_{mn}^{(I)}(R^0)}{\partial R_J^0} \right) \\ &= -\hbar \sum_{J=1}^N \sum_{n,m=1}^F \sum_{k=1}^F \frac{P_J(R^0, P^0, \dot{R}^0, \dot{P}^0) (\dot{\psi}_0^{(m)} \dot{p}_0^{(n)} - \dot{\psi}_0^{(n)} \dot{p}_0^{(m)})}{M_J} d_{nk}^{(I)}(R^0) d_{km}^{(J)}(R^0) . \end{aligned} \quad 116$$

1
2
3
4 It is important to note that, in general $\frac{\partial d_{mn}^{(J)}(\mathbf{R})}{\partial R_I^0} - \frac{\partial d_{mn}^{(I)}(\mathbf{R})}{\partial R_J^0} = 0$ does not always hold for $I \neq J$, except
5
6

7 for two-electronic-state systems. So eq 116 is not always equal to zero. The term of eq 116 cancels out the
8 third term of eq 114. The last term of the RHS of eq 114 can be recast into
9
10

$$\begin{aligned} & \sum_{n,m=1}^F \left(E_n(\mathbf{R}) \mathcal{X}_0^{(m)} \mathcal{X}_0^{(m)} - E_m(\mathbf{R}) \mathcal{P}_0^{(m)} \mathcal{P}_0^{(m)} \right) d_{nm}^{(I)}(\mathbf{R}) \\ &= \frac{1}{2} \sum_{n,m=1}^F \left(E_n(\mathbf{R}) - E_m(\mathbf{R}) \right) \left(\mathcal{X}_0^{(m)} \mathcal{X}_0^{(m)} + \mathcal{P}_0^{(m)} \mathcal{P}_0^{(m)} \right) d_{nm}^{(I)}(\mathbf{R}) \end{aligned} \quad . \quad 117$$

11
12
13
14
15
16
17
18 Equation 114 then becomes
19

$$\begin{aligned} & \dot{\mathbf{P}}_I(\mathbf{R}, \mathbf{P}, \mathbf{x}, \mathbf{p}) \\ &= - \sum_{k=1}^F \frac{\partial E_k(\mathbf{R})}{\partial R_I} \left(\frac{1}{2} \left((\mathcal{X}_0^{(k)})^2 + (\mathcal{P}_0^{(k)})^2 \right) - \gamma \right) - \sum_{n,m=1}^F \left(E_n(\mathbf{R}) - E_m(\mathbf{R}) \right) d_{mn}^{(I)}(\mathbf{R}) \frac{1}{2} \left(\mathcal{X}_0^{(n)} \mathcal{X}_0^{(m)} + \mathcal{P}_0^{(n)} \mathcal{P}_0^{(m)} \right) \end{aligned}$$

20
21
22
23
24
25
26
27
28
29
30
31
32
33
34
35
36
37
38
39
40
41
42
43
44
45
46
47
48
49
50
51
52
53
54
55
56
57
58
59
60 which is equivalent to the second equation of eq 77 of the main text. It indicates that the canonical momentum in
the diabatic representation is covariant with *kinematic* momentum \mathbf{P} rather than canonical momentum \mathbf{P}^c in
adiabatic representation unless all nonadiabatic coupling terms vanish. This is consistent with the spirit of the
work of Cotton *et. al.* in ref¹⁸⁴. Because the EOMs (eq 71 and eq 77) of the main text are identical to Hamilton's
EOMs generated by eq 108, the mapping Hamiltonian (eq 80 or eq 108) is conserved during the evolution in the
adiabatic representation.

3. The relationship between the constraint coordinate-momentum phase space and Stratonovich phase space

Stratonovich's original work¹⁰⁰ in 1956 maps a 2-state (spin-1/2) system onto a two-dimensional sphere. We review two kinds of further developments of the Stratonovich-Weyl mapping phase space representations for F -state quantum system: the first one based on the SU(2) structure^{103, 113} and the second one based on the SU(F) structure¹¹⁴. We show the relationship between constrained coordinate-momentum phase space representation that we use in the Focus Article and the two kinds of Stratonovich phase space representations.

In the SU(2) Stratonovich phase space representation, an F -state system is treated as a spin- j system (where $F = 2j + 1$). The basis set consists of $|j, m\rangle$, the eigenstate of the square of total angular momentum

\hat{J}^2 and the z -component of angular momentum \hat{J}_z with quantum numbers j and m , respectively. The mapping kernel is

$$\hat{K}_{\text{ele}}^{\text{SU}(2)}(\theta, \varphi; s) = \sqrt{\frac{\pi}{2j+1}} \sum_{l=0}^{2j} (C_{jj,l0}^{jj})^{-s} \sum_{m=-l}^l Y_{lm}^*(\theta, \varphi) \hat{T}_{lm}^j, \quad s \in \mathbb{i} \quad 119$$

where \hat{T}_{lm}^j is the irreducible tensor operator defined as²⁹⁹

$$\hat{T}_{lm}^j = \sqrt{\frac{2l+1}{2j+1}} \sum_{m',n=-j}^j C_{jm',lm}^{jn} |j,n\rangle\langle j,m'|. \quad 120$$

Here $C_{j_1 m_1, j_2 m_2}^{jm} = \langle jm | j_1 m_1, j_2 m_2 \rangle$ is the well-known Clebsch-Gordan coefficient for the angular momentum coupling, and $Y_{lm}(\theta, \varphi)$ is the spherical harmonic function. The inverse kernel of $\hat{K}_{\text{ele}}^{\text{SU}(2)}(\theta, \varphi; s)$ is simply $\hat{K}_{\text{ele}}^{\text{SU}(2)}(\theta, \varphi; -s)$. We note that, although $s = 1, 0$, and -1 are traditionally associated with the Q , Wigner, and P -functions respectively and used in the literature^{111, 128}, parameter s of eq 119 can in principle take *any* real value.

When $F > 2$, the SU(2) Stratonovich phase space (θ, φ) does *not* have a phase point-to-phase point mapping to constraint coordinate-momentum phase space, although the relation can only be constructed by virtue of the density matrix. Only when $F = 2$ as in the original work of Stratonovich, there exists a phase point-to-phase point mapping to constraint coordinate-momentum phase space. The mapping kernel can be expressed in terms of the spin-coherent state,

$$\hat{K}_{\text{ele}}^{\text{SU}(2)}(\theta, \varphi; s) = 3^{(1+s)/2} |\theta, \varphi\rangle\langle\theta, \varphi| + \frac{\hat{\mathbf{I}}}{2} [1 - 3^{(1+s)/2}] \quad . \quad 121$$

In eq 121 spin coherent state $|\theta, \varphi\rangle$ is

$$|\theta, \varphi\rangle = \begin{pmatrix} e^{-i\varphi} \sin(\theta/2) \\ \cos(\theta/2) \end{pmatrix}, \quad 122$$

where (θ, φ) are the spherical coordinate variables on the two-dimensional spherical phase space. The range of θ is $[0, \pi]$ and that for φ is $[0, 2\pi)$. When $F = 2$, the explicit transformation of (θ, φ) to the constrained coordinate-momentum phase space $(x^{(1)}, x^{(2)}, p^{(1)}, p^{(2)})$ is

$$\begin{aligned} \begin{pmatrix} x^{(1)} \\ p^{(1)} \end{pmatrix} &= \sqrt{2(1+2\gamma)} \begin{pmatrix} \cos\psi & -\sin\psi \\ \sin\psi & \cos\psi \end{pmatrix} \begin{pmatrix} \cos\varphi \sin(\theta/2) \\ -\sin\varphi \sin(\theta/2) \end{pmatrix}, \\ \begin{pmatrix} x^{(2)} \\ p^{(2)} \end{pmatrix} &= \sqrt{2(1+2\gamma)} \begin{pmatrix} \cos\psi & -\sin\psi \\ \sin\psi & \cos\psi \end{pmatrix} \begin{pmatrix} \cos(\theta/2) \\ 0 \end{pmatrix} \end{aligned} \quad , \quad 123$$

where ψ is an additional global phase.

The second kind of representation is the $SU(F)$ Stratonovich phase space¹¹⁴, which is diffeomorphic to the quotient set $SU(F)/U(F-1)$, parameterized by $(2F-2)$ angle variables $(\boldsymbol{\theta}, \boldsymbol{\varphi}) = (\theta_1, \theta_2, \dots, \theta_{F-1}, \varphi_1, \varphi_2, \dots, \varphi_{F-1})$. The range of each angle θ_i is $[0, \pi/2]$ and that for each angle φ_i is $[0, 2\pi)$. The $SU(F)$ Stratonovich phase space of Tilma *et.al.*¹¹⁴ has been used to prepare the initial condition for the Meyer-Miller mapping model of non-adiabatic dynamics in ref¹⁹⁷.

The mapping kernel of the $SU(F)$ Stratonovich phase space is

$$\hat{K}_{\text{ele}}^{\text{SU}(F)}(\boldsymbol{\theta}, \boldsymbol{\varphi}; s) = (1+F)^{(1+s)/2} |\boldsymbol{\theta}, \boldsymbol{\varphi}\rangle \langle \boldsymbol{\theta}, \boldsymbol{\varphi}| + \frac{\hat{\mathbf{I}}}{F} (1 - (1+F)^{(1+s)/2}), \quad s \in \mathbb{i} \quad 124$$

and the inverse kernel is $\hat{K}_{\text{ele}}^{\text{SU}(F)}(\boldsymbol{\theta}, \boldsymbol{\varphi}; -s)$. The explicit form of the generalized coherent state $|\boldsymbol{\theta}, \boldsymbol{\varphi}\rangle$ is^{300, 301}

$$|\boldsymbol{\theta}, \boldsymbol{\varphi}\rangle = \sum_{n=1}^F c_n |n\rangle \quad , \quad 125$$

where the coefficients are

$$\begin{pmatrix} c_1 \\ c_2 \\ c_3 \\ \vdots \\ c_{F-3} \\ c_{F-2} \\ c_{F-1} \\ c_F \end{pmatrix} = \begin{pmatrix} e^{i(\varphi_1+\varphi_2+\dots+\varphi_{F-1})} \cos(\theta_1) \cos(\theta_2) \dots \cos(\theta_{F-2}) \sin(\theta_{F-1}) \\ -e^{i(-\varphi_1+\varphi_2+\dots+\varphi_{F-1})} \sin(\theta_1) \cos(\theta_2) \dots \cos(\theta_{F-2}) \sin(\theta_{F-1}) \\ -e^{i(\varphi_3+\varphi_4+\dots+\varphi_{F-1})} \sin(\theta_2) \cos(\theta_3) \dots \cos(\theta_{F-2}) \sin(\theta_{F-1}) \\ \vdots \\ -e^{i(\varphi_{F-3}+\varphi_{F-2}+\varphi_{F-1})} \sin(\theta_{F-4}) \cos(\theta_{F-3}) \cos(\theta_{F-2}) \sin(\theta_{F-1}) \\ -e^{i(\varphi_{F-2}+\varphi_{F-1})} \sin(\theta_{F-3}) \cos(\theta_{F-2}) \sin(\theta_{F-1}) \\ -e^{i(\varphi_{F-1})} \sin(\theta_{F-2}) \sin(\theta_{F-1}) \\ \cos(\theta_{F-1}) \end{pmatrix}. \quad 126$$

As derived first in Appendix A of ref¹³² in the spirit of ref¹³¹ and then in the Supporting Information of ref¹³⁴, the mapping kernel of constraint coordinate-momentum phase space for a set of F states (eq 30 of the main text) is denoted as,

$$\hat{K}_{\text{ele}}(\mathbf{x}, \mathbf{p}; \gamma) = \sum_{m,n=1}^F \left[\frac{(x^{(m)} - i p^{(m)})(x^{(n)} + i p^{(n)})}{2} - \gamma \delta_{mn} \right] |n\rangle \langle m| = |\mathbf{x}, \mathbf{p}\rangle \langle \mathbf{x}, \mathbf{p}| - \gamma \hat{\mathbf{I}}, \quad 127$$

1
2
3 where the non-normalized state $|\mathbf{x}, \mathbf{p}\rangle$ is
4
5

$$\sum_{n=1}^F \frac{x^{(n)} + i p^{(n)}}{\sqrt{2}} |n\rangle. \quad 128$$

6
7
8
9 The $U(F)$ constraint coordinate-momentum phase space of the $(2F-1)$ -dimensional sphere is
10
11
12 diffeomorphic to $U(F)/U(F-1)$. (The difference between $U(F)$ and $SU(F) \times U(1)$ is excluded by
13
14 the division over $U(F-1)$.) Comparison of $\hat{K}_{\text{ele}}^{\text{SU}(F)}(\boldsymbol{\theta}, \boldsymbol{\varphi}; s)$ to $\hat{K}_{\text{ele}}(\mathbf{x}, \mathbf{p}; \gamma)$ implies that the two
15
16 kernels are closely related. The correspondence between parameters s and γ reads
17
18

$$1 + F\gamma = (1 + F)^{(1+s)/2}. \quad 129$$

19
20
21 It is evident (from eq 129, the relation between constraint coordinate-momentum phase space and the $SU(F)$
22
23 Stratonovich phase space) that parameter s can be any real number in eq 124, *not* limited to $s = 1, 0$, or -1 ,
24
25 where the corresponding value of parameter γ of constraint coordinate-momentum phase space is
26
27 $\gamma = 1, (\sqrt{1+F} - 1)/F$, or 0 . This has been clearly mentioned in refs^{57, 58, 134}.
28
29

30 Any normalized pure state of the F -dimensional Hilbert space uniquely corresponds to a state on constraint
31
32 coordinate-momentum phase space, $|\mathbf{x}, \mathbf{p}\rangle$, which is equivalent to $\exp[i\psi]|\boldsymbol{\theta}, \boldsymbol{\varphi}\rangle$ with ψ as the global
33
34 phase. That is, the correspondence between $(\boldsymbol{\theta}, \boldsymbol{\varphi})$ and (\mathbf{x}, \mathbf{p}) is
35
36

$$\begin{pmatrix} x^{(n)} \\ p^{(n)} \end{pmatrix} = \sqrt{2(1+F\gamma)} \begin{pmatrix} \cos\psi & -\sin\psi \\ \sin\psi & \cos\psi \end{pmatrix} \begin{pmatrix} \text{Re}\langle n | \boldsymbol{\theta}, \boldsymbol{\varphi} \rangle \\ \text{Im}\langle n | \boldsymbol{\theta}, \boldsymbol{\varphi} \rangle \end{pmatrix}. \quad 130$$

37
38
39
40
41 Under the transformation, eq 130, mapping functions $A_C(\boldsymbol{\theta}, \boldsymbol{\varphi}; s) = \text{Tr}[\hat{A} \hat{K}_{\text{ele}}^{\text{SU}(F)}(\boldsymbol{\theta}, \boldsymbol{\varphi}; s)]$ and
42
43
44 $A_C(\mathbf{x}, \mathbf{p}; \gamma) = \text{Tr}[\hat{A} \hat{K}_{\text{ele}}(\mathbf{x}, \mathbf{p}; \gamma)]$ of an operator \hat{A} share the same value. The global phase, ψ , which
45
46 is missing in the $SU(F)$ Stratonovich phase space, however, is important for the expression of quantum
47
48 dynamics.
49

50
51 When we consider quantum dynamics in a finite F -dimensional Hilbert space, if the Hamiltonian operator
52 includes linear components beyond the identity operator and generator operators of phase space group, it is
53
54 impossible to derive trajectory-based exact dynamics. The $SU(2)$ group involves the identity operator and
55
56 angular momentum operators as generators on S^2 sphere. It produces trajectory-based exact dynamics only
57
58 for two-state systems, but fails to do so for all $F > 2$ cases. It is claimed that trajectory-based dynamics is a
59
60

good approximation for the large spin limit ($F \rightarrow \infty$) though^{109, 111, 302}. Except for the $F = 2$ case, the expression of quantum dynamics on the $SU(2)$ Stratonovich phase space has no direct relation to the trajectory-based exact dynamics on constrained coordinate-momentum phase space.

The $SU(F)$ Stratonovich phase space, however, produces trajectory-based exact dynamics for the finite F -dimensional Hilbert space. This is because that the evolution generated by any Hamiltonian of the F -dimensional Hilbert space is the action of some group element of $SU(F)$.³⁰³ The inherent symplectic structure of Stratonovich phase space indicates that the trajectory-based exact dynamics can be produced by the corresponding mapping Hamiltonian function $H_C = \text{Tr}[\hat{H}\hat{K}_{\text{ele}}^{\text{SU}(F)}(\theta, \varphi; s)]$, i.e.,

$$\begin{cases} \dot{\theta}_i = -\sum_{j=1}^{F-1} \frac{A_{ji}}{(1+F)^{(1+s)/2}} \frac{\partial H_C}{\partial \varphi_j} \\ \dot{\varphi}_i = +\sum_{j=1}^{F-1} \frac{A_{ij}}{(1+F)^{(1+s)/2}} \frac{\partial H_C}{\partial \theta_j} \end{cases} \quad 131$$

The elements, $\{A_{ij}\}$, of the $(F-1) \times (F-1)$ matrix, \mathbf{A} , are

$$A_{ij} = \begin{cases} \frac{1}{2} \csc(2\theta_1) \csc^2 \theta_{F-1} \prod_{k=2}^{F-2} \sec^2 \theta_k, & i = j = 1; \\ -\frac{1}{2} \cot(2\theta_1) \csc^2 \theta_{F-1} \prod_{k=2}^{F-2} \sec^2 \theta_k, & (i-1) = j = 1; \\ \csc(2\theta_i) \csc^2 \theta_{F-1} \prod_{k=i+1}^{F-2} \sec^2 \theta_k, & 2 \leq i = j \leq F-2; \\ -\frac{1}{2} \cot(\theta_i) \csc^2 \theta_{F-1} \prod_{k=i+1}^{F-2} \sec^2 \theta_k, & 2 \leq (i-1) = j \leq F-2; \\ -\csc(2\theta_{F-1}), & i = j = (F-1). \end{cases} \quad 132$$

The explicit expression of the EOMs of eq 131 is, however, much complicated. In addition, because trigonometric functions are involved in eq 132, singularities are inevitable in the EOMs on the $SU(F)$ Stratonovich phase space for $F > 2$. This makes the expression of quantum dynamics on the $SU(F)$ Stratonovich phase space numerically unfavorable. In comparison, on (weighted) constrained coordinate-momentum phase space, Hamilton's EOMs are simply linear in derivatives with coefficients independent of phase variables, as well as exact.

The relation of eq 130 implies that there exists a one-to-one correspondence between exact trajectory-base dynamics on the $SU(F)$ Stratonovich phase space and that on constraint coordinate-momentum phase space.

The addition of the global phase, ψ , is critical to obtain the one-to-one correspondence. The EOM of ψ reads

$$\dot{\psi} = \left[-\frac{\partial}{\partial \lambda} + \frac{\tan \theta_{F-1}}{2\lambda} \frac{\partial}{\partial \theta_{F-1}} \right] H_C^{(\lambda)}(\boldsymbol{\theta}, \boldsymbol{\phi}; s) \Big|_{\lambda=(1+F)^{\frac{1+s}{2}}}, \quad 133$$

where the extended mapping Hamiltonian function is defined by

$$H_C^{(\lambda)}(\boldsymbol{\theta}, \boldsymbol{\phi}; s) = \text{Tr} \left[\hat{K}_{\text{ele}}^{\text{SU}(F), (\lambda)}(\boldsymbol{\theta}, \boldsymbol{\phi}; s) \hat{H} \right] \quad 134$$

for the extended $\text{SU}(F)$ Stratonovich mapping ‘kernel’

$$\hat{K}_{\text{ele}}^{\text{SU}(F), (\lambda)}(\boldsymbol{\theta}, \boldsymbol{\phi}; s) = \lambda |\boldsymbol{\theta}, \boldsymbol{\phi}\rangle\langle\boldsymbol{\theta}, \boldsymbol{\phi}| + \frac{\hat{I}}{F} \left(1 - (1+F)^{\frac{1+s}{2}} \right). \quad 135$$

In eq 135 λ is treated as an ‘invariant’ variable. The evolution of state $\sqrt{\lambda} e^{i\psi} |\boldsymbol{\theta}, \boldsymbol{\phi}\rangle \equiv |\mathbf{x}, \mathbf{p}\rangle$ generates

$$\begin{cases} \dot{\lambda} = \frac{\partial}{\partial \psi} H_C^{(\lambda)}(\boldsymbol{\theta}, \boldsymbol{\phi}; s) = 0 \\ \dot{\psi} = \left[-\frac{\partial}{\partial \lambda} + \frac{\tan \theta_{F-1}}{2\lambda} \frac{\partial}{\partial \theta_{F-1}} \right] H_C^{(\lambda)}(\boldsymbol{\theta}, \boldsymbol{\phi}; s) \\ \dot{\theta}_i = -\sum_{j=1}^{F-1} \frac{A_{ji}}{\lambda} \frac{\partial}{\partial \phi_j} H_C^{(\lambda)}(\boldsymbol{\theta}, \boldsymbol{\phi}; s) - \delta_{i,F-1} \frac{\tan \theta_{F-1}}{2\lambda} \frac{\partial}{\partial \psi} H_C^{(\lambda)}(\boldsymbol{\theta}, \boldsymbol{\phi}; s) \\ \dot{\phi}_i = +\sum_{j=1}^{F-1} \frac{A_{ij}}{\lambda} \frac{\partial}{\partial \theta_j} H_C^{(\lambda)}(\boldsymbol{\theta}, \boldsymbol{\phi}; s) \end{cases}. \quad 136$$

It is straightforward to show that under the bijection,

$$\begin{pmatrix} \mathbf{x}^{(n)} \\ \mathbf{p}^{(n)} \end{pmatrix} = \sqrt{2\lambda} \begin{pmatrix} \cos \psi & -\sin \psi \\ \sin \psi & \cos \psi \end{pmatrix} \begin{pmatrix} \text{Re}\langle n | \boldsymbol{\theta}, \boldsymbol{\phi} \rangle \\ \text{Im}\langle n | \boldsymbol{\theta}, \boldsymbol{\phi} \rangle \end{pmatrix}, \quad 137$$

between variables $(\lambda, \psi, \boldsymbol{\theta}, \boldsymbol{\phi})$ and (\mathbf{x}, \mathbf{p}) , eq 136 leads to the EOMS of phase variables of (weighted) constraint phase space

$$\begin{aligned} \dot{\mathbf{x}}^{(n)} &= + \frac{\partial H_C}{\partial \mathbf{p}^{(n)}} \\ \dot{\mathbf{p}}^{(n)} &= - \frac{\partial H_C}{\partial \mathbf{x}^{(n)}} \end{aligned} \quad 138$$

by the chain rules, i.e.,

$$\mathbf{x}^{(n)} = \sum_{i=1}^{2F} \frac{\partial \mathbf{x}^{(n)}}{\partial z_i} \mathbf{z}_i$$

$$\mathbf{p}^{(n)} = \sum_{i=1}^{2F} \frac{\partial \mathbf{p}^{(n)}}{\partial z_i} \mathbf{z}_i$$

139

and

$$\frac{\partial H_C}{\partial z_i} = \sum_{n=1}^F \frac{\partial \mathbf{x}^{(n)}}{\partial z_i} \frac{\partial H_C}{\partial \mathbf{x}^{(n)}} + \sum_{n=1}^F \frac{\partial \mathbf{p}^{(n)}}{\partial z_i} \frac{\partial H_C}{\partial \mathbf{p}^{(n)}},$$

140

where $\{z_i\}$ denote variables $\{\lambda, \psi, \theta, \phi\}$.

4. Marginal distribution functions on symmetrically weighted coordinate-momentum phase space

As demonstrated in Figure 5, the marginal distribution functions on symmetrically weighted constraint coordinate-momentum phase space demonstrate a hollow structure. Equation 51 leads to the marginal functions on symmetrically weighted coordinate-momentum phase space

$$\begin{aligned} K_{\uparrow\uparrow}(x^{(1)}, x^{(2)}) &= \frac{1-2\Delta^2+2\Delta}{4\Delta} \frac{1+(x^{(1)})^2/2-(x^{(2)})^2/2}{2\pi(1+2\Delta)} \Big|_{(x^{(1)})^2+(x^{(2)})^2 \leq 2(1+2\Delta)} \\ &\quad - \frac{1-2\Delta^2-2\Delta}{4\Delta} \frac{1+(x^{(1)})^2/2-(x^{(2)})^2/2}{2\pi(1-2\Delta)} \Big|_{(x^{(1)})^2+(x^{(2)})^2 \leq 2(1-2\Delta)} \\ K_{\uparrow\downarrow}(x^{(1)}, x^{(2)}) &= K_{\downarrow\uparrow}(x^{(1)}, x^{(2)}) = \frac{1-2\Delta^2+2\Delta}{4\Delta} \frac{x^{(1)}x^{(2)}}{2\pi(1+2\Delta)} \Big|_{(x^{(1)})^2+(x^{(2)})^2 \leq 2(1+2\Delta)} \\ &\quad - \frac{1-2\Delta^2-2\Delta}{4\Delta} \frac{x^{(1)}x^{(2)}}{2\pi(1-2\Delta)} \Big|_{(x^{(1)})^2+(x^{(2)})^2 \leq 2(1-2\Delta)} \\ K_{\downarrow\downarrow}(x^{(1)}, x^{(2)}) &= \frac{1-2\Delta^2+2\Delta}{4\Delta} \frac{1-(x^{(1)})^2/2+(x^{(2)})^2/2}{2\pi(1+2\Delta)} \Big|_{(x^{(1)})^2+(x^{(2)})^2 \leq 2(1+2\Delta)} \\ &\quad - \frac{1-2\Delta^2-2\Delta}{4\Delta} \frac{1-(x^{(1)})^2/2+(x^{(2)})^2/2}{2\pi(1-2\Delta)} \Big|_{(x^{(1)})^2+(x^{(2)})^2 \leq 2(1-2\Delta)} \end{aligned}$$

141

As $\Delta \rightarrow 0^+$, $K_{nm}(x^{(1)}, x^{(2)})$ approaches zero in region $(x^{(1)})^2 + (x^{(2)})^2 \leq 2(1-F\Delta)$, yielding the hollow structure.

References

1. Lee HW, Scully MO. A new approach to molecular-collisions - statistical quasiclassical method. *The Journal of Chemical Physics* 1980, 73:2238-2242.
2. Lee HW, Scully MO. The Wigner phase-space description of collision processes. *Foundations of Physics* 1983, 13:61-72.
3. Heller EJ. Wigner phase space method: Analysis for semiclassical applications. *The Journal of Chemical Physics* 1976, 65:1289.
4. Sun X, Wang H, Miller WH. Semiclassical theory of electronically nonadiabatic dynamics: Results of a linearized approximation to the initial value representation. *The Journal of Chemical Physics* 1998, 109:7064-7074.
5. Wang H, Sun X, Miller WH. Semiclassical approximations for the calculation of thermal rate constants for chemical reactions in complex molecular systems. *The Journal of Chemical Physics* 1998, 108:9726-9736.
6. Pollak E, Liao J-L. A new quantum transition state theory. *The Journal of Chemical Physics* 1998, 108:2733-2743.
7. Shao J, Liao J-L, Pollak E. Quantum transition state theory: Perturbation expansion. *The Journal of Chemical Physics* 1998, 108:9711-9725.
8. Hernandez R, Voth GA. Quantum time correlation functions and classical coherence. *Chemical Physics* 1998, 233:243-255.
9. Liu J, Miller WH. Using the thermal Gaussian approximation for the Boltzmann operator in semiclassical initial value time correlation functions. *The Journal of Chemical Physics* 2006, 125:224104.
10. Liu J, Miller WH. Linearized semiclassical initial value time correlation functions using the thermal Gaussian approximation: applications to condensed phase systems. *The Journal of Chemical Physics* 2007, 127:114506.
11. Liu J, Miller WH. Real time correlation function in a single phase space integral beyond the linearized semiclassical initial value representation. *The Journal of Chemical Physics* 2007, 126:234110.
12. Liu J, Miller WH. Linearized semiclassical initial value time correlation functions with maximum entropy analytic continuation. *The Journal of Chemical Physics* 2008, 129:124111.
13. Liu J, Miller WH. Test of the consistency of various linearized semiclassical initial value time correlation functions in application to inelastic neutron scattering from liquid para-hydrogen. *The Journal of Chemical Physics* 2008, 128:144511.
14. Liu J, Miller WH, Paesani F, Zhang W, Case DA. Quantum dynamical effects in liquid water: A semiclassical study on the diffusion and the infrared absorption spectrum. *The Journal of Chemical Physics* 2009, 131:164509.
15. Liu J, Miller WH. A simple model for the treatment of imaginary frequencies in chemical reaction rates and molecular liquids. *The Journal of Chemical Physics* 2009, 131:074113.
16. Liu J, Alder BJ, Miller WH. A semiclassical study of the thermal conductivity of low temperature liquids. *The Journal of Chemical Physics* 2011, 135:114105.
17. Liu J, Miller WH, Fanourgakis GS, Xantheas SS, Imoto S, Saito S. Insights in quantum dynamical effects in the infrared spectroscopy of liquid water from a semiclassical study with an ab initio-based flexible and polarizable force field. *The Journal of Chemical Physics* 2011, 135:244503.
18. Liu J. Recent advances in the linearized semiclassical initial value representation/classical Wigner model for the thermal correlation function. *International Journal of Quantum Chemistry* 2015, 115:657-670.
19. Liu X, Liu J. Critical role of quantum dynamical effects in the Raman spectroscopy of liquid water. *Molecular Physics* 2018, 116:755-779.
20. Shi Q, Geva E. Semiclassical theory of vibrational energy relaxation in the condensed phase. *Journal of Physical Chemistry A* 2003, 107:9059-9069.
21. Shi Q, Geva E. A relationship between semiclassical and centroid correlation functions. *The Journal of Chemical Physics* 2003, 118:8173-8184.
22. Ka BJ, Geva E. Vibrational energy relaxation of polyatomic molecules in liquid solution via the linearized semiclassical method. *Journal of Physical Chemistry A* 2006, 110:9555-9567.
23. Poulsen JA, Nyman G, Rossky PJ. Practical evaluation of condensed phase quantum correlation functions: A Feynman-Kleinert variational linearized path integral method. *The Journal of Chemical Physics* 2003, 119:12179-12193.
24. Poulsen JA, Nyman G, Rossky PJ. Feynman-Kleinert linearized path integral (FK-LPI) algorithms for quantum molecular dynamics, with application to water and He(4). *Journal of Chemical Theory and Computation* 2006, 2:1482-1491.
25. Shao J, Makri N. Forward-Backward Semiclassical Dynamics with Linear Scaling. *The Journal of Physical Chemistry A* 1999, 103:9479-9486.
26. Shao J, Makri N. Forward-Backward Semiclassical Dynamics without Prefactors. *The Journal of Physical Chemistry A* 1999, 103:7753-7756.
27. Liu J, Nakayama A, Makri N. Long-time behaviour of quantized distributions in forward-backward semiclassical dynamics. *Molecular Physics* 2006, 104:1267-1274.
28. Liu J, Makri N. Symmetries and detailed balance in forward-backward semiclassical dynamics. *Chemical Physics* 2006, 322:23-29.
29. Makri N, Nakayama A, Wright NJ. Forward-backward semiclassical simulation of dynamical properties in liquids. *Journal of Theoretical and Computational Chemistry* 2004, 3:391-417.

- 1
2
3
4
5
6
7
8
9
10
11
12
13
14
15
16
17
18
19
20
21
22
23
24
25
26
27
28
29
30
31
32
33
34
35
36
37
38
39
40
41
42
43
44
45
46
47
48
49
50
51
52
53
54
55
56
57
58
59
60
30. Makri N. Quantum-classical path integral: A rigorous approach to condensed phase dynamics. *International Journal of Quantum Chemistry* 2015, 115:1209-1214.
 31. Walters PL, Makri N. Quantum-Classical Path Integral Simulation of Ferrocene-Ferrocenium Charge Transfer in Liquid Hexane. *Journal of Physical Chemistry Letters* 2015, 6:4959-4965.
 32. Kryvohuz M, Cao JS. Quantum-classical correspondence in response theory. *Physical Review Letters* 2005, 95:180405.
 33. Donoso A, Martens CC. Quantum tunneling using entangled classical trajectories. *Physical Review Letters* 2001, 87:223202.
 34. Donoso A, Zheng Y, Martens CC. Simulation of quantum processes using entangled trajectory molecular dynamics. *Journal of Chemical Physics* 2003, 119:5010-5020.
 35. Wang A, Zheng Y, Martens CC, Ren W. Quantum tunneling dynamics using entangled trajectories: general potentials. *Physical Chemistry Chemical Physics* 2009, 11:1588-1594.
 36. Xu F, Martens CC, Zheng Y. Entanglement dynamics with a trajectory-based formulation. *Physical Review A* 2017, 96:022138.
 37. Liu J, Miller WH. An approach for generating trajectory-based dynamics which conserves the canonical distribution in the phase space formulation of quantum mechanics. I. Theories. *The Journal of Chemical Physics* 2011, 134:104101.
 38. Liu J, Miller WH. An approach for generating trajectory-based dynamics which conserves the canonical distribution in the phase space formulation of quantum mechanics. II. Thermal correlation functions. *The Journal of Chemical Physics* 2011, 134:104102.
 39. Liu J. Two more approaches for generating trajectory-based dynamics which conserves the canonical distribution in the phase space formulation of quantum mechanics. *The Journal of Chemical Physics* 2011, 134:194110.
 40. Liu J. Path integral Liouville dynamics for thermal equilibrium systems. *The Journal of Chemical Physics* 2014, 140:224107.
 41. Liu J, Zhang Z. Path integral Liouville dynamics: Applications to infrared spectra of OH, water, ammonia, and methane. *The Journal of Chemical Physics* 2016, 144:034307.
 42. Liu J, Li D, Liu X. Further study of path integral Liouville dynamics. *Scientia Sinica Chimica* 2016, 46:27-37.
 43. Zhang Z, Chen Z, Liu J. Path integral Liouville dynamics simulations of vibrational spectra of formaldehyde and hydrogen peroxide. *Chinese Journal of Chemical Physics* 2020, 33:613-622.
 44. Liu X, Zhang L, Liu J. Machine learning phase space quantum dynamics approaches. *The Journal of Chemical Physics* 2021, 154:184104.
 45. Smith KKG, Poulsen JA, Nyman G, Cunsolo A, Rossky PJ. Application of a new ensemble conserving quantum dynamics simulation algorithm to liquid para-hydrogen and ortho-deuterium. *Journal of Chemical Physics* 2015, 142:244113.
 46. Smith KKG, Poulsen JA, Nyman G, Rossky PJ. A new class of ensemble conserving algorithms for approximate quantum dynamics: Theoretical formulation and model problems. *Journal of Chemical Physics* 2015, 142:244112.
 47. Willatt MJ, Ceriotti M, Althorpe SC. Approximating Matsubara dynamics using the planetary model: Tests on liquid water and ice. *Journal of Chemical Physics* 2018, 148:102336.
 48. Orr L, de la Pena LH, Roy P-N. Formulation of state projected centroid molecular dynamics: Microcanonical ensemble and connection to the Wigner distribution. *Journal of Chemical Physics* 2017, 146:214116.
 49. Bonella S, Montemayor D, Coker DF. Linearized path integral approach for calculating nonadiabatic time correlation functions. *Proceedings of the National Academy of Sciences* 2005, 102:6715-6719.
 50. Nassimi A, Bonella S, Kapral R. Analysis of the quantum-classical Liouville equation in the mapping basis. *The Journal of Chemical Physics* 2010, 133:134115.
 51. Weinrib J, Ferry DK. Recent advances in Wigner function approaches. *Applied Physics Reviews* 2018, 5:041104.
 52. Pie T, Huppert S, Finocchi F, Depondt P, Bonella S. Sampling the thermal Wigner density via a generalized Langevin dynamics. *Journal of Chemical Physics* 2019, 151:114114.
 53. Kapral R, Ciccotti G. Mixed quantum-classical dynamics. *The Journal of Chemical Physics* 1999, 110:8919-8929.
 54. Kapral R. Quantum dynamics in open quantum-classical systems. *Journal of Physics: Condensed Matter* 2015, 27:073201.
 55. Bai S, Xie W, Zhu L, Shi Q. Calculation of absorption spectra involving multiple excited states: Approximate methods based on the mixed quantum classical Liouville equation. *Journal of Chemical Physics* 2014, 140:084105.
 56. Tao G, Miller WH. Semiclassical Description of Electronic Excitation Population Transfer in a Model Photosynthetic System. *Journal of Physical Chemistry Letters* 2010, 1:891-894.
 57. He X, Wu B, Gong Z, Liu J. Commutator Matrix in Phase Space Mapping Models for Nonadiabatic Quantum Dynamics. *The Journal of Physical Chemistry A* 2021, 125:6845-6863.
 58. Liu J, He X, Wu B. Unified Formulation of Phase Space Mapping Approaches for Nonadiabatic Quantum Dynamics. *Accounts of chemical research* 2021, 54:4215-4228.

- 1
2
3 59. Orioli AP, Safavi-Naini A, Wall ML, Rey AM. Nonequilibrium dynamics of spin-boson models from phase-space methods. *Physical Review A* 2017, 96:033607.
4
5 60. Lang H, Vendrell O, Hauke P. Generalized discrete truncated Wigner approximation for nonadiabatic quantum-classical dynamics. *Journal of Chemical Physics* 2021, 155:024111.
6
7 61. Glauber RJ. Coherent and Incoherent States of Radiation Field. *Physical Review* 1963, 131:2766.
8
9 62. Sudarshan ECG. Equivalence of Semiclassical and Quantum Mechanical Descriptions of Statistical Light Beams. *Physical Review Letters* 1963, 10:277.
10
11 63. Cahill KE, Glauber RJ. Ordered expansions in boson amplitude operators. *Physical Review* 1969, 177:1857.
12
13 64. Cahill KE, Glauber RJ. Density operators and quasiprobability distributions. *Physical Review* 1969, 177:1882.
14
15 65. Arecchi FT, Thomas H, Gilmore R, Courtens E. Atomic coherent states in quantum optics. *Physical Review A* 1972, 6:2211.
16
17 66. Drummond PD, Gardiner CW. Generalized P-Representations in Quantum Optics. *Journal of Physics A: Mathematical and General* 1980, 13:2353-2368.
18
19 67. Walls D, Millburn G. *Quantum Optics*. Berlin: Springer-Verlag; 1994.
20
21 68. Gardiner C, Zoller P. *Quantum Noise*. 3rd edition ed. Berlin Heidelberg: Springer-Verlag; 2004.
22
23 69. Schleich WP. Quantum Optics in Phase Space. *Quantum Optics in Phase Space* 2001:716.
24
25 70. Deleglise S, Dotsenko I, Sayrin C, Bernu J, Brune M, Raimond JM, Haroche S. Reconstruction of non-classical cavity field states with snapshots of their decoherence. *Nature* 2008, 455:510-514.
26
27 71. Steel MJ, Olsen MK, Plimak LI, Drummond PD, Tan SM, Collett MJ, Walls DF, Graham R. Dynamical quantum noise in trapped Bose-Einstein condensates. *Physical Review A* 1998, 58:4824-4835.
28
29 72. Sinatra A, Lobo C, Castin Y. The truncated Wigner method for Bose-condensed gases: limits of validity and applications. *Journal of Physics B: Atomic Molecular and Optical Physics* 2002, 35:3599-3631.
30
31 73. Blakie PB, Bradley AS, Davis MJ, Ballagh RJ, Gardiner CW. Dynamics and statistical mechanics of ultra-cold Bose gases using c-field techniques. *Advances in Physics* 2008, 57:363-455.
32
33 74. Polkovnikov A. Phase space representation of quantum dynamics. *Annals of Physics* 2010, 325:1790-1852.
34
35 75. Mukherjee R, Mirasola AE, Hollingsworth J, White IG, Hazzard KRA. Geometric representation of spin correlations and applications to ultracold systems. *Physical Review A* 2018, 97:043606.
36
37 76. Zurek WH. Sub-Planck structure in phase space and its relevance for quantum decoherence. *Nature* 2001, 412:712-717.
38
39 77. Miquel C, Paz JP, Saraceno M. Quantum computers in phase space. *Physical Review A* 2002, 65:062309.
40
41 78. Wootters WK. Picturing Qubits in Phase Space. *IBM Journal of Research and Development* 2004, 48:99-110.
42
43 79. Paz JP, Roncaglia AJ, Saraceno M. Qubits in phase space: Wigner-function approach to quantum-error correction and the mean-king problem. *Physical Review A* 2005, 72:012309.
44
45 80. Braunstein SL, van Loock P. Quantum information with continuous variables. *Reviews of Modern Physics* 2005, 77:513-577.
46
47 81. Delfosse N, Guerin PA, Bian J, Raussendorf R. Wigner function negativity and contextuality in quantum computation on rebits. *Physical Review X* 2015, 5:021003.
48
49 82. Schachenmayer J, Pikovski A, Rey AM. Many-Body Quantum Spin Dynamics with Monte-Carlo Trajectories on a Discrete Phase Space. *Physical Review X* 2015, 5:011022.
50
51 83. Schachenmayer J, Pikovski A, Rey AM. Dynamics of correlations in two-dimensional quantum spin models with long-range interactions: a phase-space Monte-Carlo study. *New Journal of Physics* 2015, 17:065009.
52
53 84. Bermejo-Vega J, Delfosse N, Browne DE, Okay C, Raussendorf R. Contextuality as a resource for models of quantum computation with qubits. *Physical Review Letters* 2017, 119:120505.
54
55 85. Rundle RP, Mills PW, Tilma T, Samson JH, Everitt MJ. Simple procedure for phase-space measurement and entanglement validation. *Physical Review A* 2017, 96:022117.
56
57 86. Zhu B, Rey AM, Schachenmayer J. A generalized phase space approach for solving quantum spin dynamics. *New Journal of Physics* 2019, 21:082001.
58
59 87. Rundle RP, Everitt MJ. Overview of the Phase Space Formulation of Quantum Mechanics with Application to Quantum Technologies. *Advanced Quantum Technologies* 2021, 4:2100016.
60
61 88. Weyl H. Quantum mechanics and Group theory. *Zeitschrift Fur Physik* 1927, 46:1-46.
62
63 89. Wigner E. On the Quantum Correction For Thermodynamic Equilibrium. *Physical Review* 1932, 40:749-759.
64
65 90. Hillery M, Oconnell RF, Scully MO, Wigner EP. Distribution-functions in physics - fundamentals. *Physics Reports-Review Section of Physics Letters* 1984, 106:121-167.

- 1
2
3
4
5
6
7
8
9
10
11
12
13
14
15
16
17
18
19
20
21
22
23
24
25
26
27
28
29
30
31
32
33
34
35
36
37
38
39
40
41
42
43
44
45
46
47
48
49
50
51
52
53
54
55
56
57
58
59
60
91. Lee HW. Theory and Application of the Quantum Phase-Space Distribution Functions. *Physics Reports-Review Section of Physics Letters* 1995, 259:147-211.
92. Cohen L. Generalized Phase-Space Distribution Functions. *Journal of Mathematical Physics* 1966, 7:781-786.
93. Groenewold HJ. On the Principles of Elementary Quantum Mechanics. *Physica* 1946, 12:405-460.
94. Moyal JE. Quantum mechanics as a statistical theory. *Mathematical Proceedings of the Cambridge Philosophical Society* 1949, 45:99-124.
95. Bopp F. *Werner Heisenberg und die Physik unserer Zeit*. Braunschweig: Vieweg; 1961.
96. Miller WH. Quantum dynamics of complex molecular systems. *Proceedings of the National Academy of Sciences* 2005, 102:6660-6664.
97. Miller WH. Including quantum effects in the dynamics of complex (i.e., large) molecular systems. *The Journal of Chemical Physics* 2006, 125:132305.
98. Miller WH. Classical-limit quantum mechanics and the theory of molecular collisions. *Advances in Chemical Physics* 1974, 25:69-177.
99. Miller WH. The classical S-matrix in molecular collisions. *Advances in Chemical Physics* 1975, 30:77.
100. Stratonovich RL. On distributions in representation space. *Zh. Eksp. Teor. Fiz.* 1956, 31:1012.
101. Feynman RP. Negative probability. In: Hiley BJ, Peat D, eds. *Quantum Implications: Essays in Honour of David Bohm*. New York: Routledge; 1987, 235-248.
102. Wootters WK. A Wigner-function formulation of finite-state quantum mechanics. *Annals of Physics* 1987, 176:1-21.
103. Várilly JC, Gracia-Bondía J. The Moyal representation for spin. *Annals of Physics* 1989, 190:107-148.
104. Amiet JP, Cibils MB. Description of quantum spin using functions on the sphere S₂. *Journal of Physics A: Mathematical and General* 1991, 24:1515-1535.
105. Amiet JP, Weigert S. Discrete Q- and P-symbols for spin s. *Journal of Optics B-Quantum and Semiclassical Optics* 2000, 2:118-121.
106. Dowling JP, Agarwal GS, Schleich WP. Wigner distribution of a general angular-momentum state - Applications to a collection of 2-level atoms. *Physical Review A* 1994, 49:4101-4109.
107. Brif C, Mann A. Phase-space Formulation of Quantum Mechanics and Quantum-state Reconstruction for Physical Systems with Lie-group Symmetries. *Physical Review A* 1999, 59:971-987.
108. Cunha MOT, Man'ko VI, Scully MO. Quasiprobability and probability distributions for spin-1/2 states. *Foundations of Physics Letters* 2001, 14:103-117.
109. Klimov AB, Espinoza P. Moyal-like form of the star product for generalized SU(2) Stratonovich-Weyl symbols. *Journal of Physics A: Mathematical and General* 2002, 35:8435-8447.
110. Klimov AB, Romero JL. A Generalized Wigner Function for Quantum Systems with the SU(2) Dynamical Symmetry Group. *Journal of Physics A: Mathematical and Theoretical* 2008, 41:055303.
111. Klimov AB, Romero JL, de Guise H. Generalized SU(2) Covariant Wigner Functions and Some of Their Applications. *Journal of Physics A: Mathematical and Theoretical* 2017, 50:323001.
112. Adam P, Andreev VA, Man'ko MA, Man'ko VI, Mechler M. SU(2) Symmetry of Qubit States and Heisenberg-Weyl Symmetry of Systems with Continuous Variables in the Probability Representation of Quantum Mechanics. *Symmetry-Basel* 2020, 12:23.
113. Koczor B, Zeier R, Glaser SJ. Continuous Phase-space Representations for Finite-dimensional Quantum States and Their Tomography. *Physical Review A* 2020, 101:022318.
114. Tilma T, Nemoto K. SU(N)-symmetric quasi-probability distribution functions. *Journal of Physics A: Mathematical and Theoretical* 2012, 45:14.
115. Tilma T, Everitt MJ, Samson JH, Munro WJ, Nemoto K. Wigner Functions for Arbitrary Quantum Systems. *Physical Review Letters* 2016, 117:180401.
116. Marchiolli MA, Galetti D. On the discrete Wigner function for SU(N). *Journal of Physics A: Mathematical and Theoretical* 2019, 52:405305.
117. Rundle RP, Tilma T, Samson JH, Dwyer VM, Bishop RF, Everitt MJ. General Approach to Quantum Mechanics As a Statistical Theory. *Physical Review A* 2019, 99:012115.
118. Cohenet O, Combe P, Sirugue M, Siruguecollin M. A stochastic treatment of the dynamics of an integer spin. *Journal of Physics A: Mathematical and General* 1988, 21:2875-2883.
119. Leonhardt U. Quantum-state tomography and discrete Wigner function. *Physical Review Letters* 1995, 74:4101-4105.
120. Leonhardt U. Discrete Wigner function and quantum-state tomography. *Physical Review A* 1996, 53:2998-3013.
121. Gibbons KS, Hoffman MJ, Wootters WK. Discrete phase space based on finite fields. *Physical Review A* 2004, 70:062101.
122. Wootters WK. Quantum Measurements and Finite Geometry. *Foundations of Physics* 2006, 36:112-126.
123. Ruzzi M, Marchiolli MA, Galetti D. Extended Cahill-Glauber formalism for finite-dimensional spaces: I. Fundamentals. *Journal of Physics A: Mathematical and General* 2005, 38:6239-6251.

- 1
2
3 124. Chaturvedi S, Ercolessi E, Marmo G, Morandi G, Mukunda N, Simon R. Wigner distributions for finite dimensional quantum systems: An algebraic approach. *Pramana* 2005, 65:981-993.
- 4 125. Chaturvedi S, Ercolessi E, Marmo G, Morandi G, Mukunda N, Simon R. Wigner-Weyl correspondence in quantum mechanics for continuous and discrete systems-a Dirac-inspired view. *Journal of Physics A: Mathematical and General* 2006, 39:1405-1423.
- 5 126. Gross D. Hudson's theorem for finite-dimensional quantum systems. *Journal of Mathematical Physics* 2006, 47:25.
- 6 127. Valtierra IF, Romero JL, Klimov AB. TWA versus semiclassical unitary approximation for spin-like systems. *Annals of Physics* 2017, 383:620-634.
- 7 128. Valtierra IF, Klimov AB, Leuchs G, Sánchez-Soto LL. Quasiprobability currents on the sphere. *Physical Review A* 2020, 101:033803.
- 8 129. Czischek S. Discrete Truncated Wigner Approximation. In: *Springer Theses*: Springer International Publishing; 2020, 85-109.
- 9 130. Morales-Hernández GE, Castellanos JC, Romero JL, Klimov AB. Semi-classical Discretization and Long-time Evolution of Variable Spin Systems. *Entropy* 2021, 23:684.
- 10 131. Liu J. A unified theoretical framework for mapping models for the multi-state Hamiltonian. *The Journal of Chemical Physics* 2016, 145:204105.
- 11 132. He X, Liu J. A new perspective for nonadiabatic dynamics with phase space mapping models. *The Journal of Chemical Physics* 2019, 151:024105.
- 12 133. Liu J. Isomorphism between the multi-state Hamiltonian and the second-quantized many-electron Hamiltonian with only 1-electron interactions. *The Journal of Chemical Physics* 2017, 146:024110.
- 13 134. He X, Gong Z, Wu B, Liu J. Negative Zero-Point-Energy Parameter in the Meyer-Miller Mapping Model for Nonadiabatic Dynamics. *The journal of physical chemistry letters* 2021, 12:2496-2501.
- 14 135. Domcke W, Yarkony DR, Köppel H. *Conical Intersections: Theory, Computation and Experiment*. Singapore: World Scientific; 2011.
- 15 136. Yonehara T, Hanasaki K, Takatsuka K. Fundamental Approaches to Nonadiabaticity: Toward a Chemical Theory beyond the Born-Oppenheimer Paradigm. *Chemical Reviews* 2011, 112:499-542.
- 16 137. Tully JC. Perspective: Nonadiabatic dynamics theory. *The Journal of Chemical Physics* 2012, 137:22A301.
- 17 138. Miller WH, Cotton SJ. Classical molecular dynamics simulation of electronically non-adiabatic processes. *Faraday Discussions* 2016, 195:9-30.
- 18 139. Levine BG, Martinez TJ. Isomerization through conical intersections. *Annual Review of Physical Chemistry* 2007, 58:613-634.
- 19 140. Martinez TJ. Seaming is believing. *Nature* 2010, 467:412-413.
- 20 141. Sisto A, Glowacki DR, Martinez TJ. Ab Initio Nonadiabatic Dynamics of Multichromophore Complexes: A Scalable Graphical-Processing-Unit-Accelerated Exciton Framework. *Accounts of Chemical Research* 2014, 47:2857-2866.
- 21 142. Makarov DV, Glover WJ, Martinez TJ, Shalashilin DV. Ab initio multiple cloning algorithm for quantum nonadiabatic molecular dynamics. *The Journal of Chemical Physics* 2014, 141:054110.
- 22 143. Mai S, Marquetand P, Gonzalez L. Nonadiabatic dynamics: The SHARC approach. *Wiley Interdisciplinary Reviews-Computational Molecular Science* 2018, 8:e1370.
- 23 144. Mai S, Gonzalez L. Molecular Photochemistry: Recent Developments in Theory. *Angewandte Chemie-International Edition* 2020, 59:16832-16846.
- 24 145. Subotnik JE, Jain A, Landry B, Petit A, Ouyang W, Bellonzi N. Understanding the Surface Hopping View of Electronic Transitions and Decoherence. In: Johnson MA, Martinez TJ, eds. *Annual Review of Physical Chemistry*, Vol 67. Vol. 67: Annual Reviews; 2016, 387-417.
- 25 146. Fang W-H. Ab Initio Determination of Dark Structures in Radiationless Transitions for Aromatic Carbonyl Compounds. *Accounts of Chemical Research* 2008, 41:452-457.
- 26 147. Long R, Prezhdo OV, Fang W-H. Nonadiabatic charge dynamics in novel solar cell materials. *Wiley Interdisciplinary Reviews-Computational Molecular Science* 2017, 7:e1305.
- 27 148. Feng W, Xu L, Li X-Q, Fang W-H, Yan Y. Nonadiabatic molecular dynamics simulation: An approach based on quantum measurement picture. *AIP Advances* 2014, 4:077131.
- 28 149. Lan Z, Shao J. Approximate Theoretical Methods for Nonadiabatic Dynamics of Polyatomic Molecules. *Progress in Chemistry* 2012, 24:1105-1119.
- 29 150. Wang Y-C, Ke Y, Zhao Y. The hierarchical and perturbative forms of stochastic Schrödinger equations and their applications to carrier dynamics in organic materials. *Wiley Interdisciplinary Reviews-Computational Molecular Science* 2019, 9:e1375.
- 30 151. Nelson T, Fernandez-Alberti S, Roitberg AE, Tretiak S. Nonadiabatic Excited-State Molecular Dynamics: Modeling Photophysics in Organic Conjugated Materials. *Accounts of Chemical Research* 2014, 47:1155-1164.
- 31 152. Crespo-Otero R, Barbatti M. Recent Advances and Perspectives on Nonadiabatic Mixed Quantum-Classical Dynamics. *Chemical Reviews* 2018, 118:7026-7068.

- 1
2
3 153. Meyer H-D, Miller WH. A classical analog for electronic degrees of freedom in nonadiabatic collision processes. *The Journal of Chemical Physics* 1979, 70:3214-3223.
- 4 154. Stock G, Thoss M. Semiclassical description of nonadiabatic quantum dynamics. *Physical Review Letters* 1997, 78:578-581.
- 5 155. Wigner EP. *Perspectives in Quantum Theory*. Cambridge: MIT; 1971.
- 6 156. Husimi K. Some Formal Properties of the Density Matrix. *Proceedings of the Physico-Mathematical Society of Japan* 1940, 22:264-314.
- 7 157. Glauber RJ. Optical Coherence and Photon Statistics. In: deWitt C, Blandin A, C. C-T, eds. *Quantum Optics and Electronics*. New York: Gordon and Breach; 1965.
- 8 158. Kirkwood JG. Quantum Statistics of Almost Classical Assemblies. *Physical Review* 1933, 44:31.
- 9 159. Rihaczek AW. Signal Energy Distribution in Time and Frequency. *IEEE Transactions on Information Theory* 1968, 14:369-374.
- 10 160. Mehta CL. Phase-Space Formulation of the Dynamics of Canonical Variables. *Journal of Mathematical Physics* 1964, 5:677-686.
- 11 161. Rivier DC. On a One-to-One Correspondence between Infinitesimal Canonical Transformations and Infinitesimal Unitary Transformations. *Physical Review* 1951, 83:862.
- 12 162. Margenau H, Hill RN. Correlation between Measurements in Quantum Theory. *Progress of Theoretical Physics* 1961, 26:722-738.
- 13 163. Born M, Jordan P. On quantum mechanics. *Zeitschrift fur Physik* 1925, 34:858-888.
- 14 164. Meyer H-D, Miller WH. Classical-Models for Electronic Degrees of Freedom: Derivation Via Spin Analogy and Application to $F^* + H_2 \rightarrow F + H_2$. *The Journal of Chemical Physics* 1979, 71:2156-2169.
- 15 165. Gray SK, Miller WH. Classical model for electronic degrees of freedom: charge transfer in Na + I collisions. *Chemical Physics Letters* 1982, 93:341-344.
- 16 166. Ali DP, Miller WH. Effect of electronic transition dynamics on iodine atom recombination in liquids. *The Journal of Chemical Physics* 1983, 78:6640-6645.
- 17 167. Ali DP, Miller WH. Classical models for electronic degrees of freedom: Quenching of Br*(2P1/2) by collision with H₂ in three dimensions. *Chemical Physics Letters* 1984, 103:470-474.
- 18 168. Stock G, Miller WH. A classical model for time- and frequency-resolved spectroscopy of nonadiabatic excited-state dynamics. *Chemical Physics Letters* 1992, 197:396-404.
- 19 169. Stock G, Miller WH. Classical formulation of the spectroscopy of nonadiabatic excited-state dynamics. *The Journal of Chemical Physics* 1993, 99:1545-1555.
- 20 170. Sun X, Miller WH. Semiclassical initial value representation for electronically nonadiabatic molecular dynamics. *The Journal of Chemical Physics* 1997, 106:6346-6353.
- 21 171. Coronado EA, Batista VS, Miller WH. Nonadiabatic photodissociation dynamics of CN in the A continuum: A semiclassical initial value representation study. *The Journal of Chemical Physics* 2000, 112:5566-5575.
- 22 172. Coronado EA, Xing J, Miller WH. Ultrafast non-adiabatic dynamics of systems with multiple surface crossings: a test of the Meyer-Miller Hamiltonian with semiclassical initial value representation methods. *Chemical Physics Letters* 2001, 349:521-529.
- 23 173. Ananth N, Venkataraman C, Miller WH. Semiclassical description of electronically nonadiabatic dynamics via the initial value representation. *The Journal of Chemical Physics* 2007, 127:084114.
- 24 174. Miller WH. Electronically Nonadiabatic Dynamics via Semiclassical Initial Value Methods. *Journal of Physical Chemistry A* 2009, 113:1405-1415.
- 25 175. Ananth N, Miller TF. Exact quantum statistics for electronically nonadiabatic systems using continuous path variables. *The Journal of Chemical Physics* 2010, 133:234103.
- 26 176. Cotton SJ, Miller WH. Symmetrical Windowing for Quantum States in Quasi-Classical Trajectory Simulations. *Journal of Physical Chemistry A* 2013, 117:7190-7194.
- 27 177. Cotton SJ, Miller WH. Symmetrical windowing for quantum states in quasi-classical trajectory simulations: Application to electronically non-adiabatic processes. *The Journal of Chemical Physics* 2013, 139:234112.
- 28 178. Cotton SJ, Igumenshchev K, Miller WH. Symmetrical windowing for quantum states in quasi-classical trajectory simulations: Application to electron transfer. *The Journal of Chemical Physics* 2014, 141:084104.
- 29 179. Cotton SJ, Miller WH. A Symmetrical Quasi-Classical Spin-Mapping Model for the Electronic Degrees of Freedom in Non-Adiabatic Processes. *Journal of Physical Chemistry A* 2015, 119:12138-12145.
- 30 180. Miller WH, Cotton SJ. Communication: Note on detailed balance in symmetrical quasi-classical models for electronically non-adiabatic dynamics. *The Journal of Chemical Physics* 2015, 142:131103.
- 31 181. Cotton SJ, Miller WH. A new symmetrical quasi-classical model for electronically non-adiabatic processes: Application to the case of weak non-adiabatic coupling. *The Journal of Chemical Physics* 2016, 145:144108.

- 1
2
3 182. Cotton SJ, Miller WH. The Symmetrical Quasi-Classical Model for Electronically Non-Adiabatic Processes Applied to Energy Transfer Dynamics
4 in Site-Exciton Models of Light-Harvesting Complexes. *Journal of Chemical Theory and Computation* 2016, 12:983-991.
5
6 183. Miller WH, Cotton SJ. Communication: Wigner functions in action-angle variables, Bohr-Sommerfeld quantization, the Heisenberg
7 correspondence principle, and a symmetrical quasi-classical approach to the full electronic density matrix. *The Journal of Chemical Physics*
8 2016, 145:081102.
9
10 184. Cotton SJ, Liang R, Miller WH. On the adiabatic representation of Meyer-Miller electronic-nuclear dynamics. *The Journal of Chemical Physics*
11 2017, 147:064112.
12
13 185. Liang R, Cotton SJ, Binder R, Hegger R, Burghardt I, Miller WH. The symmetrical quasi-classical approach to electronically nonadiabatic
14 dynamics applied to ultrafast exciton migration processes in semiconducting polymers. *The Journal of Chemical Physics* 2018, 149:044101.
15
16 186. Cotton SJ, Miller WH. A symmetrical quasi-classical windowing model for the molecular dynamics treatment of non-adiabatic processes
17 involving many electronic states. *The Journal of Chemical Physics* 2019, 150:104101.
18
19 187. Cotton SJ, Miller WH. Trajectory-adjusted electronic zero point energy in classical Meyer-Miller vibronic dynamics: Symmetrical quasiclassical
20 application to photodissociation. *The Journal of Chemical Physics* 2019, 150:194110.
21
22 188. Muller U, Stock G. Flow of zero-point energy and exploration of phase space in classical simulations of quantum relaxation dynamics. II.
23 Application to nonadiabatic processes. *Journal of Chemical Physics* 1999, 111:77-88.
24
25 189. Stock G, Muller U. Flow of zero-point energy and exploration of phase space in classical simulations of quantum relaxation dynamics. *Journal*
26 *of Chemical Physics* 1999, 111:65-76.
27
28 190. Stock G, Muller U. Flow of zero-point energy and exploration of phase space in classical simulations of quantum relaxation dynamics. II.
29 allication to nonadiabatic processes. *The Journal of Chemical Physics* 1999, 111:77-88.
30
31 191. Stock G, Thoss M. Classical Description of Nonadiabatic Quantum Dynamics. In: Rice SA, ed. *Advances in Chemical Physics*. Vol. 131: John
32 Wiley and Sons, Inc.; 2005, 243-375.
33
34 192. Thoss M, Miller WH, Stock G. Semiclassical description of nonadiabatic quantum dynamics: Application to the S1-S2 conical intersection in
35 pyrazine. *The Journal of Chemical Physics* 2000, 112:10282-10292.
36
37 193. Thoss M, Stock G. Mapping approach to the semiclassical description of nonadiabatic quantum dynamics. *Physical Review A* 1999, 59:64-79.
38
39 194. Golosov AA, Reichman DR. Classical mapping approaches for nonadiabatic dynamics: Short time analysis. *The Journal of Chemical Physics*
40 2001, 114:1065-1074.
41
42 195. Saller MAC, Kelly A, Richardson JO. On the identity of the identity operator in nonadiabatic linearized semiclassical dynamics. *The Journal of*
43 *Chemical Physics* 2019, 150:071101.
44
45 196. Saller MAC, Kelly A, Richardson JO. Improved population operators for multi-state nonadiabatic dynamics with the mixed quantum-classical
46 mapping approach. *Faraday Discussions* 2020, 221:150-167.
47
48 197. Runeson JE, Richardson JO. Generalized spin mapping for quantum-classical dynamics. *The Journal of Chemical Physics* 2020, 152:084110.
49
50 198. Kananenka AA, Hsieh CY, Cao JS, Geva E. Nonadiabatic Dynamics via the Symmetrical Quasi-Classical Method in the Presence of
51 Anharmonicity. *Journal of Physical Chemistry Letters* 2018, 9:319-326.
52
53 199. Mulvihill E, Gao X, Liu Y, Schubert A, Dunietz BD, Geva E. Combining the mapping Hamiltonian linearized semiclassical approach with the
54 generalized quantum master equation to simulate electronically nonadiabatic molecular dynamics. *The Journal of Chemical Physics* 2019,
55 151:074103.
56
57 200. Gao X, Geva E. Improving the Accuracy of Quasiclassical Mapping Hamiltonian Methods by Treating the Window Function Width as an
58 Adjustable Parameter. *Journal of Physical Chemistry A* 2020, 124:11006-11016.
59
60 201. Gao X, Lai Y, Geva E. Simulating Absorption Spectra of Multiexcitonic Systems via Quasiclassical Mapping Hamiltonian Methods. *Journal of*
61 *Chemical Theory and Computation* 2020, 16:6465-6480.
62
63 202. Gao X, Sailer MAC, Liu Y, Kelly A, Richardson JO, Geva E. Benchmarking Quasiclassical Mapping Hamiltonian Methods for Simulating
64 Electronically Nonadiabatic Molecular Dynamics. *Journal of Chemical Theory and Computation* 2020, 16:2883-2895.
65
66 203. Liu Y, Gao X, Lai Y, Mulvihill E, Geva E. Electronic Dynamics through Conical Intersections via Quasiclassical Mapping Hamiltonian Methods.
67 *Journal of Chemical Theory and Computation* 2020, 16:4479-4488.
68
69 204. Saller MAC, Kelly A, Geva E. Benchmarking Quasiclassical Mapping Hamiltonian Methods for Simulating Cavity-Modified Molecular Dynamics.
70 *Journal of Physical Chemistry Letters* 2021, 12:3163-3170.
71
72 205. Bonella S, Coker DF. A semiclassical limit for the mapping Hamiltonian approach to electronically nonadiabatic dynamics. *The Journal of*
73 *Chemical Physics* 2001, 114:7778-7789.
74
75 206. Bonella S, Coker DF. Semiclassical implementation of the mapping Hamiltonian approach for nonadiabatic dynamics using focused initial
76 distribution sampling. *The Journal of Chemical Physics* 2003, 118:4370-4385.

- 1
2
3 207. Bonella S, Coker DF. LAND-map, a linearized approach to nonadiabatic dynamics using the mapping formalism. *The Journal of Chemical Physics* 2005, 122:194102.
4
5 208. Huo PF, Coker DF. Semi-classical path integral non-adiabatic dynamics: a partial linearized classical mapping Hamiltonian approach. *Molecular Physics* 2012, 110:1035-1052.
6
7 209. Tang D, Fang W-H, Shen L, Cui G. Combining Meyer-Miller Hamiltonian with electronic structure methods for on-the-fly nonadiabatic dynamics
8 simulations: implementation and application. *Physical Chemistry Chemical Physics* 2019, 21:17109-17117.
9
10 210. Zheng J, Xie Y, Jiang S, Long Y, Ning X, Lan Z. Ultrafast Electron Transfer with Symmetrical Quasi-classical Dynamics based on Mapping
11 Hamiltonian and Quantum Dynamics based on ML-MCTDH. *Chinese Journal of Chemical Physics* 2017, 30:800-810.
12
13 211. Xie Y, Zheng J, Lan Z. Performance evaluation of the symmetrical quasi-classical dynamics method based on Meyer-Miller mapping Hamiltonian
14 in the treatment of site-exciton models. *The Journal of Chemical Physics* 2018, 149:174105.
15
16 212. Zheng J, Xie Y, Jiang S, Long Y, Ning X, Lan Z. Initial sampling in symmetrical quasiclassical dynamics based on Li-Miller mapping Hamiltonian.
17 *Physical Chemistry Chemical Physics* 2019, 21:26502-26514.
18
19 213. Zheng J, Peng J, Xie Y, Long Y, Ning X, Lan Z. Study of the exciton dynamics in perylene bisimide (PBI) aggregates with symmetrical
20 quasiclassical dynamics based on the Meyer-Miller mapping Hamiltonian. *Physical Chemistry Chemical Physics* 2020, 22:18192-18204.
21
22 214. Peng J, Xie Y, Hu D, Lan Z. Analysis of bath motion in MM-SQC dynamics via dimensionality reduction approach: Principal component analysis.
23 *The Journal of Chemical Physics* 2021, 154:094122.
24
25 215. Hu D, Xie Y, Peng J, Lan Z. On-the-Fly Symmetrical Quasi-Classical Dynamics with Meyer-Miller Mapping Hamiltonian for the Treatment of
26 Nonadiabatic Dynamics at Conical Intersections. *Journal of Chemical Theory and Computation* 2021, 17:3267-3279.
27
28 216. Tao G. A multi-state trajectory method for non-adiabatic dynamics simulations. *The Journal of Chemical Physics* 2016, 144:094108.
29
30 217. Tao G. Coherence-Controlled Nonadiabatic Dynamics via State-Space Decomposition: A Consistent Way To Incorporate Ehrenfest and Born-
31 Oppenheimer-Like Treatments of Nuclear Motion. *Journal of Physical Chemistry Letters* 2016, 7:4335-4339.
32
33 218. Tao G. Multi-state trajectory approach to non-adiabatic dynamics: General formalism and the active state trajectory approximation. *The Journal
34 of Chemical Physics* 2017, 147:044107.
35
36 219. Schwinger J. In: Biedenharn LC, VanDam H, eds. *Quantum Theory of Angular Momentum*. New York: Academic; 1965.
37
38 220. Sakurai JJ. *Modern Quantum Mechanics*. New York: Addison-Wesley; 1994.
39
40 221. Flammia ST, Liu Y-K. Direct Fidelity Estimation from Few Pauli Measurements. *Physical Review Letters* 2011, 106:230501.
41
42 222. Sperling J, Walmsley IA. Quasiprobability representation of quantum coherence. *Physical Review A* 2018, 97:062327.
43
44 223. Bohmann M, Agudelo E, Sperling J. Probing nonclassicality with matrices of phase-space distributions. *Quantum* 2020, 4:16.
45
46 224. Bohmann M, Agudelo E. Phase-space inequalities beyond negativities. *Physical Review Letters* 2020, 124:133601.
47
48 225. Lutterbach LG, Davidovich L. Method for direct measurement of the Wigner function in cavity QED and ion traps. *Physical Review Letters* 1997,
49 78:2547-2550.
50
51 226. Signoles A, Facon A, Grosso D, Dotsenko I, Haroche S, Raimond JM, Brune M, Gleyzes S. Confined quantum Zeno dynamics of a watched
52 atomic arrow. *Nature Physics* 2014, 10:715-719.
53
54 227. Leiner D, Glaser SJ. Wigner process tomography: Visualization of spin propagators and their spinor properties. *Physical Review A* 2018,
55 98:012112.
56
57 228. Tian Y, Wang Z, Zhang P, Li G, Li J, Zhang T. Measurement of complete and continuous Wigner functions for discrete atomic systems. *Physical
58 Review A* 2018, 97:013840.
59
60 229. Chen B, Geng J, Zhou F, Song L, Shen H, Xu N. Quantum state tomography of a single electron spin in diamond with Wigner function
reconstruction. *Applied Physics Letters* 2019, 114:041102.
230. Jing Y, Fadel M, Ivannikov V, Byrnes T. Split spin-squeezed Bose-Einstein condensates. *New Journal of Physics* 2019, 21:093038.
231. Song C, Xu K, Li H, Zhang Y-R, Zhang X, Liu W, Guo Q, Wang Z, Ren W, Hao J, et al. Generation of multicomponent atomic Schrodinger cat
states of up to 20 qubits. *Science* 2019, 365:574-577.
232. Eichler C, Lang C, Fink JM, Govenius J, Filipp S, Wallraff A. Observation of Entanglement between Itinerant Microwave Photons and a
Superconducting Qubit. *Physical Review Letters* 2012, 109:240501.
233. Morin O, Huang K, Liu J, Le Jeannic H, Fabre C, Laurat J. Remote creation of hybrid entanglement between particle-like and wave-like optical
qubits. *Nature Photonics* 2014, 8:570-574.
234. Agudelo E, Sperling J, Costanzo LS, Bellini M, Zavatta A, Vogel W. Conditional Hybrid Nonclassicality. *Physical Review Letters* 2017,
119:120403.
235. Banaszek K, Radzewicz C, Wodkiewicz K, Krasinski JS. Direct measurement of the Wigner function by photon counting. *Physical Review A*
1999, 60:674-677.

- 1
2
3 236. Garon A, Zeier R, Glaser SJ. Visualizing operators of coupled spin systems. *Physical Review A* 2015, 91:042122.
4 237. Koczor B, Zeier R, Glaser SJ. Time evolution of coupled spin systems in a generalized Wigner representation. *Annals of Physics* 2019, 408:1-
5 50.
6 238. Davies BI, Rundle RP, Dwyer VM, Samson JH, Tilma T, Everitt MJ. Visualizing spin degrees of freedom in atoms and molecules. *Physical Review*
7 A 2019, 100:042102.
8 239. Rundle RP, Davies BI, Dwyer VM, Tilma T, Everitt MJ. Visualization of correlations in hybrid discrete-continuous variable quantum systems.
9 *Journal of Physics Communications* 2020, 4:025002.
10 240. Ehrenfest P. Bemerkung über die angenäherte Gültigkeit der klassischen Mechanik innerhalb der Quantenmechanik. *Zeitschrift für Physik* 1927,
11 45:455-457.
12 241. Li X, Tully JC, Schlegel HB, Frisch MJ. Ab initio Ehrenfest dynamics. *The Journal of Chemical Physics* 2005, 123:084106.
13 242. Tully JC. Molecular dynamics with electronic transitions. *The Journal of Chemical Physics* 1990, 93:1061-1071.
14 243. Wang LJ, Akimov A, Prezhdo OV. Recent Progress in Surface Hopping: 2011-2015. *Journal of Physical Chemistry Letters* 2016, 7:2100-2112.
15 244. Peng J, Xie Y, Hu D, Du L, Lan Z. Treatment of Nonadiabatic Dynamics by On-The-Fly Trajectory Surface Hopping Dynamics. *Acta Physico-*
16 *Chimica Sinica* 2019, 35:28-48.
17 245. Meyer KR, Offin DC. *Introduction to Hamiltonian Dynamical Systems and the N-Body Problem*. New York: Springer Science+Business Media,
18 LLC; 1992.
19 246. Yarkony DR. Conical Intersections: Diabolical and Often Misunderstood. *Accounts of Chemical Research* 1998, 31:511-518.
20 247. Paterson MJ, Bearpark MJ, Robb MA, Blancafort L, Worth GA. Conical intersections: A perspective on the computation of spectroscopic Jahn-
21 Teller parameters and the degenerate 'intersection space'. *Physical Chemistry Chemical Physics* 2005, 7:2100-2115.
22 248. Matsika S, Krause P. Nonadiabatic Events and Conical Intersections. In: Leone SR, Cremer PS, Groves JT, Johnson MA, eds. *Annual Review*
23 *of Physical Chemistry*, Vol 62. Vol. 62: Annual Reviews; 2011, 621-643.
24 249. Makarov DE, Makri N. Path-Integrals for Dissipative Systems by Tensor Multiplication - Condensed-Phase Quantum Dynamics for Arbitrarily
25 Long-Time. *Chemical Physics Letters* 1994, 221:482-491.
26 250. Makri N, Makarov DE. Tensor Propagator for Iterative Quantum Time Evolution of Reduced Density-Matrices .2. Numerical Methodology. *Journal*
27 *of Chemical Physics* 1995, 102:4611-4618.
28 251. Makri N, Makarov DE. Tensor Propagator for Iterative Quantum Time Evolution of Reduced Density-Matrices .1. Theory. *Journal of Chemical*
29 *Physics* 1995, 102:4600-4610.
30 252. Topaler M, Makri N. Path integral calculation of quantum nonadiabatic rates in model condensed phase reactions. *Journal of Physical Chemistry*
31 1996, 100:4430-4436.
32 253. Tanimura Y, Kubo R. Time Evolution of a Quantum System in Contact with a Nearly Gaussian-Markoffian Noise Bath. *Journal of the Physical*
33 *Society of Japan* 1989, 58:101-114.
34 254. Yan Y-A, Yang F, Liu Y, Shao J. Hierarchical approach based on stochastic decoupling to dissipative systems. *Chemical Physics Letters* 2004,
35 395:216-221.
36 255. Xu R-X, Cui P, Li X-Q, Mo Y, Yan Y. Exact quantum master equation via the calculus on path integrals. *The Journal of Chemical Physics* 2005,
37 122:041103.
38 256. Shao J. Stochastic description of quantum open systems: Formal solution and strong dissipation limit. *Chemical Physics* 2006, 322:187-192.
39 257. Moix JM, Cao J. A hybrid stochastic hierarchy equations of motion approach to treat the low temperature dynamics of non-Markovian open
40 quantum systems. *The Journal of Chemical Physics* 2013, 139:134106.
41 258. Tanimura Y. Reduced hierarchical equations of motion in real and imaginary time: Correlated initial states and thermodynamic quantities. *The*
42 *Journal of Chemical Physics* 2014, 141:044114.
43 259. Yan Y. Theory of open quantum systems with bath of electrons and phonons and spins: Many-dissipaton density matrixes approach. *The*
44 *Journal of Chemical Physics* 2014, 140:054105.
45 260. Tang Z, Ouyang X, Gong Z, Wang H, Wu J. Extended hierarchy equation of motion for the spin-boson model. *The Journal of Chemical Physics*
46 2015, 143:224112.
47 261. Tanimura Y. Real-time and imaginary-time quantum hierarchical Fokker-Planck equations. *The Journal of Chemical Physics* 2015, 142:144110.
48 262. Meyer H-D, Manthe U, Cederbaum LS. The multi-configurational time-dependent Hartree approach. *Chemical Physics Letters* 1990, 165:73-
49 78.
50 263. Thoss M, Wang H, Miller WH. Self-consistent hybrid approach for complex systems: Application to the spin-boson model with Debye spectral
51 density. *The Journal of Chemical Physics* 2001, 115:2991-3005.

- 1
2
3
4
5
6
7
8
9
10
11
12
13
14
15
16
17
18
19
20
21
22
23
24
25
26
27
28
29
30
31
32
33
34
35
36
37
38
39
40
41
42
43
44
45
46
47
48
49
50
51
52
53
54
55
56
57
58
59
60
264. Wang H, Thoss M, Miller WH. Systematic convergence in the dynamical hybrid approach for complex systems: A numerically exact methodology. *The Journal of Chemical Physics* 2001, 115:2979-2990.
265. Wang H, Thoss M. Multilayer formulation of the multiconfiguration time-dependent Hartree theory. *The Journal of Chemical Physics* 2003, 119:1289-1299.
266. Wang H, Thoss M. From coherent motion to localization: dynamics of the spin-boson model at zero temperature. *New Journal of Physics* 2008, 10:115005.
267. Worth GA, Meyer H-D, Köppel H, Cederbaum LS, Burghardt I. Using the MCTDH wavepacket propagation method to describe multimode non-adiabatic dynamics. *International Reviews in Physical Chemistry* 2008, 27:569-606.
268. Wang H, Thoss M. From coherent motion to localization: II. Dynamics of the spin-boson model with sub-Ohmic spectral density at zero temperature. *Chemical Physics* 2010, 370:78-86.
269. Craig IR, Thoss M, Wang H. Proton transfer reactions in model condensed-phase environments: Accurate quantum dynamics using the multilayer multiconfiguration time-dependent Hartree approach. *The Journal of Chemical Physics* 2007, 127:144503.
270. Wang H. Iterative Calculation of Energy Eigenstates Employing the Multi layer Multiconfiguration Time-Dependent Hartree Theory. *Journal of Physical Chemistry A* 2014, 118:9253-9261.
271. Purcell EM. Spontaneous Emission Probabilities at Radio Frequencies. In: Burstein E, Weisbuch C, eds. *Confined Electrons and Photons: New Physics and Applications*. Boston, MA: Springer US; 1995, 839-839.
272. Krasnok AE, Slobozhanyuk AP, Simovski CR, Tretyakov SA, Poddubny AN, Miroshnichenko AE, Kivshar YS, Belov PA. An antenna model for the Purcell effect. *Scientific Reports* 2015, 5:12956.
273. Rybin MV, Mingaleev SF, Limonov MF, Kivshar YS. Purcell effect and Lamb shift as interference phenomena. *Scientific Reports* 2016, 6:20599.
274. Holsteen AL, Raza S, Fan P, Kik PG, Brongersma ML. Purcell effect for active tuning of light scattering from semiconductor optical antennas. *Science* 2017, 358:1407-1410.
275. Alagappan G, Krivitsky LA, Png CE. Diamond in a Nanopocket: A New Route to a Strong Purcell Effect. *ACS Omega* 2018, 3:4733-4742.
276. Gallego J, Alt W, Macha T, Martinez-Dorantes M, Pandey D, Meschede D. Strong Purcell Effect on a Neutral Atom Trapped in an Open Fiber Cavity. *Physical Review Letters* 2018, 121:173603.
277. Ren T, Dong Y, Xu S, Gong X. Strong Purcell effect in deep subwavelength coaxial cavity with GeSn active medium. *Optics Letters* 2021, 46:3889-3892.
278. Carmichael HJ, Brecha RJ, Raizen MG, Kimble HJ, Rice PR. Subnatural linewidth averaging for coupled atomic and cavity-mode oscillators. *Physical Review A* 1989, 40:5516-5519.
279. Zhu Y, Gauthier DJ, Morin SE, Wu Q, Carmichael HJ, Mossberg TW. Vacuum Rabi splitting as a feature of linear-dispersion theory: Analysis and experimental observations. *Physical Review Letters* 1990, 64:2499-2502.
280. Field JE. Vacuum-Rabi-splitting-induced transparency. *Physical Review A* 1993, 47:5064-5067.
281. Abram II, Oudar JL. Spontaneous emission in planar semiconductor microcavities displaying vacuum Rabi splitting. *Physical Review A* 1995, 51:4116-4122.
282. Li K, Wang W, Chen Z, Gao N, Yang W, Li W, Chen H, Li S, Li H, Jin P, et al. Vacuum Rabi splitting of exciton-polariton emission in an AlN film. *Scientific Reports* 2013, 3:3551.
283. Toida H, Nakajima T, Komiyama S. Vacuum Rabi splitting in a semiconductor circuit QED system. *Physical Review Letters* 2013, 110:066802.
284. Guerin W, Santo T, Weiss P, Cipris A, Schachenmayer J, Kaiser R, Bachelard R. Collective Multimode Vacuum Rabi Splitting. *Physical Review Letters* 2019, 123:243401.
285. Yan Y, Ergogo TT, Lu Z, Chen L, Luo J, Zhao Y. Lamb Shift and the Vacuum Rabi Splitting in a Strongly Dissipative Environment. *The Journal of Physical Chemistry Letters* 2021, 12:9919-9925.
286. Meystre P. *Elements of Quantum Optics*. Berlin New York: Springer; 2007.
287. Hoffmann NM, Schafer C, Rubio A, Kelly A, Appel H. Capturing vacuum fluctuations and photon correlations in cavity quantum electrodynamics with multitrajectory Ehrenfest dynamics. *Physical Review A* 2019, 99:063819.
288. Hoffmann NM, Schäfer C, Säkkinen N, Rubio A, Appel H, Kelly A. Benchmarking semiclassical and perturbative methods for real-time simulations of cavity-bound emission and interference. *The Journal of Chemical Physics* 2019, 151:244113.
289. Li TE, Chen HT, Nitzan A, Subotnik JE. Quasiclassical modeling of cavity quantum electrodynamics. *Physical Review A* 2020, 101:033831.
290. Levine BG, Ko C, Quenneville J, Martinez TJ. Conical intersections and double excitations in time-dependent density functional theory. *Molecular Physics* 2006, 104:1039-1051.
291. Halcrow MA. Jahn-Teller distortions in transition metal compounds, and their importance in functional molecular and inorganic materials. *Chemical Society Reviews* 2013, 42:1784-1795.

- 1
2
3 292. Bersuker IB. The Jahn-Teller and Pseudo-Jahn-Teller Effects: A Unique and Only Source of Spontaneous Symmetry Breaking in Atomic Matter.
4 *Symmetry* 2021, 13:1577.
5
6 293. Qin A, Lam JYW, Tang BZ. Luminogenic polymers with aggregation-induced emission characteristics. *Progress in Polymer Science* 2012,
7 37:182-209.
8
9 294. Schneider R, Domcke W. S1-S2 Conical intersection and ultrafast S2->S1 Internal conversion in pyrazine. *Chemical Physics Letters* 1988,
10 150:235-242.
11
12 295. Hacker B, Welte S, Daiss S, Shaukat A, Ritter S, Li L, Rempe G. Deterministic creation of entangled atom-light Schrodinger-cat states. *Nature*
13 *Photonics* 2019, 13:110–115.
14
15 296. Vlastakis B, Petrenko A, Ofek N, Sun L, Leghtas Z, Sliwa K, Liu Y, Hatridge M, Blumoff J, Frunzio L, et al. Characterizing entanglement of an
16 artificial atom and a cavity cat state with Bell's inequality. *Nature Communications* 2015, 6:8970.
17
18 297. Isserlis L. On a formula for the product-moment coefficient of any order of a normal frequency distribution in any number of variables. *Biometrika*
19 1918, 12:134-139.
20
21 298. Wang MC, Uhlenbeck GE. On the theory of the Brownian motion-II. *Reviews of Modern Physics* 1945, 17:323-342.
22
23 299. Fano U. Geometrical characterization of nuclear states and the theory of angular correlations. *Physical Review* 1953, 90:577-579.
24
25 300. Tilma T, Sudarshan ECG. Generalized Euler angle parameterization for U(N) with applications to SU(N) coset volume measures. *Journal of*
26 *Geometry and Physics* 2004, 52:263-283.
27
28 301. Tilma T, Sudarshan ECG. Generalized Euler angle parametrization for SU(N). *Journal of Physics A: Mathematical and General* 2002, 35:10467-
29 10501.
30
31 302. Klimov AB. Exact evolution equations for SU(2) quasidistribution functions. *Journal of Mathematical Physics* 2002, 43:2202-2213.
32
33 303. Bóna P. Classical Mechanical Projections of QM. In: Bóna P, ed. *Classical Systems in Quantum Mechanics*. Cham: Springer International
34 Publishing; 2020.

New Phase Space Formulations and Quantum Dynamics Approaches

Article Type:

OPINION

PRIMER

OVERVIEW

ADVANCED REVIEW

FOCUS ARTICLE

SOFTWARE FOCUS

Authors:

Xin He (co-first author)

Beijing National Laboratory for Molecular Sciences, Institute of Theoretical and Computational Chemistry, College of Chemistry and Molecular Engineering, Peking University, Beijing 100871, China

ORCID ID: 0000-0002-5189-7204

Baihua Wu (co-first author)

Beijing National Laboratory for Molecular Sciences, Institute of Theoretical and Computational Chemistry, College of Chemistry and Molecular Engineering, Peking University, Beijing 100871, China

ORCID ID: 0000-0002-1256-6859

Youhao Shang

Beijing National Laboratory for Molecular Sciences, Institute of Theoretical and Computational Chemistry, College of Chemistry and Molecular Engineering, Peking University, Beijing 100871, China

ORCID ID: 0000-0002-9297-6654

Bingqi Li

Beijing National Laboratory for Molecular Sciences, Institute of Theoretical and Computational Chemistry, College of Chemistry and Molecular Engineering, Peking University, Beijing 100871, China

ORCID ID: 0000-0001-7273-8299

Xiangsong Cheng

1
2
3 Beijing National Laboratory for Molecular Sciences, Institute of Theoretical and Computational
4 Chemistry, College of Chemistry and Molecular Engineering, Peking University, Beijing 100871,
5 China
6
7 ORCID ID: 0000-0001-8793-5092
8
9

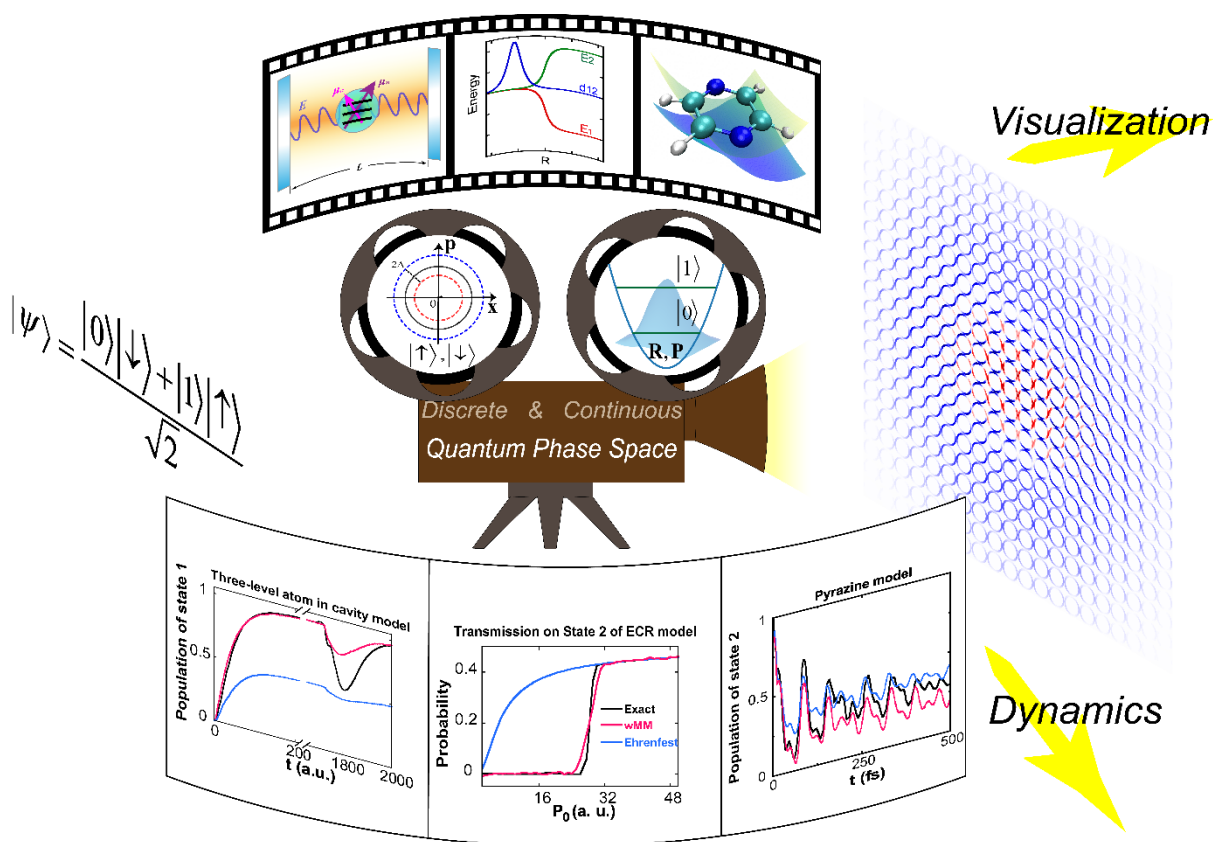
10 Jian Liu^{*} (Corresponding author)
11
12

13 Beijing National Laboratory for Molecular Sciences, Institute of Theoretical and Computational
14 Chemistry, College of Chemistry and Molecular Engineering, Peking University, Beijing 100871,
15 China
16
17 ORCID ID: 0000-0002-2906-5858
18
19 Email: jianliupku@pku.edu.cn
20
21
22

23
24 **Abstract**
25

26 We report recent progress on the phase space formulation of quantum mechanics with coordinate-momentum
27 variables, focusing more on new theory of (weighted) constraint coordinate-momentum phase space for discrete-
28 variable quantum systems. This leads to a general coordinate-momentum phase space formulation of composite
29 quantum systems, where conventional representations on infinite phase space are employed for continuous
30 variables. It is convenient to utilize (weighted) constraint coordinate-momentum phase space for representing
31 the quantum state and describing nonclassical features. Various numerical tests demonstrate that new trajectory-
32 based quantum dynamics approaches derived from the (weighted) constraint phase space representation are useful
33 and practical for describing dynamical processes of composite quantum systems in gas phase as well as in
34 condensed phase.
35
36
37
38
39
40
41
42
43
44
45
46
47
48
49
50
51
52
53
54
55
56
57
58
59
60

Graphical/Visual Abstract and Caption



Schematic representation of dynamics of composite quantum systems via phase space formulations.

1. INTRODUCTION

Phase space with coordinate-momentum variables is a fundamental concept and offers a convenient tool to describe statistics as well as dynamics in classical mechanics. In comparison to other equivalent interpretations of quantum mechanics, phase space formulations offer more insight and understanding between quantum and classical counterpart concepts, which are widely used in chemical and biological dynamics and spectroscopy¹⁻⁶⁰, quantum optics^{51, 61-70}, cryogenic physics/chemistry⁷¹⁻⁷⁵, quantum information and computation⁷⁶⁻⁸⁷, etc.

Phase space formulations of quantum mechanics have been developed since two important pioneering works, the Weyl transform in 1927, of which the original formulation converted a Hamiltonian on classical phase space into a quantum mechanical operator⁸⁸, and the Wigner function in 1932 that in principle depicts the inverse transform although a pure state was used for demonstration⁸⁹. The most essential element is the one-to-one correspondence mapping between quantum operators and classical functions often defined on a smooth manifold, namely, phase space. Because of the commutation relation of conjugate operators, the mapping is not unique in quantum mechanics^{90, 91}.

When infinite phase space is employed for a continuous-variable quantum system, most phase space formulations can be described by Cohen's generalized form⁹² in 1966. Quantum dynamics with phase space variables is expressed by the Moyal or Moyal-like bracket as first proposed by Groenewold⁹³ in 1946 and Moyal⁹⁴ in 1949. The Wigner and Husimi representations are most often used for the continuous-variable system. When the Moyal bracket is approximated by the Poisson bracket in the Wigner phase space expression of the quantum Liouville theorem, which was also derived as the linearized semiclassical initial value representation (LSC-IVR) or classical Wigner model^{4-8, 11, 20, 23} for the quantum correlation function, it reproduces exact quantum correlation functions even of nonlinear operators (i.e., nonlinear functions of the coordinate or momentum operator) in the harmonic or classical limit. The truncated Wigner approximation⁷⁴ with the time-dependent generalization of the Bopp representation^{90, 95} is similar to the LSC-IVR, but the former requests more demanding evaluation of the stability matrix elements along the trajectory when nonlinear operators are involved in the correlation function. Ref. ¹⁵ suggests a practical way to implement the imaginary time path integral treatment of the Boltzmann density operator in the LSC-IVR for general molecular systems that often contain imaginary frequencies. Its recent application illustrates that quantum dynamical effects play a critical role in reproducing the peaks in the intermediate region between the librational and bending bands, those between the bending and stretching bands, and the double-peak in the stretching band in the experimental isotropic Raman spectrum of liquid water¹⁹ (as shown in Figure 1). In addition that more advanced versions of SC-IVR⁹⁶⁻⁹⁹ are capable of

improving over the LSC-IVR, in ref¹¹ we first employed the quantum Liouville theorem in the phase space formulation to develop trajectory-based approaches to satisfy the two fundamental criteria: conservation of the quantum Boltzmann distribution for the thermal equilibrium system and being exact for any quantum thermal correlation functions in the classical and harmonic limits. Such trajectory-based approaches can in principle be further improved by higher order corrections of the exact series expansion of the phase space propagator as demonstrated in ref⁴⁴. More progress along this line can be found in refs³⁷⁻⁴⁷. (Figure 2 shows molecular vibrational spectra produced by the new phase space quantum dynamics methods.)

Phase space representations of a finite discrete F -state quantum system were first independently described by Stratonovich¹⁰⁰ in 1956, Feynman¹⁰¹ in 1987, and Wootters¹⁰² in 1987. Further developments of Stratonovich's formulation have focused on an SU(2) or SU(F) structure of phase space¹⁰³⁻¹¹⁷, while those on the construction of a discrete phase space are described in Refs^{78, 118-126}. Other than the 2-state (or spin 1/2) system, the exact equations of motion (EOMs) of phase variables (expressed by the Moyal-like bracket) involved in these approaches for the finite discrete multi-state system are often tedious (and nonlinear)^{109, 127-130}. Recent theoretical progress on exactly mapping the finite discrete F -state quantum system onto *constraint* coordinate-momentum phase space suggests that there exists a novel unified framework to derive comprehensive exact mapping Hamiltonians^{44, 57, 131, 132}, of which the quantum EOMs of mapping coordinate-momentum variables are simply linear^{44, 57, 131-134}.

The unified mapping formulation on coordinate-momentum phase space^{44, 57, 131-134} then offers a useful tool to treat dynamics of a composite quantum system, in which both continuous and finite discrete degrees of freedom (DOFs) are involved and coupled with one another. Because a typical molecular system has vibrational, rotational, and translational motion, it is often much more convenient to employ continuous coordinate space rather than Hilbert space with dense states to describe the nuclear DOFs. On the other hand, the energy gap between different electronic states of interest is often significantly larger such that the (adiabatic or diabatic) state representation is more useful to depict the electronic DOFs. It is evident that a general description of the molecular system leads to a composite quantum system, especially in the nonadiabatic region¹³⁵⁻¹⁵². A comprehensive version of the Meyer-Miller mapping Hamiltonian model^{153, 154} can rigorously be formulated in the general coordinate-momentum phase space formulation^{44, 57, 131-134}.

In the Focus Article we focus on novel developments on the phase space formulation of quantum mechanics with coordinate-momentum variables for discrete-variable systems as well as for composite systems^{44, 57, 131-134}. In Section 2 we first review the general coordinate-momentum phase space formulation, where infinite space is

used for describing continuous variables and constraint space is employed for mapping discrete variables. We then propose a weighted constraint phase space representation that is also an exact formulation for mapping discrete-variable quantum systems. Section 3 demonstrates several examples and discusses implications of the (weighted) constraint coordinate-momentum phase space for studying and illustrating discrete-variable or composite quantum systems. When we use the weighted constraint phase space representation for mapping composite quantum systems, the mapping Hamiltonian (we use the Meyer-Miller mapping Hamiltonian for demonstration throughout the article, albeit that other mapping Hamiltonians are also available^{57, 58, 131, 132}) yields a novel trajectory-based approximate approach for composite systems. Such a new method satisfies the frozen nuclei limit [i.e., the dynamics reproduces the exact evolution when only finite discrete (electronic) DOFs are involved]. In Section 4 the performance of new trajectory-based quantum dynamics approaches on (weighted) constraint phase space is extensively tested for a few typical benchmark composite systems in gas phase as well as in condensed phase. Finally, conclusion remarks are presented in Section 5.

2. GENERAL COORDINATE-MOMENTUM PHASE SPACE FORMULATION OF QUANTUM MECHANICS

Consider a (molecular) system with N continuous (nuclear) DOFs and F discrete (electronic) states, of which the Hamiltonian reads

$$\hat{H} = \sum_{n,m=1}^F H_{nm}(\hat{\mathbf{R}}, \hat{\mathbf{P}}) |n\rangle\langle m| = \sum_{n,m=1}^F \left[\frac{1}{2} \hat{\mathbf{P}}^T \mathbf{M}^{-1} \hat{\mathbf{P}} \delta_{nm} + V_{nm}(\hat{\mathbf{R}}) \right] |n\rangle\langle m| , \quad 1$$

where \mathbf{R} and \mathbf{P} are the nuclear coordinate and momentum variables, respectively, \mathbf{M} is the diagonal mass matrix, and the F states form an orthonormal complete basis sets, i.e.,

$$\langle m|n \rangle = \delta_{mn}, \quad \hat{I}_{\text{ele}} = \sum_{n=1}^F |n\rangle\langle n| . \quad 2$$

\hat{I}_{ele} and \hat{I}_{nuc} stand for the identity operator of the discrete (electronic) DOFs and that of the continuous (nuclear) DOFs. For simplicity, eq 1 employs the (electronically) diabatic representation, where the Hermitian potential matrix $\mathbf{V}(\mathbf{R})$ is a function of only the coordinate vector. (In applications $\mathbf{V}(\mathbf{R})$ is often a real symmetric matrix.) More discussion on the adiabatic representation of discrete (electronic) DOFs is available in Section-4.1.

The unified formulation of mapping phase space with coordinate-momentum variables offers a useful exact approach to describe the composite system. The trace of a product of two quantum operators is expressed as an integral of two functions on mapping phase space, *i.e.*,

$$\text{Tr}_{n,e} [\hat{A}\hat{B}] = \int d\mu_{\text{nuc}}(\mathbf{R}, \mathbf{P}) \int_{\mathcal{S}(\mathbf{x}, \mathbf{p})} d\mu_{\text{ele}}(\mathbf{x}, \mathbf{p}) A_C(\mathbf{R}, \mathbf{P}; \mathbf{x}, \mathbf{p}) \tilde{B}_C(\mathbf{R}, \mathbf{P}; \mathbf{x}, \mathbf{p}) \quad 3$$

with

$$A_C(\mathbf{R}, \mathbf{P}; \mathbf{x}, \mathbf{p}) = \text{Tr}_{n,e} [\hat{A}\hat{K}_{\text{nuc}}(\mathbf{R}, \mathbf{P}) \otimes \hat{K}_{\text{ele}}(\mathbf{x}, \mathbf{p})] \quad 4$$

$$\tilde{B}_C(\mathbf{R}, \mathbf{P}; \mathbf{x}, \mathbf{p}) = \text{Tr}_{n,e} [\hat{K}_{\text{nuc}}^{-1}(\mathbf{R}, \mathbf{P}) \otimes \hat{K}_{\text{ele}}^{-1}(\mathbf{x}, \mathbf{p}) \hat{B}] \quad 5$$

$d\mu_{\text{nuc}}(\mathbf{R}, \mathbf{P}) = (2\pi\hbar)^{-N} d\mathbf{R} d\mathbf{P}$ and $d\mu_{\text{ele}}(\mathbf{x}, \mathbf{p}) = F d\mathbf{x} d\mathbf{p}$ as the integration measure on nuclear phase space and that on electronic phase space, respectively, and $\text{Tr}_{n,e}$ represents the trace over the corresponding nuclear and electronic Hilbert space. The integral over the mapping phase space variables for the finite discrete (electronic) DOFs in eq 3 is performed as

$$\int_{\mathcal{S}(\mathbf{x}, \mathbf{p})} F d\mathbf{x} d\mathbf{p} g(\mathbf{x}, \mathbf{p}) = \int F d\mathbf{x} d\mathbf{p} \frac{1}{\Omega} \mathcal{S}(\mathbf{x}, \mathbf{p}) g(\mathbf{x}, \mathbf{p}) = \int F d\mathbf{x} d\mathbf{p} \bar{\mathcal{S}}(\mathbf{x}, \mathbf{p}) g(\mathbf{x}, \mathbf{p}) \quad 6$$

where the area of constraint space $\mathcal{S}(\mathbf{x}, \mathbf{p})$

$$\Omega = \int d\mathbf{x} d\mathbf{p} \mathcal{S}(\mathbf{x}, \mathbf{p}) \quad 7$$

is the normalization constant, and $\bar{\mathcal{S}}(\mathbf{x}, \mathbf{p})$ is the normalized constraint space.

The normalization of the (inverse) mapping kernel reads

$$\text{Tr}_n [\hat{K}_{\text{nuc}}(\mathbf{R}, \mathbf{P})] = \text{Tr}_n [\hat{K}_{\text{nuc}}^{-1}(\mathbf{R}, \mathbf{P})] = 1 \quad 8$$

$$\text{Tr}_e [\hat{K}_{\text{ele}}(\mathbf{x}, \mathbf{p})] = \text{Tr}_e [\hat{K}_{\text{ele}}^{-1}(\mathbf{x}, \mathbf{p})] = 1 \quad 9$$

and

$$\int d\mu_{\text{nuc}}(\mathbf{R}, \mathbf{P}) \hat{K}_{\text{nuc}}(\mathbf{R}, \mathbf{P}) = \int d\mu_{\text{nuc}}(\mathbf{R}, \mathbf{P}) \hat{K}_{\text{nuc}}^{-1}(\mathbf{R}, \mathbf{P}) = \hat{I}_{\text{nuc}} \quad 10$$

$$\int_{\mathcal{S}(\mathbf{x}, \mathbf{p})} d\mu_{\text{ele}}(\mathbf{x}, \mathbf{p}) \hat{K}_{\text{ele}}(\mathbf{x}, \mathbf{p}) = \int_{\mathcal{S}(\mathbf{x}, \mathbf{p})} d\mu_{\text{ele}}(\mathbf{x}, \mathbf{p}) \hat{K}_{\text{ele}}^{-1}(\mathbf{x}, \mathbf{p}) = \hat{I}_{\text{ele}} \quad . \quad 11$$

The one-to-one correspondence mapping from phase space function $A_c(\mathbf{R}, \mathbf{P}; \mathbf{x}, \mathbf{p})$ or $\tilde{B}_c(\mathbf{R}, \mathbf{P}; \mathbf{x}, \mathbf{p})$ of Eq 4 back to operator \hat{A} or \hat{B} is

$$\begin{aligned}\hat{A} &= \int d\mu_{\text{nuc}}(\mathbf{R}, \mathbf{P}) \int_{S(x,p)} d\mu_{\text{ele}}(\mathbf{x}, \mathbf{p}) A_c(\mathbf{R}, \mathbf{P}; \mathbf{x}, \mathbf{p}) \hat{K}_{\text{nuc}}^{-1}(\mathbf{R}, \mathbf{P}) \otimes \hat{K}_{\text{ele}}^{-1}(\mathbf{x}, \mathbf{p}) \\ \hat{B} &= \int d\mu_{\text{nuc}}(\mathbf{R}, \mathbf{P}) \int_{S(x,p)} d\mu_{\text{ele}}(\mathbf{x}, \mathbf{p}) \tilde{B}_c(\mathbf{R}, \mathbf{P}; \mathbf{x}, \mathbf{p}) \hat{K}_{\text{nuc}}(\mathbf{R}, \mathbf{P}) \otimes \hat{K}_{\text{ele}}(\mathbf{x}, \mathbf{p})\end{aligned}. \quad 12$$

The nuclear or electronic kernel should satisfy five criteria, namely, linearity, reality, standardization (normalization), traciality, and covariance^{93, 94, 100, 115}.

2.1 Mapping kernel for continuous (nuclear) degrees of freedom

The integrals for (\mathbf{R}, \mathbf{P}) in eqs 3, 10, and 12 are over infinite (nuclear) phase space. The mapping kernel and its inverse for the nuclear DOFs are

$$\begin{aligned}\hat{K}_{\text{nuc}}(\mathbf{R}, \mathbf{P}) &= \left(\frac{\hbar}{2\pi} \right)^N \int d\zeta \int d\eta e^{i\zeta \cdot (\hat{\mathbf{R}} - \mathbf{R}) + i\eta \cdot (\hat{\mathbf{P}} - \mathbf{P})} f(\zeta, \eta) \\ \hat{K}_{\text{nuc}}^{-1}(\mathbf{R}, \mathbf{P}) &= \left(\frac{\hbar}{2\pi} \right)^N \int d\zeta \int d\eta e^{i\zeta \cdot (\hat{\mathbf{R}} - \mathbf{R}) + i\eta \cdot (\hat{\mathbf{P}} - \mathbf{P})} [f(-\zeta, -\eta)]^{-1}\end{aligned}, \quad 13$$

where $f(\zeta, \eta)$ is a scalar function. E.g., we have the Wigner function^{89, 155}

$$f(\zeta, \eta) = 1, \quad 14$$

the Husimi function¹⁵⁶

$$f(\zeta, \eta) = \exp \left(-\frac{\zeta^T \Gamma^{-1} \zeta}{4} - \frac{\hbar^2}{4} \eta^T \Gamma \eta \right), \quad 15$$

the anti-Husimi function

$$f(\zeta, \eta) = \exp \left(\frac{\zeta^T \Gamma^{-1} \zeta}{4} + \frac{\hbar^2}{4} \eta^T \Gamma \eta \right), \quad 16$$

the Glauber-Sudarshan P function^{61, 62, 66} (with the characteristic frequency matrix ω of the system)

$$f(\zeta, \eta) = \exp \left[\frac{\hbar}{4} \zeta^T \mathbf{M}^{-1/2} \omega^{-1} \mathbf{M}^{-1/2} \zeta + \frac{\hbar}{4} \eta^T \mathbf{M}^{1/2} \omega \mathbf{M}^{1/2} \eta \right] \quad 17$$

and its generalized versions⁶⁶, the Glauber Q function¹⁵⁷

$$f(\zeta, \eta) = \exp\left[-\frac{\hbar}{4}\zeta^T \mathbf{M}^{-1/2} \boldsymbol{\omega}^{-1} \mathbf{M}^{-1/2} \zeta - \frac{\hbar}{4}\eta^T \mathbf{M}^{1/2} \boldsymbol{\omega} \mathbf{M}^{1/2} \eta\right], \quad 18$$

the normal-antinormal ordered function⁹¹

$$f(\zeta, \eta) = \cosh\left[\frac{\hbar}{4}\zeta^T \mathbf{M}^{-1/2} \boldsymbol{\omega}^{-1} \mathbf{M}^{-1/2} \zeta + \frac{\hbar}{4}\eta^T \mathbf{M}^{1/2} \boldsymbol{\omega} \mathbf{M}^{1/2} \eta\right], \quad 19$$

the Kirkwood antistandard-ordered function^{158, 159}

$$f(\zeta, \eta) = e^{i\hbar\zeta^T \eta/2}, \quad 20$$

the Mehta standard-ordered function¹⁶⁰

$$f(\zeta, \eta) = e^{-i\hbar\zeta^T \eta/2}, \quad 21$$

the Rivier function^{161, 162}

$$f(\zeta, \eta) = \cos\left[\frac{1}{2}\hbar\zeta^T \eta\right], \quad 22$$

and the distribution function of Born and Jordan¹⁶³

$$f(\zeta, \eta) = \frac{\sin\left[\frac{1}{2}\hbar\zeta^T \eta\right]}{\frac{1}{2}\hbar\zeta^T \eta}, \quad 23$$

etc.

When operator \hat{A} is a function of only the nuclear DOFs, its phase space function from Eq 4 and the dual function from eq 5 become

$$A_{\text{nuc}}(\mathbf{R}, \mathbf{P}) = \text{Tr}_n\left[\hat{A}\hat{K}_{\text{nuc}}(\mathbf{R}, \mathbf{P})\right] \quad 24$$

and

$$\tilde{A}_{\text{nuc}}(\mathbf{R}, \mathbf{P}) = \text{Tr}_n\left[\hat{K}_{\text{nuc}}^{-1}(\mathbf{R}, \mathbf{P})\hat{A}\right]. \quad 25$$

When the Wigner function eq 14 is used, the mapping kernel and its inverse are the same, i.e., $\hat{K}_{\text{nuc}}(\mathbf{x}, \mathbf{p}) = \hat{K}_{\text{nuc}}^{-1}(\mathbf{x}, \mathbf{p})$. The Wigner phase space function of operator \hat{A} (from eq 24) is identical to its dual (from eq 25),

$$A_{\text{nuc}}^W(\mathbf{R}, \mathbf{P}) = \tilde{A}_{\text{nuc}}^W(\mathbf{R}, \mathbf{P}) . \quad 26$$

When the Husimi phase space (eq 15) is employed, it is straightforward to show the relation between the Wigner and Husimi phase space functions (obtained from eq 24)

$$A_{\text{nuc}}^H(\mathbf{R}, \mathbf{P}) = \exp \left[\frac{1}{4} \left(\frac{\mathbf{d}}{\mathbf{d}\mathbf{R}} \right)^T \boldsymbol{\Gamma}^{-1} \left(\frac{\mathbf{d}}{\mathbf{d}\mathbf{R}} \right) + \frac{\hbar^2}{4} \left(\frac{\mathbf{d}}{\mathbf{d}\mathbf{P}} \right)^T \boldsymbol{\Gamma} \left(\frac{\mathbf{d}}{\mathbf{d}\mathbf{P}} \right) \right] A_{\text{nuc}}^W(\mathbf{R}, \mathbf{P}) , \quad 27$$

and the relation between the dual function of Husimi phase space $\tilde{A}_{\text{nuc}}^H(\mathbf{R}, \mathbf{P})$ and the Wigner phase space function $A_{\text{nuc}}^W(\mathbf{R}, \mathbf{P})$

$$\tilde{A}_{\text{nuc}}^H(\mathbf{R}, \mathbf{P}) = \exp \left[-\frac{1}{4} \left(\frac{\mathbf{d}}{\mathbf{d}\mathbf{R}} \right)^T \boldsymbol{\Gamma}^{-1} \left(\frac{\mathbf{d}}{\mathbf{d}\mathbf{R}} \right) - \frac{\hbar^2}{4} \left(\frac{\mathbf{d}}{\mathbf{d}\mathbf{P}} \right)^T \boldsymbol{\Gamma} \left(\frac{\mathbf{d}}{\mathbf{d}\mathbf{P}} \right) \right] A_{\text{nuc}}^W(\mathbf{R}, \mathbf{P}) . \quad 28$$

Because any choice of $f(\zeta, \eta)$ in eq 13 leads to an informationally complete representation of the continuous-variable quantum system, it is not difficult to establish the relation between different (dual) phase space functions in addition to eq 27 and eq 28.

2.2 Mapping kernel on constraint space for discrete (electronic) degrees of freedom

As derived first in Appendix A of ref¹³² in the spirit of Ref¹³¹ and then in the Supporting Information of ref¹³⁴, the kernel that maps a set of F states onto constraint phase space $\mathcal{S}(\mathbf{x}, \mathbf{p})$ reads

$$\hat{K}_{\text{ele}}(\mathbf{x}, \mathbf{p}) = \sum_{n,m=1}^F \left[\frac{1}{2} (x^{(n)} + ip^{(n)}) (x^{(m)} - ip^{(m)}) - \gamma \delta_{nm} \right] |n\rangle\langle m| \quad 29$$

and the corresponding inverse kernel is

$$\hat{K}_{\text{ele}}^{-1}(\mathbf{x}, \mathbf{p}) = \sum_{n,m=1}^F \left[\frac{1+F}{2(1+F\gamma)^2} (x^{(n)} + ip^{(n)}) (x^{(m)} - ip^{(m)}) - \frac{1-\gamma}{1+F\gamma} \delta_{nm} \right] |n\rangle\langle m| . \quad 30$$

As naturally required by eq 9, constraint phase space $\mathcal{S}(\mathbf{x}, \mathbf{p})$ is defined by

$$\delta\left(\sum_{n=1}^F \frac{(x^{(n)})^2 + (p^{(n)})^2}{2} - (1+F\gamma)\right) , \quad 31$$

of which the area is

$$\Omega(\gamma) = \int d\mathbf{x}d\mathbf{p} \delta\left(\sum_{n=1}^F \frac{(x^{(n)})^2 + (p^{(n)})^2}{2} - (1+F\gamma)\right) . \quad 32$$

The normalized constraint phase space is $\bar{\mathcal{S}}(\mathbf{x}, \mathbf{p}) = \mathcal{S}(\mathbf{x}, \mathbf{p})/\Omega(\gamma)$.

Equations 29-32 define the mapping kernel and inverse kernel as well as constraint phase space, which are the key elements of the coordinate-momentum phase space formulation of the discrete-variable quantum system that we first established in refs^{131, 132} and further developed in refs^{57, 58, 134}. As yielded from eq 4, when the Wigner function eq 14 is used for the nuclear DOFs, the mapping Hamiltonian for the quantum Hamiltonian operator eq 1 reads

$$H_C(\mathbf{R}, \mathbf{P}; \mathbf{x}, \mathbf{p}; \gamma) = \frac{1}{2} \mathbf{P}^T \mathbf{M}^{-1} \mathbf{P} + \sum_{n,m=1}^F V_{mn}(\mathbf{R}) \left[\frac{1}{2} (x^{(n)} + ip^{(n)}) (x^{(m)} - ip^{(m)}) - \gamma \delta_{nm} \right] . \quad 33$$

Because $\mathbf{V}(\mathbf{R})$ is Hermitian, the mapping Hamiltonian is real. As $\mathbf{V}(\mathbf{R})$ is often a real symmetric matrix, eq 33 becomes

$$H_C(\mathbf{R}, \mathbf{P}; \mathbf{x}, \mathbf{p}; \gamma) = \frac{1}{2} \mathbf{P}^T \mathbf{M}^{-1} \mathbf{P} + \sum_{n,m=1}^F \left[\frac{1}{2} (x^{(n)} x^{(m)} + p^{(n)} p^{(m)}) - \gamma \delta_{nm} \right] V_{mn}(\mathbf{R}) , \quad 34$$

which is the seminal Meyer-Miller Hamiltonian¹⁵³ that has extensively been implemented for nonadiabatic dynamics in the literature^{4, 56, 60, 138, 154, 164-218}. In refs^{58, 131, 132} it is shown that there also exist other comprehensive mapping Hamiltonian models in the general coordinate-momentum phase space formulation of quantum mechanics. When the mapping Hamiltonian is employed to generate trajectory-based dynamics in the phase space formulation for a composite quantum system, we denote it the classical mapping model (CMM) approach. It satisfies the frozen nuclei limit. We use the Meyer-Miller Hamiltonian for demonstration throughout the Focus Article.

When Meyer and Miller proposed the conventional Meyer-Miller mapping Hamiltonian model for the nonadiabatic system in 1979, they did not invoke the phase space formulation. In 1997 Stock and Thoss¹⁵⁴ utilized the Schwinger oscillator theory of angular momentum^{219, 220} to derive the Meyer-Miller mapping Hamiltonian¹⁵³. Its LSC-IVR approximation⁴ in principle includes *infinite* Wigner phase space for the finite set of (electronic) states. The applications, however, suggest that the LSC-IVR approximation in the framework of

refs^{4, 154, 170} is not good^{172, 177, 181, 187, 195, 200, 202}. More advanced semiclassical approaches^{96, 97} improve the performance but request more computational effort^{172, 173}. The symmetric-window-function and other techniques have been introduced to practically overcome the drawbacks^{177, 181, 187, 195, 200, 202}. Recent progress along this line is briefly summarized in ref¹³⁸.

Equation 31 indicates that parameter γ lies in region $(-1/F, \infty)$. It is shown that parameter γ can be either positive or negative^{131, 134} and should be interpreted as a special case of the commutator matrix^{57, 58, 131, 134} rather than the conventional zero-point-energy parameter^{153, 154}. There exist three key elements for a trajectory-based quantum dynamics method to evaluate the evolution of the expectation/ensemble average of a physical property, namely,

- 1) the EOMs of the trajectory,
- 2) the initial condition of the trajectory, and
- 3) the integral expression for the expectation/ensemble average of the physical property of interest.

In the frozen-nuclei limit, Hamilton's EOMs governed by the Meyer-Miller mapping Hamiltonian is isomorphic to exact dynamics. While it is reasonable to employ the mapping Hamiltonian to define the EOMs of the trajectory, the left two elements are also important to consider such that the trajectory-based dynamics method is consistent. The constraint coordinate-momentum phase space formulation then offers a more advanced platform to consider all the three key elements.

It is evident that eq 31 is a special choice of constraint phase space $\mathcal{S}(\mathbf{x}, \mathbf{p})$. The interpretation of parameter γ in refs^{57, 58, 131, 134} hints that a more comprehensive choice of normalized constraint phase space $\bar{\mathcal{S}}(\mathbf{x}, \mathbf{p})$ is

$$\int_{-1/F}^{\infty} d\gamma w(\gamma) \frac{1}{\Omega(\gamma)} \delta\left(\sum_{n=1}^F \frac{(x^{(n)})^2 + (p^{(n)})^2}{2} - (1+F\gamma)\right) , \quad 35$$

with the *quasi*-probability distribution function

$$\int_{-1/F}^{\infty} d\gamma w(\gamma) = 1 . \quad 36$$

Equation 6, the integral over the mapping phase space variables for the finite discrete (electronic) DOFs then becomes

$$\int_{\mathcal{S}(\mathbf{x}, \mathbf{p})} F d\mathbf{x} d\mathbf{p} g(\mathbf{x}, \mathbf{p}) = \int_{-1/F}^{\infty} d\gamma w(\gamma) \int F d\mathbf{x} d\mathbf{p} \frac{1}{\Omega(\gamma)} \delta \left(\sum_{n=1}^F \frac{(x^{(n)})^2 + (p^{(n)})^2}{2} - (1+F\gamma) \right) g(\mathbf{x}, \mathbf{p}) . \quad 37$$

If we require that the kernel is the same as its inverse, i.e.,

$$\hat{K}_{\text{ele}}(\mathbf{x}, \mathbf{p}) = \hat{K}_{\text{ele}}^{-1}(\mathbf{x}, \mathbf{p}) = \sum_{n,m=1}^F \left[\frac{1}{2} (x^{(n)} + ip^{(n)}) (x^{(m)} - ip^{(m)}) - \gamma \delta_{nm} \right] |n\rangle \langle m| , \quad 38$$

it is then not difficult to obtain

$$\int_{-1/F}^{\infty} d\gamma w(\gamma) \chi(\gamma) = 1 \quad 39$$

with

$$\chi(\gamma) = F\gamma^2 + 2\gamma . \quad 40$$

(See Appendix 1 of Supporting Information for more discussion.) Equations 35-40 define normalized constraint phase space $\bar{\mathcal{S}}(\mathbf{x}, \mathbf{p})$, the mapping kernel and inverse kernel, and the *quasi*-probability distribution function $w(\gamma)$ of parameter γ . The weighted constraint phase space formulation for the discrete-variable quantum system is the key new theoretical result of the Focus Article. When the Wigner function eq 14 is used for the nuclear DOFs, where $\hat{K}_{\text{nuc}}(\mathbf{x}, \mathbf{p}) = \hat{K}_{\text{nuc}}^{-1}(\mathbf{x}, \mathbf{p})$, eq 4 is then identical to eq 5 when $\hat{A} = \hat{B}$. The mapping Hamiltonian for the quantum Hamiltonian operator eq 1 produced by either of eq 4 and eq 5 leads to the same expression as eq 34. When the mapping Hamiltonian is utilized to produce the trajectory-based dynamics for a composite system, it is denoted the weighted mapping model (wMM) approach. The frozen nuclei limit is satisfied in wMM.

Many choices are possible for the discrete or continuous version of the normalized quasi-probability distribution function $w(\gamma)$ in the weighted constraint phase space mapping theory. In the Focus Article we consider only the simplest cases of the discrete version. When but a single value of parameter γ is chosen in eq 39, i.e., $w(\gamma) = \delta(\gamma - \gamma_1)$, we obtain

$$F\gamma^2 + 2\gamma = 1 , \quad 41$$

of which the non-trivial solution is

$$\gamma = \frac{\sqrt{1+F} - 1}{F} \quad . \quad 42$$

In this case, the weighted constraint phase space formulation is identical to the constraint phase space formulation, and wMM becomes CMM when trajectory-based dynamics is considered. When only two values of parameter γ are selected, i.e.,

$$w(\gamma) = \sum_{j=1}^2 w(\gamma_j) \delta(\gamma - \gamma_j) \quad , \quad 43$$

eq 36 and eq 39 lead to

$$\begin{aligned} w(\gamma_1) &= \frac{1 - \chi(\gamma_2)}{\chi(\gamma_1) - \chi(\gamma_2)} \\ w(\gamma_2) &= \frac{\chi(\gamma_1) - 1}{\chi(\gamma_1) - \chi(\gamma_2)} \end{aligned} \quad . \quad 44$$

When the values of parameter γ are close to zero or smaller than zero in region $(-1/F, \infty)$, trajectories produced by the Meyer-Miller mapping Hamiltonian eq 34 for nonadiabatic molecular dynamics are stable. For demonstration in the paper we choose

$$\gamma_1 = -\gamma_2 = \Delta \quad 45$$

with Δ a reasonably small positive real number in region $(0, 1/F)$. Figure 3 presents the constraint coordinate-momentum phase space formulation when a single value of parameter γ is used (Figure 3a) as well as the weighted formulation when two values of parameter γ suggested by eq 45 are used (Figure 3b).

3. PHASE SPACE REPRESENTATION OF THE NONCLASSICAL FEATURE OF QUANTUM SYSTEMS

Recent advance on quantum technologies makes it possible to control and manipulate quantum states in experiment. Because the phase space formulation offers an informationally complete description of the density matrix, direct measurements of phase space of the quantum system with continuous DOFs, those of the quantum system with discrete DOFs, and those of the composite quantum system have been realized in experiment^{70, 85, 221-234}. While the celebrated Wigner phase space has long been used for illustration of the negative *quasi*-probability for continuous-variable systems^{225, 235}, Stratonovich phase space has recently been proposed for visualization and tomography of discrete-variable systems^{85, 113, 227-229, 231, 236, 237}. A combination of these two spaces has been used for illustration of nonclassical correlations or entanglement between the discrete DOF and the continuous DOF of

the composite system^{238, 239}. (In Appendix 3 of Supporting Information, we briefly review Stratonovich phase space with an either SU(2) or SU(F) structure, as well as the relationship between Stratonovich phase space and constraint coordinate-momentum phase space as already pointed out in refs^{57, 58}.)

As coordinate-momentum phase space is well-established in classical mechanics, the formulation of (weighted) constraint coordinate-momentum phase space described in Section 2 offers a potentially useful approach for describing correlations and dynamics in the discrete-variable system as well as the composite system in quantum mechanics. When (weighted) constraint coordinate-momentum phase space is used for mapping an F -state system, the phase space distribution is

$$\rho_C(\mathbf{x}, \mathbf{p}) = \sum_{m,n=1}^F \rho_{mn} K_{nm}(\mathbf{x}, \mathbf{p}), \quad 46$$

where $\rho_{mn} = \langle m | \hat{\rho} | n \rangle$ and $K_{nm}(\mathbf{x}, \mathbf{p}) = \langle n | \hat{K}_{\text{ele}}(\mathbf{x}, \mathbf{p}) | m \rangle$ with $\hat{K}_{\text{ele}}(\mathbf{x}, \mathbf{p})$ defined in eq 38. For the sake of visualization, it is convenient to further reduce constraint phase space variables (\mathbf{x}, \mathbf{p}) to two relevant variables, $(x^{(n)}, x^{(m)})$ or $(x^{(n)}, p^{(m)})$ for describing the correlation on arbitrary two states $|n\rangle$ and $|m\rangle$. We define the marginal function, $\mathcal{K}_{(n,m)}(x^{(n)}, x^{(m)})$, on constraint coordinate-momentum phase space (Figure 4),

$$\mathcal{K}_{(n,m)}(x^{(n)}, x^{(m)}) = \int F d\mathbf{x}_\perp d\mathbf{p} \frac{1}{\Omega(\gamma)} \delta \left(\sum_{j=1}^F \frac{(x^{(j)})^2 + (p^{(j)})^2}{2} - (1+F\gamma) \right) K_{nm}(\mathbf{x}, \mathbf{p}; \gamma), \quad 47$$

where \mathbf{x}_\perp represents all $x^{(i)}$ other than $\{x^{(n)}, x^{(m)}\}$, and that on weighted constraint phase space,

$$\mathcal{K}_{(n,m)}(x^{(n)}, x^{(m)}) = \int_{-1/F}^{\infty} d\gamma w(\gamma) \frac{1}{\Omega(\gamma)} \int F d\mathbf{x}_\perp d\mathbf{p} \delta \left(\sum_{j=1}^F \frac{(x^{(j)})^2 + (p^{(j)})^2}{2} - (1+F\gamma) \right) K_{nm}(\mathbf{x}, \mathbf{p}; \gamma). \quad 48$$

Figure 5 demonstrates the case of eq 48 when the quasi-probability distribution function $w(\gamma)$ is defined by eqs 43-45 where two symmetrical values of parameter γ are used. Similar definitions also apply for $\mathcal{K}_{(n,m)}(x^{(n)}, p^{(m)})$. The explicit formula of these marginal functions can be derived by using the integral techniques in Appendix 1 of Supporting Information.

Figures 4-5 demonstrate a composite system that consists of a discrete DOF for spin-1/2 and a continuous DOF for a harmonic oscillator. The marginal joint distribution function of the composite system reads

$$\rho_C^{(n,m)}(\mathbf{R}, \mathbf{P}; x^{(n)}, x^{(m)}) = \text{Tr}_{n,e} \left[\hat{\rho} \hat{K}_{\text{nuc}}(\mathbf{R}, \mathbf{P}) \otimes |n\rangle \langle m| \mathcal{K}_{(n,m)}(x^{(n)}, x^{(m)}) \right]. \quad 49$$

The marginal quasi-probability distribution functions of the continuous variable for both the pure state and the mixed state are presented in Figure 4a, where infinite Wigner phase space is employed. The marginal functions of the discrete variables (based on eq 47) of the spin-1/2 system read

$$\begin{aligned} & \begin{pmatrix} \mathcal{K}_{\uparrow\uparrow}(x^{(1)}, x^{(2)}) & \mathcal{K}_{\uparrow\downarrow}(x^{(1)}, x^{(2)}) \\ \mathcal{K}_{\downarrow\uparrow}(x^{(1)}, x^{(2)}) & \mathcal{K}_{\downarrow\downarrow}(x^{(1)}, x^{(2)}) \end{pmatrix} \\ &= \frac{1}{2\pi(1+2\gamma)} \begin{pmatrix} 1 + \frac{1}{2}(x^{(1)})^2 - \frac{1}{2}(x^{(2)})^2 & x^{(1)}x^{(2)} \\ x^{(1)}x^{(2)} & 1 - \frac{1}{2}(x^{(1)})^2 + \frac{1}{2}(x^{(2)})^2 \end{pmatrix}, \end{aligned} \quad 50$$

where notations \uparrow, \downarrow are used to represent the two discrete states.

The marginal functions for the discrete variable are demonstrated on constraint coordinate-momentum phase space in Figure 4b and on weighted constraint space in Figure 5b. More interestingly, the identical angular behaviour and the radial cancellation behaviour of two weighted components lead to a hollow ring structure on weighted constraint phase space (Figure 5a, also see Appendix 4 of Supporting Information). The difference between the Schrodinger cat state and the mixed state is distinct in either Figure 4b on constraint space or Figure 5b on weighted constraint space.

The marginal joint function of a pure Bell entangled state, $(|0\rangle|\downarrow\rangle + |1\rangle|\uparrow\rangle)/2$, of the composite system is demonstrated in Figure 4c (by adopting the similar strategy of refs^{238, 239}), where constraint coordinate-momentum phase space is used for the discrete DOF at each grid, as well as in Figure 5c where weighted constraint space is employed for the discrete DOF at each grid. The two-dimensional grids represent variables (R, P) of infinite Wigner phase space for the continuous DOF in either of Figure 4c and Figure 5c. When the pure Bell entangled state is studied, both Figure 4c and Figure 5c clearly demonstrate a Gaussian decay of the joint marginal function against Wigner phase space variables (R, P) of the continuous DOF. Either Figure 4c or Figure 5c also shows the pattern of the correlation between the continuous DOF and the discrete DOF. It is convenient to distinguish the pure Bell entangled state, $(|0\rangle|\downarrow\rangle + |1\rangle|\uparrow\rangle)/2$, from the direct product of the Schrodinger cat states, $(|0\rangle + |1\rangle) \otimes (|\uparrow\rangle + |\downarrow\rangle)/2$, when the hybrid representation of the general coordinate-momentum phase space is used.

4. DYNAMICS OF COMPOSITE QUANTUM SYSTEMS

The quantum Liouville theorem can be expressed as a generalized Moyal bracket on hybrid coordinate-momentum phase space. When the Poisson bracket for classical Hamilton's EOMs governed by the mapping Hamiltonian, eq 34, is used to approximate the generalized Moyal bracket on phase space, we have CMM when constraint space is used, and wMM when weighted constraint space is employed. We compare the new wMM and CMM approaches to Ehrenfest dynamics^{240, 241} as well as the fewest-switches surface hopping (FSSH) method²⁴²⁻²⁴⁴, two prevailing trajectory-based dynamics methods for a few typical composite quantum systems. (In this section we set $\hbar = 1$ for simplicity if it is not specifically stated).

4.1 Equations of motion governed by the mapping Hamiltonian

In eq 1, the 'complete' set of diabatic states $\{|n\rangle\}$ is independent of nuclear coordinate/configuration \mathbf{R} . The mapping variables for discrete (electronic) DOFs, (\mathbf{x}, \mathbf{p}) , are independent of \mathbf{R} . Define $\mathbf{g} = \mathbf{x} + i\mathbf{p}$. The EOMs governed by eq 33, the mapping Hamiltonian of eq 1, then read,

$$\dot{\mathbf{g}} = -i\mathbf{V}(\mathbf{R})\mathbf{g} \quad . \quad 51$$

$$\dot{\mathbf{R}} = \mathbf{M}^{-1}\mathbf{P} \quad 52$$

$$\dot{\mathbf{P}} = -\sum_{n,m=1}^F (\nabla_{\mathbf{R}} V_{mn}(\mathbf{R})) \left(\frac{1}{2} (x^{(n)} + ip^{(n)}) (x^{(m)} - ip^{(m)}) - \gamma \delta_{nm} \right) \quad . \quad 53$$

Diabatic potential matrix $\mathbf{V}(\mathbf{R})$ is Hermitian, so is the force matrix, $\{\nabla_{\mathbf{R}} V_{mn}(\mathbf{R})\}$. It is trivial to verify that the mean force of the right-hand side (RHS) of eq 53 is always real. When $\mathbf{V}(\mathbf{R})$ is a real symmetric matrix, the EOMs become

$$\begin{aligned} \dot{\mathbf{x}} &= \mathbf{V}(\mathbf{R})\mathbf{p} \\ \dot{\mathbf{p}} &= -\mathbf{V}(\mathbf{R})\mathbf{x} \\ \dot{\mathbf{R}} &= \mathbf{M}^{-1}\mathbf{P} \\ \dot{\mathbf{P}} &= -\sum_{n,m=1}^F (\nabla_{\mathbf{R}} V_{mn}(\mathbf{R})) \left[\frac{1}{2} (x^{(n)} x^{(m)} + p^{(n)} p^{(m)}) - \gamma \delta_{nm} \right] \end{aligned} \quad . \quad 54$$

Consider the full Hamiltonian of nuclei and electrons of the molecular system,

$$\hat{H} = \frac{1}{2} \hat{\mathbf{P}}^T \mathbf{M}^{-1} \hat{\mathbf{P}} + \hat{H}_{el}(\hat{\mathbf{R}}) \quad , \quad 55$$

where $\hat{H}_{el}(\hat{\mathbf{R}})$ is the electronic Hamiltonian. Its representation in the diabatic basis reads

$$\hat{H}_{el}(\mathbf{R}) = \sum_{n,m} V_{nm}(\mathbf{R}) |n\rangle \langle m| \quad 56$$

and that in the adiabatic basis is

$$\hat{H}_{el}(\mathbf{R}) = \sum_k E_k(\mathbf{R}) |\phi_k(\mathbf{R})\rangle\langle\phi_k(\mathbf{R})| , \quad 57$$

where $E_k(\mathbf{R})$ denotes the adiabatic potential energy surface of the k -th adiabatic electronic state. Assume that the unitary transformation between a set of diabatic basis states, $\{|m\rangle\}$, and a set of adiabatic basis states, $\{|\phi_k(\mathbf{R})\rangle\}$, is

$$|\phi_k(\mathbf{R})\rangle = \sum_m U_{mk}(\mathbf{R}) |m\rangle , \quad 58$$

$$|n\rangle = \sum_k U_{nk}^*(\mathbf{R}) |\phi_k(\mathbf{R})\rangle$$

where $U_{mk}(\mathbf{R}) = \langle m | \phi_k(\mathbf{R}) \rangle$. This states the diagonalization of the diabatic potential matrix,

$$\sum_{n,m} U_{nj}^*(\mathbf{R}) V_{nm}(\mathbf{R}) U_{mk}(\mathbf{R}) = E_k(\mathbf{R}) \delta_{kj} , \quad 59$$

or equivalently,

$$V_{mn}(\mathbf{R}) = \sum_k U_{mk}(\mathbf{R}) E_k(\mathbf{R}) U_{nk}^*(\mathbf{R}) . \quad 60$$

Define the nonadiabatic coupling vector,

$$\mathbf{d}_{mn}(\mathbf{R}) = \left\langle \phi_m(\mathbf{R}) \left| \frac{\partial \phi_n(\mathbf{R})}{\partial \mathbf{R}} \right. \right\rangle . \quad 61$$

It is trivial to show

$$\mathbf{d}_{mn}(\mathbf{R}) = -\mathbf{d}_{nm}^*(\mathbf{R}) \quad 62$$

because of the orthonormality of the basis set, i.e., $\langle \phi_m(\mathbf{R}) | \phi_n(\mathbf{R}) \rangle = \delta_{mn}$. We then obtain

$$\nabla_{\mathbf{R}} U_{mk}^*(\mathbf{R}) = \langle \nabla_{\mathbf{R}} \phi_k(\mathbf{R}) | m \rangle = \sum_n \langle \nabla_{\mathbf{R}} \phi_k(\mathbf{R}) | \phi_n \rangle \langle \phi_n | m \rangle$$

$$= \sum_n \mathbf{d}_{nk}^*(\mathbf{R}) U_{mn}^*(\mathbf{R}) = -\sum_n \mathbf{d}_{kn}(\mathbf{R}) U_{mn}^*(\mathbf{R}) \quad 63$$

and

$$\nabla_{\mathbf{R}} U_{mk}(\mathbf{R}) = -\sum_n \mathbf{d}_{kn}^*(\mathbf{R}) U_{mn}(\mathbf{R}) = \sum_n U_{mn}(\mathbf{R}) \mathbf{d}_{nk}(\mathbf{R}) . \quad 64$$

Below we show the explicit form of the EOMs, eqs 51-53, under the diabatic-to-adiabatic transformation, eq 58.

The covariant transformation for mapping variables corresponding to the diabatic-to-adiabatic transformation, eq 58, reads

$$\tilde{x}^{(n)}(\mathbf{R}) + i\tilde{p}^{(n)}(\mathbf{R}) = \sum_m U_{mn}^*(\mathbf{R}) (x^{(m)} + ip^{(m)}) \quad 65$$

or

$$x^{(n)} + ip^{(n)} = \sum_m U_{nm}(\mathbf{R}) (\tilde{x}^{(m)}(\mathbf{R}) + i\tilde{p}^{(m)}(\mathbf{R})) \quad 66$$

Denote $\tilde{\mathbf{g}}(\mathbf{R}) = \tilde{\mathbf{x}}(\mathbf{R}) + i\tilde{\mathbf{p}}(\mathbf{R})$. Equations 65-66 become

$$\begin{aligned} \tilde{\mathbf{g}}(\mathbf{R}) &= \mathbf{U}^\dagger(\mathbf{R}) \mathbf{g} \\ \mathbf{g} &= \mathbf{U}(\mathbf{R}) \tilde{\mathbf{g}}(\mathbf{R}) \end{aligned} \quad 67$$

The electronic mapping kernel, eq 29, is

$$\hat{K}_{\text{ele}} = \sum_{n,m} \left[\frac{1}{2} (\tilde{x}^{(n)} + i\tilde{p}^{(n)}) (\tilde{x}^{(m)} - i\tilde{p}^{(m)}) - \gamma \delta_{nm} \right] |\phi_n\rangle \langle \phi_m| \quad 68$$

under the transformation for a specific nuclear configuration, \mathbf{R} . Substitution of eq 63 into eq 65 yields

$$\nabla_{\mathbf{R}} (\tilde{x}^{(n)}(\mathbf{R}) + i\tilde{p}^{(n)}(\mathbf{R})) = - \sum_k \mathbf{d}_{nk}(\mathbf{R}) (\tilde{x}^{(k)}(\mathbf{R}) + i\tilde{p}^{(k)}(\mathbf{R})) \quad 69$$

The total time derivative of $\tilde{x}^{(n)} + i\tilde{p}^{(n)}$ reads

$$\begin{aligned} \frac{d}{dt} (\tilde{x}^{(n)} + i\tilde{p}^{(n)}) &= \sum_m U_{mn}^*(\mathbf{R}) \left(\frac{d}{dt} (x^{(m)} + ip^{(m)}) \right) + \sum_m \left(\frac{d}{dt} U_{mn}^*(\mathbf{R}) \right) (x^{(m)} + ip^{(m)}) \\ &= -i \sum_k \delta_{nk} E_k(\mathbf{R}) (\tilde{x}^{(k)} + i\tilde{p}^{(k)}) - \sum_k \dot{\mathbf{R}} \cdot \mathbf{d}_{nk}(\mathbf{R}) (\tilde{x}^{(k)} + i\tilde{p}^{(k)}) \\ &= -i \sum_k [E_k(\mathbf{R}) \delta_{nk} - i \dot{\mathbf{R}} \cdot \mathbf{d}_{nk}(\mathbf{R})] (\tilde{x}^{(k)} + i\tilde{p}^{(k)}) \end{aligned} \quad 70$$

Equation 70 is the EOMs for mapping variables of electronic DOFs in the adiabatic representation.

We then consider the EOMs of nuclear mapping variables under the transformation eq 58. Equation 52 remains invariant under the transformation. Substitution of eqs 60, 63, 64, and 69 into eq 53 produces

$$\begin{aligned}
\dot{\mathbf{P}} = & - \sum_{n,m=1}^F (\nabla_{\mathbf{R}} V_{mn}(\mathbf{R})) \left[\frac{1}{2} (x^{(n)} + ip^{(n)}) (x^{(m)} - ip^{(m)}) - \gamma \delta_{nm} \right] \\
= & - \sum_{n,m} \nabla_{\mathbf{R}} \left(\sum_k U_{mk}(\mathbf{R}) E_k(\mathbf{R}) U_{nk}^*(\mathbf{R}) \right) \left[\frac{1}{2} (x^{(n)} + ip^{(n)}) (x^{(m)} - ip^{(m)}) - \gamma \delta_{nm} \right] \quad 71 \\
= & \sum_{k,l} \mathbf{d}_{lk}(\mathbf{R}) (E_l(\mathbf{R}) - E_k(\mathbf{R})) \left[\frac{1}{2} (\tilde{x}^{(k)} + i\tilde{p}^{(k)}) (\tilde{x}^{(l)} - i\tilde{p}^{(l)}) - \gamma \delta_{kl} \right] \\
& - \sum_{k,l} \nabla_{\mathbf{R}} E_k(\mathbf{R}) \delta_{kl} \left[\frac{1}{2} (\tilde{x}^{(k)} + i\tilde{p}^{(k)}) (\tilde{x}^{(l)} - i\tilde{p}^{(l)}) - \gamma \delta_{kl} \right]
\end{aligned}$$

Since force matrix $\{\mathbf{F}_{kl} = \nabla_{\mathbf{R}} E_k(\mathbf{R}) \delta_{kl} + (E_k(\mathbf{R}) - E_l(\mathbf{R})) \mathbf{d}_{lk}(\mathbf{R})\}$ is Hermitian, the mean force of the RHS of eq 71 stays real. Under the diabatic-to-adiabatic transformation, eq 58, the EOMs of nuclear phase variables (eqs 52-53) are then recast into

$$\dot{\mathbf{R}} = \mathbf{M}^{-1} \mathbf{P}$$

$$\dot{\mathbf{P}} = - \sum_{k,l} \left[\nabla_{\mathbf{R}} E_k(\mathbf{R}) \delta_{kl} + (E_k(\mathbf{R}) - E_l(\mathbf{R})) \mathbf{d}_{lk}(\mathbf{R}) \right] \left[\frac{1}{2} (\tilde{x}^{(k)} + i\tilde{p}^{(k)}) (\tilde{x}^{(l)} - i\tilde{p}^{(l)}) - \gamma \delta_{kl} \right]. \quad 72$$

Define the effective potential matrix, $\mathbf{V}^{(\text{eff})}$, whose element is a function of the nuclear phase variables,

$$V_{nk}^{(\text{eff})}(\mathbf{R}, \mathbf{P}) = E_n(\mathbf{R}) \delta_{nk} - i \dot{\mathbf{R}} \cdot \mathbf{d}_{nk}(\mathbf{R}) = E_n(\mathbf{R}) \delta_{nk} - i \mathbf{M}^{-1} \mathbf{P} \cdot \mathbf{d}_{nk}(\mathbf{R}). \quad 73$$

A more compact form of eq 70 for the electronic phase variables becomes

$$\dot{\tilde{\mathbf{g}}} = -i \mathbf{V}^{(\text{eff})}(\mathbf{R}, \mathbf{P}) \tilde{\mathbf{g}}. \quad 74$$

Equations 72 and 74 are the final EOMs under the covariant transformation eq 65.

When the electronic wavefunction of the basis set is always real, i.e., $\langle r | \phi_n(\mathbf{R}) \rangle$ is real for any n , which is often the case for molecular systems, eq 62 leads to

$$\mathbf{d}_{mn}(\mathbf{R}) = -\mathbf{d}_{nm}(\mathbf{R}) \quad . \quad 75$$

Equation 72 is simplified to

$$\begin{aligned}
\dot{\mathbf{R}} = & \mathbf{M}^{-1} \mathbf{P} \\
\dot{\mathbf{P}} = & - \sum_{k,l} \left[\nabla_{\mathbf{R}} E_k(\mathbf{R}) \delta_{kl} + (E_k(\mathbf{R}) - E_l(\mathbf{R})) \mathbf{d}_{lk}(\mathbf{R}) \right] \left[\frac{1}{2} (\tilde{x}^{(k)} \tilde{x}^{(l)} + \tilde{p}^{(k)} \tilde{p}^{(l)}) - \gamma \delta_{kl} \right] \quad . \quad 76
\end{aligned}$$

Note that the mapping Hamiltonian of eq 33 (obtained in the diabatic representation) becomes

$$H_C(\mathbf{R}, \mathbf{P}, \mathbf{x}(\tilde{\mathbf{x}}, \tilde{\mathbf{p}}), \mathbf{p}(\tilde{\mathbf{x}}, \tilde{\mathbf{p}})) = \frac{1}{2} \mathbf{P}^T \mathbf{M}^{-1} \mathbf{P} + \sum_{n=1}^F E_n(\mathbf{R}) \left(\frac{1}{2} \left((\tilde{x}^{(n)}(\mathbf{R}))^2 + (\tilde{p}^{(n)}(\mathbf{R}))^2 \right) - \gamma \right) \quad 77$$

under the transformation defined by eq 60 and eq 65. The new EOMs, eq 72 and eq 74, conserve the mapping Hamiltonian of eq 77. The diabatic-to-adiabatic transformation depends on nuclear coordinate \mathbf{R} , which is also a time-dependent variable of the evolution. The time-dependent canonical transformation for the Hamiltonian system yields a new set of EOMs by the chain rule²⁴⁵.

In eqs 71-74 and eqs 76-77 \mathbf{P} corresponds to the mapping momentum in the diabatic representation, but *not* the canonical momentum in the adiabatic representation because eq 71 is *not* generated from Hamilton's equations of motion. Equations 74 and 76 share a similar form to the EOMs proposed by Cotton *et al* in ref 184 and discussed in the Supporting Information of ref⁵⁷. Define the covariant transformation for nuclear phase variables,

$$\tilde{\mathbf{R}} = \mathbf{R} \quad 78$$

$$\tilde{\mathbf{P}} = \mathbf{P} + i \sum_{m,n} \left[\frac{1}{2} (\tilde{x}^{(n)} + i\tilde{p}^{(n)}) (\tilde{x}^{(m)} - i\tilde{p}^{(m)}) - \gamma \delta_{nm} \right] \mathbf{d}_{mn}(\mathbf{R})$$

The Hamiltonian of eq 77 becomes

$$H_C(\tilde{\mathbf{R}}, \tilde{\mathbf{P}}, \tilde{\mathbf{x}}, \tilde{\mathbf{p}}) = \frac{1}{2} \mathbf{P}(\tilde{\mathbf{P}}, \tilde{\mathbf{x}}, \tilde{\mathbf{p}}, \tilde{\mathbf{R}})^T \mathbf{M}^{-1} \mathbf{P}(\tilde{\mathbf{P}}, \tilde{\mathbf{x}}, \tilde{\mathbf{p}}, \tilde{\mathbf{R}}) + \sum_{n=1}^F E_n(\tilde{\mathbf{R}}) \left(\frac{1}{2} \left((\tilde{x}^{(n)}(\tilde{\mathbf{R}}))^2 + (\tilde{p}^{(n)}(\tilde{\mathbf{R}}))^2 \right) - \gamma \right), \quad 79$$

of which the canonical variables are $\{\tilde{\mathbf{R}}, \tilde{\mathbf{P}}, \tilde{\mathbf{x}}, \tilde{\mathbf{p}}\}$ instead of $\{\mathbf{R}, \mathbf{P}, \mathbf{x}, \mathbf{p}\}$. (See more discussions in Appendix 2 of Supporting Information). The mapping diabatic momentum, \mathbf{P} , is related to the kinematic momentum of the adiabatic representation. Although we can directly use Hamilton's EOMs for $\{\tilde{\mathbf{R}}, \tilde{\mathbf{P}}, \tilde{\mathbf{x}}, \tilde{\mathbf{p}}\}$, it is more convenient to employ the EOMs for $\{\mathbf{R}, \mathbf{P}, \mathbf{x}, \mathbf{p}\}$ instead to avoid the derivative of nonadiabatic coupling terms. This is indeed the strategy suggested by Cotton *et al* in ref¹⁸⁴. When the initial condition does not involve nonadiabatic coupling terms, the sampling of \mathbf{P} in the diabatic representation is the same for that of $\tilde{\mathbf{P}}$ in the adiabatic representation. This is the case in the following applications, where FSSH has to be used in the adiabatic representation. By applying the covariance relation under the diabatic-to-adiabatic transformation, the EOMs on mapping phase space are independent of the representation of the (electronic) basis set, which is also the merit of Ehrenfest dynamics.

We note that either eq 51 or eq 74 can analytically be solved by a symplectic approach that employs an exact propagator on electronic phase space at each nuclear phase point. For example, for eq 74 we use

$$\tilde{\mathbf{U}}(\mathbf{R}, \mathbf{P}; \Delta t) = \exp[-i\Delta t \mathbf{V}^{(\text{eff})}] \quad 80$$

such that the evolution of electronic phase variables follows $\tilde{\mathbf{g}}(t + \Delta t) = \tilde{\mathbf{U}}(\mathbf{R}, \mathbf{P}; \Delta t)\tilde{\mathbf{g}}(t)$.

We then test a range of benchmark systems, including two-site dissipative models, Tully's scattering models, atomic systems in cavity interacted with a number of field modes, and linear vibronic coupling model systems that involve the conical intersection^{135, 246-248}. They are typical composite quantum systems in chemistry, physics, condensed matter science, quantum optics, and quantum information.

4.2 Spin-boson models at low-temperature in condensed phase

The first model illustrated is the spin-boson model, which describes a two-site system interacted with an environmental bath in condense phase. It is also a simplified model for electron transfer and energy transfer in chemical and biological reactions. Several numerically exact benchmark methods for solving the spin-boson model include quasi-adiabatic propagator path integral (QuAPI)²⁴⁹⁻²⁵², hierarchy equations of motion (HEOM)²⁵³⁻²⁶¹, (multi-layer) multi-configuration time-dependent Hartree [(ML-)MCTDH]²⁶²⁻²⁶⁸, but their numerical costs typically increase exponentially as the number of DOFs increases. Quantum dynamics of the spin-boson model exhibits interesting dissipative characters, of which the asymptotic behaviours are often missed by either of Ehrenfest dynamics and FSSH in the low temperature regime⁵⁸. Spin-boson models with strong coupling in the low temperature regime presents challenging tests for trajectory-based dynamics methods.

The Hamiltonian of the spin-boson model is divided to three parts, $\hat{H} = \hat{H}_s + \hat{H}_b + \hat{H}_{sb}$. Here $\hat{H}_s = \varepsilon \hat{\sigma}_z + \Delta_c \hat{\sigma}_x$ describes a two-site system with the bias ε and tunneling Δ_c , while the bath part of the Hamiltonian is discretized into a combination of a number of quantum harmonic oscillators $\hat{H}_b = \sum_{j=1}^{N_b} (\hat{P}_j^2 + \omega_j^2 \hat{R}_j^2)/2$. The system-bath coupling adopts a bilinear interaction, $\hat{H}_{sb} = -\sum_{j=1}^{N_b} c_j \hat{R}_j \hat{\sigma}_z$. Here we use an Ohmic bath spectral density $J(\omega) = (\pi/2) \alpha \omega e^{-\omega/\omega_c}$, where α is the Kondo parameter and ω_c is the cut-off frequency. Its discrete frequencies and coupling strengths $\{\omega_j, c_j\}$ are sampled^{269, 270} from

$$\begin{cases} \omega_j = -\omega_c \ln[1 - j/(1+N_b)] \\ c_j = \omega_j \sqrt{\alpha \omega_c / (1+N_b)} \end{cases}, \quad j = 1, \dots, N_b \quad 81$$

The initial density is set as $|1\rangle_s\langle 1|_s \otimes \hat{\rho}_b$, where the system is in excited state $|1\rangle_s$ while all bath modes are at thermal equilibrium with $\hat{\rho}_b = e^{-\beta\hat{H}_b} / Z_b$. Initial nuclear DOFs are sampled from the Wigner distribution of $\hat{\rho}_b$, while initial electronic DOFs are sampled from (weighted) constraint coordinate-momentum phase space $\mathcal{S}(\mathbf{x}, \mathbf{p})$. The continuous spectral density is discretized into $N_b = 300$ effective bath modes to guarantee numerical convergence in simulations.

In Figure 6, we demonstrate results produced by wMM with parameter $\Delta = 0.05$, by wMM with $\Delta = 0.1$, and by CMM with $\gamma = (\sqrt{F+1} - 1) / F = 0.366$ that is a special case of CMM of ref.¹³⁴. Numerically exact results, as well as results yielded by Ehrenfest dynamics and FSSH, are also shown for comparison. Figure 6 indicates that wMM, as well as CMM, outperforms both Ehrenfest dynamics and FSSH dynamics, either for short-time coherences or for long-time dissipations.

4.3 Tully's gas phase scattering models

Tully's scattering models²⁴² mimic different intersection types of molecular systems, which have widely been tested for various nonadiabatic dynamics methods. They describe a two-state Hamiltonian with a central coupling area and asymptotic plateau regions where diabatic potential function $V_{nn}(R \rightarrow \pm\infty)$ is flat. All the three models, including the single avoided crossing (SAC), dual avoided crossing (DAC), and extended coupling region (ECR) problems, are used in our numerical tests.

Atomic units are used in the simulations of the Tully models. The SAC model (Panel (a1) of Figure 7) describes the simplest but essential surface crossing in molecular systems. In the diabatic representation, its diagonal potential energy surfaces (PESes) are $V_{11} = -V_{22} = A(1 - e^{-B|R|})\text{sgn}(R)$ and off-diagonal coupling terms are $V_{12} = V_{21} = Ce^{-DR^2}$. Here, the parameters are $A = 0.01$, $B = 1.6$, $C = 0.005$, and $D = 1.0$. The DAC model (Panel (b1) of Figure 7) includes two crossing points, thus different (electronic) paths are interfered with the dependence on the initial momentum. Its diagonal PESes are $V_{11} = 0$ and $V_{22} = -Ae^{-BR^2} + E_0$, and off-diagonal coupling terms are $V_{12} = V_{21} = Ce^{-DR^2}$ in the diabatic representation with parameters $A = 0.10$, $B = 0.28$, $E_0 = 0.05$, $C = 0.015$ and $D = 0.06$. The ECR model in the diabatic representation (Panel (c1) of Figure 7) has diagonal PESes $V_{11} = -V_{22} = E_0$ and coupling terms $V_{12} = V_{21} = C[e^{BR}\Theta(-R) + (2 - e^{-BR})\Theta(R)]$, with $E_0 = -0.0006$, $B = 0.9$, $C = 0.1$. Here

1
2
3 $\Theta(R)$ is the Heaviside function of coordinate R . The adiabatic PESes and nonadiabatic coupling vector of
4
5 the ECR model are also illustrated in Panel (c2) of Figure 7.
6

7 We investigate the transmission and reflection coefficients of each state. In the simulations, the initial
8 condition is a nuclear wavepacket, $\Psi(R; t=0) \propto \exp[-\alpha(R-R_0)^2/2 + i(R-R_0)P_0]$ (here we adopt
9
10 $\hbar = 1$), occupied in state 1, where $\alpha = 1$ is the Gaussian width parameter, and R_0 and P_0 are the initial
11 average coordinate and momentum. The initial average coordinate is set at $R_0 = -3.8$, -10 , and -13
12
13 for the SAC, DAC and ECR models, respectively. The initial Wigner distribution for the nuclear DOF is then
14
15 $\rho_W^{\text{nuc}}(R, P) \propto \exp[-\alpha(R-R_0)^2 - (P-P_0)^2/\alpha]$.
16

17 Figure 7a shows that all methods are capable of quantitatively describing transmission coefficients in
18 (diabatic) state 1 and state 2 of the SAC model. Figure 7b demonstrates that either wMM or CMM outperforms
19 Ehrenfest dynamics and FSSH in predicting the peak shape when the initial momentum is relatively high, e.g.,
20
21 $P_0 \geq 15$ au. This indicates that the trajectory-based approximate dynamics approaches in the mapping phase
22
23 space formulation are good for fast processes in the gas phase composite/nonadiabatic system. However, the
24 performance of either wMM or CMM in the low initial momentum region should be improved. It is important
25
26 to note that the EOMs of wMM/CMM are invariant with the representation of the electronic state, as described in
27
28 the Supporting Information of ref⁵⁷. (More discussion is also available in Appendix 2 of Supporting
29
30 Information.) That is, both the diabatic and adiabatic representations produce the same results for wMM or
31
32 CMM, which is often not satisfied in FSSH and other nonadiabatic dynamics approaches.
33

34 For the ECR model of Figure 7c, the numerically exact DVR solution indicates an energy threshold for a
35 bifurcation. Ehrenfest dynamics totally misses the step-like behaviours for the transmission coefficient in state
36
37 1, and for the reflection coefficient in either state 1 or state 2. CMM greatly improves over Ehrenfest dynamics.
38
39 It is more encouraging that wMM is capable of faithfully describing such step-like behaviours. Tully's original
40
41 FSSH algorithm is not able to well describe the ECR model²⁴², but a modified version for treating frustrated
42
43 hopping of FSSH (e.g., see ref.²⁴⁴) is capable of qualitatively capturing the step-like behaviours. As shown in
44
45 Figure 7c, in comparison to the traditional FSSH approach^{242, 244}, the overall performance of wMM for the ECR
46
47 model is better.
48

50 4.4 Atom/molecule-in-cavity models of quantum electrodynamic light-matter systems

51
52 The cavity quantum electrodynamics (cQED) focuses on studying the interaction between light and a multi-
53
54 level system (e.g., an atom or a molecule) in an optical cavity, which has many applications in the field of quantum
55

information and quantum computation. There exist many interesting and important phenomena in cQED, e.g., the Purcell effect when coupling is weak and the vacuum Rabi splitting when coupling becomes strong²⁷¹⁻²⁸⁵. When the general atomic/molecular system is coupled to multi-cavity modes, it is often intractable to solve the exact evolution in real time due to the curse of dimensionality. We test wMM for two typical models that describe an imprisoned multi-level atom coupled with a series of optical modes in a one-dimensional lossless cavity^{57, 204, 286-289}.

The total Hamiltonian consists of three parts. The optical field is depicted by N effective modes

$$\hat{H}_p = \sum_{j=1}^N \frac{1}{2} (\hat{P}_j^2 + \omega_j^2 \hat{R}_j^2) , \quad 82$$

where $\{\hat{R}_j, \hat{P}_j\}$ denote the canonical coordinate-momentum variables of j -th optical field mode with the corresponding photonic frequency ω_j . The atomic system is described by $\hat{H}_a = \sum_{n=1}^F \varepsilon_n |n\rangle\langle n|$ with ε_n representing the n -th atomic energy level. Employing the dipole approximation, one can formulate the interaction between atom and optical field as

$$\hat{H}_c = \sum_{n \neq m} \left(\sum_{j=1}^N \omega_j \lambda_j(r_0) \hat{R}_j \right) \mu_{nm} |n\rangle\langle m| . \quad 83$$

Here μ_{nm} denotes the transitional dipole moment between the n -th and m -th atomic levels, and the coupling between the j -th mode and the atom is

$$\lambda_j(r_0) = \sqrt{\frac{2}{\varepsilon_0 L}} \sin\left(\frac{j\pi r_0}{L}\right) , \quad 84$$

where L is the volume length of cavity, ε_0 denotes the vacuum permittivity, and r_0 represents the location of the atom. In the simulation, the volume length of the cavity is set to 236200 au and the atom is frozen at the central location, i.e., $r_0 = L/2$. The optical field is depicted by 400 standing-wave modes in cavity, of which the j -th frequency is $\omega_j = j\pi c/L$ with c the light speed in vacuum. We use two benchmark models for studying cQED processes, a three-level model with $\varepsilon_1 = -0.6738$, $\varepsilon_2 = -0.2798$, $\varepsilon_3 = -0.1547$, $\mu_{12} = -1.034$, $\mu_{23} = -2.536$ (all in atomic units), and a reduced two-level model where only the two lowest atomic levels are employed.

The highest atomic level of each model is initially occupied with no photon in cavity, i.e., all cavity modes are in the corresponding vacuum state. The spontaneous emission occurs at the beginning, the released photon evolves in the cavity, and the re-absorption and re-emission happen later when the photon is reflected to meet the atom. Figure 8 shows the population transfer of each atomic level of the two models. The wMM results are compared with CMM, Ehrenfest dynamics, FSSH, and exact results^{287, 288}. Results of Ehrenfest dynamics and of FSSH significantly deviate from exact results even since very short time, while CMM and wMM yield much more reasonable descriptions for all energy levels, including the transfer behaviour at short time and the revival at around $t = 1800$ au. The wMM approach shows overall better performance than CMM in most of the cases. Figure 8 implies that the trajectory-based methods in the general coordinate-momentum phase space formulation will be useful for studying cQED phenomena in the field of quantum optics and quantum information.

4.5 Linear vibronic coupling model for the molecular system involving the conical intersection

The conical intersection widely exists in molecular systems and plays a central role in many photophysical and photochemical phenomena^{135, 139, 214, 246, 247, 290-293}. The linear vibronic coupling model (LVCM) is the simplest but effective model widely used to describe dynamic properties around the conical intersection region, of which Hamiltonian in the diabatic representation is

$$\hat{H} = \hat{H}_0 + \hat{H}_l + \hat{H}_c \quad . \quad 85$$

Here, $\hat{H}_0 = \sum_{k=1}^N \omega_k (\hat{P}_k^2 + \hat{R}_k^2)/2$ is the zeroth-order harmonic oscillator Hamiltonian in normal-mode space of the electronic ground state, where $\hat{P}_k, \hat{R}_k (k = 1, \dots, N)$ denote the k -th effective weighted normal-mode variables with frequency ω_k (i.e., $P_k = p_k / \sqrt{\omega_k}$, $R_k = \sqrt{\omega_k} r_k$, where p_k, r_k are the canonical momentum, and canonical coordinate of k -th normal-mode). In eq 85,

$\hat{H}_l = \sum_{n=1}^F \left(E_n + \sum_{k=1}^N \kappa_k^{(n)} \hat{R}_k \right) |n\rangle\langle n|$ contains the vertical excitation energy, $E_n (n = 1, \dots, F)$ of F electronic states, and the linear coupling term $\kappa_k^{(n)}$ of each nuclear DOF for diagonal Hamiltonian elements, while $\hat{H}_c = \sum_{n \neq m}^F \left(\sum_{k=1}^N \lambda_k^{(nm)} \hat{R}_k \right) |n\rangle\langle m|$ includes linear coupling $\lambda_k^{(nm)}$ for each normal-mode between two different electronic states, $|n\rangle$ and $|m\rangle$.

A typical two-level 3-mode LVCM describes the S1/S2 conical intersection of the pyrazine molecule. The parameters of this model are fitted from semi-empirical electronic structure calculations by Schneiders and

Domcke in ref²⁹⁴. The excitation energies for the two electronic states are $E_1 = 3.94$ eV and $E_2 = 4.84$ eV.

The diagonal linear coupling terms of first two modes $\{\hat{R}_1, \hat{R}_2\}$ are $\kappa_1^{(1)} = 0.037$ eV, $\kappa_2^{(1)} = -0.105$ eV for the first electronic state, and $\kappa_1^{(2)} = -0.254$ eV, $\kappa_2^{(2)} = 0.149$ eV for the second electronic state, respectively. The off-diagonal linear coupling of third mode \hat{R}_3 is $\lambda_3^{(12)} = \lambda_3^{(21)} = 0.262$ eV. The normal-mode vibronic frequency of each mode is $\omega_1 = 0.126$ eV, $\omega_2 = 0.074$ eV, and $\omega_3 = 0.118$ eV, respectively. Initial conditions of nuclear DOFs are sampled from the corresponding Wigner function of the vibronic ground state while the second electronic state is occupied. All simulations employ $\sim 10^5$ trajectories and time stepsize $\Delta t = 0.01$ fs for fully converged results. Numerically exact result of this model calculated by ML-MCTDH are available in ref²¹².

Figure 9 shows population dynamics of state 2 yielded by wMM, CMM, Ehrenfest dynamics, FSSH and ML-MCTDH. It is evident that Ehrenfest dynamics performs poorly even for the short-time behaviour (before 100 fs). In comparison, wMM, CMM, and FSSH more reasonably describe the radiationless energy transfer process at short time. Interestingly, wMM describes the oscillating behaviours in the long-time region (after 300 fs) better than other approximate methods. Such oscillating behaviour in population dynamics indicates the molecular system passes through the “slopped” conical intersection region²⁹⁴.

Figures 6-9 demonstrate that the overall performance of wMM is better than CMM, especially in the gas phase scattering case of Figure 7c and the quantum electrodynamic light-matter systems of Figure 8. Both wMM and CMM approaches are able to outperform Ehrenfest dynamics as well as FSSH for condensed phase systems (e.g., in Figure 6 and Figure 8).

5. CONCLUSION REMARKS

The phase space formulation of quantum mechanics not only presents a type of convenient interpretation to describe quantum-classical correspondences as well as nonclassical correlations/entanglement, but also sets the insightful scene for developing practical and useful trajectory-based quantum dynamics approaches.

In the Focus Article we show that the constraint coordinate-momentum phase space formulation for the discrete-variable system which we have recently developed, and the weighted representation that we propose in the Focus Article are useful approaches for illustration of nonclassical features of quantum systems. The novel formulation is expected to have potential use for illustration of nonclassical features of quantum states, as well as for future phase point measurement experiment^{70, 85, 221-234}.

1
2
3 It is straightforward to show the relation between the $SU(F)/U(F-1)$ Stratonovich phase space¹¹⁴ and
4 constraint coordinate-momentum phase space, which is diffeomorphic to $U(F)/U(F-1)$. When $F > 2$, it is
5 inevitable to meet singularities in dynamics for discrete-variable systems when Stratonovich phase space is used.
6 In comparison, (weighted) constraint coordinate-momentum phase space does not cause any singularities in
7 trajectory-based exact dynamics, which is much more numerically favourable. (See more discussion in
8 Appendix 3 of Supporting Information).

9
10
11
12
13
14 When the general Moyal bracket of the quantum Liouville theorem is approximated by the corresponding
15 Poisson bracket on (weighted) constraint phase space, it reproduces the correct frozen-nuclei limit of
16 composite/nonadiabatic systems. Such trajectory-based EOMs on (weighted) constraint coordinate-momentum
17 phase space do not rely on the choice of representation of electronic states and are straightforward to obtain the
18 form under covariant transformations. Because second-order nonadiabatic coupling terms are avoided in the
19 EOMs of the adiabatic representation, it is especially useful for applications to realistic molecular systems.
20 Various benchmark model tests of from gas phase to condensed phase quantum systems (as shown in Figures 6-
21 9) indicate that wMM, the new trajectory-based approximate approach with the weighted constraint coordinate-
22 momentum phase space representation, demonstrates overall better performance than FSSH as well as Ehrenfest
23 dynamics. It is expected that more investigations on the (weighted) constraint phase space formulation will shed
24 light on more numerically favourable dynamics approaches with the Meyer-Miller mapping Hamiltonian or other
25 mapping Hamiltonians (e.g., those of ref¹³¹ and discussed in ref⁵⁸).
26
27
28
29
30
31
32
33
34
35
36
37

38 We note that the (weighted) constraint coordinate-momentum phase space formulation is established for any
39 systems with a finite set of states, not only limited to discrete electronic states, but also for finite discrete nuclear
40 states. The weighted phase space strategy that we propose can also be applied to other types of phase space
41 formulations of the discrete-variable system, such as Stratonovich phase space, and Wootters phase space, albeit
42 that the general coordinate-momentum phase space formulation presented in the Focus Article will be more
43 convenient, for experimental measurements, tomography, or characterizations of fidelity, coherence, inequalities,
44 displaced parity, atomic/molecular/optical Schrodinger cat states, and entanglement in quantum information and
45 computation^{70, 85, 221-234, 295, 296} as well as for studying dynamic processes of composite systems in physics,
46 chemistry, materials, biology, and environmental science.
47
48
49
50
51
52
53
54
55
56
57
58
59
60

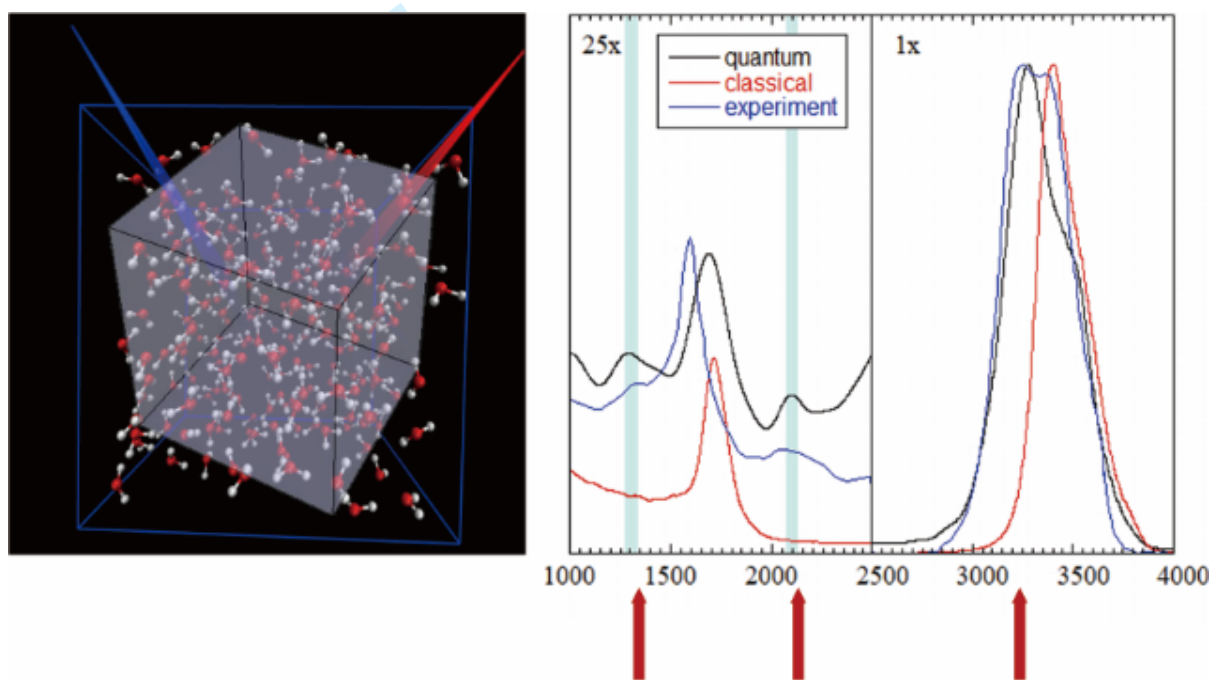
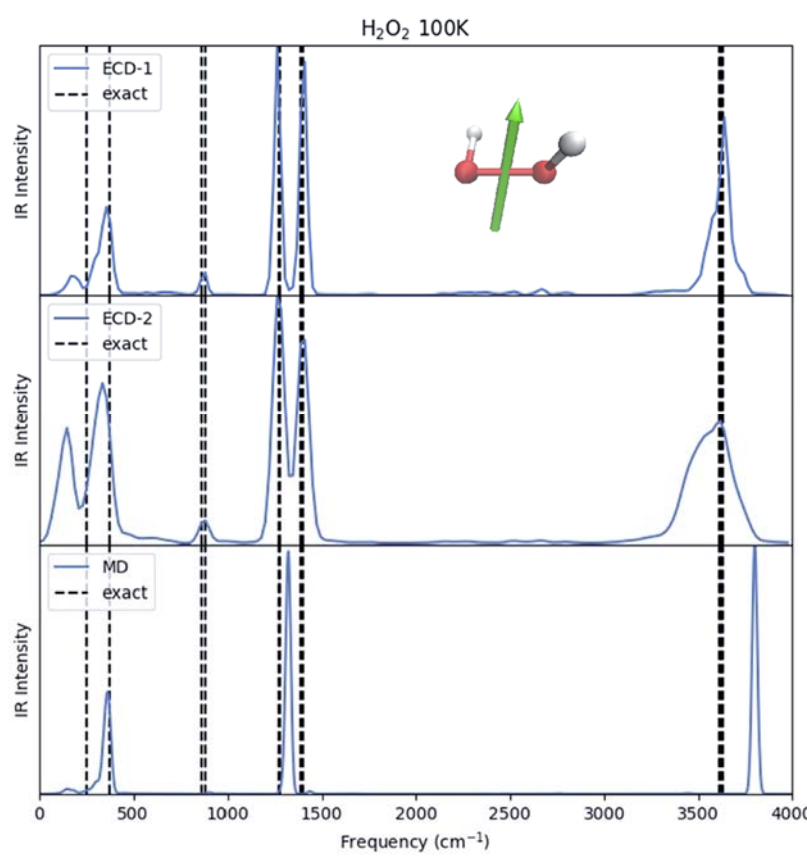
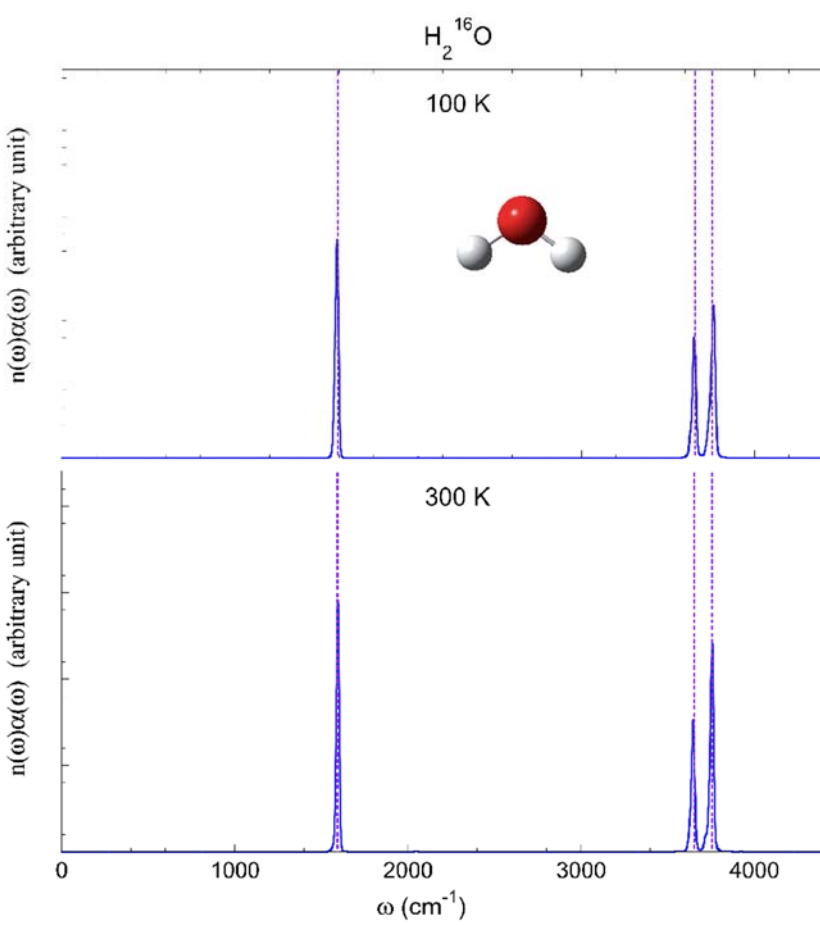
Figures and Tables

Figure 1. Quantum dynamical effects are decisive in reproducing the experimental isotropic Raman spectrum of liquid water at room temperature, as illustrated by the LSC-IVR simulation where infinite (Wigner) phase space for nuclear DOFs is used. Converged results were obtained with 216 water molecules in a box with periodic boundary conditions. (Reprinted with permission from ref¹⁹. Copyright 2018 Taylor & Francis.)

1
2
3
4
5
6
7
8
9
10
11
12
13
14
15
16
17
18
19
20
21
22
23
24
25
26
27
28
29
30
31
32
33
34
35
36
37
38
39
40
41
42
43
44
45
46
47
48
49
50
51
52
53
54
55
56
57
58
59
60

For Peer Review



1
2
3 **Figure 2.** Molecular vibrational spectra produced by more advanced trajectory-based dynamics methods with
4 infinite (Wigner) phase space used for nuclear DOFs, which satisfy the two fundamental criteria: conservation of
5 the quantum Boltzmann distribution for the thermal equilibrium system and being exact for any quantum thermal
6 correlation functions in the classical and harmonic limits. (a) Vibrational spectrum of the H_2O molecule at
7 100K and that at 300K. Adapted with permission from ref⁴¹. Copyright 2016 American Institute of Physics
8
9 Publishing. (b) Vibrational spectrum of the H_2O_2 molecule at 100K. Adapted with permission from ref⁴⁴.
10
11 Copyright 2021 American Institute of Physics Publishing.
12
13
14
15
16
17
18
19
20
21
22
23
24
25
26
27
28
29
30
31
32
33
34
35
36
37
38
39
40
41
42
43
44
45
46
47
48
49
50
51
52
53
54
55
56
57
58
59
60

For Peer Review

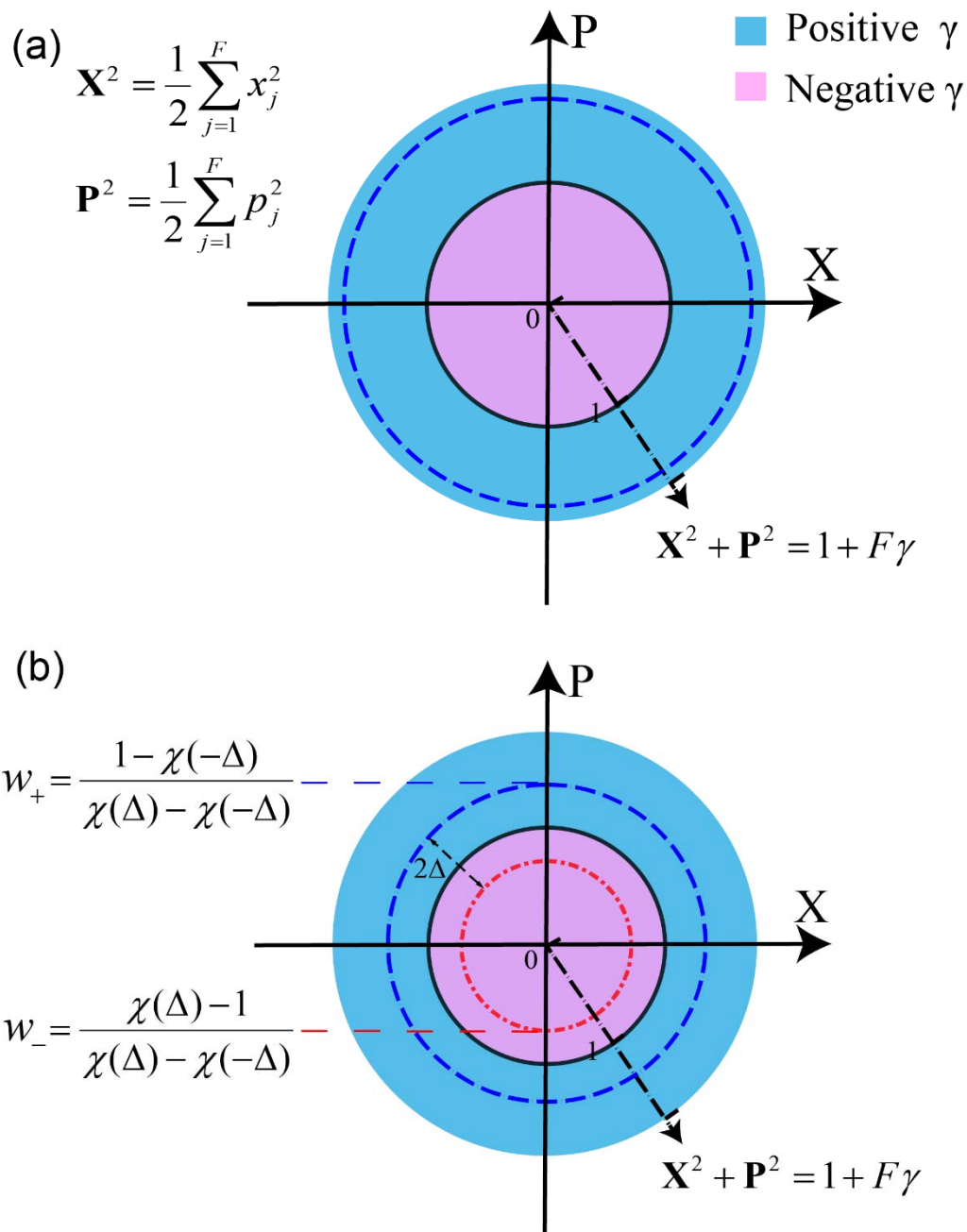
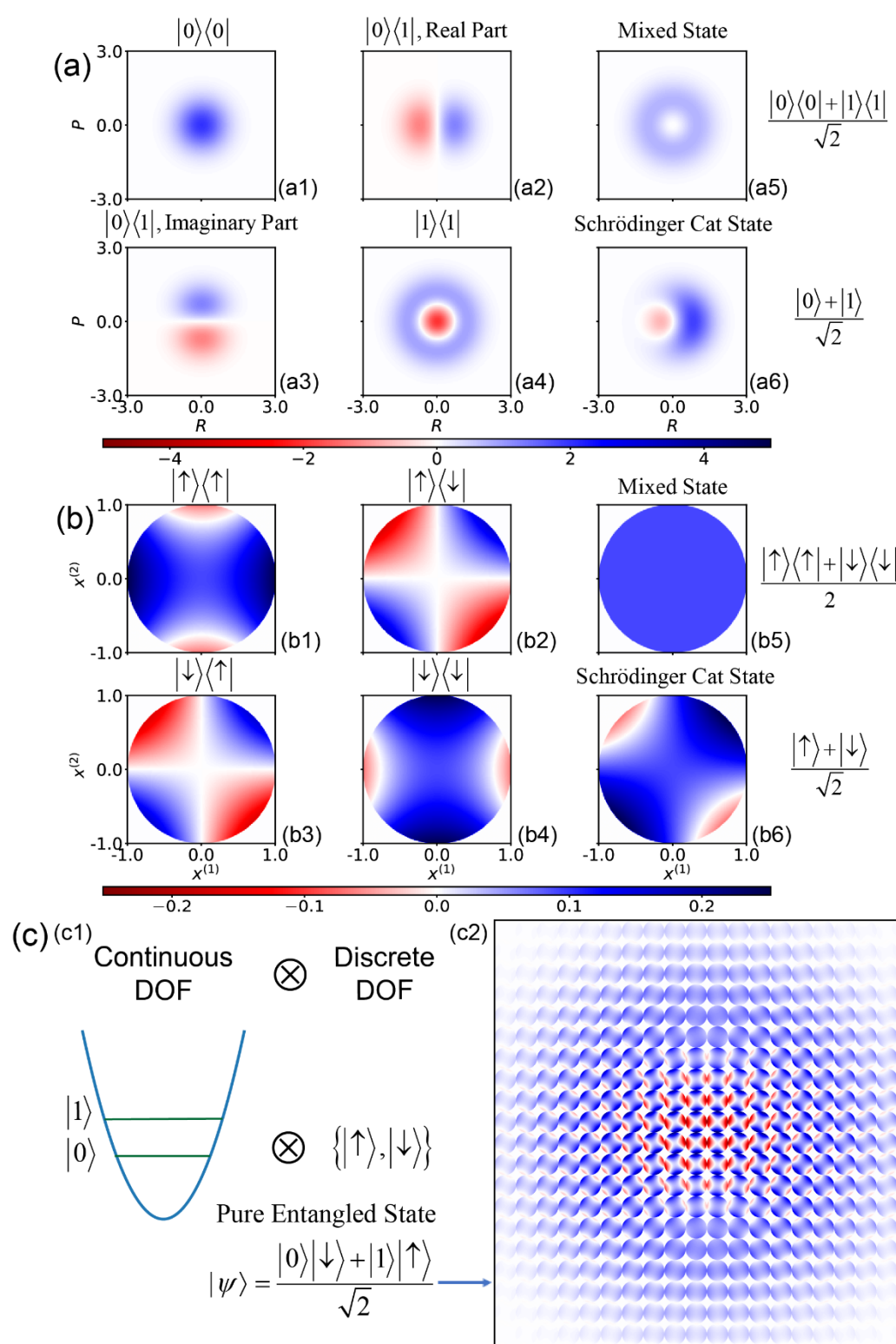


Figure 3: Illustration of the exact mapping formulation with constraint coordinate-momentum phase space. Panel (a) presents constraint phase space with only a single value of parameter γ . Panel (b) demonstrates weighted constraint phase space with two values of parameter γ , where the quasi-probability distribution function is $w(\gamma) = w_+ \delta(\gamma - \Delta) + w_- \delta(\gamma + \Delta)$. Constraint phase space with the positive weight is blue-dashed, while that with the negative weight is red dot-dashed. (Panel (a) is adapted with permission from ref¹³⁴. Copyright 2021 American Chemical Society.)

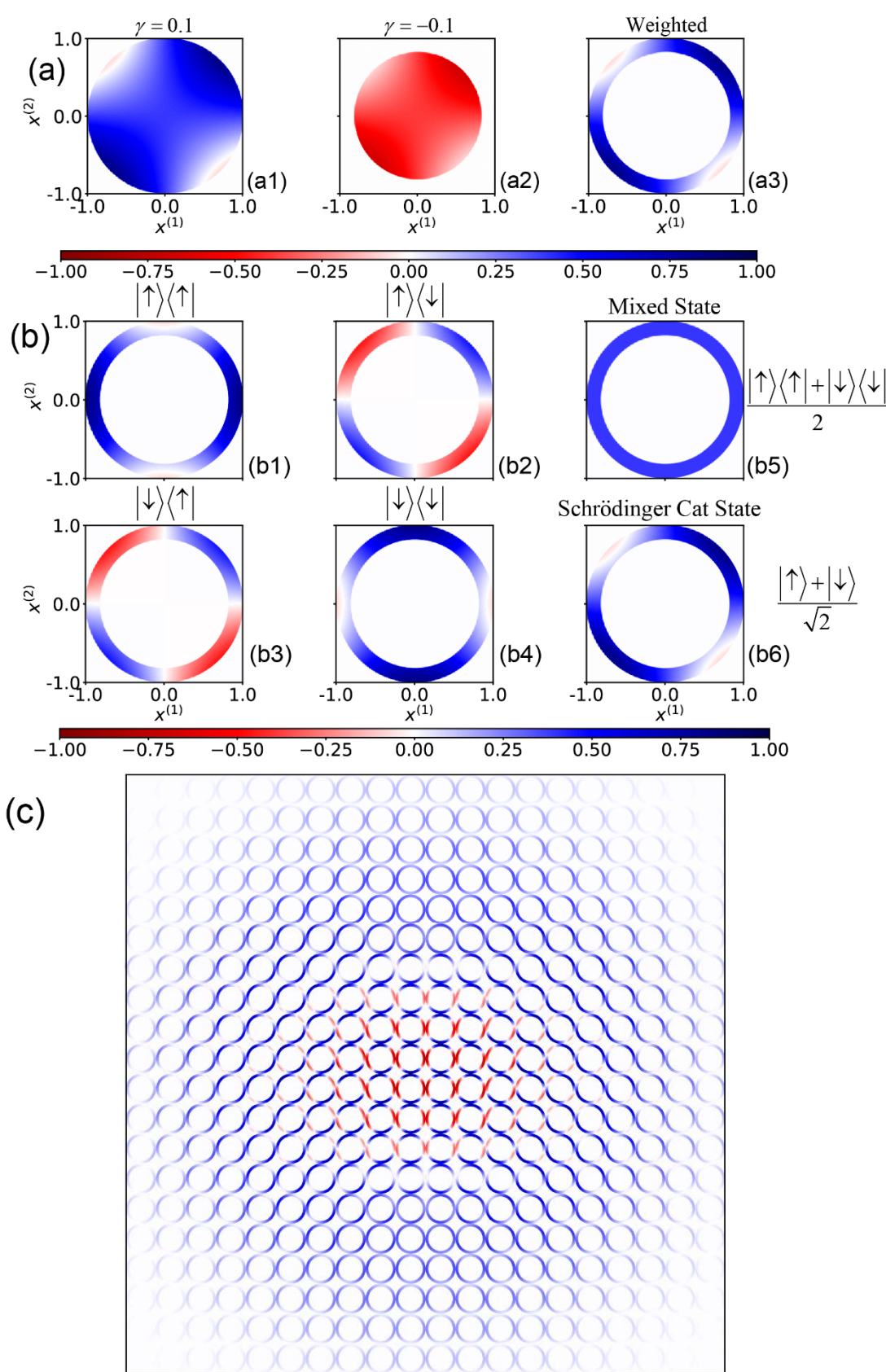


1
2
3 **Figure 4:** Illustrations of (a) Wigner representation of a continuous-variable system, (b) constraint phase space
4 representation of a discrete-variable system, and (c) hybrid coordinate-momentum phase space representation of
5 a composite system with both discrete and continuous DOFs.
6
7

8 (a) Wigner distribution for $|0\rangle\langle 0|$ (Panel a1), that for $|1\rangle\langle 1|$ (Panel a4), real part (Panel a2) and imaginary
9 part (Panel a3) of the Wigner distribution for $|0\rangle\langle 1|$, Wigner distribution for mixed state
10 $(|0\rangle\langle 0|+|1\rangle\langle 1|)/2$ (Panel a5), and that for Schrödinger cat state $(|0\rangle+|1\rangle)/\sqrt{2}$ (Panel a6). Here,
11
12 $|0\rangle$ and $|1\rangle$ are two energy levels of a continuous-variable system.
13
14

15 (b) Marginal distribution of constraint phase space coordinates $(x^{(1)}, x^{(2)})$ for $|\uparrow\rangle\langle \uparrow|$ (Panel b1), $|\downarrow\rangle\langle \downarrow|$
16 (Panel b4), that for $|\uparrow\rangle\langle \downarrow|$ (Panel b2), that for $|\downarrow\rangle\langle \uparrow|$ (Panel b3), that for mixed state
17 $(|\uparrow\rangle\langle \uparrow|+|\downarrow\rangle\langle \downarrow|)/2$ (Panel b5), and that for Schrödinger cat state $(|\uparrow\rangle+|\downarrow\rangle)/\sqrt{2}$ (Panel b6). Here,
18
19 $|\uparrow\rangle$ and $|\downarrow\rangle$ represent two discrete states of a discrete-variable system.
20
21

22 (c) Panel c1: Schematic representaton of the composite system and the pure entangled state
23 $(|0\rangle|\downarrow\rangle+|1\rangle|\uparrow\rangle)/2$; Panel c2: hybrid coordinate-momentum phase space representation of the entangled
24 state. The grid is on the Wigner phase space (R, P) for the continous DOF, and each circle of a grid stands
25 for the local marginal distribution function of constraint phase space variables $(x^{(1)}, x^{(2)})$. The notations
26 are identical to those in Panels (a)-(b).
27
28
29
30
31
32
33
34
35
36
37
38
39
40
41
42
43
44
45
46
47
48
49
50
51
52
53
54
55
56
57
58
59
60



1
2
3 **Figure 5:** Illustrations of (a) components and (b) marginal distribution functions of the weighted constraint phase
4 space representation of a discrete-variable system, and (c) weighted hybrid representation of the same composite
5 system as that of Figure 4(c).
6
7

- 8 (a) Marginal distribution of constraint phase space coordinates $(x^{(1)}, x^{(2)})$ for Schrödinger cat state
9 $(|\uparrow\rangle + |\downarrow\rangle)/\sqrt{2}$ with $\gamma = \Delta$ weighted by w_+ (Panel a1), with $\gamma = -\Delta$ weighted by w_- (Panel
10 a2). The sum of the two components yields the marginal distribution of constraint phase space coordinates
11 (x_1, x_2) of the weighted representation with two values of parameter γ for the Schrödinger cat state
12 (Panel a3). Coordinates are scaled by the larger radius $\sqrt{2(1+F\Delta)}$.
13
14 (b) Weighted marginal distribution of constraint phase space coordinates $(x^{(1)}, x^{(2)})$ for the same properties
15 as those in Figure 4(b).
16
17 (c) Same as Figure 4(c), but using weighted marginal distribution for the discrete DOF.
18
19
20
21
22
23
24
25
26
27
28
29
30
31
32
33
34
35
36
37
38
39
40
41
42
43
44
45
46
47
48
49
50
51
52
53
54
55
56
57
58
59
60

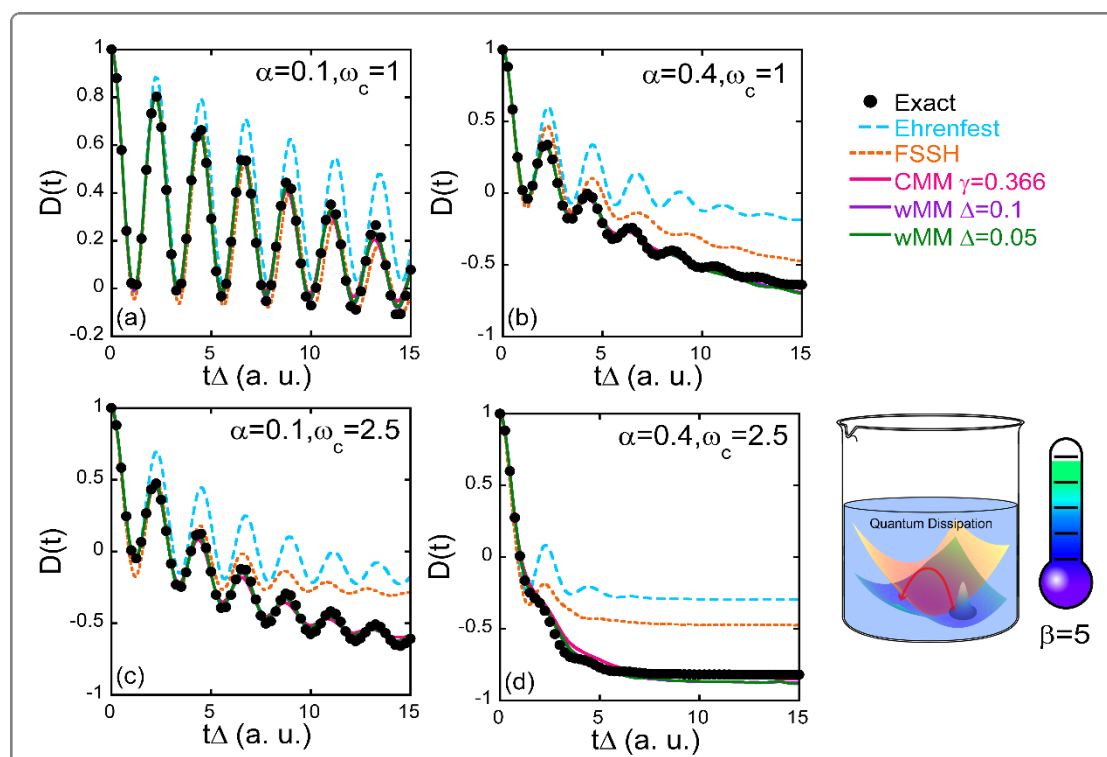
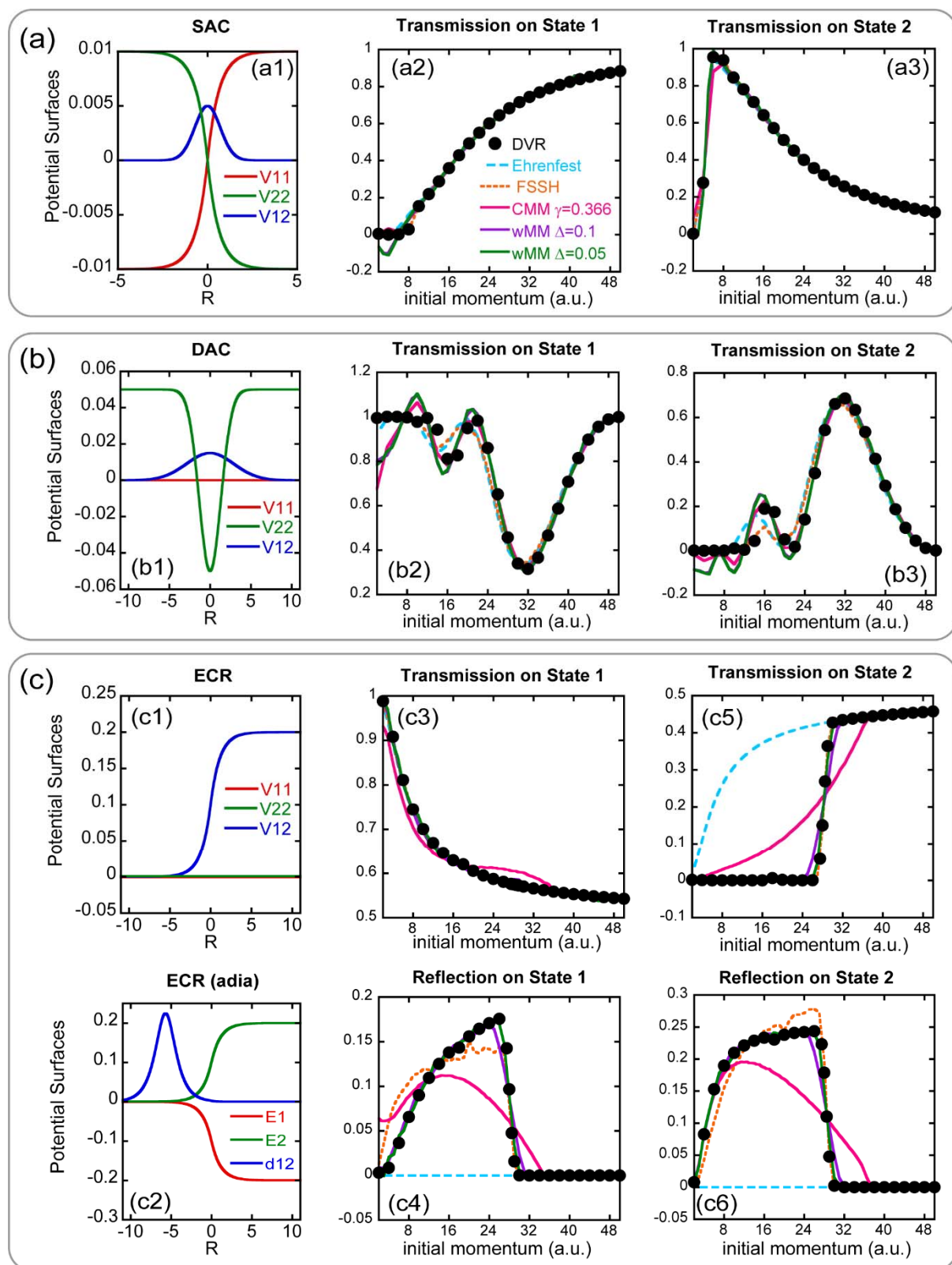


Figure 6: Results of population difference $D(t) = P_1(t) - P_0(t)$ between two states for the spin-boson model at low-temperature ($\beta = 1 / (k_B T) = 5$) with the Ohmic bath. Panel (a) reports the population dynamics of the spin-boson model with parameters $\varepsilon = \Delta_c = 1$, $\beta = 5$, $\omega_c = 1$, $\alpha = 0.1$ in Panel (a). Solid circles: Exact results produced by eHEOM reported in ref¹³⁴. Cyan dashed lines: Ehrenfest dynamics. Orange dashed lines: FSSH. Magenta solid lines: CMM with $\gamma = 0.366$. Purple and green solid lines: wMM with $\Delta = 0.1$ and 0.05 , respectively. Panel (b) is similar to Panel (a) but for $\alpha = 0.4$; Panel (c) is similar to Panel (a) but for $\omega_c = 2.5$; Panel (d) is similar to Panel (a) but for $\omega_c = 2.5$, $\alpha = 0.4$. In each model 300 continuous DOFs (i.e., effective bath modes) are used.



1
2
3 **Figure 7:** Illustration of three Tully models and simulation results. Panel (a1) denotes diabatic PESes $V_{11}(R)$
4 and $V_{22}(R)$, as well as coupling term $V_{12}(R)$ for the SAC model; Panel (b1) does so for the DAC model;
5
6 Panel (c1) does so for the ECR model. Panel (c2) demonstrates adiabatic PESes $E_1(R)$ and $E_2(R)$, as well
7
8 as nonadiabatic coupling vector $d_{12}(R)$.
9

10
11 Panels (a2)-(a3): transmission coefficients on diabatic state 1, and those on diabatic state 2 of the SAC model,
12 respectively. Panels (b2)-(b3): similar to Panels (a2)-(a3), but for the DAC model. Panels (c3) and (c4):
13 transmission/reflection coefficients on adiabatic state 1 of the ECR model; Panels (c5) and (c6): those on adiabatic
14 state 2.
15

16
17 In Panels (a2)-(a3), (b2)-(b3), and (c3)-(c6), magenta, purple and green lines stand for transmission coefficients
18 results for CMM with $\gamma = 0.366$, wMM with $\Delta = 0.1$, and wMM with $\Delta = 0.05$, respectively. Long-
19 dashed blue lines: Ehrenfest dynamics; Short-dashed orange lines: FSSH; Black points: exact DVR benchmarks.
20
21
22
23
24
25
26
27
28
29
30
31
32
33
34
35
36
37
38
39
40
41
42
43
44
45
46
47
48
49
50
51
52
53
54
55
56
57
58
59
60

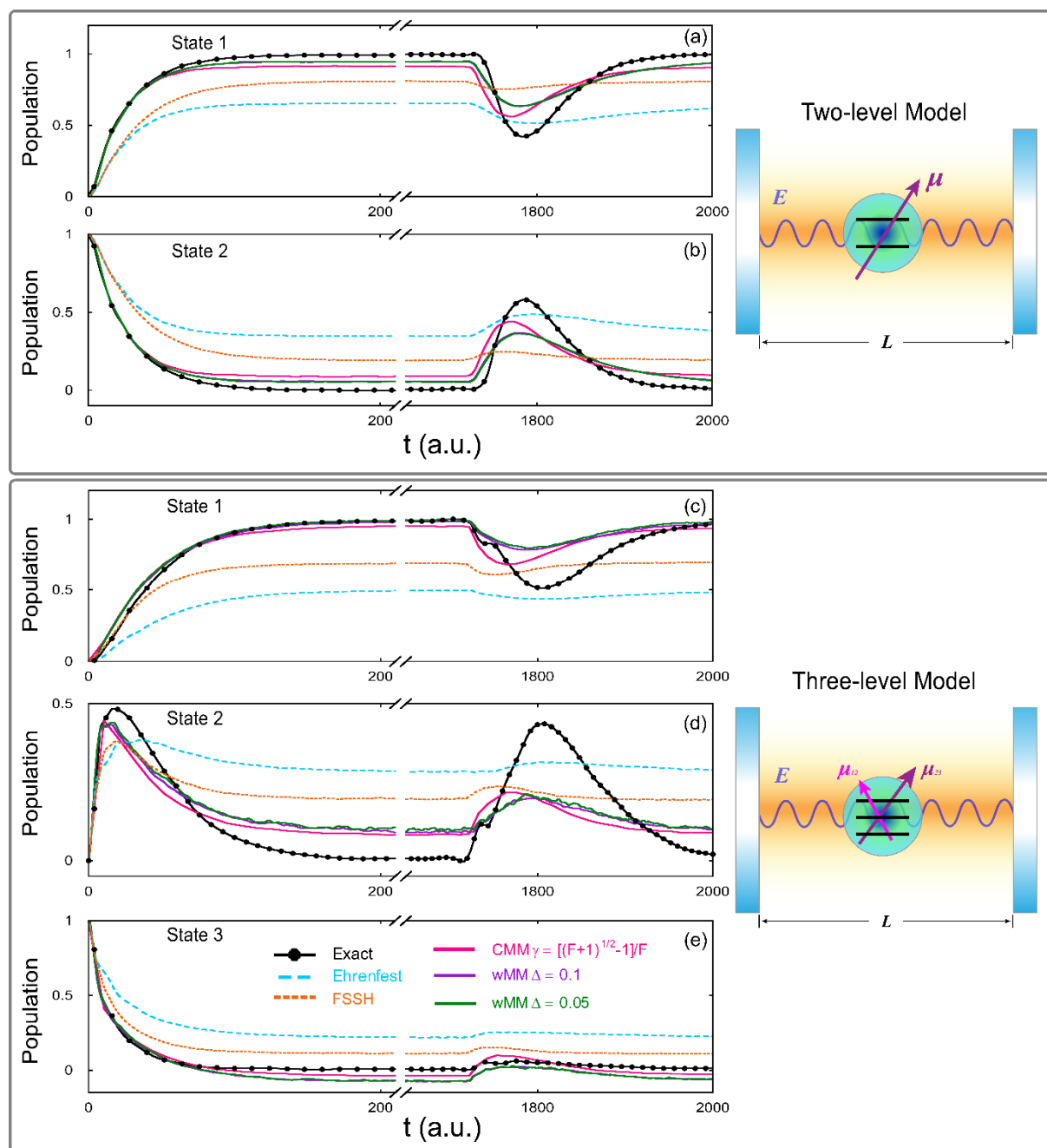


Figure 8: Results of population dynamics for the atom-in-cavity models. Panels (a)-(b) represent data of the first and second states of the two-level model, respectively. Panels (c)-(e) denote data of the first, second and third states of the three-level model, respectively. Magenta solid lines: CMM with $\gamma = (\sqrt{F+1} - 1)/F$; Purple solid lines: wMM with $\Delta = 0.1$; Green solid lines: wMM with $\Delta = 0.05$; Cyan long-dashed lines: Ehrenfest dynamics; Orange short-dashed lines: FSSH; Black solid-dotted lines: exact results from refs^{287, 288}. In each model 400 continuous DOFs (i.e., standing-wave modes) are involved.

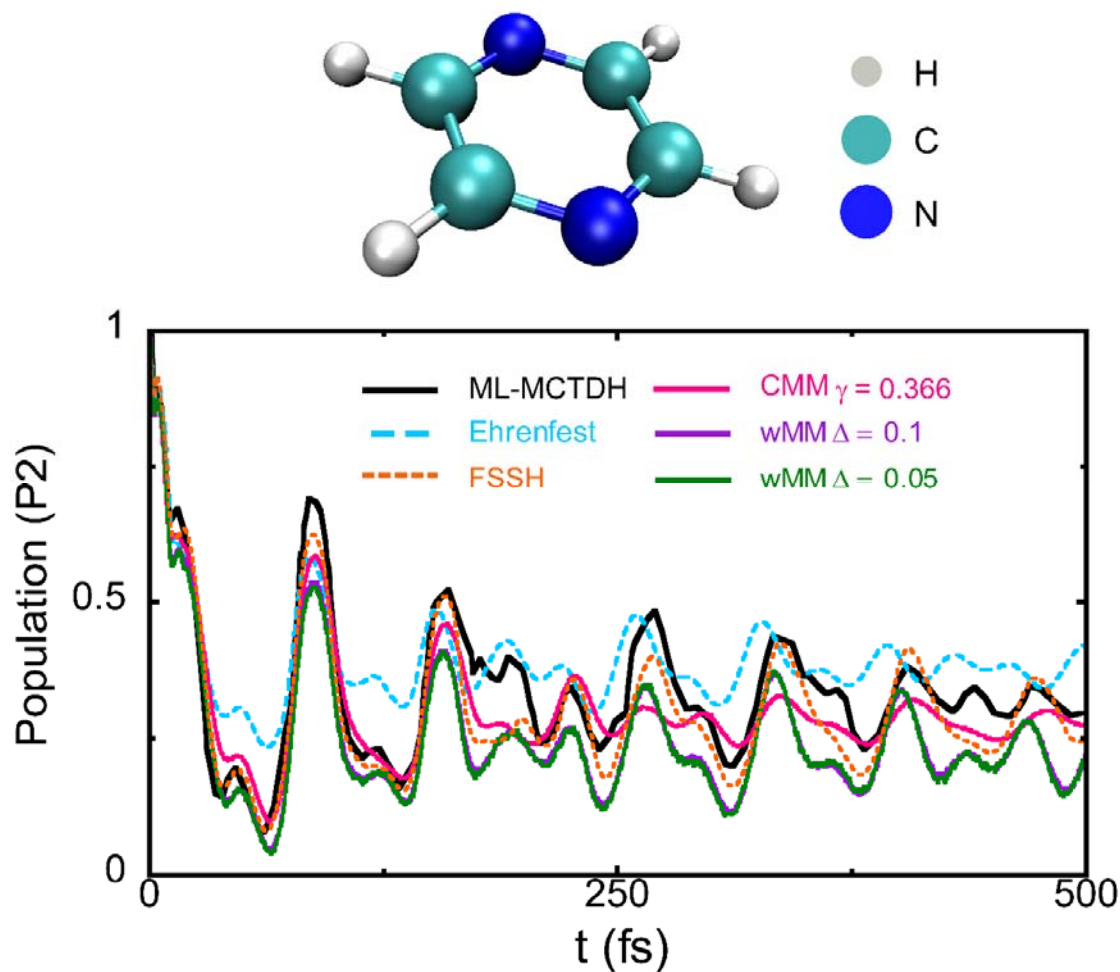


Figure 9: Results of population dynamics of the second electronic state of the 2-level 3-mode pyrazine model.

Magenta solid lines: CMM with $\gamma = (\sqrt{F+1} - 1) / F \approx 0.366$; Purple solid lines: wMM with $\Delta = 0.1$; Green solid lines: wMM with $\Delta = 0.05$. Cyan dashed lines: Ehrenfest dynamics; Orange short-dashed lines: FSSH; Black solid lines: ML-MCTDH results of ref²¹².

Funding Information

National Natural Science Foundation of China (NSFC) Grant No. 21961142017; Ministry of Science and Technology of China (MOST) Grant No. 2017YFA0204901

Research Resources

High-performance Computing Platform of Peking University, Beijing PARATERA Tech CO., Ltd., and Guangzhou supercomputer center

Acknowledgments

This work was supported by the National Natural Science Foundation of China (NSFC) Grant No. 21961142017, and by the Ministry of Science and Technology of China (MOST) Grant No. 2017YFA0204901. We acknowledge the High-performance Computing Platform of Peking University, Beijing PARATERA Tech CO., Ltd., and Guangzhou supercomputer center for providing computational resources.

Notes

The authors declare no competing financial interest.

Further Reading**Appendices****1. Derivation of the formulation of (weighted) constraint coordinate-momentum phase space.**

In this appendix, we introduce the techniques for performing integrals on constraint coordinate-momentum phase space, and show the brief derivation of the formulation of (weighted) constraint coordinate-momentum phase space. Such techniques have been expressed in Appendix A of ref¹³² as well as in Section S1 of the Supporting Information of ref¹³⁴.

Consider the expectation of any function $f(X_1, X_2, \dots, X_L)$ under the L -dimensional independent standard normal distribution (i.e., $\{X_i\} \sim N^{(L)}(0,1)$). It is closely related to that under the uniform distribution on the $(L-1)$ -dimensional constraint space, i.e.,

$$\begin{aligned}
 \langle f \rangle_{N^{(L)}(0,1)} &= \frac{1}{(2\pi)^{L/2}} \int dX_1 dX_2 \cdots dX_L e^{-\frac{1}{2} \sum_{k=1}^L X_k^2} f(X_1, X_2, \dots, X_L) \\
 &= \frac{1}{(2\pi)^{L/2}} \int_0^\infty d\xi \int dX_1 dX_2 \cdots dX_L e^{-\xi} \delta\left(\frac{1}{2} \sum_{k=1}^L X_k^2 - \xi\right) f(X_1, X_2, \dots, X_L) . \quad 86 \\
 &= \frac{1}{(2\pi)^{L/2}} \int_0^\infty d\xi e^{-\xi} S_{L-1}(\sqrt{\xi}) \langle f \rangle_{S_{L-1}(\sqrt{\xi})}
 \end{aligned}$$

Here,

$$S_{L-1}(R) = \int dX_1 dX_2 \cdots dX_L \delta\left(\frac{1}{2} \sum_{k=1}^L X_k^2 - R^2\right) \quad 87$$

denotes the area of the constraint space with radius R , and the expectation under the uniform distribution on the $(L-1)$ -dimensional constraint space, $\langle \dots \rangle_{S_{L-1}(R)}$, is given by

$$\langle f \rangle_{S_{L-1}(R)} = \frac{1}{S_{L-1}(R)} \int dX_1 dX_2 \cdots dX_L \delta\left(\frac{1}{2} \sum_{k=1}^L X_k^2 - R^2\right) f(X_1, X_2, \dots, X_L) . \quad 88$$

(Note that the constraint space with radius R defined in eq 87 is slightly different from the $(L-1)$ -sphere in mathematics.) It is trivial to verify that $S_{L-1}(R) = R^{L-2} S_{L-1}(1)$ is the scaling relation of $S_{L-1}(R)$. We can calculate $S_{L-1}(1)$ by setting $f(X_1, X_2, \dots, X_L) \equiv 1$ in eq 86, i.e.,

$$1 = \frac{1}{(2\pi)^{L/2}} \int_0^\infty d\xi e^{-\xi} S_{L-1}(\sqrt{\xi}) = \frac{1}{(2\pi)^{L/2}} S_{L-1}(1) \int_0^\infty d\xi e^{-\xi} \xi^{\frac{L-2}{2}} . \quad 89$$

Equation 89 yields

$$S_{L-1}(1) = \frac{(2\pi)^{L/2}}{\Gamma(L/2)} \quad 90$$

after we use the equality $\int_0^\infty de^{-x} x^\alpha = \Gamma(\alpha+1)$ for $\alpha > -1$, where the Gamma function is defined by

$$\Gamma(s) = \int_0^\infty dt e^{-t} t^{s-1} \quad (s > 0)$$

The k -th order moment of the uniform distribution on the $(L-1)$ -dimensional constraint space has the scaling relation,

$$\begin{aligned} \langle X_{n_1} X_{n_2} \cdots X_{n_k} \rangle_{S_{L-1}(\sqrt{\xi})} &= \frac{1}{S_{L-1}(\sqrt{\xi})} \int dX_1 dX_2 \cdots dX_L \delta\left(\frac{1}{2} \sum_{l=1}^L X_l^2 - \xi\right) X_{n_1} X_{n_2} \cdots X_{n_k} \\ &= \xi^{k/2} \langle X_{n_1} X_{n_2} \cdots X_{n_k} \rangle_{S_{L-1}(1)} \end{aligned} \quad 91$$

Substitution of eq 91 into eq 86 produces

$$\begin{aligned} \langle X_{n_1} X_{n_2} \cdots X_{n_k} \rangle_{N^{(L)}(0,1)} &= \frac{\Gamma\left(\frac{L+k}{2}\right)}{\Gamma(L/2)} \langle X_{n_1} X_{n_2} \cdots X_{n_k} \rangle_{S_{L-1}(1)} \\ &= \frac{\Gamma\left(\frac{L+k}{2}\right)}{\xi^{k/2} \Gamma(L/2)} \langle X_{n_1} X_{n_2} \cdots X_{n_k} \rangle_{S_{L-1}(\sqrt{\xi})} \end{aligned} \quad 92$$

The well-known Wick theorem (also called Isserlis's theorem)^{297, 298} for the independent and identical standard normal distribution reads

$$\langle X_{n_1} X_{n_2} \cdots X_{n_k} \rangle_{N^{(L)}(0,1)} = \begin{cases} 0, & k \text{ is odd} \\ \sum \left(\prod \langle X_{n_i} X_{n_j} \rangle_{N^{(L)}(0,1)} \right), & k \text{ is even} \end{cases} \quad 93$$

Here, the notation $\sum(\prod \cdots)$ stands for the summation of the products over all possible pair partitions of $\{X_{n_1}, X_{n_2}, \dots, X_{n_k}\}$. It is straightforward to obtain the second order moment and fourth order moment of $N^{(L)}(0,1)$,

$$\begin{aligned} \langle X_i X_j \rangle_{N(0,1)} &= \delta_{ij} \\ \langle X_i X_j X_k X_l \rangle_{N(0,1)} &= \delta_{ij} \delta_{kl} + \delta_{ik} \delta_{jl} + \delta_{il} \delta_{jk} \end{aligned} \quad 94$$

Substitution of eq 94 into eq 92 leads to

$$\begin{aligned} \langle X_i X_j \rangle_{S_{L-1}(\sqrt{\xi})} &= \frac{\xi}{L/2} \delta_{ij} \\ \langle X_i X_j X_k X_l \rangle_{S_{L-1}(\sqrt{\xi})} &= \frac{\xi^2}{\frac{L}{2} \left(\frac{L}{2} + 1 \right)} (\delta_{ij} \delta_{kl} + \delta_{ik} \delta_{jl} + \delta_{il} \delta_{jk}) \end{aligned} \quad 95$$

We then set $L = 2F$ as well as $\xi = 1 + F\gamma$ and relabel the constraint space (defined by eq 31) as $\mathcal{S}_\gamma(\mathbf{x}, \mathbf{p})$ parameterized by γ . The comparison between eq 32 and eq 87 states that the area of constraint phase space is

$$\Omega(\gamma) = S_{2F-1} \left(R = \sqrt{1+F\gamma} \right) = \frac{(2\pi)^F}{\Gamma(F)} (1+F\gamma)^{F-1} . \quad 96$$

We then obtain

$$\begin{aligned} \langle g(\mathbf{x}, \mathbf{p}) \rangle_{S_{L-1}(\sqrt{\xi})} &= \int_{S_\gamma(\mathbf{x}, \mathbf{p})} d\mathbf{X} g(\mathbf{x}, \mathbf{p}) \\ &= \int F d\mathbf{x} d\mathbf{p} \frac{1}{\Omega(\gamma)} \delta \left(\sum_{n=1}^F \frac{(x^{(n)})^2 + (p^{(n)})^2}{2} - (1+F\gamma) \right) g(\mathbf{x}, \mathbf{p}) , \end{aligned} \quad 97$$

where $\mathbf{X} = (\mathbf{x}, \mathbf{p})$. The second order moment and fourth order moment on the constraint space of eq 31 read

$$\begin{aligned} \int_{S_\gamma(\mathbf{x}, \mathbf{p})} d\mathbf{X} (X_i X_j) &= \frac{1+F\gamma}{F} \delta_{ij} \\ \int_{S_\gamma(\mathbf{x}, \mathbf{p})} d\mathbf{X} (X_i X_j X_k X_l) &= \frac{(1+F\gamma)^2}{F(F+1)} (\delta_{ij}\delta_{kl} + \delta_{ik}\delta_{jl} + \delta_{il}\delta_{jk}) \end{aligned} . \quad 98$$

Consider $\hat{A} = |m\rangle\langle n|$ and $\hat{B} = |k\rangle\langle l|$. We have

$$\text{Tr}[\hat{A}\hat{B}] = \delta_{nk}\delta_{ml} . \quad 99$$

The constraint phase space expression (i.e., eqs 3-5 when only discrete electronic DOFs exist) of the left-hand side (LHS) of eq 99 is equivalent to

$$\begin{aligned} \text{Tr}[\hat{A}\hat{B}] &= F \int_{S_\gamma(\mathbf{x}, \mathbf{p})} d\mathbf{X} \langle n | \hat{K}_{\text{ele}}(\mathbf{x}, \mathbf{p}) | m \rangle \langle l | K_{\text{ele}}^{-1}(\mathbf{x}, \mathbf{p}) | k \rangle \\ &= F \int_{S_\gamma(\mathbf{x}, \mathbf{p})} d\mathbf{X} K_{nm}^{(\text{ele})}(\mathbf{x}, \mathbf{p}) K_{(ele), lk}^{-1}(\mathbf{x}, \mathbf{p}) \end{aligned} . \quad 100$$

In eq 100, $K_{nm}^{(\text{ele})}(\mathbf{x}, \mathbf{p})$ is the element of operator $\hat{K}_{\text{ele}}(\mathbf{x}, \mathbf{p})$, and $K_{(ele), lk}^{-1}(\mathbf{x}, \mathbf{p})$ is the element of operator $K_{\text{ele}}^{-1}(\mathbf{x}, \mathbf{p})$. When the mapping kernel is given by eq 29, it is straightforward to derive that its corresponding inverse kernel is eq 30 by employing eqs 98-100. Specifically, when the mapping kernel is identical to its inverse (i.e., eq 38), the element of the (inverse) kernel operator is

$$K_{nm}(\mathbf{x}, \mathbf{p}) = K_{nm}^{-1}(\mathbf{x}, \mathbf{p}) = \frac{1}{2} (x^{(n)} + ip^{(n)}) (x^{(m)} - ip^{(m)}) - \gamma \delta_{nm} . \quad 101$$

It is trivial to use eq 98 and eq 101 to achieve the equality

$$F \int_{S_\gamma(\mathbf{x}, \mathbf{p})} d\mathbf{X} K_{nm}(\mathbf{x}, \mathbf{p}) K_{lk}^{-1}(\mathbf{x}, \mathbf{p}) = \frac{(1+F\gamma)^2}{(F+1)} \delta_{nk}\delta_{ml} + \left[\frac{(1+F\gamma)^2}{(F+1)} - 2\gamma - F\gamma^2 \right] \delta_{lk}\delta_{nm} . \quad 102$$

After employing eqs 99-100, we obtain $\gamma = (\sqrt{F+1} - 1) / F$ from eq 102 where the mapping kernel is identical to its inverse (i.e., eq 38).

Similarly, the weighting constraint phase space formulation (eqs 3-5 when only discrete electronic DOFs exist, and eq 37) leads to

$$\begin{aligned}\text{Tr}_e [\hat{A}\hat{B}] &= \int_{S(x,p)} F dxdp A_C(x,p) \tilde{B}_C(x,p) \\ &= \int_{-1/F}^{\infty} d\gamma w(\gamma) \int F dxdp \frac{1}{\Omega(\gamma)} \delta\left(\sum_{n=1}^F \frac{(x^{(n)})^2 + (p^{(n)})^2}{2} - (1+F\gamma)\right) A_C(x,p) \tilde{B}_C(x,p) \quad 103 \\ &= \int_{-1/F}^{\infty} d\gamma w(\gamma) \langle A_C(x,p) \tilde{B}_C(x,p) \rangle_{S_{L-1}(\sqrt{\xi})}\end{aligned}$$

Employing eq 99, we obtain an equation similar to eq 100

$$F \int d\gamma w(\gamma) \int_{S_\gamma(x,p)} dX K_{nm}(x,p) K_{lk}^{-1}(x,p) = \delta_{nk} \delta_{ml} \quad . \quad 104$$

Because we request eq 38 that the mapping kernel is identical to its inverse in the weighted constraint phase space formulation, eqs 101-102 also hold. Substitution of eq 102 into eq 104 generates

$$\int d\gamma w(\gamma) (F\gamma^2 + 2\gamma) = \int d\gamma w(\gamma) \chi(\gamma) = 1 \quad , \quad 105$$

which is eq 39 of the main text. When $w(\gamma)$, the quasi-probability distribution function of parameter γ , is a single Dirac delta function, the constraint coordinate-momentum phase space formulation with $\gamma = (\sqrt{F+1} - 1) / F$ is a special case of eq 105, or of eq 39 of the main text. When in eq 105 or eq 39 $w(\gamma)$ is represented by a linear combination of two symmetrical delta functions (i.e., eqs 43-45), we achieve the symmetrically weighted constraint phase space formulation employed in wMM of the Focus Article. Apparently, various other choices for quasi-probability distribution function $w(\gamma)$ are also available and can be investigated in the future.

2. More discussion on the equations of motion in the adiabatic representation

Below we will show that eq 74 and eq 76, the equations of motion (EOMs) under the diabatic-to-adiabatic transformation are intrinsically equivalent to Hamilton's EOMs generated by the Hamiltonian, eq 79, when (nuclear) canonical phase variables $(\tilde{\mathbf{R}}, \tilde{\mathbf{P}})$ are defined by eq 78. For simplicity, assume that all nonadiabatic coupling terms $\{\mathbf{d}_{mn}^{(I)}(\mathbf{R})\}$ are real. It leads to a simplified relation

106

$$\tilde{\mathbf{P}} = \mathbf{P} + \hbar \sum_{n,m=1}^F \tilde{x}^{(n)} \tilde{p}^{(m)} \mathbf{d}_{mn}(\mathbf{R})$$

in eq 78. In the adiabatic representation, $\mathbf{P} = \tilde{\mathbf{P}} - \hbar \sum_{n,m=1}^F \tilde{x}^{(n)} \tilde{p}^{(m)} \mathbf{d}_{mn}(\tilde{\mathbf{R}})$ is denoted the kinematic momentum (e.g., in ref¹⁸⁴), which is different from canonical momentum $\tilde{\mathbf{P}}$. The Hamiltonian, eq 79, is recast into

$$H_C(\tilde{\mathbf{R}}, \tilde{\mathbf{P}}, \tilde{\mathbf{x}}, \tilde{\mathbf{p}}) = \sum_{I=1}^N \frac{\left(\tilde{P}_I - \hbar \sum_{n,m=1}^F \tilde{x}^{(n)} \tilde{p}^{(m)} d_{mn}^{(I)}(\tilde{\mathbf{R}}) \right)^2}{2M_I} + \sum_{k=1}^F E_k(\tilde{\mathbf{R}}) \left(\frac{1}{2} \left((\tilde{x}^{(k)})^2 + (\tilde{p}^{(k)})^2 \right) - \gamma \right). \quad 107$$

Here, $d_{mn}^{(I)}(\tilde{\mathbf{R}})$ and \tilde{P}_I are the the I -th DOF component of $\mathbf{d}_{mn}(\tilde{\mathbf{R}})$ and that of $\tilde{\mathbf{P}}$, respectively. Note that canonical variables $(\tilde{\mathbf{R}}, \tilde{\mathbf{P}}, \tilde{\mathbf{x}}, \tilde{\mathbf{p}})$ are independent of one another. Hamilton's EOMs produced by eq 107 are

$$\begin{aligned} \dot{\tilde{x}}^{(m)} &= \frac{1}{\hbar} \frac{\partial}{\partial \tilde{p}^{(m)}} H_C(\tilde{\mathbf{R}}, \tilde{\mathbf{P}}, \tilde{\mathbf{x}}, \tilde{\mathbf{p}}) \\ &= - \sum_{J=1}^N \sum_{n=1}^F \frac{\tilde{P}_J - \hbar \sum_{k,l=1}^F \tilde{x}^{(k)} \tilde{p}^{(l)} d_{lk}^{(J)}(\tilde{\mathbf{R}})}{M_J} \tilde{x}^{(n)} d_{mn}^{(J)}(\tilde{\mathbf{R}}) + \frac{1}{\hbar} E_m(\tilde{\mathbf{R}}) \tilde{p}^{(m)}, \end{aligned} \quad 108$$

$$\begin{aligned} \dot{\tilde{p}}^{(m)} &= - \frac{1}{\hbar} \frac{\partial}{\partial \tilde{x}^{(m)}} H_C(\tilde{\mathbf{R}}, \tilde{\mathbf{P}}, \tilde{\mathbf{x}}, \tilde{\mathbf{p}}) \\ &= \sum_{J=1}^N \sum_{n=1}^F \frac{\tilde{P}_J - \hbar \sum_{k,l=1}^F \tilde{x}^{(k)} \tilde{p}^{(l)} d_{lk}^{(J)}(\tilde{\mathbf{R}})}{M_J} \tilde{p}^{(n)} d_{nm}^{(J)}(\tilde{\mathbf{R}}) - \frac{1}{\hbar} E_m(\tilde{\mathbf{R}}) \tilde{x}^{(m)}, \end{aligned} \quad 109$$

$$\dot{\tilde{R}}_I = \frac{\partial}{\partial \tilde{P}_I} H_C(\tilde{\mathbf{R}}, \tilde{\mathbf{P}}, \tilde{\mathbf{x}}, \tilde{\mathbf{p}}) = \frac{\tilde{P}_I - \hbar \sum_{n,m=1}^F \tilde{x}^{(n)} \tilde{p}^{(m)} d_{mn}^{(I)}(\tilde{\mathbf{R}})}{M_I}, \quad 110$$

$$\begin{aligned} \dot{\tilde{P}}_I &= - \frac{\partial}{\partial \tilde{R}_I} H_C(\tilde{\mathbf{R}}, \tilde{\mathbf{P}}, \tilde{\mathbf{x}}, \tilde{\mathbf{p}}) \\ &= \hbar \sum_{J=1}^N \sum_{n,m=1}^F \frac{\tilde{P}_J - \hbar \sum_{k,l=1}^F \tilde{x}^{(k)} \tilde{p}^{(l)} d_{lk}^{(J)}(\tilde{\mathbf{R}})}{M_J} \tilde{x}^{(n)} \tilde{p}^{(m)} \frac{\partial d_{mn}^{(J)}(\tilde{\mathbf{R}})}{\partial \tilde{R}_I} \\ &\quad - \sum_{k=1}^F \frac{\partial E_k(\tilde{\mathbf{R}})}{\partial \tilde{R}_I} \left(\frac{1}{2} \left((\tilde{x}^{(k)})^2 + (\tilde{p}^{(k)})^2 \right) - \gamma \right) \end{aligned} \quad 111$$

It is evident that eqs 108-109 are identical to eq 70 and that eq 110 is the same as the first equation of eq 76.

We will then prove that eq 111 is equivalent to the second equation of eq 76.

Consider the full time-derivative of canonical momentum \tilde{P}_I ,

$$\begin{aligned}\dot{\tilde{P}}_I &= \dot{P}_I(\tilde{\mathbf{R}}, \tilde{\mathbf{P}}, \tilde{\mathbf{x}}, \tilde{\mathbf{p}}) + \hbar \frac{d}{dt} \sum_{n,m=1}^F \tilde{x}^{(m)} \tilde{p}^{(n)} d_{nm}^{(I)}(\tilde{\mathbf{R}}) \\ &= \dot{P}_I + \hbar \sum_{n,m=1}^F \dot{\tilde{x}}^{(m)} \tilde{p}^{(n)} d_{nm}^{(I)}(\tilde{\mathbf{R}}) + \hbar \sum_{n,m=1}^F \tilde{x}^{(m)} \dot{\tilde{p}}^{(n)} d_{nm}^{(I)}(\tilde{\mathbf{R}}) + \hbar \sum_{n,m=1}^F \tilde{x}^{(m)} \tilde{p}^{(n)} \sum_{J=1}^N \frac{\partial d_{nm}^{(I)}(\tilde{\mathbf{R}})}{\partial \tilde{R}_J} \dot{\tilde{R}}_J.\end{aligned}\quad 112$$

Substitution of eqs 108-111 into eq 112 yields,

$$\begin{aligned}\dot{P}_I(\tilde{\mathbf{R}}, \tilde{\mathbf{P}}, \tilde{\mathbf{x}}, \tilde{\mathbf{p}}) &= \hbar \sum_{J=1}^N \sum_{n,m=1}^F \frac{P_J(\tilde{\mathbf{R}}, \tilde{\mathbf{P}}, \tilde{\mathbf{x}}, \tilde{\mathbf{p}})}{M_J} \tilde{x}^{(n)} \tilde{p}^{(m)} \left(\frac{\partial d_{mn}^{(J)}(\tilde{\mathbf{R}})}{\partial \tilde{R}_I} - \frac{\partial d_{mn}^{(I)}(\tilde{\mathbf{R}})}{\partial \tilde{R}_J} \right) \\ &\quad - \sum_{k=1}^F \frac{\partial E_k(\tilde{\mathbf{R}})}{\partial \tilde{R}_I} \left(\frac{1}{2} \left((\tilde{x}^{(k)})^2 + (\tilde{p}^{(k)})^2 \right) - \gamma \right) \\ &\quad + \hbar \sum_{n,m=1}^F \sum_{J=1}^N \sum_{k=1}^F \frac{P_J(\tilde{\mathbf{R}}, \tilde{\mathbf{P}}, \tilde{\mathbf{x}}, \tilde{\mathbf{p}})}{M_J} d_{nk}^{(I)}(\tilde{\mathbf{R}}) d_{km}^{(J)}(\tilde{\mathbf{R}}) (\tilde{x}^{(m)} \tilde{p}^{(n)} - \tilde{x}^{(n)} \tilde{p}^{(m)}) \\ &\quad + \sum_{n,m=1}^F (E_n(\tilde{\mathbf{R}}) \tilde{x}^{(n)} \tilde{x}^{(m)} - E_m(\tilde{\mathbf{R}}) \tilde{p}^{(m)} \tilde{p}^{(n)}) d_{nm}^{(I)}(\tilde{\mathbf{R}}).\end{aligned}\quad 113$$

Since the derivative of the first-order nonadiabatic coupling is

$$\begin{aligned}\frac{\partial d_{mn}^{(J)}}{\partial \tilde{R}_I} &= \frac{\partial}{\partial \tilde{R}_I} \left\langle \phi_m \left| \frac{\partial}{\partial \tilde{R}_J} \phi_n \right. \right\rangle = \left\langle \frac{\partial}{\partial \tilde{R}_I} \phi_m \left| \frac{\partial}{\partial \tilde{R}_J} \phi_n \right. \right\rangle + \left\langle \phi_m \left| \frac{\partial^2}{\partial \tilde{R}_I \partial \tilde{R}_J} \phi_n \right. \right\rangle, \\ &= \sum_{k=1}^F d_{km}^{(I)} d_{kn}^{(J)} + D_{mn}^{(IJ)},\end{aligned}\quad 114$$

where $D_{mn}^{(IJ)} = \left\langle \phi_m \left| \frac{\partial^2}{\partial \tilde{R}_I \partial \tilde{R}_J} \phi_n \right. \right\rangle$ is a symmetric tensor of nuclear index, i.e., $D_{mn}^{(IJ)} = D_{mn}^{(JI)}$, the first term of

the RHS of eq 113 becomes

$$\begin{aligned}&\hbar \sum_{J=1}^N \sum_{n,m=1}^F \frac{P_J(\tilde{\mathbf{R}}, \tilde{\mathbf{P}}, \tilde{\mathbf{x}}, \tilde{\mathbf{p}})}{M_J} \tilde{x}^{(n)} \tilde{p}^{(m)} \left(\frac{\partial d_{mn}^{(J)}(\tilde{\mathbf{R}})}{\partial \tilde{R}_I} - \frac{\partial d_{mn}^{(I)}(\tilde{\mathbf{R}})}{\partial \tilde{R}_J} \right) \\ &= -\hbar \sum_{J=1}^N \sum_{n,m=1}^F \sum_{k=1}^F \frac{P_J(\tilde{\mathbf{R}}, \tilde{\mathbf{P}}, \tilde{\mathbf{x}}, \tilde{\mathbf{p}})}{M_J} (\tilde{x}^{(m)} \tilde{p}^{(n)} - \tilde{x}^{(n)} \tilde{p}^{(m)}) d_{nk}^{(I)}(\tilde{\mathbf{R}}) d_{km}^{(J)}(\tilde{\mathbf{R}}).\end{aligned}\quad 115$$

1
2
3
4 It is important to note that, in general $\frac{\partial d_{mn}^{(J)}(\tilde{\mathbf{R}})}{\partial \tilde{R}_I} - \frac{\partial d_{mn}^{(I)}(\tilde{\mathbf{R}})}{\partial \tilde{R}_J} = 0$ does not always hold for $I \neq J$, except
5
6

7 for two-electronic-state systems. So eq 115 is not always equal to zero. The term of eq 115 cancels out the
8 third term of eq 113. The last term of the RHS of eq 113 can be recast into
9
10

$$\begin{aligned} & \sum_{n,m=1}^F \left(E_n(\tilde{\mathbf{R}}) \tilde{x}^{(n)} \tilde{x}^{(m)} - E_m(\tilde{\mathbf{R}}) \tilde{p}^{(m)} \tilde{p}^{(n)} \right) d_{nm}^{(I)}(\tilde{\mathbf{R}}) \\ &= \frac{1}{2} \sum_{n,m=1}^F \left(E_n(\tilde{\mathbf{R}}) - E_m(\tilde{\mathbf{R}}) \right) \left(\tilde{x}^{(n)} \tilde{x}^{(m)} + \tilde{p}^{(n)} \tilde{p}^{(m)} \right) d_{nm}^{(I)}(\tilde{\mathbf{R}}) \end{aligned} \quad . \quad 116$$

18 Equation 113 then becomes
19

$$\begin{aligned} & \dot{P}_I(\tilde{\mathbf{R}}, \tilde{\mathbf{P}}, \tilde{\mathbf{x}}, \tilde{\mathbf{p}}) \\ &= -\sum_{k=1}^F \frac{\partial E_k(\tilde{\mathbf{R}})}{\partial R_I} \left(\frac{1}{2} \left((\tilde{x}^{(k)})^2 + (\tilde{p}^{(k)})^2 \right) - \gamma \right) - \sum_{n,m=1}^F \left(E_n(\tilde{\mathbf{R}}) - E_m(\tilde{\mathbf{R}}) \right) d_{mn}^{(I)}(\tilde{\mathbf{R}}) \frac{1}{2} \left(\tilde{x}^{(n)} \tilde{x}^{(m)} + \tilde{p}^{(n)} \tilde{p}^{(m)} \right) \end{aligned}$$

20
21
22
23
24
25
26
27
28
29
30
31
32
33
34
35
36
37
38
39
40
41
42
43
44
45
46
47
48
49
50
51
52
53
54
55
56
57
58
59
60

which is equivalent to the second equation of eq 76 of the main text. It indicates that the canonical momentum in the diabatic representation is covariant with *kinematic* momentum \mathbf{P} rather than canonical momentum $\tilde{\mathbf{P}}$ in adiabatic representation unless all nonadiabatic coupling terms vanish. This is consistent with the spirit of the work of Cotton *et. al.* in ref¹⁸⁴. Because the EOMs (eq 70 and eq 76) of the main text are identical to Hamilton's EOMs generated by eq 107, the mapping Hamiltonian (eq 79 or eq 107) is conserved during the evolution in the adiabatic representation.

3. The relationship between the constraint coordinate-momentum phase space and Stratonovich phase space

Stratonovich's original work¹⁰⁰ in 1956 maps a 2-state (spin-1/2) system onto a two-dimensional sphere. We review two kinds of further developments of the Stratonovich-Weyl mapping phase space representations for F -state quantum system: the first one based on the SU(2) structure^{103, 113} and the second one based on the SU(F) structure¹¹⁴. We show the relationship between constrained coordinate-momentum phase space representation that we use in the Focus Article and the two kinds of Stratonovich phase space representations.

In the SU(2) Stratonovich phase space representation, an F -state system is treated as a spin- j system (where $F = 2j + 1$). The basis set consists of $| j, m \rangle$, the eigenstate of the square of total angular momentum

\hat{J}^2 and the z -component of angular momentum \hat{J}_z with quantum numbers j and m , respectively. The mapping kernel is

$$\hat{K}_{\text{ele}}^{\text{SU}(2)}(\theta, \varphi; s) = \sqrt{\frac{\pi}{2j+1}} \sum_{l=0}^{2j} (C_{jj,l0})^{-s} \sum_{m=-l}^l Y_{lm}^*(\theta, \varphi) \hat{T}_{lm}^j, \quad s \in \mathbb{R} \quad 118$$

where \hat{T}_{lm}^j is the irreducible tensor operator defined as²⁹⁹

$$\hat{T}_{lm}^j = \sqrt{\frac{2l+1}{2j+1}} \sum_{m',n=-j}^j C_{jm',lm}^{jn} | j, n \rangle \langle j, m' |. \quad 119$$

Here $C_{j_1 m_1, j_2 m_2}^{jm} = \langle jm | j_1 m_1, j_2 m_2 \rangle$ is the well-known Clebsch-Gordan coefficient for the angular momentum coupling, and $Y_{lm}(\theta, \varphi)$ is the spherical harmonic function. The inverse kernel of $\hat{K}_{\text{ele}}^{\text{SU}(2)}(\theta, \varphi; s)$ is simply $\hat{K}_{\text{ele}}^{\text{SU}(2)}(\theta, \varphi; -s)$. We note that, although $s = 1, 0$, and -1 are traditionally associated with the Q , Wigner, and P -functions respectively and used in the literature^{111, 128}, parameter s of eq 118 can in principle take *any* real value.

When $F > 2$, the SU(2) Stratonovich phase space (θ, φ) does *not* have a phase point-to-phase point mapping to constraint coordinate-momentum phase space, although the relation can only be constructed by virtue of the density matrix. Only when $F = 2$ as in the original work of Stratonovich, there exists a phase point-to-phase point mapping to constraint coordinate-momentum phase space. The mapping kernel can be expressed in terms of the spin-coherent state,

$$\hat{K}_{\text{ele}}^{\text{SU}(2)}(\theta, \varphi; s) = 3^{(1+s)/2} |\theta, \varphi\rangle \langle \theta, \varphi| + \frac{\hat{\mathbf{I}}}{2} [1 - 3^{(1+s)/2}] \quad . \quad 120$$

In eq 120 spin coherent state $|\theta, \varphi\rangle$ is

$$|\theta, \varphi\rangle = \begin{pmatrix} e^{-i\varphi} \sin(\theta/2) \\ \cos(\theta/2) \end{pmatrix}, \quad 121$$

where (θ, φ) are the spherical coordinate variables on the two-dimensional spherical phase space. The range of θ is $[0, \pi]$ and that for φ is $[0, 2\pi)$. When $F = 2$, the explicit transformation of (θ, φ) to the constrained coordinate-momentum phase space $(x^{(1)}, x^{(2)}, p^{(1)}, p^{(2)})$ is

$$\begin{aligned} \begin{pmatrix} x^{(1)} \\ p^{(1)} \end{pmatrix} &= \sqrt{2(1+2\gamma)} \begin{pmatrix} \cos\psi & -\sin\psi \\ \sin\psi & \cos\psi \end{pmatrix} \begin{pmatrix} \cos\varphi \sin(\theta/2) \\ -\sin\varphi \sin(\theta/2) \end{pmatrix}, \\ \begin{pmatrix} x^{(2)} \\ p^{(2)} \end{pmatrix} &= \sqrt{2(1+2\gamma)} \begin{pmatrix} \cos\psi & -\sin\psi \\ \sin\psi & \cos\psi \end{pmatrix} \begin{pmatrix} \cos(\theta/2) \\ 0 \end{pmatrix} \end{aligned} \quad , \quad 122$$

where ψ is an additional global phase.

The second kind of representation is the $SU(F)$ Stratonovich phase space¹¹⁴, which is diffeomorphic to the quotient set $SU(F)/U(F-1)$, parameterized by $(2F-2)$ angle variables $(\boldsymbol{\theta}, \boldsymbol{\varphi}) = (\theta_1, \theta_2, \dots, \theta_{F-1}, \varphi_1, \varphi_2, \dots, \varphi_{F-1})$. The range of each angle θ_i is $[0, \pi/2]$ and that for each angle φ_i is $[0, 2\pi)$. The $SU(F)$ Stratonovich phase space of Tilma *et.al.*¹¹⁴ has been used to prepare the initial condition for the Meyer-Miller mapping model of non-adiabatic dynamics in ref¹⁹⁷.

The mapping kernel of the $SU(F)$ Stratonovich phase space is

$$\hat{K}_{\text{ele}}^{\text{SU}(F)}(\boldsymbol{\theta}, \boldsymbol{\varphi}; s) = (1+F)^{(1+s)/2} |\boldsymbol{\theta}, \boldsymbol{\varphi}\rangle \langle \boldsymbol{\theta}, \boldsymbol{\varphi}| + \frac{\hat{\mathbf{I}}}{F} \left(1 - (1+F)^{(1+s)/2} \right), \quad s \in \mathbb{R} \quad 123$$

and the inverse kernel is $\hat{K}_{\text{ele}}^{\text{SU}(F)}(\boldsymbol{\theta}, \boldsymbol{\varphi}; -s)$. The explicit form of the generalized coherent state $|\boldsymbol{\theta}, \boldsymbol{\varphi}\rangle$ is^{300, 301}

$$|\boldsymbol{\theta}, \boldsymbol{\varphi}\rangle = \sum_{n=1}^F c_n |n\rangle \quad , \quad 124$$

where the coefficients are

$$\begin{pmatrix} c_1 \\ c_2 \\ c_3 \\ \vdots \\ c_{F-3} \\ c_{F-2} \\ c_{F-1} \\ c_F \end{pmatrix} = \begin{pmatrix} e^{i(\varphi_1+\varphi_2+\dots+\varphi_{F-1})} \cos(\theta_1) \cos(\theta_2) \dots \cos(\theta_{F-2}) \sin(\theta_{F-1}) \\ -e^{i(-\varphi_1+\varphi_2+\dots+\varphi_{F-1})} \sin(\theta_1) \cos(\theta_2) \dots \cos(\theta_{F-2}) \sin(\theta_{F-1}) \\ -e^{i(\varphi_3+\varphi_4+\dots+\varphi_{F-1})} \sin(\theta_2) \cos(\theta_3) \dots \cos(\theta_{F-2}) \sin(\theta_{F-1}) \\ \vdots \\ -e^{i(\varphi_{F-3}+\varphi_{F-2}+\varphi_{F-1})} \sin(\theta_{F-4}) \cos(\theta_{F-3}) \cos(\theta_{F-2}) \sin(\theta_{F-1}) \\ -e^{i(\varphi_{F-2}+\varphi_{F-1})} \sin(\theta_{F-3}) \cos(\theta_{F-2}) \sin(\theta_{F-1}) \\ -e^{i(\varphi_{F-1})} \sin(\theta_{F-2}) \sin(\theta_{F-1}) \\ \cos(\theta_{F-1}) \end{pmatrix}. \quad 125$$

As derived first in Appendix A of ref¹³² in the spirit of ref¹³¹ and then in the Supporting Information of ref¹³⁴, the mapping kernel of constraint coordinate-momentum phase space for a set of F states (eq 29 of the main text) is denoted as,

$$\hat{K}_{\text{ele}}(\mathbf{x}, \mathbf{p}; \gamma) = \sum_{m,n=1}^F \left[\frac{(x^{(m)} - i p^{(m)})(x^{(n)} + i p^{(n)})}{2} - \gamma \delta_{mn} \right] |n\rangle \langle m| = |\mathbf{x}, \mathbf{p}\rangle \langle \mathbf{x}, \mathbf{p}| - \gamma \hat{\mathbf{I}}, \quad 126$$

1
2
3 where the non-normalized state $|\mathbf{x}, \mathbf{p}\rangle$ is
4
5

$$\sum_{n=1}^F \frac{x^{(n)} + i p^{(n)}}{\sqrt{2}} |n\rangle. \quad 127$$

6
7
8
9 The $U(F)$ constraint coordinate-momentum phase space of the $(2F-1)$ -dimensional sphere is
10
11
12 diffeomorphic to $U(F)/U(F-1)$. (The difference between $U(F)$ and $SU(F) \times U(1)$ is excluded by
13
14 the division over $U(F-1)$.) Comparison of $\hat{K}_{\text{ele}}^{\text{SU}(F)}(\boldsymbol{\theta}, \boldsymbol{\varphi}; s)$ to $\hat{K}_{\text{ele}}(\mathbf{x}, \mathbf{p}; \gamma)$ implies that the two
15
16 kernels are closely related. The correspondence between parameters s and γ reads
17
18

$$1 + F\gamma = (1 + F)^{(1+s)/2}. \quad 128$$

19
20 It is evident (from eq 128, the relation between constraint coordinate-momentum phase space and the $SU(F)$
21
22 Stratonovich phase space) that parameter s can be any real number in eq 123, *not* limited to $s = 1, 0$, or -1 ,
23
24 where the corresponding value of parameter γ of constraint coordinate-momentum phase space is
25
26 $\gamma = 1, (\sqrt{1+F} - 1)/F$, or 0 . This has been clearly mentioned in refs^{57, 58, 134}.

27
28
29 Any normalized pure state of the F -dimensional Hilbert space uniquely corresponds to a state on constraint
30
31 coordinate-momentum phase space, $|\mathbf{x}, \mathbf{p}\rangle$, which is equivalent to $\exp[i\psi]|\boldsymbol{\theta}, \boldsymbol{\varphi}\rangle$ with ψ as the global
32
33 phase. That is, the correspondence between $(\boldsymbol{\theta}, \boldsymbol{\varphi})$ and (\mathbf{x}, \mathbf{p}) is
34
35

$$\begin{pmatrix} x^{(n)} \\ p^{(n)} \end{pmatrix} = \sqrt{2(1+F\gamma)} \begin{pmatrix} \cos\psi & -\sin\psi \\ \sin\psi & \cos\psi \end{pmatrix} \begin{pmatrix} \text{Re}\langle n | \boldsymbol{\theta}, \boldsymbol{\varphi} \rangle \\ \text{Im}\langle n | \boldsymbol{\theta}, \boldsymbol{\varphi} \rangle \end{pmatrix}. \quad 129$$

36
37
38 Under the transformation, eq 129, mapping functions $A_C(\boldsymbol{\theta}, \boldsymbol{\varphi}; s) = \text{Tr}[\hat{A} \hat{K}_{\text{ele}}^{\text{SU}(F)}(\boldsymbol{\theta}, \boldsymbol{\varphi}; s)]$ and
39
40
41
42
43
44
45
46
47
48
49
50
51
52
53
54
55
56
57
58
59
60
 $A_C(\mathbf{x}, \mathbf{p}; \gamma) = \text{Tr}[\hat{A} \hat{K}_{\text{ele}}(\mathbf{x}, \mathbf{p}; \gamma)]$ of an operator \hat{A} share the same value. The global phase, ψ , which
is missing in the $SU(F)$ Stratonovich phase space, however, is important for the expression of quantum
dynamics.

When we consider quantum dynamics in a finite F -dimensional Hilbert space, if the Hamiltonian operator includes linear components beyond the identity operator and generator operators of phase space group, it is impossible to derive trajectory-based exact dynamics. The $SU(2)$ group involves the identity operator and angular momentum operators as generators on \mathbb{S}^2 sphere. It produces trajectory-based exact dynamics only for two-state systems, but fails to do so for all $F > 2$ cases. It is claimed that trajectory-based dynamics is a

good approximation for the large spin limit ($F \rightarrow \infty$) though^{109, 111, 302}. Except for the $F = 2$ case, the expression of quantum dynamics on the $SU(2)$ Stratonovich phase space has no direct relation to the trajectory-based exact dynamics on constrained coordinate-momentum phase space.

The $SU(F)$ Stratonovich phase space, however, produces trajectory-based exact dynamics for the finite F -dimensional Hilbert space. This is because that the evolution generated by any Hamiltonian of the F -dimensional Hilbert space is the action of some group element of $SU(F)$.³⁰³ The inherent symplectic structure of Stratonovich phase space indicates that the trajectory-based exact dynamics can be produced by the corresponding mapping Hamiltonian function $H_C = \text{Tr}[\hat{H}\hat{K}_{\text{ele}}^{\text{SU}(F)}(\theta, \varphi; s)]$, i.e.,

$$\begin{cases} \dot{\theta}_i = -\sum_{j=1}^{F-1} \frac{A_{ji}}{(1+F)^{(1+s)/2}} \frac{\partial H_C}{\partial \varphi_j} \\ \dot{\varphi}_i = +\sum_{j=1}^{F-1} \frac{A_{ij}}{(1+F)^{(1+s)/2}} \frac{\partial H_C}{\partial \theta_j} \end{cases}. \quad 130$$

The elements, $\{A_{ij}\}$, of the $(F-1) \times (F-1)$ matrix, \mathbf{A} , are

$$A_{ij} = \begin{cases} \frac{1}{2} \csc(2\theta_1) \csc^2 \theta_{F-1} \prod_{k=2}^{F-2} \sec^2 \theta_k, & i = j = 1; \\ -\frac{1}{2} \cot(2\theta_1) \csc^2 \theta_{F-1} \prod_{k=2}^{F-2} \sec^2 \theta_k, & (i-1) = j = 1; \\ \csc(2\theta_i) \csc^2 \theta_{F-1} \prod_{k=i+1}^{F-2} \sec^2 \theta_k, & 2 \leq i = j \leq F-2; \\ -\frac{1}{2} \cot(\theta_i) \csc^2 \theta_{F-1} \prod_{k=i+1}^{F-2} \sec^2 \theta_k, & 2 \leq (i-1) = j \leq F-2; \\ -\csc(2\theta_{F-1}), & i = j = (F-1). \end{cases}. \quad 131$$

The explicit expression of the EOMs of eq 130 is, however, much complicated. In addition, because trigonometric functions are involved in eq 131, singularities are inevitable in the EOMs on the $SU(F)$ Stratonovich phase space for $F > 2$. This makes the expression of quantum dynamics on the $SU(F)$ Stratonovich phase space numerically unfavorable. In comparison, on (weighted) constrained coordinate-momentum phase space, Hamilton's EOMs are simply linear in derivatives with coefficients independent of phase variables, as well as exact.

The relation of eq 129 implies that there exists a one-to-one correspondence between exact trajectory-base dynamics on the $SU(F)$ Stratonovich phase space and that on constraint coordinate-momentum phase space.

The addition of the global phase, ψ , is critical to obtain the one-to-one correspondence. The EOM of ψ reads

$$\dot{\psi} = \left[-\frac{\partial}{\partial \lambda} + \frac{\tan \theta_{F-1}}{2\lambda} \frac{\partial}{\partial \theta_{F-1}} \right] H_C^{(\lambda)}(\boldsymbol{\theta}, \boldsymbol{\phi}; s) \Big|_{\lambda=(1+F)^{\frac{1+s}{2}}}, \quad 132$$

where the extended mapping Hamiltonian function is defined by

$$H_C^{(\lambda)}(\boldsymbol{\theta}, \boldsymbol{\phi}; s) = \text{Tr} \left[\hat{K}_{\text{ele}}^{\text{SU}(F),(\lambda)}(\boldsymbol{\theta}, \boldsymbol{\phi}; s) \hat{H} \right] \quad 133$$

for the extended $\text{SU}(F)$ Stratonovich mapping ‘kernel’

$$\hat{K}_{\text{ele}}^{\text{SU}(F),(\lambda)}(\boldsymbol{\theta}, \boldsymbol{\phi}; s) = \lambda |\boldsymbol{\theta}, \boldsymbol{\phi}\rangle \langle \boldsymbol{\theta}, \boldsymbol{\phi}| + \frac{\hat{I}}{F} \left(1 - (1+F)^{\frac{1+s}{2}} \right). \quad 134$$

In eq 134 λ is treated as an ‘invariant’ variable. The evolution of state $\sqrt{\lambda} e^{i\psi} |\boldsymbol{\theta}, \boldsymbol{\phi}\rangle \equiv |\mathbf{x}, \mathbf{p}\rangle$ generates

$$\begin{cases} \dot{\lambda} = \frac{\partial}{\partial \psi} H_C^{(\lambda)}(\boldsymbol{\theta}, \boldsymbol{\phi}; s) = 0 \\ \dot{\psi} = \left[-\frac{\partial}{\partial \lambda} + \frac{\tan \theta_{F-1}}{2\lambda} \frac{\partial}{\partial \theta_{F-1}} \right] H_C^{(\lambda)}(\boldsymbol{\theta}, \boldsymbol{\phi}; s) \\ \dot{\theta}_i = -\sum_{j=1}^{F-1} \frac{A_{ji}}{\lambda} \frac{\partial}{\partial \varphi_j} H_C^{(\lambda)}(\boldsymbol{\theta}, \boldsymbol{\phi}; s) - \delta_{i,F-1} \frac{\tan \theta_{F-1}}{2\lambda} \frac{\partial}{\partial \psi} H_C^{(\lambda)}(\boldsymbol{\theta}, \boldsymbol{\phi}; s) \\ \dot{\varphi}_i = +\sum_{j=1}^{F-1} \frac{A_{ij}}{\lambda} \frac{\partial}{\partial \theta_j} H_C^{(\lambda)}(\boldsymbol{\theta}, \boldsymbol{\phi}; s) \end{cases}. \quad 135$$

It is straightforward to show that under the bijection,

$$\begin{pmatrix} x^{(n)} \\ p^{(n)} \end{pmatrix} = \sqrt{2\lambda} \begin{pmatrix} \cos \psi & -\sin \psi \\ \sin \psi & \cos \psi \end{pmatrix} \begin{pmatrix} \text{Re} \langle n | \boldsymbol{\theta}, \boldsymbol{\phi} \rangle \\ \text{Im} \langle n | \boldsymbol{\theta}, \boldsymbol{\phi} \rangle \end{pmatrix}, \quad 136$$

between variables $(\lambda, \psi, \boldsymbol{\theta}, \boldsymbol{\phi})$ and (\mathbf{x}, \mathbf{p}) , eq 135 leads to the EOMS of phase variables of (weighted) constraint phase space

$$\begin{aligned} \dot{x}^{(n)} &= +\frac{\partial H_C}{\partial p^{(n)}} \\ \dot{p}^{(n)} &= -\frac{\partial H_C}{\partial x^{(n)}} \end{aligned} \quad 137$$

by the chain rules, i.e.,

$$\dot{x}^{(n)} = \sum_{i=1}^{2F} \frac{\partial x^{(n)}}{\partial z_i} \dot{z}_i$$

$$\dot{p}^{(n)} = \sum_{i=1}^{2F} \frac{\partial p^{(n)}}{\partial z_i} \dot{z}_i$$

138

and

$$\frac{\partial H_C}{\partial z_i} = \sum_{n=1}^F \frac{\partial x^{(n)}}{\partial z_i} \frac{\partial H_C}{\partial x^{(n)}} + \sum_{n=1}^F \frac{\partial p^{(n)}}{\partial z_i} \frac{\partial H_C}{\partial p^{(n)}},$$

where $\{z_i\}$ denote variables $\{\lambda, \psi, \theta, \phi\}$.

4. Marginal distribution functions on symmetrically weighted coordinate-momentum phase space

As demonstrated in Figure 5, the marginal distribution functions on symmetrically weighted constraint coordinate-momentum phase space demonstrate a hollow structure. Equation 50 leads to the marginal functions on symmetrically weighted coordinate-momentum phase space

$$\begin{aligned} \mathcal{K}_{\uparrow\uparrow}(x^{(1)}, x^{(2)}) &= \frac{1-2\Delta^2+2\Delta}{4\Delta} \frac{1+(x^{(1)})^2/2-(x^{(2)})^2/2}{2\pi(1+2\Delta)} \Big|_{(x^{(1)})^2+(x^{(2)})^2 \leq 2(1+2\Delta)} \\ &\quad - \frac{1-2\Delta^2-2\Delta}{4\Delta} \frac{1+(x^{(1)})^2/2-(x^{(2)})^2/2}{2\pi(1-2\Delta)} \Big|_{(x^{(1)})^2+(x^{(2)})^2 \leq 2(1-2\Delta)} \\ \mathcal{K}_{\uparrow\downarrow}(x^{(1)}, x^{(2)}) &= \mathcal{K}_{\downarrow\uparrow}(x^{(1)}, x^{(2)}) = \frac{1-2\Delta^2+2\Delta}{4\Delta} \frac{x^{(1)}x^{(2)}}{2\pi(1+2\Delta)} \Big|_{(x^{(1)})^2+(x^{(2)})^2 \leq 2(1+2\Delta)} \\ &\quad - \frac{1-2\Delta^2-2\Delta}{4\Delta} \frac{x^{(1)}x^{(2)}}{2\pi(1-2\Delta)} \Big|_{(x^{(1)})^2+(x^{(2)})^2 \leq 2(1-2\Delta)} \\ \mathcal{K}_{\downarrow\downarrow}(x^{(1)}, x^{(2)}) &= \frac{1-2\Delta^2+2\Delta}{4\Delta} \frac{1-(x^{(1)})^2/2+(x^{(2)})^2/2}{2\pi(1+2\Delta)} \Big|_{(x^{(1)})^2+(x^{(2)})^2 \leq 2(1+2\Delta)} \\ &\quad - \frac{1-2\Delta^2-2\Delta}{4\Delta} \frac{1-(x^{(1)})^2/2+(x^{(2)})^2/2}{2\pi(1-2\Delta)} \Big|_{(x^{(1)})^2+(x^{(2)})^2 \leq 2(1-2\Delta)} \end{aligned}$$

140

As $\Delta \rightarrow 0^+$, $\mathcal{K}_{nm}(x^{(1)}, x^{(2)})$ approaches zero in region $(x^{(1)})^2 + (x^{(2)})^2 \leq 2(1-F\Delta)$, yielding the hollow structure.

References

1. Lee HW, Scully MO. A new approach to molecular-collisions - statistical quasiclassical method. *The Journal of Chemical Physics* 1980, 73:2238-2242.
2. Lee HW, Scully MO. The Wigner phase-space description of collision processes. *Foundations of Physics* 1983, 13:61-72.
3. Heller EJ. Wigner phase space method: Analysis for semiclassical applications. *The Journal of Chemical Physics* 1976, 65:1289.
4. Sun X, Wang H, Miller WH. Semiclassical theory of electronically nonadiabatic dynamics: Results of a linearized approximation to the initial value representation. *The Journal of Chemical Physics* 1998, 109:7064-7074.
5. Wang H, Sun X, Miller WH. Semiclassical approximations for the calculation of thermal rate constants for chemical reactions in complex molecular systems. *The Journal of Chemical Physics* 1998, 108:9726-9736.
6. Pollak E, Liao J-L. A new quantum transition state theory. *The Journal of Chemical Physics* 1998, 108:2733-2743.
7. Shao J, Liao J-L, Pollak E. Quantum transition state theory: Perturbation expansion. *The Journal of Chemical Physics* 1998, 108:9711-9725.
8. Hernandez R, Voth GA. Quantum time correlation functions and classical coherence. *Chemical Physics* 1998, 233:243-255.
9. Liu J, Miller WH. Using the thermal Gaussian approximation for the Boltzmann operator in semiclassical initial value time correlation functions. *The Journal of Chemical Physics* 2006, 125:224104.
10. Liu J, Miller WH. Linearized semiclassical initial value time correlation functions using the thermal Gaussian approximation: applications to condensed phase systems. *The Journal of Chemical Physics* 2007, 127:114506.
11. Liu J, Miller WH. Real time correlation function in a single phase space integral beyond the linearized semiclassical initial value representation. *The Journal of Chemical Physics* 2007, 126:234110.
12. Liu J, Miller WH. Linearized semiclassical initial value time correlation functions with maximum entropy analytic continuation. *The Journal of Chemical Physics* 2008, 129:124111.
13. Liu J, Miller WH. Test of the consistency of various linearized semiclassical initial value time correlation functions in application to inelastic neutron scattering from liquid para-hydrogen. *The Journal of Chemical Physics* 2008, 128:144511.
14. Liu J, Miller WH, Paesani F, Zhang W, Case DA. Quantum dynamical effects in liquid water: A semiclassical study on the diffusion and the infrared absorption spectrum. *The Journal of Chemical Physics* 2009, 131:164509.
15. Liu J, Miller WH. A simple model for the treatment of imaginary frequencies in chemical reaction rates and molecular liquids. *The Journal of Chemical Physics* 2009, 131:074113.
16. Liu J, Alder BJ, Miller WH. A semiclassical study of the thermal conductivity of low temperature liquids. *The Journal of Chemical Physics* 2011, 135:114105.
17. Liu J, Miller WH, Fanourgakis GS, Xantheas SS, Imoto S, Saito S. Insights in quantum dynamical effects in the infrared spectroscopy of liquid water from a semiclassical study with an ab initio-based flexible and polarizable force field. *The Journal of Chemical Physics* 2011, 135:244503.
18. Liu J. Recent advances in the linearized semiclassical initial value representation/classical Wigner model for the thermal correlation function. *International Journal of Quantum Chemistry* 2015, 115:657-670.
19. Liu X, Liu J. Critical role of quantum dynamical effects in the Raman spectroscopy of liquid water. *Molecular Physics* 2018, 116:755-779.
20. Shi Q, Geva E. Semiclassical theory of vibrational energy relaxation in the condensed phase. *Journal of Physical Chemistry A* 2003, 107:9059-9069.
21. Shi Q, Geva E. A relationship between semiclassical and centroid correlation functions. *The Journal of Chemical Physics* 2003, 118:8173-8184.
22. Ka BJ, Geva E. Vibrational energy relaxation of polyatomic molecules in liquid solution via the linearized semiclassical method. *Journal of Physical Chemistry A* 2006, 110:9555-9567.
23. Poulsen JA, Nyman G, Rossky PJ. Practical evaluation of condensed phase quantum correlation functions: A Feynman-Kleinert variational linearized path integral method. *The Journal of Chemical Physics* 2003, 119:12179-12193.

- 1
2
3 24. Poulsen JA, Nyman G, Rossky PJ. Feynman-Kleinert linearized path integral (FK-LPI) algorithms for quantum molecular dynamics, with application to water and He(4). *Journal of Chemical Theory and Computation* 2006, 2:1482-1491.
- 4 25. Shao J, Makri N. Forward-Backward Semiclassical Dynamics with Linear Scaling. *The Journal of Physical Chemistry A* 1999, 103:9479-9486.
- 5 26. Shao J, Makri N. Forward-Backward Semiclassical Dynamics without Prefactors. *The Journal of Physical Chemistry A* 1999, 103:7753-7756.
- 6 27. Liu J, Nakayama A, Makri N. Long-time behaviour of quantized distributions in forward-backward semiclassical dynamics. *Molecular Physics* 2006, 104:1267-1274.
- 7 28. Liu J, Makri N. Symmetries and detailed balance in forward-backward semiclassical dynamics. *Chemical Physics* 2006, 322:23-29.
- 8 29. Makri N, Nakayama A, Wright NJ. Forward-backward semiclassical simulation of dynamical properties in liquids. *Journal of Theoretical and Computational Chemistry* 2004, 3:391-417.
- 9 30. Makri N. Quantum-classical path integral: A rigorous approach to condensed phase dynamics. *International Journal of Quantum Chemistry* 2015, 115:1209-1214.
- 10 31. Walters PL, Makri N. Quantum-Classical Path Integral Simulation of Ferrocene-Ferrocenium Charge Transfer in Liquid Hexane. *Journal of Physical Chemistry Letters* 2015, 6:4959-4965.
- 11 32. Kryvohuz M, Cao JS. Quantum-classical correspondence in response theory. *Physical Review Letters* 2005, 95:180405.
- 12 33. Donoso A, Martens CC. Quantum tunneling using entangled classical trajectories. *Physical Review Letters* 2001, 87:223202.
- 13 34. Donoso A, Zheng Y, Martens CC. Simulation of quantum processes using entangled trajectory molecular dynamics. *Journal of Chemical Physics* 2003, 119:5010-5020.
- 14 35. Wang A, Zheng Y, Martens CC, Ren W. Quantum tunneling dynamics using entangled trajectories: general potentials. *Physical Chemistry Chemical Physics* 2009, 11:1588-1594.
- 15 36. Xu F, Martens CC, Zheng Y. Entanglement dynamics with a trajectory-based formulation. *Physical Review A* 2017, 96:022138.
- 16 37. Liu J, Miller WH. An approach for generating trajectory-based dynamics which conserves the canonical distribution in the phase space formulation of quantum mechanics. I. Theories. *The Journal of Chemical Physics* 2011, 134:104101.
- 17 38. Liu J, Miller WH. An approach for generating trajectory-based dynamics which conserves the canonical distribution in the phase space formulation of quantum mechanics. II. Thermal correlation functions. *The Journal of Chemical Physics* 2011, 134:104102.
- 18 39. Liu J. Two more approaches for generating trajectory-based dynamics which conserves the canonical distribution in the phase space formulation of quantum mechanics. *The Journal of Chemical Physics* 2011, 134:194110.
- 19 40. Liu J. Path integral Liouville dynamics for thermal equilibrium systems. *The Journal of Chemical Physics* 2014, 140:224107.
- 20 41. Liu J, Zhang Z. Path integral Liouville dynamics: Applications to infrared spectra of OH, water, ammonia, and methane. *The Journal of Chemical Physics* 2016, 144:034307.
- 21 42. Liu J, Li D, Liu X. Further study of path integral Liouville dynamics. *Scientia Sinica Chimica* 2016, 46:27-37.
- 22 43. Zhang Z, Chen Z, Liu J. Path integral Liouville dynamics simulations of vibrational spectra of formaldehyde and hydrogen peroxide. *Chinese Journal of Chemical Physics* 2020, 33:613-622.
- 23 44. Liu X, Zhang L, Liu J. Machine learning phase space quantum dynamics approaches. *The Journal of Chemical Physics* 2021, 154:184104.
- 24 45. Smith KKG, Poulsen JA, Nyman G, Cunsolo A, Rossky PJ. Application of a new ensemble conserving quantum dynamics simulation algorithm to liquid para-hydrogen and ortho-deuterium. *Journal of Chemical Physics* 2015, 142:244113.
- 25 46. Smith KKG, Poulsen JA, Nyman G, Rossky PJ. A new class of ensemble conserving algorithms for approximate quantum dynamics: Theoretical formulation and model problems. *Journal of Chemical Physics* 2015, 142:244112.
- 26 47. Willatt MJ, Ceriotti M, Althorpe SC. Approximating Matsubara dynamics using the planetary model: Tests on liquid water and ice. *Journal of Chemical Physics* 2018, 148:102336.
- 27 48. Orr L, de la Pena LH, Roy P-N. Formulation of state projected centroid molecular dynamics: Microcanonical ensemble and connection to the Wigner distribution. *Journal of Chemical Physics* 2017, 146:214116.
- 28 49. Bonella S, Montemayor D, Coker DF. Linearized path integral approach for calculating nonadiabatic time correlation functions. *Proceedings of the National Academy of Sciences* 2005, 102:6715-6719.

- 1
2
3 50. Nassimi A, Bonella S, Kapral R. Analysis of the quantum-classical Liouville equation in the
4 mapping basis. *The Journal of Chemical Physics* 2010, 133:134115.
5 51. Weinbub J, Ferry DK. Recent advances in Wigner function approaches. *Applied Physics
Reviews* 2018, 5:041104.
6 52. Pie T, Huppert S, Finocchi F, Depondt P, Bonella S. Sampling the thermal Wigner density via
7 a generalized Langevin dynamics. *Journal of Chemical Physics* 2019, 151:114114.
8 53. Kapral R, Ciccotti G. Mixed quantum-classical dynamics. *The Journal of Chemical Physics*
9 1999, 110:8919-8929.
10 54. Kapral R. Quantum dynamics in open quantum-classical systems. *Journal of Physics:
Condensed Matter* 2015, 27:073201.
11 55. Bai S, Xie W, Zhu L, Shi Q. Calculation of absorption spectra involving multiple excited states:
12 Approximate methods based on the mixed quantum classical Liouville equation. *Journal of
Chemical Physics* 2014, 140:084105.
13 56. Tao G, Miller WH. Semiclassical Description of Electronic Excitation Population Transfer in a
14 Model Photosynthetic System. *Journal of Physical Chemistry Letters* 2010, 1:891-894.
15 57. He X, Wu B, Gong Z, Liu J. Commutator Matrix in Phase Space Mapping Models for
16 Nonadiabatic Quantum Dynamics. *The Journal of Physical Chemistry A* 2021, 125:6845-6863.
17 58. Liu J, He X, Wu B. Unified Formulation of Phase Space Mapping Approaches for Nonadiabatic
18 Quantum Dynamics. *Accounts of chemical research* 2021, 54:4215-4228.
19 59. Orioli AP, Safavi-Naini A, Wall ML, Rey AM. Nonequilibrium dynamics of spin-boson models
20 from phase-space methods. *Physical Review A* 2017, 96:033607.
21 60. Lang H, Vendrell O, Hauke P. Generalized discrete truncated Wigner approximation for
22 nonadiabatic quantum-classical dynamics. *Journal of Chemical Physics* 2021, 155:024111.
23 61. Glauber RJ. Coherent and Incoherent States of Radiation Field. *Physical Review* 1963,
24 131:2766.
25 62. Sudarshan ECG. Equivalence of Semiclassical and Quantum Mechanical Descriptions of
26 Statistical Light Beams. *Physical Review Letters* 1963, 10:277.
27 63. Cahill KE, Glauber RJ. Ordered expansions in boson amplitude operators. *Physical Review*
28 1969, 177:1857.
29 64. Cahill KE, Glauber RJ. Density operators and quasiprobability distributions. *Physical Review*
30 1969, 177:1882.
31 65. Arecchi FT, Thomas H, Gilmore R, Courtens E. Atomic coherent states in quantum optics.
32 *Physical Review A* 1972, 6:2211.
33 66. Drummond PD, Gardiner CW. Generalized P-Representations in Quantum Optics. *Journal of
34 Physics A: Mathematical and General* 1980, 13:2353-2368.
35 67. Walls D, Millburn G. *Quantum Optics*. Berlin: Springer-Verlag; 1994.
36 68. Gardiner C, Zoller P. *Quantum Noise*. 3rd edition ed. Berlin Heidelberg: Springer-Verlag; 2004.
37 69. Schleich WP. Quantum Optics in Phase Space. *Quantum Optics in Phase Space* 2001:716.
38 70. Deleglise S, Dotsenko I, Sayrin C, Bernu J, Brune M, Raimond JM, Haroche S. Reconstruction
39 of non-classical cavity field states with snapshots of their decoherence. *Nature* 2008, 455:510-
40 514.
41 71. Steel MJ, Olsen MK, Plimak LI, Drummond PD, Tan SM, Collett MJ, Walls DF, Graham R.
42 Dynamical quantum noise in trapped Bose-Einstein condensates. *Physical Review A* 1998,
43 58:4824-4835.
44 72. Sinatra A, Lobo C, Castin Y. The truncated Wigner method for Bose-condensed gases: limits
45 of validity and applications. *Journal of Physics B: Atomic Molecular and Optical Physics* 2002,
46 35:3599-3631.
47 73. Blakie PB, Bradley AS, Davis MJ, Ballagh RJ, Gardiner CW. Dynamics and statistical
48 mechanics of ultra-cold Bose gases using c-field techniques. *Advances in Physics* 2008,
49 57:363-455.
50 74. Polkovnikov A. Phase space representation of quantum dynamics. *Annals of Physics* 2010,
51 325:1790-1852.
52 75. Mukherjee R, Mirasola AE, Hollingsworth J, White IG, Hazzard KRA. Geometric representation
53 of spin correlations and applications to ultracold systems. *Physical Review A* 2018, 97:043606.
54 76. Zurek WH. Sub-Planck structure in phase space and its relevance for quantum decoherence.
55 *Nature* 2001, 412:712-717.
56 77. Miquel C, Paz JP, Saraceno M. Quantum computers in phase space. *Physical Review A* 2002,
57 65:062309.
58 78. Wootters WK. Picturing Qubits in Phase Space. *IBM Journal of Research and Development*
59 2004, 48:99-110.

- 1
2
3 79. Paz JP, Roncaglia AJ, Saraceno M. Qubits in phase space: Wigner-function approach to
4 quantum-error correction and the mean-king problem. *Physical Review A* 2005, 72:012309.
5 80. Braunstein SL, van Loock P. Quantum information with continuous variables. *Reviews of
Modern Physics* 2005, 77:513-577.
6 81. Delfosse N, Guerin PA, Bian J, Raussendorf R. Wigner function negativity and contextuality in
7 quantum computation on rebits. *Physical Review X* 2015, 5:021003.
8 82. Schachenmayer J, Pikovski A, Rey AM. Many-Body Quantum Spin Dynamics with Monte-Carlo
9 Trajectories on a Discrete Phase Space. *Physical Review X* 2015, 5:011022.
10 83. Schachenmayer J, Pikovski A, Rey AM. Dynamics of correlations in two-dimensional quantum
11 spin models with long-range interactions: a phase-space Monte-Carlo study. *New Journal of
12 Physics* 2015, 17:065009.
13 84. Bermejo-Vega J, Delfosse N, Browne DE, Okay C, Raussendorf R. Contextuality as a resource
14 for models of quantum computation with qubits. *Physical Review Letters* 2017, 119:120505.
15 85. Rundle RP, Mills PW, Tilma T, Samson JH, Everitt MJ. Simple procedure for phase-space
16 measurement and entanglement validation. *Physical Review A* 2017, 96:022117.
17 86. Zhu B, Rey AM, Schachenmayer J. A generalized phase space approach for solving quantum
18 spin dynamics. *New Journal of Physics* 2019, 21:082001.
19 87. Rundle RP, Everitt MJ. Overview of the Phase Space Formulation of Quantum Mechanics with
20 Application to Quantum Technologies. *Advanced Quantum Technologies* 2021, 4:2100016.
21 88. Weyl H. Quantum mechanics and Group theory. *Zeitschrift Fur Physik* 1927, 46:1-46.
22 89. Wigner E. On the Quantum Correction For Thermodynamic Equilibrium. *Physical Review* 1932,
23 40:749-759.
24 90. Hillery M, Oconnell RF, Scully MO, Wigner EP. Distribution-functions in physics - fundamentals.
25 *Physics Reports-Review Section of Physics Letters* 1984, 106:121-167.
26 91. Lee HW. Theory and Application of the Quantum Phase-Space Distribution Functions. *Physics
Reports-Review Section of Physics Letters* 1995, 259:147-211.
27 92. Cohen L. Generalized Phase-Space Distribution Functions. *Journal of Mathematical Physics*
28 1966, 7:781-786.
29 93. Groenewold HJ. On the Principles of Elementary Quantum Mechanics. *Physica* 1946, 12:405-
30 460.
31 94. Moyal JE. Quantum mechanics as a statistical theory. *Mathematical Proceedings of the
Cambridge Philosophical Society* 1949, 45:99-124.
32 95. Bopp F. *Werner Heisenberg und die Physik unserer Zeit*. Braunschweig: Vieweg; 1961.
33 96. Miller WH. Quantum dynamics of complex molecular systems. *Proceedings of the National
Academy of Sciences* 2005, 102:6660-6664.
34 97. Miller WH. Including quantum effects in the dynamics of complex (i.e., large) molecular systems.
35 *The Journal of Chemical Physics* 2006, 125:132305.
36 98. Miller WH. Classical-limit quantum mechanics and the theory of molecular collisions. *Advances
in Chemical Physics* 1974, 25:69-177.
37 99. Miller WH. The classical S-matrix in molecular collisions. *Advances in Chemical Physics* 1975,
38 30:77.
39 100. Stratonovich RL. On distributions in representation space. *Zh. Eksp. Teor. Fiz.* 1956, 31:1012.
40 101. Feynman RP. Negative probability. In: Hiley BJ, Peat D, eds. *Quantum Implications: Essays in
Honour of David Bohm*. New York: Routledge; 1987, 235-248.
41 102. Wootters WK. A Wigner-function formulation of finite-state quantum mechanics. *Annals of
Physics* 1987, 176:1-21.
42 103. Várilly JC, Gracia-Bondía J. The Moyal representation for spin. *Annals of Physics* 1989,
43 190:107-148.
44 104. Amiet JP, Cibils MB. Description of quantum spin using functions on the sphere S2. *Journal of
Physics A: Mathematical and General* 1991, 24:1515-1535.
45 105. Amiet JP, Weigert S. Discrete Q- and P-symbols for spin s. *Journal of Optics B-Quantum and
Semiclassical Optics* 2000, 2:118-121.
46 106. Dowling JP, Agarwal GS, Schleich WP. Wigner distribution of a general angular-momentum
47 state - Applications to a collection of 2-level atoms. *Physical Review A* 1994, 49:4101-4109.
48 107. Brif C, Mann A. Phase-space Formulation of Quantum Mechanics and Quantum-state
49 Reconstruction for Physical Systems with Lie-group Symmetries. *Physical Review A* 1999,
50 59:971-987.
51 108. Cunha MOT, Man'ko VI, Scully MO. Quasiprobability and probability distributions for spin-1/2
52 states. *Foundations of Physics Letters* 2001, 14:103-117.
53
54
55
56
57
58
59
60

- 1
2
3 109. Klimov AB, Espinoza P. Moyal-like form of the star product for generalized SU(2) Stratonovich-Weyl symbols. *Journal of Physics A: Mathematical and General* 2002, 35:8435-8447.
4 110. Klimov AB, Romero JL. A Generalized Wigner Function for Quantum Systems with the SU(2)
5 Dynamical Symmetry Group. *Journal of Physics A: Mathematical and Theoretical* 2008,
6 41:055303.
7 111. Klimov AB, Romero JL, de Guise H. Generalized SU(2) Covariant Wigner Functions and Some
8 of Their Applications. *Journal of Physics A: Mathematical and Theoretical* 2017, 50:323001.
9 112. Adam P, Andreev VA, Man'ko MA, Man'ko VI, Mechler M. SU(2) Symmetry of Qubit States and
10 Heisenberg-Weyl Symmetry of Systems with Continuous Variables in the Probability
11 Representation of Quantum Mechanics. *Symmetry-Basel* 2020, 12:23.
12 113. Koczor B, Zeier R, Glaser SJ. Continuous Phase-space Representations for Finite-dimensional
13 Quantum States and Their Tomography. *Physical Review A* 2020, 101:022318.
14 114. Tilma T, Nemoto K. SU(N)-symmetric quasi-probability distribution functions. *Journal of Physics*
15 *A: Mathematical and Theoretical* 2012, 45:14.
16 115. Tilma T, Everitt MJ, Samson JH, Munro WJ, Nemoto K. Wigner Functions for Arbitrary Quantum
17 Systems. *Physical Review Letters* 2016, 117:180401.
18 116. Marchiolli MA, Galetti D. On the discrete Wigner function for SU(N). *Journal of Physics A: Mathematical and Theoretical* 2019, 52:405305.
19 117. Rundle RP, Tilma T, Samson JH, Dwyer VM, Bishop RF, Everitt MJ. General Approach to
20 Quantum Mechanics As a Statistical Theory. *Physical Review A* 2019, 99:012115.
21 118. Cohendet O, Combe P, Sirugue M, Siruguecollin M. A stochastic treatment of the dynamics of
22 an integer spin. *Journal of Physics A: Mathematical and General* 1988, 21:2875-2883.
23 119. Leonhardt U. Quantum-state tomography and discrete Wigner function. *Physical Review Letters*
24 1995, 74:4101-4105.
25 120. Leonhardt U. Discrete Wigner function and quantum-state tomography. *Physical Review A*
26 1996, 53:2998-3013.
27 121. Gibbons KS, Hoffman MJ, Wootters WK. Discrete phase space based on finite fields. *Physical*
28 *Review A* 2004, 70:062101.
29 122. Wootters WK. Quantum Measurements and Finite Geometry. *Foundations of Physics* 2006,
30 36:112-126.
31 123. Ruzzi M, Marchiolli MA, Galetti D. Extended Cahill-Glauber formalism for finite-dimensional
32 spaces: I. Fundamentals. *Journal of Physics A: Mathematical and General* 2005, 38:6239-6251.
33 124. Chaturvedi S, Ercolessi E, Marmo G, Morandi G, Mukunda N, Simon R. Wigner distributions
34 for finite dimensional quantum systems: An algebraic approach. *Pramana* 2005, 65:981-993.
35 125. Chaturvedi S, Ercolessi E, Marmo G, Morandi G, Mukunda N, Simon R. Wigner-Weyl
36 correspondence in quantum mechanics for continuous and discrete systems-a Dirac-inspired
37 view. *Journal of Physics A: Mathematical and General* 2006, 39:1405-1423.
38 126. Gross D. Hudson's theorem for finite-dimensional quantum systems. *Journal of Mathematical*
39 *Physics* 2006, 47:25.
40 127. Valtierra IF, Romero JL, Klimov AB. TWA versus semiclassical unitary approximation for spin-
41 like systems. *Annals of Physics* 2017, 383:620-634.
42 128. Valtierra IF, Klimov AB, Leuchs G, Sánchez-Soto LL. Quasiprobability currents on the sphere.
43 *Physical Review A* 2020, 101:033803.
44 129. Czischek S. Discrete Truncated Wigner Approximation. In: *Springer Theses*: Springer
45 International Publishing; 2020, 85-109.
46 130. Morales-Hernndez GE, Castellanos JC, Romero JL, Klimov AB. Semi-classical Discretization
47 and Long-time Evolution of Variable Spin Systems. *Entropy* 2021, 23:684.
48 131. Liu J. A unified theoretical framework for mapping models for the multi-state Hamiltonian. *The*
49 *Journal of Chemical Physics* 2016, 145:204105.
50 132. He X, Liu J. A new perspective for nonadiabatic dynamics with phase space mapping models.
51 *The Journal of Chemical Physics* 2019, 151:024105.
52 133. Liu J. Isomorphism between the multi-state Hamiltonian and the second-quantized many-
53 electron Hamiltonian with only 1-electron interactions. *The Journal of Chemical Physics* 2017,
54 146:024110.
55 134. He X, Gong Z, Wu B, Liu J. Negative Zero-Point-Energy Parameter in the Meyer-Miller Mapping
56 Model for Nonadiabatic Dynamics. *The journal of physical chemistry letters* 2021, 12:2496-
57 2501.
58 135. Domcke W, Yarkony DR, Köppel H. *Conical Intersections: Theory, Computation and*
59 *Experiment*. Singapore: World Scientific; 2011.

- 1
2
3 136. Yonehara T, Hanasaki K, Takatsuka K. Fundamental Approaches to Nonadiabaticity: Toward
4 a Chemical Theory beyond the Born-Oppenheimer Paradigm. *Chemical Reviews* 2011,
5 112:499-542.
- 6 137. Tully JC. Perspective: Nonadiabatic dynamics theory. *The Journal of Chemical Physics* 2012,
7 137:22A301.
- 8 138. Miller WH, Cotton SJ. Classical molecular dynamics simulation of electronically non-adiabatic
9 processes. *Faraday Discussions* 2016, 195:9-30.
- 10 139. Levine BG, Martinez TJ. Isomerization through conical intersections. *Annual Review of Physical
11 Chemistry* 2007, 58:613-634.
- 12 140. Martinez TJ. Seaming is believing. *Nature* 2010, 467:412-413.
- 13 141. Sisto A, Glowacki DR, Martinez TJ. Ab Initio Nonadiabatic Dynamics of Multichromophore
14 Complexes: A Scalable Graphical-Processing-Unit-Accelerated Exciton Framework. *Accounts
15 of Chemical Research* 2014, 47:2857-2866.
- 16 142. Makhov DV, Glover WJ, Martinez TJ, Shalashilin DV. Ab initio multiple cloning algorithm for
17 quantum nonadiabatic molecular dynamics. *The Journal of Chemical Physics* 2014,
18 141:054110.
- 19 143. Mai S, Marquetand P, Gonzalez L. Nonadiabatic dynamics: The SHARC approach. *Wiley
20 Interdisciplinary Reviews-Computational Molecular Science* 2018, 8:e1370.
- 21 144. Mai S, Gonzalez L. Molecular Photochemistry: Recent Developments in Theory. *Angewandte
22 Chemie-International Edition* 2020, 59:16832-16846.
- 23 145. Subotnik JE, Jain A, Landry B, Petit A, Ouyang W, Bellonzi N. Understanding the Surface
24 Hopping View of Electronic Transitions and Decoherence. In: Johnson MA, Martinez TJ, eds.
25 *Annual Review of Physical Chemistry*, Vol 67. Vol. 67: Annual Reviews; 2016, 387-417.
- 26 146. Fang W-H. Ab Initio Determination of Dark Structures in Radiationless Transitions for Aromatic
27 Carbonyl Compounds. *Accounts of Chemical Research* 2008, 41:452-457.
- 28 147. Long R, Prezhdo OV, Fang W-H. Nonadiabatic charge dynamics in novel solar cell materials.
29 *Wiley Interdisciplinary Reviews-Computational Molecular Science* 2017, 7:e1305.
- 30 148. Feng W, Xu L, Li X-Q, Fang W-H, Yan Y. Nonadiabatic molecular dynamics simulation: An
31 approach based on quantum measurement picture. *AIP Advances* 2014, 4:077131.
- 32 149. Lan Z, Shao J. Approximate Theoretical Methods for Nonadiabatic Dynamics of Polyatomic
33 Molecules. *Progress in Chemistry* 2012, 24:1105-1119.
- 34 150. Wang Y-C, Ke Y, Zhao Y. The hierarchical and perturbative forms of stochastic Schrodinger
35 equations and their applications to carrier dynamics in organic materials. *Wiley Interdisciplinary
36 Reviews-Computational Molecular Science* 2019, 9:e1375.
- 37 151. Nelson T, Fernandez-Alberti S, Roitberg AE, Tretiak S. Nonadiabatic Excited-State Molecular
38 Dynamics: Modeling Photophysics in Organic Conjugated Materials. *Accounts of Chemical
39 Research* 2014, 47:1155-1164.
- 40 152. Crespo-Otero R, Barbatti M. Recent Advances and Perspectives on Nonadiabatic Mixed
41 Quantum-Classical Dynamics. *Chemical Reviews* 2018, 118:7026-7068.
- 42 153. Meyer H-D, Miller WH. A classical analog for electronic degrees of freedom in nonadiabatic
43 collision processes. *The Journal of Chemical Physics* 1979, 70:3214-3223.
- 44 154. Stock G, Thoss M. Semiclassical description of nonadiabatic quantum dynamics. *Physical
45 Review Letters* 1997, 78:578-581.
- 46 155. Wigner EP. *Perspectives in Quantum Theory*. Cambridge: MIT; 1971.
- 47 156. Husimi K. Some Formal Properties of the Density Matrix. *Proceedings of the Physico-
48 Mathematical Society of Japan* 1940, 22:264-314.
- 49 157. Glauber RJ. Optical Coherence and Photon Statistics. In: deWitt C, Blandin A, C. C-T, eds.
50 *Quantum Optics and Electronics*. New York: Gordon and Breach; 1965.
- 51 158. Kirkwood JG. Quantum Statistics of Almost Classical Assemblies. *Physical Review* 1933, 44:31.
- 52 159. Rihaczek AW. Signal Energy Distribution in Time and Frequency. *IEEE Transactions on
53 Information Theory* 1968, 14:369-374.
- 54 160. Mehta CL. Phase-Space Formulation of the Dynamics of Canonical Variables. *Journal of
55 Mathematical Physics* 1964, 5:677-686.
- 56 161. Rivier DC. On a One-to-One Correspondence between Infinitesimal Canonical Transformations
57 and Infinitesimal Unitary Transformations. *Physical Review* 1951, 83:862.
- 58 162. Margenau H, Hill RN. Correlation between Measurements in Quantum Theory. *Progress of
59 Theoretical Physics* 1961, 26:722-738.
- 60 163. Born M, Jordan P. On quantum mechanics. *Zeitschrift fur Physik* 1925, 34:858-888.

- 1
2
3 164. Meyer H-D, Miller WH. Classical-Models for Electronic Degrees of Freedom: Derivation Via
4 Spin Analogy and Application to $F^*+H_2 \rightarrow F+H_2$. *The Journal of Chemical Physics* 1979,
5 71:2156-2169.
6 165. Gray SK, Miller WH. Classical model for electronic degrees of freedom: charge transfer in Na^+ + I collisions. *Chemical Physics Letters* 1982, 93:341-344.
7 166. Ali DP, Miller WH. Effect of electronic transition dynamics on iodine atom recombination in
8 liquids. *The Journal of Chemical Physics* 1983, 78:6640-6645.
9 167. Ali DP, Miller WH. Classical models for electronic degrees of freedom: Quenching of $Br^*(2P1/2)$
10 by collision with H_2 in three dimensions. *Chemical Physics Letters* 1984, 103:470-474.
11 168. Stock G, Miller WH. A classical model for time- and frequency-resolved spectroscopy of
12 nonadiabatic excited-state dynamics. *Chemical Physics Letters* 1992, 197:396-404.
13 169. Stock G, Miller WH. Classical formulation of the spectroscopy of nonadiabatic excited-state
14 dynamics. *The Journal of Chemical Physics* 1993, 99:1545-1555.
15 170. Sun X, Miller WH. Semiclassical initial value representation for electronically nonadiabatic
16 molecular dynamics. *The Journal of Chemical Physics* 1997, 106:6346-6353.
17 171. Coronado EA, Batista VS, Miller WH. Nonadiabatic photodissociation dynamics of CN in the A
18 continuum: A semiclassical initial value representation study. *The Journal of Chemical Physics*
19 2000, 112:5566-5575.
21 172. Coronado EA, Xing J, Miller WH. Ultrafast non-adiabatic dynamics of systems with multiple
22 surface crossings: a test of the Meyer-Miller Hamiltonian with semiclassical initial value
23 representation methods. *Chemical Physics Letters* 2001, 349:521-529.
24 173. Ananth N, Venkataraman C, Miller WH. Semiclassical description of electronically nonadiabatic
25 dynamics via the initial value representation. *The Journal of Chemical Physics* 2007,
26 127:084114.
27 174. Miller WH. Electronically Nonadiabatic Dynamics via Semiclassical Initial Value Methods.
28 *Journal of Physical Chemistry A* 2009, 113:1405-1415.
29 175. Ananth N, Miller TF. Exact quantum statistics for electronically nonadiabatic systems using
30 continuous path variables. *The Journal of Chemical Physics* 2010, 133:234103.
31 176. Cotton SJ, Miller WH. Symmetrical Windowing for Quantum States in Quasi-Classical
32 Trajectory Simulations. *Journal of Physical Chemistry A* 2013, 117:7190-7194.
33 177. Cotton SJ, Miller WH. Symmetrical windowing for quantum states in quasi-classical trajectory
34 simulations: Application to electronically non-adiabatic processes. *The Journal of Chemical
35 Physics* 2013, 139:234112.
36 178. Cotton SJ, Igumenshchev K, Miller WH. Symmetrical windowing for quantum states in quasi-
37 classical trajectory simulations: Application to electron transfer. *The Journal of Chemical
38 Physics* 2014, 141:084104.
39 179. Cotton SJ, Miller WH. A Symmetrical Quasi-Classical Spin-Mapping Model for the Electronic
40 Degrees of Freedom in Non-Adiabatic Processes. *Journal of Physical Chemistry A* 2015,
41 119:12138-12145.
42 180. Miller WH, Cotton SJ. Communication: Note on detailed balance in symmetrical quasi-classical
43 models for electronically non-adiabatic dynamics. *The Journal of Chemical Physics* 2015,
44 142:131103.
45 181. Cotton SJ, Miller WH. A new symmetrical quasi-classical model for electronically non-adiabatic
46 processes: Application to the case of weak non-adiabatic coupling. *The Journal of Chemical
47 Physics* 2016, 145:144108.
48 182. Cotton SJ, Miller WH. The Symmetrical Quasi-Classical Model for Electronically Non-Adiabatic
49 Processes Applied to Energy Transfer Dynamics in Site-Exciton Models of Light-Harvesting
50 Complexes. *Journal of Chemical Theory and Computation* 2016, 12:983-991.
51 183. Miller WH, Cotton SJ. Communication: Wigner functions in action-angle variables, Bohr-
52 Sommerfeld quantization, the Heisenberg correspondence principle, and a symmetrical quasi-
53 classical approach to the full electronic density matrix. *The Journal of Chemical Physics* 2016,
54 145:081102.
55 184. Cotton SJ, Liang R, Miller WH. On the adiabatic representation of Meyer-Miller electronic-
56 nuclear dynamics. *The Journal of Chemical Physics* 2017, 147:064112.
57 185. Liang R, Cotton SJ, Binder R, Hegger R, Burghardt I, Miller WH. The symmetrical quasi-
58 classical approach to electronically nonadiabatic dynamics applied to ultrafast exciton migration
59 processes in semiconducting polymers. *The Journal of Chemical Physics* 2018, 149:044101.
60 186. Cotton SJ, Miller WH. A symmetrical quasi-classical windowing model for the molecular
dynamics treatment of non-adiabatic processes involving many electronic states. *The Journal
of Chemical Physics* 2019, 150:104101.

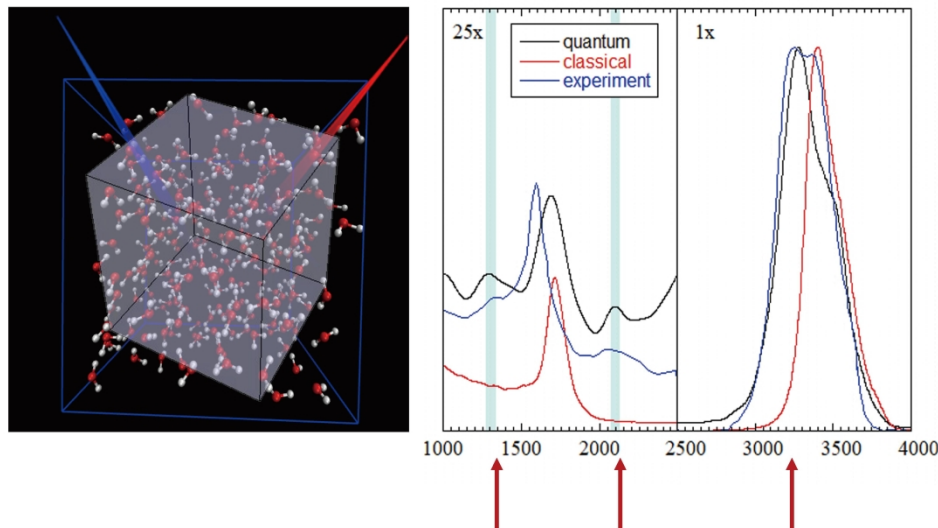
- 1
2
3 187. Cotton SJ, Miller WH. Trajectory-adjusted electronic zero point energy in classical Meyer-Miller
4 vibronic dynamics: Symmetrical quasiclassical application to photodissociation. *The Journal of
5 Chemical Physics* 2019, 150:194110.
- 6 188. Muller U, Stock G. Flow of zero-point energy and exploration of phase space in classical
7 simulations of quantum relaxation dynamics. II. Application to nonadiabatic processes. *Journal
8 of Chemical Physics* 1999, 111:77-88.
- 9 189. Stock G, Muller U. Flow of zero-point energy and exploration of phase space in classical
10 simulations of quantum relaxation dynamics. *Journal of Chemical Physics* 1999, 111:65-76.
- 11 190. Stock G, Muller U. Flow of zero-point energy and exploration of phase space in classical
12 simulations of quantum relaxation dynamics. II. application to nonadiabatic processes. *The
13 Journal of Chemical Physics* 1999, 111:77-88.
- 14 191. Stock G, Thoss M. Classical Description of Nonadiabatic Quantum Dynamics. In: Rice SA, ed.
15 *Advances in Chemical Physics*. Vol. 131: John Wiley and Sons, Inc.; 2005, 243-375.
- 16 192. Thoss M, Miller WH, Stock G. Semiclassical description of nonadiabatic quantum dynamics:
17 Application to the S1-S2 conical intersection in pyrazine. *The Journal of Chemical Physics* 2000,
18 112:10282-10292.
- 19 193. Thoss M, Stock G. Mapping approach to the semiclassical description of nonadiabatic quantum
20 dynamics. *Physical Review A* 1999, 59:64-79.
- 21 194. Golosov AA, Reichman DR. Classical mapping approaches for nonadiabatic dynamics: Short
22 time analysis. *The Journal of Chemical Physics* 2001, 114:1065-1074.
- 23 195. Saller MAC, Kelly A, Richardson JO. On the identity of the identity operator in nonadiabatic
24 linearized semiclassical dynamics. *The Journal of Chemical Physics* 2019, 150:071101.
- 25 196. Saller MAC, Kelly A, Richardson JO. Improved population operators for multi-state nonadiabatic
26 dynamics with the mixed quantum-classical mapping approach. *Faraday Discussions* 2020,
27 221:150-167.
- 28 197. Runeson JE, Richardson JO. Generalized spin mapping for quantum-classical dynamics. *The
29 Journal of Chemical Physics* 2020, 152:084110.
- 30 198. Kananenka AA, Hsieh CY, Cao JS, Geva E. Nonadiabatic Dynamics via the Symmetrical
31 Quasi-Classical Method in the Presence of Anharmonicity. *Journal of Physical Chemistry
Letters* 2018, 9:319-326.
- 32 199. Mulvihill E, Gao X, Liu Y, Schubert A, Dunietz BD, Geva E. Combining the mapping Hamiltonian
33 linearized semiclassical approach with the generalized quantum master equation to simulate
34 electronically nonadiabatic molecular dynamics. *The Journal of Chemical Physics* 2019,
35 151:074103.
- 36 200. Gao X, Geva E. Improving the Accuracy of Quasiclassical Mapping Hamiltonian Methods by
37 Treating the Window Function Width as an Adjustable Parameter. *Journal of Physical
Chemistry A* 2020, 124:11006-11016.
- 38 201. Gao X, Lai Y, Geva E. Simulating Absorption Spectra of Multiexcitonic Systems via
39 Quasiclassical Mapping Hamiltonian Methods. *Journal of Chemical Theory and Computation*
40 2020, 16:6465-6480.
- 41 202. Gao X, Sailer MAC, Liu Y, Kelly A, Richardson JO, Geva E. Benchmarking Quasiclassical
42 Mapping Hamiltonian Methods for Simulating Electronically Nonadiabatic Molecular Dynamics.
43 *Journal of Chemical Theory and Computation* 2020, 16:2883-2895.
- 44 203. Liu Y, Gao X, Lai Y, Mulvihill E, Geva E. Electronic Dynamics through Conical Intersections via
45 Quasiclassical Mapping Hamiltonian Methods. *Journal of Chemical Theory and Computation*
46 2020, 16:4479-4488.
- 47 204. Saller MAC, Kelly A, Geva E. Benchmarking Quasiclassical Mapping Hamiltonian Methods for
48 Simulating Cavity-Modified Molecular Dynamics. *Journal of Physical Chemistry Letters* 2021,
49 12:3163-3170.
- 50 205. Bonella S, Coker DF. A semiclassical limit for the mapping Hamiltonian approach to
51 electronically nonadiabatic dynamics. *The Journal of Chemical Physics* 2001, 114:7778-7789.
- 52 206. Bonella S, Coker DF. Semiclassical implementation of the mapping Hamiltonian approach for
53 nonadiabatic dynamics using focused initial distribution sampling. *The Journal of Chemical
54 Physics* 2003, 118:4370-4385.
- 55 207. Bonella S, Coker DF. LAND-map, a linearized approach to nonadiabatic dynamics using the
56 mapping formalism. *The Journal of Chemical Physics* 2005, 122:194102.
- 57 208. Huo PF, Coker DF. Semi-classical path integral non-adiabatic dynamics: a partial linearized
58 classical mapping Hamiltonian approach. *Molecular Physics* 2012, 110:1035-1052.

- 1
2
3 209. Tang D, Fang W-H, Shen L, Cui G. Combining Meyer-Miller Hamiltonian with electronic
4 structure methods for on-the-fly nonadiabatic dynamics simulations: implementation and
5 application. *Physical Chemistry Chemical Physics* 2019, 21:17109-17117.
- 6 210. Zheng J, Xie Y, Jiang S, Long Y, Ning X, Lan Z. Ultrafast Electron Transfer with Symmetrical
7 Quasi-classical Dynamics based on Mapping Hamiltonian and Quantum Dynamics based on
8 ML-MCTDH. *Chinese Journal of Chemical Physics* 2017, 30:800-810.
- 9 211. Xie Y, Zheng J, Lan Z. Performance evaluation of the symmetrical quasi-classical dynamics
10 method based on Meyer-Miller mapping Hamiltonian in the treatment of site-exciton models.
11 *The Journal of Chemical Physics* 2018, 149:174105.
- 12 212. Zheng J, Xie Y, Jiang S, Long Y, Ning X, Lan Z. Initial sampling in symmetrical quasiclassical
13 dynamics based on Li-Miller mapping Hamiltonian. *Physical Chemistry Chemical Physics* 2019,
14 21:26502-26514.
- 15 213. Zheng J, Peng J, Xie Y, Long Y, Ning X, Lan Z. Study of the exciton dynamics in perylene
16 bisimide (PBI) aggregates with symmetrical quasiclassical dynamics based on the Meyer-Miller
17 mapping Hamiltonian. *Physical Chemistry Chemical Physics* 2020, 22:18192-18204.
- 18 214. Peng J, Xie Y, Hu D, Lan Z. Analysis of bath motion in MM-SQC dynamics via dimensionality
19 reduction approach: Principal component analysis. *The Journal of Chemical Physics* 2021,
20 154:094122.
- 21 215. Hu D, Xie Y, Peng J, Lan Z. On-the-Fly Symmetrical Quasi-Classical Dynamics with
22 Meyer-Miller Mapping Hamiltonian for the Treatment of Nonadiabatic Dynamics at Conical
23 Intersections. *Journal of Chemical Theory and Computation* 2021, 17:3267-3279.
- 24 216. Tao G. A multi-state trajectory method for non-adiabatic dynamics simulations. *The Journal of
Chemical Physics* 2016, 144:094108.
- 25 217. Tao G. Coherence-Controlled Nonadiabatic Dynamics via State-Space Decomposition: A
26 Consistent Way To Incorporate Ehrenfest and Born-Oppenheimer-Like Treatments of Nuclear
27 Motion. *Journal of Physical Chemistry Letters* 2016, 7:4335-4339.
- 28 218. Tao G. Multi-state trajectory approach to non-adiabatic dynamics: General formalism and the
29 active state trajectory approximation. *The Journal of Chemical Physics* 2017, 147:044107.
- 30 219. Schwinger J. In: Biedenharn LC, VanDam H, eds. *Quantum Theory of Angular Momentum*.
31 New York: Academic; 1965.
- 32 220. Sakurai JJ. *Modern Quantum Mechanics*. New York: Addison-Wesley; 1994.
- 33 221. Flammia ST, Liu Y-K. Direct Fidelity Estimation from Few Pauli Measurements. *Physical
34 Review Letters* 2011, 106:230501.
- 35 222. Sperling J, Walmsley IA. Quasiprobability representation of quantum coherence. *Physical
36 Review A* 2018, 97:062327.
- 37 223. Bohmann M, Agudelo E, Sperling J. Probing nonclassicality with matrices of phase-space
38 distributions. *Quantum* 2020, 4:16.
- 39 224. Bohmann M, Agudelo E. Phase-space inequalities beyond negativities. *Physical Review
40 Letters* 2020, 124:133601.
- 41 225. Lutterbach LG, Davidovich L. Method for direct measurement of the Wigner function in cavity
42 QED and ion traps. *Physical Review Letters* 1997, 78:2547-2550.
- 43 226. Signoles A, Facon A, Grosso D, Dotsenko I, Haroche S, Raimond JM, Brune M, Gleyzes S.
44 Confined quantum Zeno dynamics of a watched atomic arrow. *Nature Physics* 2014, 10:715-
719.
- 45 227. Leiner D, Glaser SJ. Wigner process tomography: Visualization of spin propagators and their
46 spinor properties. *Physical Review A* 2018, 98:012112.
- 47 228. Tian Y, Wang Z, Zhang P, Li G, Li J, Zhang T. Measurement of complete and continuous Wigner
48 functions for discrete atomic systems. *Physical Review A* 2018, 97:013840.
- 49 229. Chen B, Geng J, Zhou F, Song L, Shen H, Xu N. Quantum state tomography of a single electron
50 spin in diamond with Wigner function reconstruction. *Applied Physics Letters* 2019, 114:041102.
- 51 230. Jing Y, Fadel M, Ivannikov V, Byrnes T. Split spin-squeezed Bose-Einstein condensates. *New
52 Journal of Physics* 2019, 21:093038.
- 53 231. Song C, Xu K, Li H, Zhang Y-R, Zhang X, Liu W, Guo Q, Wang Z, Ren W, Hao J, et al.
54 Generation of multicomponent atomic Schrodinger cat states of up to 20 qubits. *Science* 2019,
55 365:574-577.
- 56 232. Eichler C, Lang C, Fink JM, Govenius J, Filipp S, Wallraff A. Observation of Entanglement
57 between Itinerant Microwave Photons and a Superconducting Qubit. *Physical Review Letters*
58 2012, 109:240501.

- 1
2
3 233. Morin O, Huang K, Liu J, Le Jeannic H, Fabre C, Laurat J. Remote creation of hybrid
4 entanglement between particle-like and wave-like optical qubits. *Nature Photonics* 2014, 8:570-
5 574.
- 6 234. Agudelo E, Sperling J, Costanzo LS, Bellini M, Zavatta A, Vogel W. Conditional Hybrid
7 Nonclassicality. *Physical Review Letters* 2017, 119:120403.
- 8 235. Banaszek K, Radzewicz C, Wodkiewicz K, Krasinski JS. Direct measurement of the Wigner
9 function by photon counting. *Physical Review A* 1999, 60:674-677.
- 10 236. Garon A, Zeier R, Glaser SJ. Visualizing operators of coupled spin systems. *Physical Review*
11 *A* 2015, 91:042122.
- 12 237. Koczor B, Zeier R, Glaser SJ. Time evolution of coupled spin systems in a generalized Wigner
13 representation. *Annals of Physics* 2019, 408:1-50.
- 14 238. Davies BI, Rundle RP, Dwyer VM, Samson JH, Tilma T, Everitt MJ. Visualizing spin degrees of
15 freedom in atoms and molecules. *Physical Review A* 2019, 100:042102.
- 16 239. Rundle RP, Davies BI, Dwyer VM, Tilma T, Everitt MJ. Visualization of correlations in hybrid
17 discrete-continuous variable quantum systems. *Journal of Physics Communications* 2020,
18 4:025002.
- 19 240. Ehrenfest P. Bemerkung über die angenäherte Gültigkeit der klassischen Mechanik innerhalb
20 der Quantenmechanik. *Zeitschrift für Physik* 1927, 45:455-457.
- 21 241. Li X, Tully JC, Schlegel HB, Frisch MJ. Ab initio Ehrenfest dynamics. *The Journal of Chemical*
22 *Physics* 2005, 123:084106.
- 23 242. Tully JC. Molecular dynamics with electronic transitions. *The Journal of Chemical Physics* 1990,
24 93:1061-1071.
- 25 243. Wang LJ, Akimov A, Prezhdo OV. Recent Progress in Surface Hopping: 2011-2015. *Journal of*
26 *Physical Chemistry Letters* 2016, 7:2100-2112.
- 27 244. Peng J, Xie Y, Hu D, Du L, Lan Z. Treatment of Nonadiabatic Dynamics by On-The-Fly
28 Trajectory Surface Hopping Dynamics. *Acta Physico-Chimica Sinica* 2019, 35:28-48.
- 29 245. Meyer KR, Offin DC. *Introduction to Hamiltonian Dynamical Systems and the N-Body Problem*.
30 New York: Springer Science+Business Media, LLC; 1992.
- 31 246. Yarkony DR. Conical Intersections: Diabolical and Often Misunderstood. *Accounts of Chemical*
32 *Research* 1998, 31:511-518.
- 33 247. Paterson MJ, Bearpark MJ, Robb MA, Blancfort L, Worth GA. Conical intersections: A
34 perspective on the computation of spectroscopic Jahn-Teller parameters and the degenerate
35 'intersection space'. *Physical Chemistry Chemical Physics* 2005, 7:2100-2115.
- 36 248. Matsika S, Krause P. Nonadiabatic Events and Conical Intersections. In: Leone SR, Cremer
37 PS, Groves JT, Johnson MA, eds. *Annual Review of Physical Chemistry*, Vol 62. Vol. 62:
38 Annual Reviews; 2011, 621-643.
- 39 249. Makarov DE, Makri N. Path-Integrals for Dissipative Systems by Tensor Multiplication -
40 Condensed-Phase Quantum Dynamics for Arbitrarily Long-Time. *Chemical Physics Letters*
41 1994, 221:482-491.
- 42 250. Makri N, Makarov DE. Tensor Propagator for Iterative Quantum Time Evolution of Reduced
43 Density-Matrices .2. Numerical Methodology. *Journal of Chemical Physics* 1995, 102:4611-
44 4618.
- 45 251. Makri N, Makarov DE. Tensor Propagator for Iterative Quantum Time Evolution of Reduced
46 Density-Matrices .1. Theory. *Journal of Chemical Physics* 1995, 102:4600-4610.
- 47 252. Topaler M, Makri N. Path integral calculation of quantum nonadiabatic rates in model
48 condensed phase reactions. *Journal of Physical Chemistry* 1996, 100:4430-4436.
- 49 253. Tanimura Y, Kubo R. Time Evolution of a Quantum System in Contact with a Nearly Gaussian-
50 Markoffian Noise Bath. *Journal of the Physical Society of Japan* 1989, 58:101-114.
- 51 254. Yan Y-A, Yang F, Liu Y, Shao J. Hierarchical approach based on stochastic decoupling to
52 dissipative systems. *Chemical Physics Letters* 2004, 395:216-221.
- 53 255. Xu R-X, Cui P, Li X-Q, Mo Y, Yan Y. Exact quantum master equation via the calculus on path
54 integrals. *The Journal of Chemical Physics* 2005, 122:041103.
- 55 256. Shao J. Stochastic description of quantum open systems: Formal solution and strong
56 dissipation limit. *Chemical Physics* 2006, 322:187-192.
- 57 257. Moix JM, Cao J. A hybrid stochastic hierarchy equations of motion approach to treat the low
58 temperature dynamics of non-Markovian open quantum systems. *The Journal of Chemical*
59 *Physics* 2013, 139:134106.
- 60 258. Tanimura Y. Reduced hierarchical equations of motion in real and imaginary time: Correlated
initial states and thermodynamic quantities. *The Journal of Chemical Physics* 2014,
141:044114.

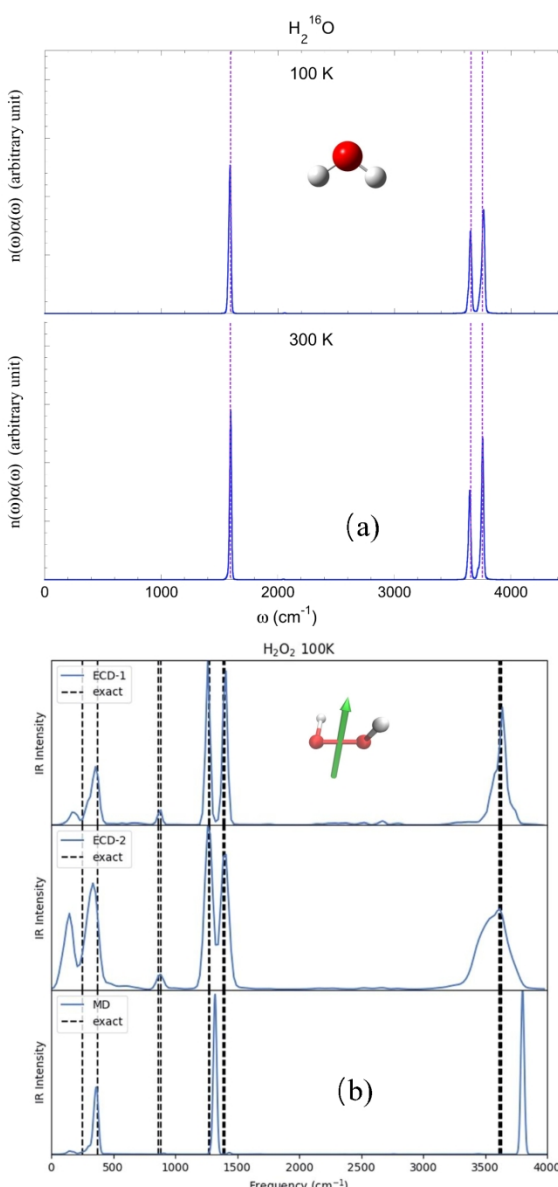
- 1
2
3 259. Yan Y. Theory of open quantum systems with bath of electrons and phonons and spins: Many-
4 dissipaton density matrixes approach. *The Journal of Chemical Physics* 2014, 140:054105.
5 260. Tang Z, Ouyang X, Gong Z, Wang H, Wu J. Extended hierarchy equation of motion for the spin-
6 boson model. *The Journal of Chemical Physics* 2015, 143:224112.
7 261. Tanimura Y. Real-time and imaginary-time quantum hierachal Fokker-Planck equations. *The
8 Journal of Chemical Physics* 2015, 142:144110.
9 262. Meyer H-D, Manthe U, Cederbaum LS. The multi-configurational time-dependent Hartree
10 approach. *Chemical Physics Letters* 1990, 165:73-78.
11 263. Thoss M, Wang H, Miller WH. Self-consistent hybrid approach for complex systems: Application
12 to the spin-boson model with Debye spectral density. *The Journal of Chemical Physics* 2001,
13 115:2991-3005.
14 264. Wang H, Thoss M, Miller WH. Systematic convergence in the dynamical hybrid approach for
15 complex systems: A numerically exact methodology. *The Journal of Chemical Physics* 2001,
16 115:2979-2990.
17 265. Wang H, Thoss M. Multilayer formulation of the multiconfiguration time-dependent Hartree
18 theory. *The Journal of Chemical Physics* 2003, 119:1289-1299.
19 266. Wang H, Thoss M. From coherent motion to localization: dynamics of the spin-boson model at
20 zero temperature. *New Journal of Physics* 2008, 10:115005.
21 267. Worth GA, Meyer H-D, Köppel H, Cederbaum LS, Burghardt I. Using the MCTDH wavepacket
22 propagation method to describe multimode non-adiabatic dynamics. *International Reviews in
23 Physical Chemistry* 2008, 27:569-606.
24 268. Wang H, Thoss M. From coherent motion to localization: II. Dynamics of the spin-boson model
25 with sub-Ohmic spectral density at zero temperature. *Chemical Physics* 2010, 370:78-86.
26 269. Craig IR, Thoss M, Wang H. Proton transfer reactions in model condensed-phase environments:
27 Accurate quantum dynamics using the multilayer multiconfiguration time-dependent Hartree
28 approach. *The Journal of Chemical Physics* 2007, 127:144503.
29 270. Wang H. Iterative Calculation of Energy Eigenstates Employing the Multi layer
30 Multiconfiguration Time-Dependent Hartree Theory. *Journal of Physical Chemistry A* 2014,
31 118:9253-9261.
32 271. Purcell EM. Spontaneous Emission Probabilities at Radio Frequencies. In: Burstein E,
33 Weisbuch C, eds. *Confined Electrons and Photons: New Physics and Applications*. Boston, MA:
34 Springer US; 1995, 839-839.
35 272. Krasnok AE, Slobozhanyuk AP, Simovski CR, Tretyakov SA, Poddubny AN, Miroshnichenko
36 AE, Kivshar YS, Belov PA. An antenna model for the Purcell effect. *Scientific Reports* 2015,
37 5:12956.
38 273. Rybin MV, Mingaleev SF, Limonov MF, Kivshar YS. Purcell effect and Lamb shift as
39 interference phenomena. *Scientific Reports* 2016, 6:20599.
40 274. Holsteen AL, Raza S, Fan P, Kik PG, Brongersma ML. Purcell effect for active tuning of light
41 scattering from semiconductor optical antennas. *Science* 2017, 358:1407-1410.
42 275. Alagappan G, Krivitsky LA, Png CE. Diamond in a Nanopocket: A New Route to a Strong Purcell
43 Effect. *ACS Omega* 2018, 3:4733-4742.
44 276. Gallego J, Alt W, Macha T, Martinez-Dorantes M, Pandey D, Meschede D. Strong Purcell Effect
45 on a Neutral Atom Trapped in an Open Fiber Cavity. *Physical Review Letters* 2018, 121:173603.
46 277. Ren T, Dong Y, Xu S, Gong X. Strong Purcell effect in deep subwavelength coaxial cavity with
47 GeSn active medium. *Optics Letters* 2021, 46:3889-3892.
48 278. Carmichael HJ, Brecha RJ, Raizen MG, Kimble HJ, Rice PR. Subnatural linewidth averaging
49 for coupled atomic and cavity-mode oscillators. *Physical Review A* 1989, 40:5516-5519.
50 279. Zhu Y, Gauthier DJ, Morin SE, Wu Q, Carmichael HJ, Mossberg TW. Vacuum Rabi splitting as
51 a feature of linear-dispersion theory: Analysis and experimental observations. *Physical Review
52 Letters* 1990, 64:2499-2502.
53 280. Field JE. Vacuum-Rabi-splitting-induced transparency. *Physical Review A* 1993, 47:5064-5067.
54 281. Abram II, Oudar JL. Spontaneous emission in planar semiconductor microcavities displaying
55 vacuum Rabi splitting. *Physical Review A* 1995, 51:4116-4122.
56 282. Li K, Wang W, Chen Z, Gao N, Yang W, Li W, Chen H, Li S, Li H, Jin P, et al. Vacuum Rabi
57 splitting of exciton-polariton emission in an AlN film. *Scientific Reports* 2013, 3:3551.
58 283. Toida H, Nakajima T, Komiya S. Vacuum Rabi splitting in a semiconductor circuit QED
59 system. *Physical Review Letters* 2013, 110:066802.
60 284. Guerin W, Santo T, Weiss P, Cipris A, Schachenmayer J, Kaiser R, Bachelard R. Collective
Multimode Vacuum Rabi Splitting. *Physical Review Letters* 2019, 123:243401.

- 1
2
3 285. Yan Y, Ergogo TT, Lu Z, Chen L, Luo J, Zhao Y. Lamb Shift and the Vacuum Rabi Splitting in
4 a Strongly Dissipative Environment. *The Journal of Physical Chemistry Letters* 2021, 12:9919-
5 9925.
6 286. Meystre P. *Elements of Quantum Optics*. Berlin New York: Springer; 2007.
7 287. Hoffmann NM, Schafer C, Rubio A, Kelly A, Appel H. Capturing vacuum fluctuations and photon
8 correlations in cavity quantum electrodynamics with multitrajectory Ehrenfest dynamics.
9 *Physical Review A* 2019, 99:063819.
10 288. Hoffmann NM, Schäfer C, Säkkinen N, Rubio A, Appel H, Kelly A. Benchmarking semiclassical
11 and perturbative methods for real-time simulations of cavity-bound emission and interference.
12 *The Journal of Chemical Physics* 2019, 151:244113.
13 289. Li TE, Chen HT, Nitzan A, Subotnik JE. Quasiclassical modeling of cavity quantum
14 electrodynamics. *Physical Review A* 2020, 101:033831.
15 290. Levine BG, Ko C, Quenneville J, Martinez TJ. Conical intersections and double excitations in
16 time-dependent density functional theory. *Molecular Physics* 2006, 104:1039-1051.
17 291. Halcrow MA. Jahn-Teller distortions in transition metal compounds, and their importance in
18 functional molecular and inorganic materials. *Chemical Society Reviews* 2013, 42:1784-1795.
19 292. Bersuker IB. The Jahn-Teller and Pseudo-Jahn-Teller Effects: A Unique and Only Source of
20 Spontaneous Symmetry Breaking in Atomic Matter. *Symmetry* 2021, 13:1577.
21 293. Qin A, Lam JWY, Tang BZ. Luminogenic polymers with aggregation-induced emission
22 characteristics. *Progress in Polymer Science* 2012, 37:182-209.
23 294. Schneider R, Domcke W. S1-S2 Conical intersection and ultrafast S2->S1 Internal conversion
24 in pyrazine. *Chemical Physics Letters* 1988, 150:235-242.
25 295. Hacker B, Welte S, Daiss S, Shaukat A, Ritter S, Li L, Rempe G. Deterministic creation of
26 entangled atom-light Schrödinger-cat states. *Nature Photonics* 2019, 13:110–115.
27 296. Vlastakis B, Petrenko A, Ofek N, Sun L, Leghtas Z, Sliwa K, Liu Y, Hatridge M, Blumoff J,
28 Frunzio L, et al. Characterizing entanglement of an artificial atom and a cavity cat state with
29 Bell's inequality. *Nature Communications* 2015, 6:8970.
30 297. Isserlis L. On a formula for the product-moment coefficient of any order of a normal frequency
31 distribution in any number of variables. *Biometrika* 1918, 12:134-139.
32 298. Wang MC, Uhlenbeck GE. On the theory of the Brownian motion-II. *Reviews of Modern Physics*
33 1945, 17:323-342.
34 299. Fano U. Geometrical characterization of nuclear states and the theory of angular correlations.
35 *Physical Review* 1953, 90:577-579.
36 300. Tilma T, Sudarshan ECG. Generalized Euler angle parameterization for U(N) with applications
37 to SU(N) coset volume measures. *Journal of Geometry and Physics* 2004, 52:263-283.
38 301. Tilma T, Sudarshan ECG. Generalized Euler angle parametrization for SU(N). *Journal of
39 Physics A: Mathematical and General* 2002, 35:10467-10501.
40 302. Klimov AB. Exact evolution equations for SU(2) quasidistribution functions. *Journal of
41 Mathematical Physics* 2002, 43:2202-2213.
42 303. Bóna P. Classical Mechanical Projections of QM. In: Bóna P, ed. *Classical Systems in Quantum
43 Mechanics*. Cham: Springer International Publishing; 2020.
- 44
45
46
47
48
49
50
51
52
53
54
55
56
57
58
59
60



Quantum dynamical effects are decisive in reproducing the experimental isotropic Raman spectrum of liquid water at room temperature, as illustrated by the LSC-IVR simulation where the infinite (Wigner) phase space for nuclear DOFs is used. Converged results were obtained with 216 water molecules in a box with periodic boundary conditions. (Reprinted with permission from ref 19. Copyright 2018 Taylor & Francis.)

180x106mm (600 x 600 DPI)



Molecular vibrational spectra produced by more advanced trajectory-based dynamics methods with infinite (Wigner) phase space used for nuclear DOFs, which satisfy the two fundamental criteria: conservation of the quantum Boltzmann distribution for the thermal equilibrium system and being exact for any quantum thermal correlation functions in the classical and harmonic limits. (a) Vibrational spectrum of the H_2O molecule at 100K and that at 300K. Adapted with permission from ref 41. Copyright 2016 American Institute of Physics Publishing. (b) Vibrational spectrum of the H_2O_2 molecule at 100K. Adapted with permission from ref 44. Copyright 2021 American Institute of Physics Publishing.

249x479mm (144 x 144 DPI)

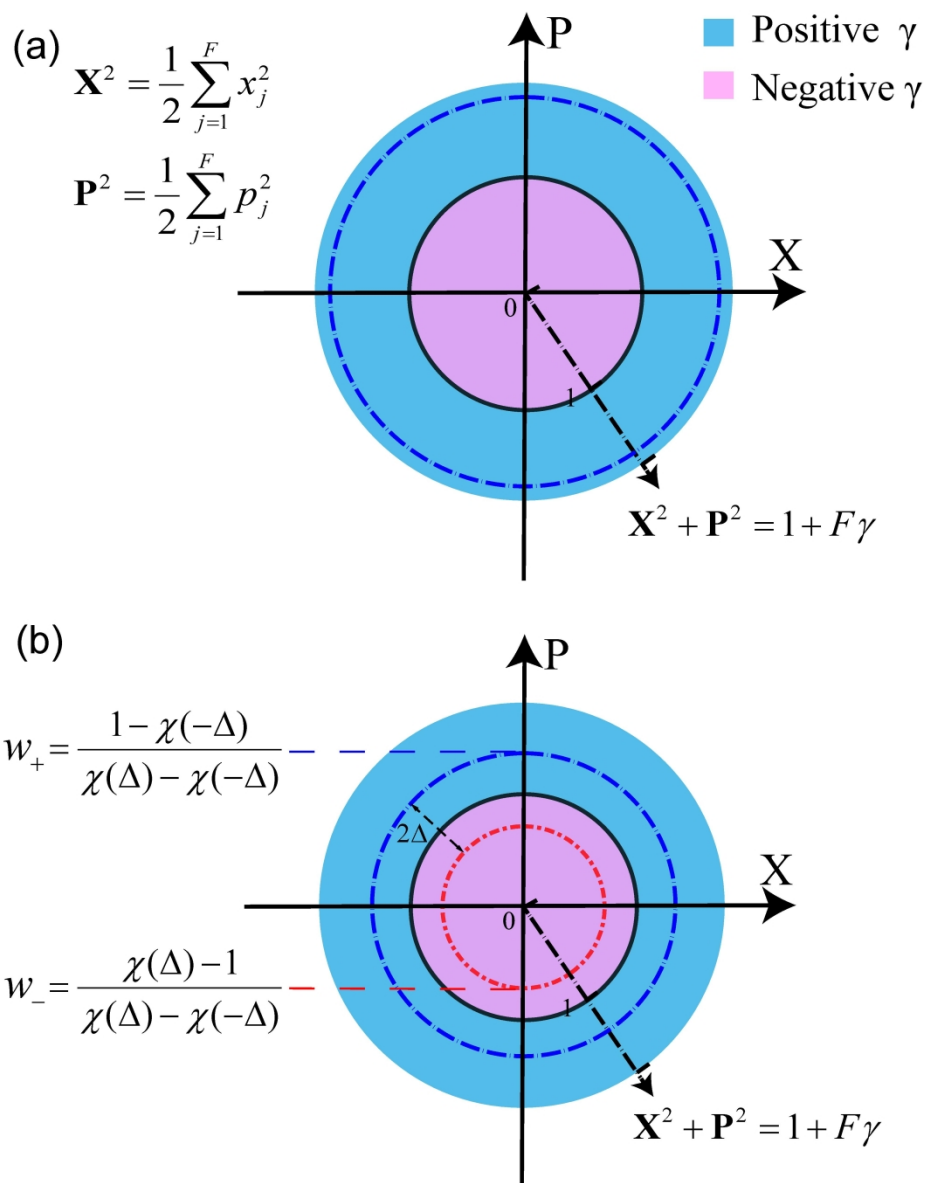
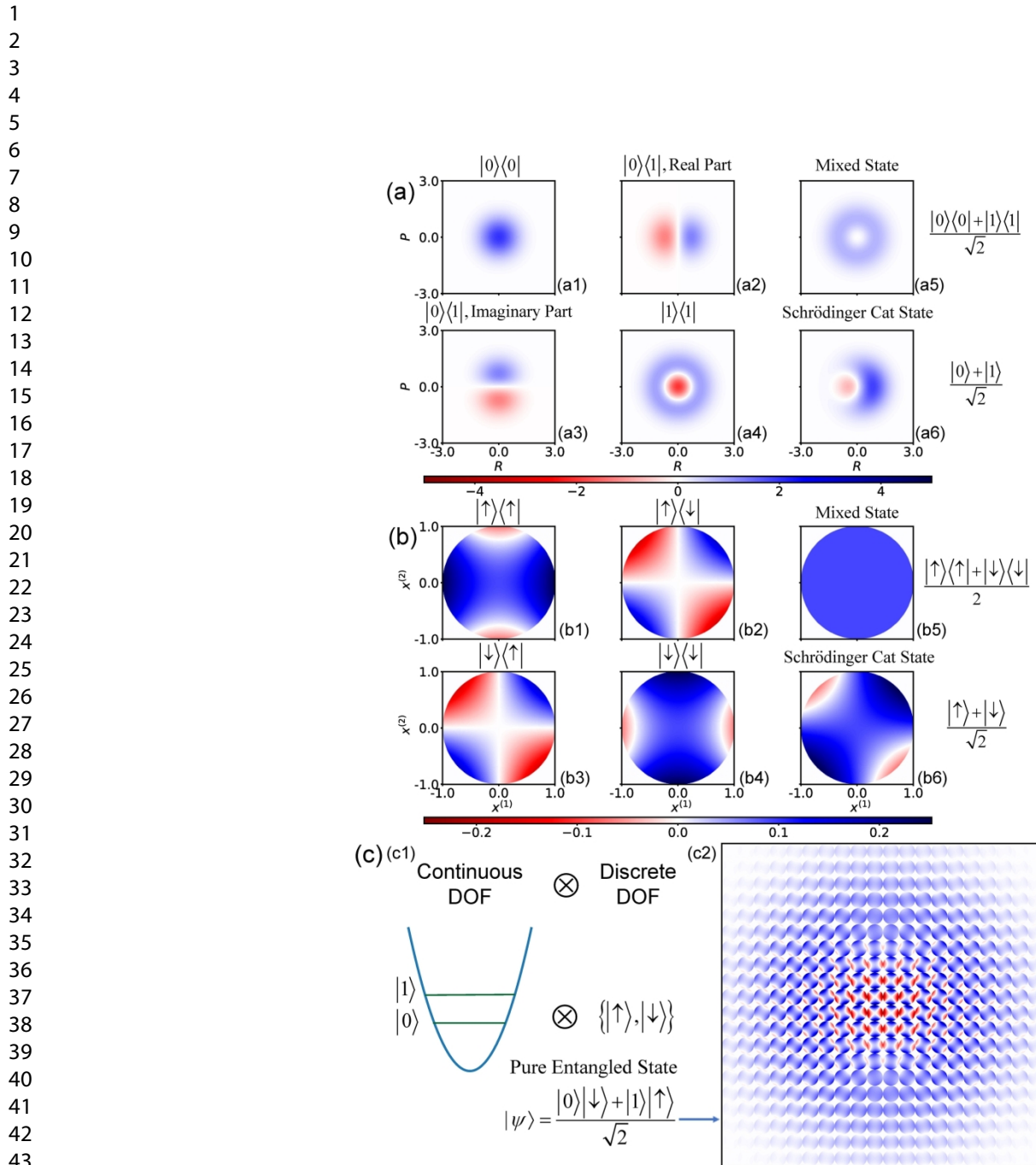


Illustration of the exact mapping formulation with constraint coordinate-momentum phase space. Panel (a) presents constraint phase space with only a single value of parameter γ . Panel (b) demonstrates weighted constraint phase space with two values of parameter γ , where the quasi-probability distribution function is $w(\gamma) = w_+ \delta(\gamma - \Delta) + w_- \delta(\gamma + \Delta)$. Constraint phase space with the positive weight is blue-dashed, while that with the negative weight is red dot-dashed. (Panel (a) is adapted with permission from ref 134. Copyright 2021 American Chemical Society.)

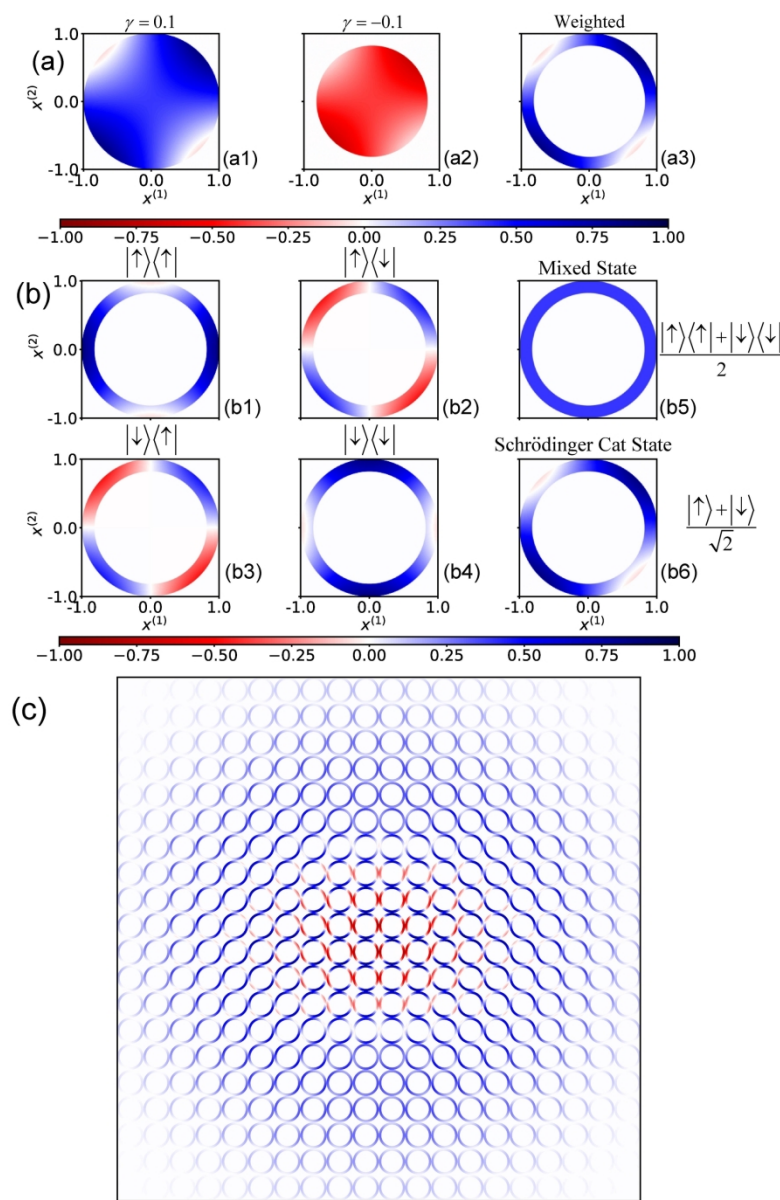
180x212mm (600 x 600 DPI)



Illustrations of (a) Wigner representation of a continuous-variable system, (b) constraint phase space representation of a discrete-variable system, and (c) hybrid coordinate-momentum phase space representation of a composite system with both discrete and continuous DOFs. (a) Wigner distribution for $|0\rangle\langle 0|$ (Panel a1), that for $|1\rangle\langle 1|$ (Panel a4), real part (Panel a2) and imaginary part (Panel a3) of the Wigner distribution for $|0\rangle\langle 1|$, Wigner distribution for mixed state $(|0\rangle\langle 0| + |1\rangle\langle 1|)/2$ (Panel a5), and that for Schrödinger cat state $(|0\rangle + |1\rangle)/\sqrt{2}$ (Panel a6). Here, $|0\rangle$ and $|1\rangle$ are two energy levels of a continuous-variable system. (b) Marginal distribution of constraint phase space coordinates $(x^{(1)}, x^{(2)})$ for $|\uparrow\rangle\langle \uparrow|$ (Panel b1), $|\downarrow\rangle\langle \downarrow|$ (Panel b4), that for $|\uparrow\rangle\langle \downarrow|$ (Panel b2), that for $|\downarrow\rangle\langle \uparrow|$ (Panel b3), that for mixed state $(|\uparrow\rangle\langle \uparrow| + |\downarrow\rangle\langle \downarrow|)/2$ (Panel b5), and that for Schrödinger cat state $(|\uparrow\rangle\langle \uparrow| + |\downarrow\rangle\langle \downarrow|)/\sqrt{2}$ (Panel b6). Here, $|\uparrow\rangle$ and $|\downarrow\rangle$ represent two discrete states of a discrete-variable system. (c) Panel c1: Schematic representation of the composite system and the pure entangled state $(|0\rangle|\downarrow\rangle + |1\rangle|\uparrow\rangle)/\sqrt{2}$; Panel c2: hybrid coordinate-momentum phase space representation of the entangled state. The grid is on the Wigner phase space (R, P) for the continuous DOF, and each circle of a grid stands for the local marginal distribution function of

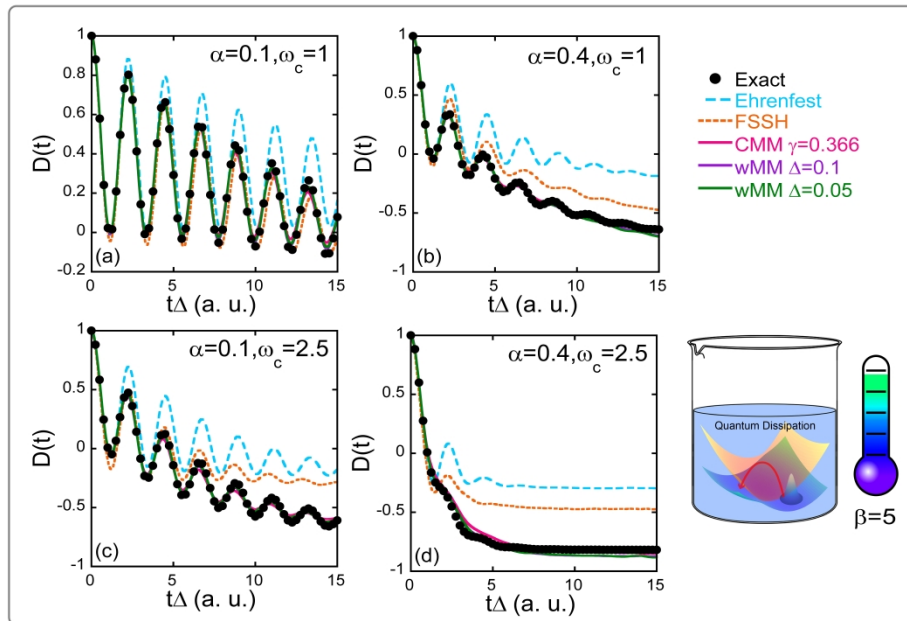
constraint phase space variables ($x^{(1)}, x^{(2)}$). The notations are identical to those in Panels (a)-(b).

180x251mm (300 x 300 DPI)



Illustrations of (a) components and (b) marginal distribution functions of the weighted constraint phase space representation of a discrete-variable system, and (c) weighted hybrid representation of the same composite system as that of Figure 4(c). (a) Marginal distribution of constraint phase space coordinates $(x^{(1)}, x^{(2)})$ for Schrödinger cat state $(|\uparrow\rangle + |\downarrow\rangle)/\sqrt{2}$ with $\gamma = \Delta$ weighted by w_+ (Panel a1), with $\gamma = -\Delta$ weighted by w_- (Panel a2). The sum of the two components yields the marginal distribution of constraint phase space coordinates $(x^{(1)}, x^{(2)})$ of the weighted representation with two values of parameter γ for the Schrödinger cat state (Panel a3). Coordinates are scaled by the larger radius $\sqrt{2(1+F\Delta)}$. (b) Weighted marginal distribution of constraint phase space coordinates $(x^{(1)}, x^{(2)})$ for the same properties as those in Figure 4(b). (c) Same as Figure 4(c), but using weighted marginal distribution for the discrete DOF.

180x274mm (300 x 300 DPI)



Results of population difference $D(t)=P_1(t) - P_0(t)$ between two states for the spin-boson model at low-temperature ($\beta=1/(k_B T)=5$) with the Ohmic bath. Panel (a) reports the population dynamics of the spin-boson model with parameter $\varepsilon=\Delta_c=1$, $\beta=5$, $\omega_c=1$, $\alpha=0.1$ in Panel (a). Solid circles: Exact results produced by eHEOM reported in ref 134. Cyan dashed lines: Ehrenfest dynamics. Orange dashed lines: FSSH. Magenta solid lines: CMM with $\gamma=0.366$. Purple and green solid lines: wMM with $\Delta=0.1$ and 0.05 , respectively. Panel (b) is similar to Panel (a) but for $\alpha=0.4$; Panel (c) is similar to Panel (a) but for $\omega_c=2.5$; Panel (d) is similar to Panel (a) but for $\omega_c=2.5$, $\alpha=0.4$. In each model 300 continuous DOFs (i.e., effective bath modes) are used.

579x515mm (600 x 600 DPI)

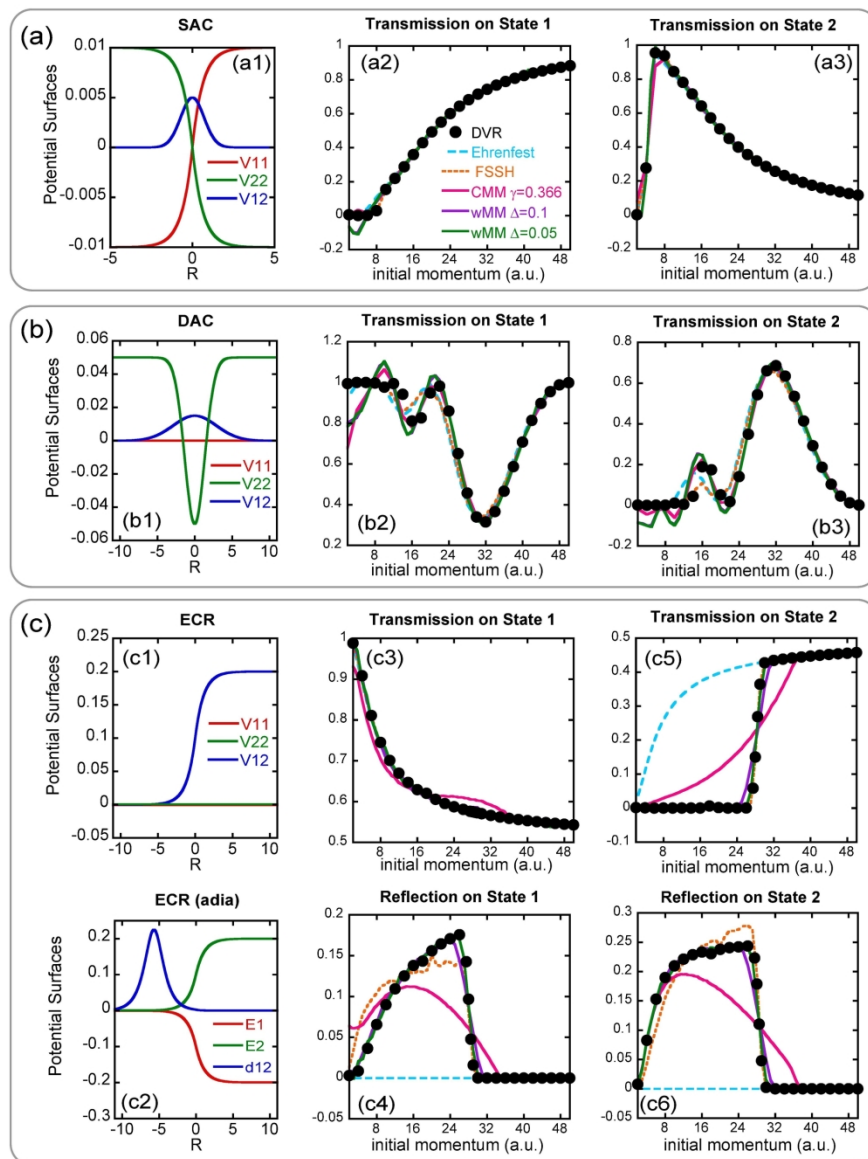
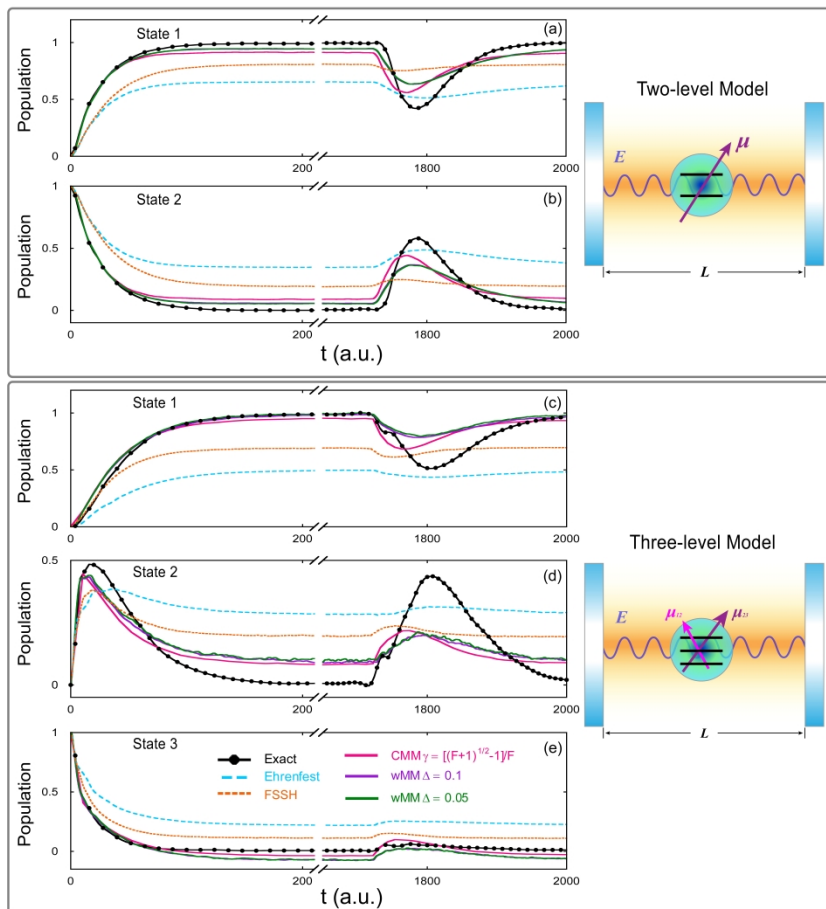


Illustration of three Tully models and simulation results. Panel (a1) denotes diabatic PESes $V_{11}(R)$ and $V_{22}(R)$, as well as coupling term $V_{12}(R)$ for the SAC model; Panel (b1) does so for the DAC model; Panel (c1) does so for the ECR model. Panel (c2) demonstrates adiabatic PESes $E_1(R)$ and $E_2(R)$, as well as nonadiabatic coupling vector $d_{12}(R)$. Panels (a2)-(a3): transmission coefficients on diabatic state 1, and those on diabatic state 2 of the SAC model, respectively. Panels (b2)-(b3): similar to Panels (a2)-(a3), but for the DAC model. Panels (c3) and (c4): transmission/reflection coefficients on adiabatic state 1 of the ECR model; Panels (c5) and (c6): those on adiabatic state 2. In Panels (a2)-(a3), (b2)-(b3), and (c3)-(c6), magenta, purple and green lines stand for transmission coefficients results for CMM with $\gamma = 0.366$, wMM with $\Delta = 0.1$, and wMM with $\Delta = 0.05$, respectively. Long-dashed blue lines: Ehrenfest dynamics; Short-dashed orange lines: FSSH; Black points: exact DVR benchmarks.

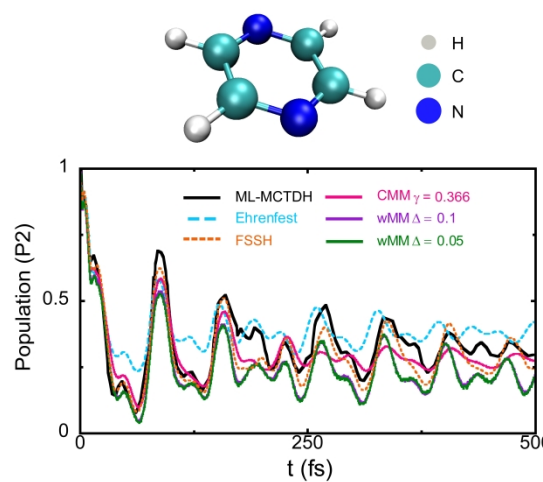
180x239mm (300 x 300 DPI)

1
2
3
4
5
6
7
8
9
10
11
12
13
14
15
16
17
18
19
20
21
22
23
24
25
26
27
28
29
30
31
32
33
34
35
36
37
38
39
40
41
42
43
44
45
46
47
48
49
50
51
52
53
54
55
56
57
58
59
60



Results of population dynamics for the atom-in-cavity models. Panels (a)-(b) represent data of the first and second states of the two-level model, respectively. Panels (c)-(e) denote data of the first, second and third states of the three-level model, respectively. Magenta solid lines: CMM with $\gamma = (\sqrt{F+1}-1)/F$; Purple solid lines: wMM with $\Delta = 0.1$; Green solid lines: wMM with $\Delta = 0.05$; Cyan long-dashed lines: Ehrenfest dynamics; Orange short-dashed lines: FSSH; Black solid-dotted lines: exact results of refs 287, 288. In each model 400 continuous DOFs (i.e., standing-wave modes) are involved.

840x1188mm (600 x 600 DPI)



Results of population dynamics of the second electronic state of the 2-level 3-mode pyrazine model.
Magenta solid lines: CMM with $\gamma = (\sqrt{F+1}-1)/F \approx 0.366$; Purple solid lines: wMM with $\Delta = 0.1$; Green solid lines: wMM with $\Delta = 0.05$. Cyan dashed lines: Ehrenfest dynamics; Orange short-dashed lines: FSSH; Black solid lines: ML-MCTDH results of ref. 212.

979x515mm (600 x 600 DPI)